

Dissertation zur Erlangung des Doktorgrades
der Fakultät für Chemie und Pharmazie
der Ludwig-Maximilians-Universität München

Protein Particle Analysis
—
Critical Factors and New Standards

Sarah Elisabeth Zölls

geb. Mickisch

aus Starnberg, Deutschland

2013

Erklärung

Diese Dissertation wurde im Sinne von § 7 der Promotionsordnung vom 28. November 2011 von Herrn Prof. Dr. Wolfgang Frieß betreut.

Eidesstattliche Versicherung

Diese Dissertation wurde eigenständig und ohne unerlaubte Hilfe erarbeitet.

München, den 27.06.2013

Sarah Zölls

Dissertation eingereicht am 27.06.2013

1. Gutachter: Prof. Dr. Wolfgang Frieß

2. Gutachter: Prof. Dr. Gerhard Winter

Mündliche Prüfung am 26.07.2013

For my family



Coriolis Pharma

Biopharmaceutical Research and Development Service



Acknowledgment

The presented thesis was prepared at the facilities of Coriolis Pharma in Martinsried in collaboration with the Department of Pharmacy, Pharmaceutical Technology and Biopharmaceutics, at the Ludwig-Maximilians-Universität (LMU) Munich and supervised by Dr. Andrea Hawe and Dr. Sun Tantipolphan from Coriolis Pharma and Prof. Dr. Wolfgang Frieß from the LMU.

First, I want to express my deepest gratitude to my first supervisor from the university, Prof. Dr. Wolfgang Frieß, for his continuous and encouraging support of my work and for his inspiration to think "outside the box". Furthermore, I would like to thank you for keeping up the great team spirit in the group which made me always feel as a part of the team although my regular work place was outside the university.

My second supervisor from the university, Prof. Dr. Gerhard Winter, is kindly acknowledged for his valuable suggestions and input for our publications and for the project. I also want to thank you for the dedicated leadership of the chair concerning both scientific and social factors and for taking over the co-referee.

I am most deeply indebted to my first supervisor from Coriolis Pharma Dr. Andrea Hawe for her outstanding and reliable support in every phase of the project. I enjoyed working with you a lot and am very grateful for all your valuable and honest advice – scientifically and personally.

Dr. Sun Tantipolphan as my second supervisor from Coriolis Pharma is cordially acknowledged for her dedicated guidance of my work and many new ideas and discussion points. I really appreciated the time you spent for my project in parallel to your regular project work.

I would like to express my deepest gratitude to Dr. Michael and Thomas Wiggenghorn who gave me the opportunity to work on this project at Coriolis Pharma and supported my work by providing outstanding working conditions. I also want to thank you very much for the possibility to present my work at

several conferences worldwide. Furthermore, I appreciated all your efforts for sustaining the fascinating team spirit in the group by numerous social activities.

Prof. Dr. Wim Jiskoot from Leiden University is kindly acknowledged for our great collaboration and for very helpful comments and advice on our joint publications. Thanks a lot for your continuously fast feedback!

I would like to thank our collaboration partners Axel Wilde from Anasysta and Josh Geib from Fluid Imaging for allocating the FlowCAM systems for extended test periods, Dr. Jürgen Lühmann from Malvern for providing access to the Sysmex FPIA-3000 instrument, and Jérôme Sabathier from Occhio and Mathias Lesti from Quantachrome for providing access to the Occhio FC200S+ instrument. Furthermore, I would like to express my gratitude to Dr. Oliver Valet and Dr. Markus Lankers from rapID particle systems for providing access to the rapID LPE and SPE systems and Prof. Dr. Klaus T. Wanner and Dr. Jörg Pabel from the LMU for providing access to the Abbé refractometer.

I want to thank the whole group of Prof. Frieß and Prof. Winter for the pleasant and supportive working atmosphere. Especially, I would like to thank Kristine and Kerstin for our nice trip to Breckenridge. All colleagues from the university are kindly acknowledged for their welcoming and integrative attitude.

Many thanks go to my Coriolis colleagues who, without exception, made me feel welcome as a part of the team despite my different work topic. I especially want to thank Katharina who has always been an important and appreciated colleague for me, Franziska who has been a great office mate, and Daniel for our joint projects and publications and our inspiring discussions.

The students Richard Höchster, Marika Kutscher, Manuel Gregoritzka, and Julia Schanda are acknowledged for the good work they have done.

I want to thank my friends from the study period Carmen, Christina, Martina, Miriam, Julia, and Elena, for our valuable and long-lasting friendship. I also would like to thank my closest friends Ulrike, Teresa, and Alfons: Thank you for our continuous and precious friendship.

My mother Marion, my sisters Mirjam, Ruth, and Veronika, and my brother Daniel, I want to thank for their constant encouragement and support. Finally, I sincerely thank my husband Sebastian for his enduring patience and support over the last years. Thank you for being the most important person in my life and for your love.

Table of contents

Aims of the thesis.....	1
-------------------------	---

Chapter 1

Introduction: Particles in therapeutic protein formulations – overview of analytical methods

1	General introduction	4
2	Goals and challenges associated with particle analysis.....	10
3	Methods for particle analysis	14
	3.1 Visual inspection.....	14
	3.2 Microscopic methods	15
	3.2.1 <i>Optical microscopy</i>	15
	3.2.2 <i>Fluorescence microscopy</i>	16
	3.2.3 <i>Flow imaging microscopy</i>	17
	3.2.4 <i>Electron microscopy</i>	19
	3.2.5 <i>Atomic force microscopy</i>	19
	3.3 Light absorption/blockage methods.....	20
	3.3.1 <i>Light obscuration</i>	20
	3.3.2 <i>Nephelometry / turbidimetry</i>	22
	3.4 Light scattering techniques	23
	3.4.1 <i>Principles of light scattering</i>	23
	3.4.2 <i>Dynamic light scattering</i>	23
	3.4.3 <i>Nanoparticle tracking analysis</i>	26
	3.4.4 <i>Static light scattering / multi-angle laser light scattering</i>	27
	3.4.5 <i>Fluorescence activated particle sorting</i>	28
	3.5 Non-optical counting and sizing methods	29
	3.5.1 <i>Electrical sensing zone / Coulter counter method</i>	29
	3.5.2 <i>Resonant mass measurement / Archimedes</i>	30
	3.6 Separation methods.....	32
	3.6.1 <i>Size exclusion chromatography</i>	32
	3.6.2 <i>Centrifugation</i>	32
	3.6.3 <i>Asymmetrical flow field flow fractionation</i>	33
	3.7 Spectroscopic methods.....	34
	3.7.1 <i>Circular dichroism spectroscopy</i>	35
	3.7.2 <i>Fourier-transform infrared spectroscopy</i>	35
	3.7.3 <i>Raman spectroscopy</i>	36
	3.7.4 <i>Fluorescence methods</i>	38
	3.7.5 <i>Energy dispersive X-ray spectroscopy</i>	40
4	Conclusion	41
5	References.....	42

Chapter 2

Evaluation of novel techniques for protein particle analysis

1	Introduction.....	50
2	Materials and methods	52
	2.1 Materials	52
	2.2 Light obscuration (LO).....	53
	2.3 Micro-Flow Imaging (MFI).....	53
	2.4 Flow particle image analysis (FPIA)	53
	2.5 Flow imaging microscopy analysis (Occhio)	54
	2.6 Flow imaging microscopy analysis (FlowCAM VS1)	54
	2.7 Electrical sensing zone (ESZ, Coulter counter).....	54
	2.8 Resonant mass measurements (RMM, Archimedes).....	55
	2.9 Dynamic light scattering (DLS).....	56
	2.10 Nanoparticle tracking analysis (NTA).....	56
	2.11 Image directed Raman spectroscopy (rapID)	56
3	Results and discussion	58
	3.1 Flow imaging techniques	58
	3.2 Non-optical particle analysis.....	63
	3.3 Particle identification techniques.....	70
4	Conclusion.....	73
5	References.....	75

Chapter 3

Micro-Flow Imaging and resonant mass measurement (Archimedes) – Complementary methods to quantitatively differentiate protein particles and silicone oil droplets

1	Introduction.....	78
2	Materials and methods	81
	2.1 Materials	81
	2.2 Preparation of protein samples.....	81
	2.3 Preparation of silicone oil emulsion	82
	2.4 Preparation of individual and mixed samples of silicone oil droplets and protein particles	82
	2.5 Micro-Flow Imaging (MFI).....	83
	2.6 Development of a customized filter for MFI	83
	2.7 Resonant mass measurement (RMM)	86
3	Results and discussion	88
	3.1 Silicone oil droplets in prefilled syringes	88
	3.2 Determination of total particle concentrations (without discrimination) ...	88
	3.3 Discrimination between silicone oil droplets and protein particles.....	97
	3.3.1 <i>Discrimination between droplets and particles by MFI</i>	<i>97</i>
	3.3.2 <i>Discrimination between droplets and particles by RMM</i>	<i>102</i>
	3.4 Comparison of results for MFI and RMM.....	103
4	Recommendations and conclusions	105
5	References.....	108

Chapter 4

Flow imaging microscopy for protein particle analysis – a comparative evaluation of four different analytical instruments

1	Introduction.....	111
2	Materials and methods	115
	2.1 Materials	115
	2.2 Preparation of protein samples	115
	2.3 Preparation of silicone oil emulsion	116
	2.4 Preparation of individual and mixed samples of silicone oil droplets and protein particles	116
	2.5 Refractive index determination	117
	2.6 Light obscuration (LO).....	117
	2.7 Micro-Flow Imaging (MFI).....	117
	2.7.1 MFI4100	117
	2.7.2 MFI5200	118
	2.7.3 Particle data analysis MFI	118
	2.8 FlowCAM analysis	118
	2.8.1 FlowCAM VS1.....	118
	2.8.2 FlowCAM PV.....	119
	2.9 Performance evaluation	120
3	Results and discussion	121
	3.1 Count and size performance with polystyrene standards	121
	3.2 Image properties	126
	3.3 Quantification of protein particles	128
	3.4 Differentiation of silicone oil droplets and protein particles.....	132
	3.5 Handling of the systems	135
4	Conclusion	137
5	References.....	139

Chapter 5

Material screening and investigation of particle density for the development of standardized protein-like particles

1	Introduction.....	142
2	Materials and methods	144
	2.1 Materials	144
	2.2 Particle preparation.....	145
	2.3 Light obscuration (LO).....	147
	2.4 Micro-Flow Imaging (MFI).....	147
	2.5 Resonant mass measurements (RMM).....	147
3	Results and discussion	149
	3.1 Comparison of current standards to protein particles by LO and MFI	149
	3.2 Evaluation of novel materials	151
	3.3 Investigation of protein particle density	156
4	Conclusion	161
5	References.....	162

Chapter 6

How subvisible particles become invisible – relevance of the refractive index for protein particle analysis

1	Introduction.....	164
2	Materials and methods	166
	2.1 Materials	166
	2.2 Refractive index determination	167
	2.3 Light obscuration (LO).....	170
	2.4 Micro-Flow Imaging (MFI).....	170
	2.5 Resonant mass measurements (RMM).....	171
3	Results and discussion	172
	3.1 Transparency evaluation of protein particles	172
	3.2 Refractive index determination of protein particles.....	176
	3.3 Relevance of RI for protein particle analysis.....	178
	3.4 PTFE particles for the evaluation of the “invisible particles effect” in LO .	185
	3.5 Orthogonal techniques for protein particle analysis to cope with RI influences.....	188
4	Conclusion.....	190
5	References.....	191

Chapter 7

Summary of the thesis 193

Aims of the thesis

Protein aggregates and particles are an important instability product in formulations of therapeutic proteins, such as monoclonal antibodies, and need to be analyzed in formulation development, production, and for release. This is required by the authorities due to the potential loss of activity, increasing concerns about the immunogenicity, and to gain the broadest possible knowledge of product properties to ensure product quality. In particular the analysis of visible and subvisible particles (i.e. in the lower μm range) is currently a hot topic in the development of therapeutic protein formulations which constantly gains more importance by novel findings, additional available techniques, and new regulatory requirements.

The overall goal of this thesis is to identify and evaluate critical factors for protein particle analysis and to apply this knowledge for the development of novel standardized protein-like particles. This is crucial because up to now the analysis of particles in therapeutic protein formulations relies on the calibration of the instruments with polystyrene standards which differ clearly from protein particles in their properties.

Various techniques for protein particle analysis are available on the market and additional techniques are constantly under development. Thus, the first main objective of this thesis is to comparatively evaluate existing and novel techniques for quantification and characterization of particles in therapeutic protein formulations. This includes a comprehensive research on the state of the art of available techniques, as well as scientific applications and literature on these methods (Chapter 1).

As a second step, techniques with novel measurement principles or from different application fields which are not yet state of the art for protein particle analysis should be experimentally evaluated for their suitability to characterize proteinaceous particles (Chapter 2). This should lead to a guideline which method is suitable for which purpose and which obstacles are to be considered in the data evaluation.

Additionally, for selected techniques, the focus is set on specific critical topics of scientific interest for the development of protein pharmaceuticals: the differentiation of silicone oil droplets and protein particles, which is currently highly relevant due to the trend of protein formulation in prefilled syringes (Chapter 3), and evaluation of the performance of different flow imaging microscopy instruments, which is crucial for correct data interpretation (Chapter 4).

The second main objective of this thesis is the identification of typical and crucial properties of protein particles to enable the development of more proteinaceous particle standards. Additionally, these factors should provide the scientific basis for a better interpretation of particle analysis data generated by different measurement principles. A material screening based on the optical particle properties shape and transparency should be performed to identify potential materials and preparation methods for novel standardized protein-like particles (Chapter 5).

Furthermore, novel methods to determine the critical protein particle properties density and refractive index, which are not well characterized up to now, are to be developed (Chapter 5 and Chapter 6). Understanding these properties and their relevance for protein particle analysis should support the development of standardized protein-like particles. Additionally, potential applications of those novel standards for protein particle analysis should be evaluated. Finally, general recommendations for protein particle analysis in the future are derived (Chapter 6).

Chapter 1

Introduction: Particles in therapeutic protein formulations – overview of analytical methods

Abstract

The presence of particles is a major issue during therapeutic protein formulation development. Both proteinaceous and non-proteinaceous particles need to be analyzed not only due to the requirements of the Pharmacopeias, but also to monitor the stability of the protein formulation. Increasing concerns about the immunogenic potential together with new developments in particle analysis make a comparative description of established and novel analytical methods useful. Our review aims to provide a comprehensive overview on analytical methods for the detection and characterization of visible and subvisible particles in therapeutic protein formulations. We describe the underlying theory, benefits, shortcomings, and illustrative examples for quantification techniques, as well as characterization techniques for particle shape, morphology, structure and identity.

The following chapter was published in a slightly modified version as a review article in the Journal of Pharmaceutical Sciences and appears in this thesis with the journal's permission:

S. Zölls, R. Tantipolphan, M. Wiggerhorn, G. Winter, W. Jiskoot, W. Friess, A. Hawe: "Particles in therapeutic protein formulations, part 1: Overview of analytical methods"; J Pharm Sci 101(3):914-935 (2012)

1 General introduction

Approximately half of all new drugs approved by the FDA in the last few years are biopharmaceuticals,¹ mainly therapeutic proteins and especially monoclonal antibodies.² A major challenge during formulation development of these products is overcoming their limited stability. Among the various degradation mechanisms a protein can undergo,^{3,4} the formation of protein aggregates and particles is a particular concern.⁵ Aggregates are generally defined as assemblies of protein monomers and can vary in many aspects such as size, reversibility, and structure. For instance, their size can range from dimers in the nm range to large aggregates of hundreds of microns which are visible to the human eye. These larger aggregates are often also designated as particles.^{6,7} However, not only proteinaceous particles, but also non-proteinaceous particles, e.g. originating from packaging material or excipients, can influence product quality and therefore need to be analyzed.^{8,9}

Our review aims to give an overview on methods for both quantification and characterization of visible and subvisible particles in therapeutic protein formulations. On the basis of the current classification of protein aggregates and particles,¹⁰ for this article particles are defined as material with a size above 0.1 μm and are further classified into subvisible (0.1 – 100 μm) and visible particles (above 100 μm); submicron particles (0.1 – 1 μm) are a subgroup of subvisible particles.

Whereas particles above 10 μm have received attention in the development of therapeutic protein products already for a long time due to the requirements of the Pharmacopoeias for parenteral products,¹¹⁻¹³ the detection and characterization of subvisible particles below 10 μm has only recently gained more importance. This is due to increasing concerns about the potential immunogenicity of subvisible particles – both proteinaceous particles,¹⁴ non-proteinaceous particles,¹⁵ and non-proteinaceous particles with adsorbed protein.^{16,17} Moreover, new techniques for the analysis of subvisible particles have emerged in the last few years, enabling a more detailed characterization of these impurities or contaminants.^{8,9} Several reviews summarizing methods for the quantitative analysis of protein aggregates and particles^{6,18,19} and one

describing analytical methods for protein particles down to 2 μm^{20} are available. Our review includes not only particle quantification techniques, but also analytical characterization methods that provide information about particle characteristics such as shape, morphology, structure and identity. Moreover, we discuss new developments in particle analysis. We provide a comprehensive overview of particle analysis for pharmaceutical protein products with the presented methods summarized in Table 1-1 and Table 1-2. The sections describing the individual analytical methods are sorted according to measurement principle and cover the underlying theory, advantages, shortcomings, and illustrative examples. Analytical techniques for nanometer protein aggregates with a very limited use for subvisible and visible particles such as size-exclusion chromatography and analytical ultracentrifugation are explained only briefly. For the pharmaceutical application of the described methods in development and production of therapeutic proteins, the reader is referred to Part II "Applications in the Pharmaceutical Industry" of the review article by Narhi et al.²¹

Table 1-1: Overview of analytical methods for (protein) particle analysis, optical quantification methods.

Principle	Method	Destructive	Isolation of particles required	Further information
Visual inspection	Human or automated visual inspection	No	No	Detects only presence of visible particles
	Light microscopy	Yes	Yes	Manual data acquisition required
	Fluorescence microscopy	Yes	Yes/no ^a	Manual data acquisition required
Microscopic methods	Flow Particle Image Analyzer (Sysmex FPIA-3000)	Yes	No	-
	FlowCAM	Yes	No	-
	Micro-Flow Imaging	Yes	No	-
	Electron microscopy	Yes	Yes	-
	Atomic force microscopy	Yes	Yes	-
Light absorption / blockage	Light obscuration	Yes	No	-
	Nephelometry / turbidimetry	No	No	Detects only presence of particles / aggregates
Light scattering	Dynamic light scattering	No	No	-
	Nanoparticle tracking analysis	No	No	-
	Static light scattering	No	No	-

^a Yes/no = isolation possible, but not required; ^b ECD = equivalent circular diameter; - = no or very limited information provided

(continued from previous page)

Provided information				
Size	Size distribution	Shape	Structure	Identity
-	-	-	-	-
Actual size	Yes	Different shape factors	-	-
Actual size	Yes	Different shape factors	Hydrophobic regions by selective fluorescent dyes	Limited
Different diameters (e.g. ECD ^b ; Feret diameter)	Limited	Aspect ratio; circularity	-	-
Different diameters (e.g. ECD ^b ; Feret diameter)	Yes	Aspect ratio; circularity	Transparency related values	Fluorescence option: distinction of protein vs. non-protein material by selective fluorescent dyes
Different diameters (e.g. ECD ^b ; Feret diameter)	Yes	Aspect ratio; circularity	Transparency related values	Limited (distinction by software filters based on optical properties)
Limited	-	Limited	Surface morphology	-
Limited	-	Limited	Surface morphology	-
ECD ^b	Yes	-	-	-
-	-	-	-	-
Hydrodynamic diameter	Limited	-	-	-
Hydrodynamic diameter	Limited	-	-	-
Molecular weight	Limited	-	-	-

Table 1-2: Overview of analytical methods for (protein) particle analysis, non-optical quantification methods, separation methods and spectroscopic methods.

Principle	Method	Destructive	Isolation of particles required	Further information
Electrical sensing zone	Coulter counter	Yes	No	Sufficient buffer conductivity required
Resonant mass measurement	Archimedes	Yes	No	Density information for liquid and particles required for correct size determination
Separation methods	Size exclusion chromatography	Yes	No	Detects indirectly fraction of insoluble particles
	Analytical ultracentrifugation	Yes	No	Very limited applicability for particles
	Disk centrifugation	Yes	No	-
	Asymmetrical flow field flow fractionation	No	No	Applicability for particle analysis not fully established
	Fluorescence activated particle sorting	No	No	Preparative separation possible; applicability for particle analysis not fully established
Spectroscopic methods	Circular dichroism	No	No	-
	FT-IR spectroscopy / microscopy	No	Yes/no ^a	-
	Raman spectroscopy / microscopy	No	Yes/no ^a	-
	Intrinsic fluorescence	No	No	-
	Extrinsic fluorescent dyes	Yes	Yes/no ^a	-
	Energy dispersive X-ray spectroscopy	Yes	Yes	-

^a Yes/no = isolation possible, but not required; ^b ESD = equivalent spherical diameter; - = no or very limited information provided

(continued from previous page)

Provided information				
Size	Size distribution	Shape	Structure	Identity
ESD ^b	Yes	-	-	-
ESD ^b	Yes	-	-	Differentiation between positively and negatively buoyant particles (e.g. silicone oil droplets and protein particles)
Hydrodynamic size	-	-	-	-
Molecular weight	Yes	-	-	-
Hydrodynamic size	Yes	-	-	-
Hydrodynamic size; molecular weight if coupled with MALLS detector	-	-	-	-
Hydrodynamic size	Yes	-	-	Separation of protein vs. non-protein material by selective fluorescent dyes
-	-	-	Secondary, tertiary structure	-
Only in IR microscopy	Limited, only in IR microscopy	Limited, only in IR microscopy	Secondary structure	By comparison with database
Only in Raman microscopy	Limited, only in Raman microscopy	Limited, only in Raman microscopy	Secondary structure	By comparison with database
-	-	-	Conformational changes	-
-	-	-	Conformational changes	Limited
-	-	-	-	Atomic composition

2 Goals and challenges associated with particle analysis

The tolerated amount of visible and subvisible particles in parenteral therapeutic protein products is restricted by regulations as described in the Pharmacopoeias,^{11-13,22} which makes quantification of protein particles essential in development and production of therapeutic proteins. The size of visible particles is not specified in the Pharmacopoeias, as the detection of particles by the human eye depends amongst others on personal eyesight, light conditions, and used test settings. However, the specifications for subvisible particles include particle sizes $\geq 10 \mu\text{m}$ and $\geq 25 \mu\text{m}$,^{11,13} which makes also size determination of the counted particles necessary.

Although the identification of particles present in parenteral protein products is not required by the Pharmacopoeias, a distinction between non-proteinaceous and proteinaceous particles is relevant in case of protein therapeutics. Non-proteinaceous material, e.g. particles shed from pumps or primary packaging material (including silicone oil droplets in prefilled syringes) or particles formed by degradation of excipients (e.g. polysorbate),²³ can trigger protein aggregation by heterogeneous nucleation and might be related to increased immunogenicity.^{16,24,25} Root cause analysis to determine the source of the particles is an important part of any investigation and can result in minimizing the occurrence of non-proteinaceous particles. In addition, false positive "particles" such as air bubbles need to be distinguished from real particles for a correct evaluation of the particle load in the analytical characterization. However, only few techniques are able to discriminate between proteinaceous and non-proteinaceous particles, e.g. Raman spectroscopy/microscopy,²⁶ IR spectroscopy/microscopy,²⁷ and to a certain extent also methods involving fluorescent dyes²⁸ and flow imaging microscopy methods^{29,30} (Table 1-1, Table 1-2).

For proteinaceous particles, it can be helpful during formulation development to further discriminate the particles with respect to e.g. size, shape or structure (Table 1-3). Depending on the (stress) conditions the protein had been exposed

to, several types of aggregates and particles can be detected allowing conclusions about the susceptibility of the protein to distinct stress conditions and the identification of means to prevent this instability.³¹

Table 1-3: Overview of measurable particle properties.

Property	Reported as
Size	Hydrodynamic diameter Equivalent circular diameter (ECD) Equivalent spherical diameter (ESD) Feret diameter Molecular weight
Concentration	Total particle concentration Size distribution
Shape	Aspect ratio Circularity
Optical properties	Transparency Refractive index
Identity	Chemical identity (proteinaceous vs. non-proteinaceous) Further characterization of proteinaceous particles (secondary/tertiary structure)

Many analytical methods for (protein) particles are based on the interaction of particles with light (Figure 1-1). Methods based on light scattering require a substantial difference in refractive index of the particles and the surrounding liquid. However, protein particles are often translucent with a supposed refractive index between 1.33 and 1.4.²⁹ This value is close to that of aqueous buffers and highly-concentrated protein solutions, thereby hampering the detection by light-based systems.^{29,32} However, to our knowledge the refractive index of protein particles has not been analyzed up to now. It likely depends on the type of particle, e.g. degree of protein unfolding and packing, so the values described in the literature are only assumptions. Light-based systems for particle analysis rely on the calibration with standards, usually polystyrene beads of a clearly higher refractive index compared to protein particles. Therefore, the results obtained from these systems for protein particles need to be evaluated carefully and standards that resemble the proteinaceous nature of the particles more closely would be very helpful for data interpretation.⁹ When comparing particle size results from several analytical techniques algorithms for size determination need to be considered as particle size can be provided as various parameters (Table

1-3). A further challenge lies in the often dynamic, heterogeneous and transient nature of particles, as size and number of particles can change when larger particles dissociate into smaller ones and vice versa.^{24,33}

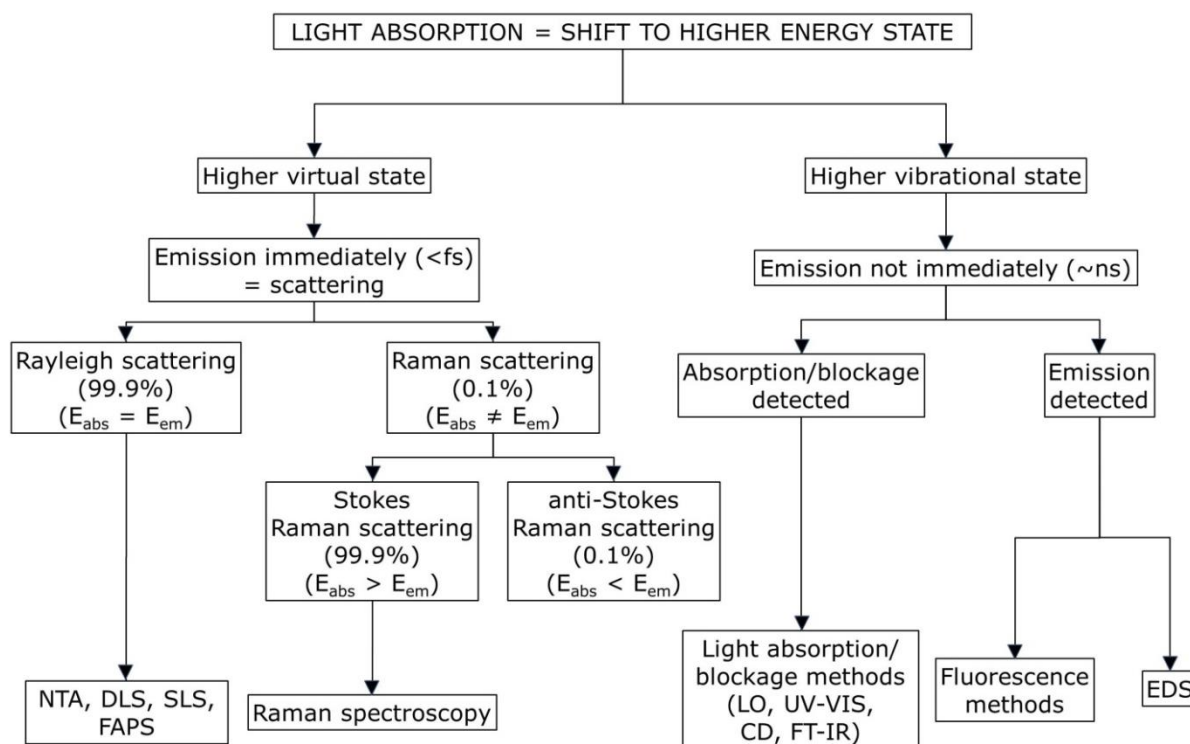


Figure 1-1: Schematic classification of analytical methods based on the interaction of particles with light. NTA, nanoparticle tracking analysis; DLS, dynamic light scattering; SLS, static light scattering; FAPS, fluorescence activated particle sorting; LO, light obscuration; CD, circular dichroism; FTIR, Fourier transform infrared spectroscopy; EDS, energy dispersive X-ray spectroscopy.

In general, several analytical methods with different underlying principles should be combined for each sample to overcome the limitations of a single method in terms of size range (Figure 1-2), concentration range or delivered parameters. This comes along with comprehensive and challenging data analysis as unequal results may be obtained for the same parameter if different measurement principles are applied. Therefore, results may not always be directly comparable and need to be evaluated considering the underlying theory. One possibility is to assess the sample with several orthogonal methods to understand the limitations and then select one or two methods for sample to sample comparison to look for trends rather than focusing on actual numbers obtained.

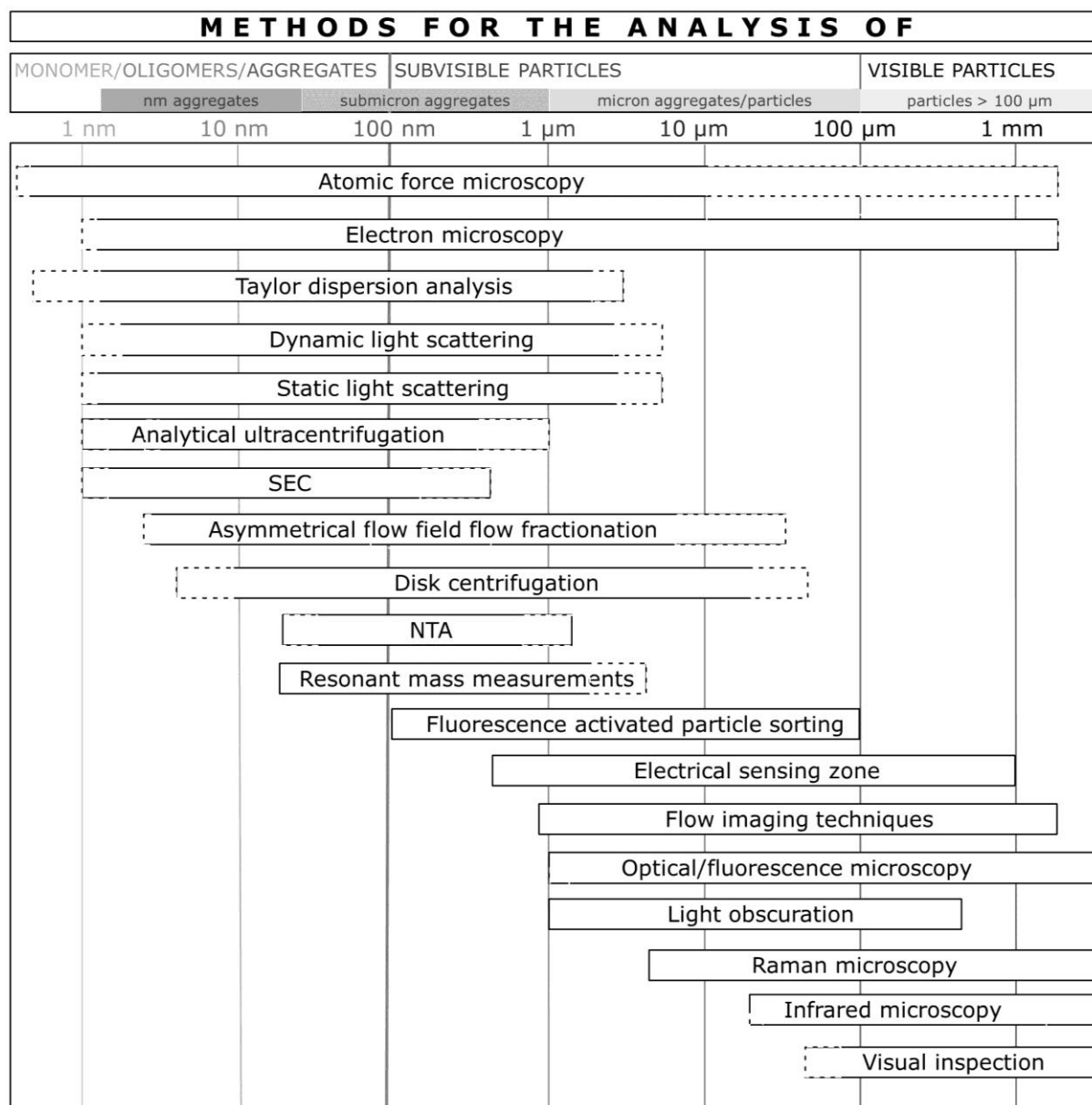


Figure 1-2: Depiction of the approximate size range of analytical methods for size determination of subvisible and visible (protein) particles.

3 Methods for particle analysis

3.1 Visual inspection

Visual inspection by definition describes the examination of particles detectable by the human eye without any auxiliary equipment. The absence of visible particles as requirement for parenterals was originally introduced because of foreign particles in pharmaceutical products, e.g. dissolved from packaging material or introduced during production, filling and packaging processes. However, as protein itself can form visible particles, the significance of this requirement has been controversially discussed. The USP requires parenteral preparations to be “essentially free from visible particulates”,²² but does not describe a specific analytical method for visual inspection. According to the Ph.Eur., injections need to be “practically free from particles”, which is to be evaluated by eye while gently swirling the formulation in its original container for 5 seconds in front of a white background and 5 seconds in front of a black background with specified light conditions.¹² Depending on the individual eyesight, experience of the operator and experimental conditions, particles larger than 50 μm ⁶ to 100 μm ⁸ can be detected by this manual method. Furthermore, intensive training of the operators, e.g. with particle test kits, is required to obtain reliable results. Due to the dependency on the operator’s ability and judgment, semi-automated and fully-automated visual inspection methods have been developed to improve and standardize the inspection process (e.g. from Seidenader GmbH, Markt Schwaben, Germany or Eisai Machinery GmbH, Tokyo, Japan). Semi-automated systems relieve the human operator from holding and swirling the container and standardize thereby the sample preparation process. Furthermore, auxiliary devices such as light from the bottom or a magnifying lens in front of the analyzed container alleviate particle detection. However, the detection process and the evaluation itself still need to be performed personally by the examiner involving again the operator’s ability and judgment. In contrast, fully-automated systems detect particles by light reflection and transmission with subsequent image analysis to distinguish particles from container defects. The threshold for vial rejection and automated sorting is set based on Knapp testing,³⁴ a validation procedure for fully-automated visual inspection systems showing that it is still a probabilistic and not an absolute method. As a major

benefit, both human and automated visual inspection allows 100% non-destructive inspection of the complete production volume. As a limitation, visual inspection originally only distinguishes between absence and presence of visible particles and does not provide information about particle properties such as number, structure or origin. Though, human inspectors can be trained with a set of standards to distinguish air bubbles, cellulose fibers, and colored particles from protein particles. For a rough estimation of the amount of visible particles, the evaluation scale provided in the "Deutscher Arzneimittel Codex" (DAC), which describes the presence of visible particles in scores from 0 (no particles visible within 5 seconds) to 10 (particles visible immediately and clearly in great quantities), can be useful.³⁵ Semi-automated visual inspection has been used to roughly detect differences in protein particles generated by several stress types in terms of number and size, thereby complementing light obscuration and turbidity results.³³ Furthermore, additional phenomena such as foam formation, turbidity or particle floating can be observed by visual inspection, supplementing information from other analytical methods.³⁶

3.2 Microscopic methods

Microscopic methods enable the visualization of particles with a resolution ranging from 1 μm (optical microscopy, fluorescence microscopy and flow imaging microscopy) down to 0.1-1 nm (electron microscopy and atomic force microscopy) (Figure 1-2). Those methods add an important aspect to results obtained from pure counting or sizing techniques. Raman microscopy and FT-IR microscopy combine microscopic and spectroscopic information. A disadvantage of all microscopic techniques is that they only analyze a small fraction of the sample which may not necessarily be representative for the complete sample.

3.2.1 Optical microscopy

Optical microscopy allows visualization, counting and sizing of particles in the range of 1 μm to several mm. The method is listed in the Ph.Eur.¹¹ and USP¹³ for the analysis of subvisible particles next to light obscuration with the same shortcoming of a large required volume of 25 mL. The compendial method requires a light microscope and includes a filtration step to isolate the protein particles onto a filter membrane. The maximum particle counts for parenteral

products are specified in the Ph.Eur.¹¹ and the USP¹³ as follows: For a total volume of 100 mL or less, the maximum particle count is specified as 3000 particles $\geq 10 \mu\text{m}$ and 300 particles $\geq 25 \mu\text{m}$, each per container. For a total volume larger than 100 mL, the maximum particle count is 12 particles $\geq 10 \mu\text{m}$ and 2 particles $\geq 25 \mu\text{m}$, each per mL.

Optical microscopy is rarely used as a single technique due to potential influences on sample properties by the initial filtration step and a very time-consuming manual evaluation of particle size and number. Thus, it is mostly combined with other techniques, e.g. it is used to get a first impression on the particle load on the filter prior to analysis by FT-IR microscopy or SEM-EDS (see below)²⁷ or applied to analyze particles observed by visual inspection (see above) in more detail, which can be done directly in solution without a filtration step.³⁶ However, microscopic evaluation of unstained particles can be difficult as translucent protein particles are hard to detect. Furthermore, it is not easy to distinguish proteinaceous from non-proteinaceous particles. Staining of the particles by protein-reactive dyes, e.g. the "reversible protein detection kit" (Sigma, St. Louis, MO), can in some cases improve the detectability and at the same time help to distinguish proteinaceous from non-proteinaceous particles by optical microscopy.³⁷

3.2.2 Fluorescence microscopy

Fluorescence microscopy comprises visualization, counting and sizing of particles stained by fluorescent dyes such as Nile Red, Congo Red, Thioflavine T or SYPRO orange³⁸ (see below), using a fluorescence microscope or a confocal microscope. The technique enables visualization of protein particles larger than ca. $0.5 \mu\text{m}$, either immobilized on a filter or even without a filtration step as the stained sample can be placed directly on a microscopic slide. Conventional fluorescence microscopes are equipped with a light source (usually a xenon or mercury lamp), excitation filters and emission filters which allow the emitted light to pass to the detector, but at the same time mask any reflected excitation light.³⁸ In confocal microscopy, only a small spot of the sample is illuminated by a laser beam, and the detection of emitted light is restricted to the same spot. Major advantages of confocal over conventional fluorescence microscopy include (1) three-dimensional information about the complete sample and (2) an increased

resolution by a factor of 1.4 compared to conventional fluorescence microscopy due to the arrangement of the optics avoiding background fluorescence.^{39,40}

A benefit of fluorescence microscopy in general is a high sensitivity for the detection of protein particles. This was for example shown for monoclonal antibodies stained by Nile Red which allowed an earlier detection of protein particles compared to UV absorbance or light microscopy and also permitted sizing and counting of the particles.^{38,41} The specificity of fluorescent dyes such as Nile Red for hydrophobic binding regions allows the distinction of hydrophobic versus hydrophilic material, e.g. particles of unfolded protein versus native protein or non-proteinaceous particles. Other dyes, such as Thioflavine T or Congo Red selectively bind to amyloid structures.³⁸ However, binding of these and other fluorescent dyes to non-proteinaceous hydrophobic material cannot be excluded. A major shortcoming of this approach is the possibility that staining of the sample may change particle properties.⁴²⁻⁴⁴

3.2.3 Flow imaging microscopy

Flow imaging techniques allow analyzing particles without isolation. The particles pass an imaging field where they are illuminated by a light source and imaged by a charge-coupled device (CCD) camera. Subsequent automated image analysis provides information about size and number in a size range from ca. 1 to 400 μm ; information about shape and different parameters connected to transparency or compactness of the particles can be obtained for particles from ca. 5 to 400 μm .⁴⁵

Three major flow imaging systems currently on the market are: Sysmex FPIA-3000 (Flow Particle Image Analyzer, Malvern Instruments, Herrenberg, Germany), FlowCAM (Fluid Imaging Technologies, Yarmouth, ME) and Micro-Flow Imaging (MFI, ProteinSimple, Santa Clara, CA). FPIA differs from the other techniques in mainly two aspects: (1) The particle suspension is analyzed "sandwiched" between "particle sheath liquid" which causes all particles in the imaging field to be orientated with their largest side perpendicular to the light beam.⁴⁶ A direct contact between "particle sheath liquid" and analyte during the measurement could potentially cause changes in the sample properties. In contrast, FlowCAM and MFI use glass flow cells of 50 to 400 μm depth as imaging

field. The imaging field allows analysis of larger sample volumes and eliminates the use of particle sheath liquid as in FPIA.^{29,47} However, protein particles can stick to the glass surface in FlowCAM and MFI and thereby disturb the analysis. (2) FPIA applies stroboscopic sample illumination potentially missing particles between the illumination intervals. In contrast, FlowCAM and MFI use an image capture rate which is balanced with the flow rate to pick up nearly all particles passing by the analysis window of the flow cell.

All imaging techniques are suitable to analyze particle properties such as size, shape, and transparency and allow the application of software filters in the data analysis to classify particles upon different properties. In addition, FlowCAM and MFI provide information about particle concentration (up to about 5,000 particles/mL for FlowCAM and 1,200,000 particles/mL for MFI, according to the manufacturer), whereas FPIA is less suitable to determine the particle concentration due to the stroboscopic illumination and the small imaging field. In return, FPIA delivers the highest image quality among the flow imaging techniques.²⁰ FPIA analyzes only a very small amount of the applied sample volume (less than 1%) whereas MFI and FlowCAM can achieve a higher efficiency of 60-80% depending on the used instrument.

A general benefit of all flow imaging techniques is the digital visualization of particles enabling profound analysis of size, shape, transparency, and related parameters. This can for example enable a differentiation between silicone oil droplets and protein particles, as shown for MFI.^{29,30} As a general shortcoming, dilution of the sample can be required if particle count limits are reached, thereby potentially changing sample properties.³² Furthermore, as a light-based technique, flow imaging microscopy relies on sufficient differences in refractive index between particle and solvent. As this is not always the case, especially not for highly-concentrated protein solutions or formulations containing high concentrations of excipients such as sugars, particle number and/or size could be underestimated.³²

Especially MFI has been recently used for the characterization of particles in therapeutic protein products. The technique has been shown to detect aggregate and particle formation earlier compared to size-exclusion chromatography or

turbidity measurements⁴⁸ and to detect higher particle counts as compared to light obscuration.^{27,49}

3.2.4 Electron microscopy

In electron microscopy, the isolated particles of the samples are illuminated by an electron beam enabling qualitative evaluation of the surface morphology down to 1 nm resolution. Information about number, size and shape is limited due to the small imaged area in the mm range. The most important electron microscopy methods for protein particle analysis are scanning electron microscopy (SEM) and transmission electron microscopy (TEM). SEM provides three-dimensional images of the particle. It requires drying and coating of the particles with a conductive layer, e.g. gold or carbon, which can influence the original sample properties and surfaces. Environmental SEM applies lower vacuum, i.e. higher pressures, thereby enabling analysis of hydrated samples,^{50,51} often in combination with energy dispersive X-ray spectroscopy²⁷ (see below). TEM does not require coating, but the electron beam itself can change the original sample structure. In addition, the sample needs to be fixed, e.g. by filtration, and stained which can also change sample properties. An alternative option is cryo-TEM where rapid freezing of the sample allows analysis in a state similar to the hydrated state in the original solution.⁵² The major advantage of both, SEM and TEM, is the high resolution, enabling detailed information about particle structure as shown by TEM for monoclonal antibody aggregates⁵³ and by both techniques for HSA aggregates.⁵⁴ Although both examples describe the analysis of relatively small protein aggregates, the techniques should in principle be applicable also for protein particles. As a major shortcoming in addition to the caveats mentioned above, both methods are not suitable for high-throughput analysis due to expensive equipment and time-consuming measurements.⁶

3.2.5 Atomic force microscopy

In atomic force microscopy (AFM), the sample surface is scanned mechanically using a cantilever. The principle of AFM including application examples is presented in the literature.⁵⁵⁻⁵⁷ As a major benefit, AFM provides three-dimensional images down to 0.1 nm resolution under ambient conditions without sample preparation by filtration or coating, i.e. the samples can be measured air-

dried or in liquid. The high resolution is not only beneficial for the early detection of protein aggregation,⁵⁸ but also for the evaluation of shape and surface structure of aggregates and particles. This was shown for heat induced aggregates of a monoclonal antibody⁵⁷ and HSA⁵⁹ in the nanometer range. It should be possible to transfer the technique to larger protein particles, but the image area in AFM is limited to μm dimensions strongly constraining information about particle number, size and shape.⁵⁵ A technical difficulty of this technique is the need to find conditions where the cantilever tip does not draw the analyzed material with it as it moves across the surface.⁵⁷ Further shortcomings include expensive equipment and time-consuming measurements similar to TEM and SEM.

3.3 Light absorption/blockage methods

3.3.1 Light obscuration

Light obscuration is a compendial method for the quantification of subvisible particles within parenteral solutions. Depending on the system, size and number of particles between 1 μm and 600 μm can be quantified. A large sample volume of 25 mL is required by both Ph.Eur.¹¹ and USP¹³ for the analysis of low volume parenterals (volume smaller than 100 mL), which is often not feasible in the case of therapeutic protein products.²¹ Approaches to reduce the volume for light obscuration measurements of pharmaceutical products have been made to overcome this drawback.^{60,61} Small volumes may come along with increased data variability,⁷ but allow at the same time the detection of vial-to-vial variations which are missed if the vials are pooled to obtain a larger measurement volume. The maximum particle counts are defined in the Ph.Eur.¹¹ and the USP¹³ as follows: For a total volume of 100 mL or less, the maximum particle count is specified as 6000 particles $\geq 10 \mu\text{m}$ and 600 particles $\geq 25 \mu\text{m}$, each per container. For a total volume larger than 100 mL, the maximum particle count is 25 particles $\geq 10 \mu\text{m}$ and 3 particles $\geq 25 \mu\text{m}$, each per mL. The discussion on the significance of these numbers for therapeutic protein formulations is ongoing.^{7-9,61} The USP is in the process of developing a biologics-specific chapter for particle analysis in the μm range, which will include appropriate sample handling and analysis of small volumes, and is also going to develop an

instructional chapter discussing some of the other technologies for this size range.

In light obscuration, particles passing a laser beam block a certain amount of light proportional to their cross-sectional area, which is recorded by a photo diode detector. Light obscuration instruments are typically calibrated with polystyrene standards and based on this calibration the equivalent circular diameter (ECD) of the analyzed particles is obtained. However, for the interpretation of the results it has to be considered that the physico-chemical properties of protein particles, with respect to shape, transparency, and refractive index, are highly different from standard beads.^{29,62} Therefore, there is a need for standard particles that better represent the properties of protein particles.^{9,27,62} The simple measurement principle is certainly an advantage of light obscuration methods leading to straightforward and fast measurements. Nevertheless, this simplicity comes along with some restrictions: the particles have to pass the laser beam individually to avoid overloading and coincidence, i.e. two particles being detected as one larger particle. Therefore, the particle concentration must not exceed a certain limit depending on the system. The following light obscuration systems are mainly used for the analysis of protein products: HIAC HRLD by Hach® (Loveland, CO)^{32,62,63} with a linear range up to 18,000 particles per mL, SVSS by PAMAS GmbH (Rutesheim, Germany)⁶⁴⁻⁶⁶ with a linear range up to 200,000 particles per mL and AccuSizer 780 by Particle Sizing Systems (Port Richey, FL)⁶⁷ for particle concentrations up to 15,000 particles per mL. Further available systems are APSS2000/LiQuilaz® by Particle Measuring Systems (Boulder, CO) and Syringe® by Klotz GmbH (Bad Liebenzell, Germany).

Light obscuration cannot differentiate between proteinaceous particles and particles of other origin. Moreover, the technique is sensitive to air bubbles, which could be introduced during sample preparation or analysis. On this account, sample preparation, e.g. reconstitution of lyophilized products and handling of highly concentrated solutions of high viscosity, can have great influence on the result.²⁰ Therefore, degassing of the sample is often performed prior to measurement, however, this procedure can also change sample properties.⁶¹ Furthermore, translucent protein particles could be underestimated

in number and size as more light passes through such particles as compared to the polystyrene standards used for calibration.^{27,49} Similar to flow imaging microscopy, analysis of highly-concentrated protein solutions or formulations containing high concentrations of excipients such as sugars can be challenging due to low differences in refractive index between particle and solvent; thus, particle number and/or size could be underestimated.³² Despite these restrictions, light obscuration has been routinely used for lot release and has enabled the manufacturing and release of drugs that are safe and efficacious.⁹ It is also regularly used for the monitoring of subvisible particle counts in therapeutic protein formulations to compare various formulations or stress conditions.^{63,64,66,68}

3.3.2 Nephelometry / turbidimetry

Nephelometry and turbidimetry are both light scattering-based methods that are listed in the Ph.Eur.⁶⁹ and in the USP.⁷⁰ Nephelometry is defined as the measurement of light scattered by the sample solution compared to a formazin reference suspension. The scattered light is measured in a nephelometer at a high wavelength, typically 850 or 860 nm, at a scattering angle of 90°. In contrast, turbidimetry is defined as the measurement of light transmitted through the sample solution compared to a formazin reference suspension. The transmitted light can be measured in a UV spectrophotometer at a wavelength where proteins do not absorb light, i.e. in the range of 320-800 nm. Ratio turbidimetry measures both light scattering and light transmission and thereby determines the ratio of scattered light to transmitted light typically at 860 nm. Ratio turbidimetry is recommended by the Pharmacopeias for colored solutions as it compensates for the reduction of the transmitted light by absorption.

These measurements are simple and useful for a non-specific comparison of samples as limited sample preparation is required and the methods are non-destructive. The results are given in various synonymous units, e.g. NTU (nephelometric turbidity units), FNU (formazine nephelometric units) or FTU (formazine turbidity units). Although nephelometry and turbidimetry do not provide information about size, concentration or nature of protein aggregates or particles, the methods are often used to detect relative changes in the aggregate status.^{33,36,68} However, high turbidity values can also originate from other factors

such as high protein concentration and do not necessarily reflect the presence of aggregates or particles.⁷¹

3.4 Light scattering techniques

3.4.1 Principles of light scattering

Light scattering techniques play a central role in particle characterization. Light scattering can be seen as a very fast sequence of photon absorption upon illumination of a sample with light and almost instantaneous emission of another photon.⁷² Photon absorption in light scattering techniques shifts electrons in the molecule for a short time to a higher virtual (=physically non-existing) state, from which photons are immediately re-emitted. In contrast, photon absorption in spectroscopic techniques such as UV/VIS spectroscopy, IR spectroscopy and fluorescence spectroscopy shifts electrons in the molecule for a longer time to a higher electronic or vibrational state.

During light scattering, the absorbed energy can be released from the virtual state as photons in two different ways: (1) The scattered photon has the same energy/frequency as the absorbed photon (elastic light scattering). This process occurs for nearly all scattered photons and is called Rayleigh scattering for scatterers smaller than the wavelength of the incident light and Mie scattering for scatterers in the range of the wavelength of the incident light and above. (2) The scattered photon has an energy/frequency different from that of the absorbed photon, which occurs only for 10^{-3} of all scattered photons (inelastic or Raman scattering).

Rayleigh/Mie scattering (1) is used for dynamic light scattering (DLS), nanoparticle tracking analysis (NTA) and static light scattering (SLS). Raman scattering (2) is the basis for Raman spectroscopy.

3.4.2 Dynamic light scattering

Dynamic light scattering (DLS), also referred to as photon correlation spectroscopy or quasielastic light scattering, is used to determine the hydrodynamic size of native proteins, as well as aggregates and particles thereof from 1 nm to about 10 μm (size limit depending on sample properties and

measurement conditions).⁷³ The technique is based on intensity fluctuations of laser light scattered by the analyte, which is moving in Brownian motion.⁷⁴ Intensity fluctuations are quantified via an autocorrelation function which compares the initial scattering intensity to the intensity after specified time periods. A slow decay in the autocorrelation function is caused by slow fluctuations in intensity indicating the presence of slowly moving large particles; a fast decay is due to fast fluctuations indicating the presence of fast moving small particles. From the measured decay the diffusion coefficient D can be obtained, which is directly proportional to the inverse radius of the particles via the Stokes-Einstein equation.^{75,76} An important assumption for the validity of Stokes-Einstein is that the analyzed molecules or particles are spherical and not interacting with each other. Provided that temperature and viscosity of the solution are known, the hydrodynamic diameter – usually reported as Z-average diameter, i.e. the mean diameter – is obtained from DLS measurements. Especially the viscosity, which affects the diffusion coefficient, plays an important role in the analysis of therapeutic protein formulations as many excipients, in particular sugars, increase the viscosity.^{32,71} Therefore, the viscosity needs to be individually determined for the respective formulation. As protein aggregates and particles are mostly not spherical but of various shapes, the delivered hydrodynamic diameter for protein particles needs to be evaluated carefully. In addition, for polydisperse samples, indicated by a high polydispersity index (PdI), Z-average values do not necessarily reflect the different sizes present in the samples. Furthermore, DLS can only distinguish two populations in the sample if they theoretically differ in size at least by a factor of two⁷⁷ or three.⁷⁸ Particle populations with a lower difference in size appear as one broader population reflecting the average distribution.

DLS measurements provide intensity-based size distributions. However, this is not the best way for characterization of polydisperse samples as the scattering intensity I depends on the diameter d to the power of six in the Rayleigh approximation (Equation 1-1).

$$I \approx d^6$$

Equation 1-1

The resulting size distribution by intensity is therefore biased to larger sizes. This can be an advantage if small amounts of larger aggregates shall be detected in the presence of monomeric protein. However, in most cases it is disturbing, as a few large aggregates/particles present in the sample can impede the measurement of many small molecules, e.g. protein monomer. Using volume, weight or number based size distributions may be a better estimation of the composition of the sample in some cases.^{79,80} Volume or weight based size distributions are still biased to larger sizes, but less than intensity based size distributions.^{73,81} For a direct comparison of particle counts of different sizes, a number based size distribution can be suitable. However, it should be noted that an inaccurate intensity distribution as obtained from DLS data will result in significant errors in the derived volume, weight or number distribution.

Another challenge lies in high particle concentrations in the sample which can lead to multiple scattering effects. A technical possibility to reduce confounding influences of very large particles or to deal with high sample concentrations is the use of laser light backscatter detection, which detects the scattered light not in the commonly used 90° angle, but at a higher angle, e.g. 173° (Zetasizer Nano S and Nano ZS by Malvern Instruments Ltd, Worcestershire, UK)⁸² or 153° (FOQELS by Brookhaven Instruments Corporation, Holtsville, NY).⁸³ In this case, the laser light does not need to pass far into the sample as the scattered light is detected close to the cuvette wall thereby circumventing multiple scattering effects.

Nevertheless, despite this improvement in the measurement of large particles, DLS is in particular suitable for the analysis of protein monomer and small aggregates in the nanometer range^{81,84-86} and less suitable for particles in the μm size range. As an advantage of DLS, measurements in plate reader-based systems can save time and material.⁸⁷ As a further benefit, the method is not destructive and requires limited sample preparation. However, sufficient protein concentration is necessary for DLS to obtain reliable signals and the results are not quantitative as no absolute values for monomer content or aggregate concentration are provided.

Taylor dispersion analysis (TDA) is a novel method for the analysis of protein aggregates and particles which also determines the hydrodynamic size based on the diffusion coefficient. In contrast to DLS, the diffusion coefficient is not based on light scattering fluctuations, but on band broadening of the UV signal of the sample analyzed in a cylindrical tube under laminar Poiseuille flow, which passes a detector twice. TDA was shown to accurately size monomers of BSA and IgG antibodies and should in principle also be applicable for protein particles.⁸⁸

3.4.3 Nanoparticle tracking analysis

Nanoparticle tracking analysis (NTA) was developed by NanoSight Ltd in 2006 for the characterization of analytes in the nanometer size range. In NTA samples are illuminated by a laser (405 nm, 532 nm or 638 nm), particle movement is recorded via light scattering by a CCD camera and a software tracks the particles as light-scattering centers moving under Brownian motion. This visualization adds the value of microscopic imaging of the sample next to the particle size and concentration information based on light scattering. In contrast to DLS, where intensity changes are measured as bulk technique for the complete sample, particles in NTA are tracked individually, which facilitates distinction of particle subpopulations. As the particles are tracked only in two dimensions in the measuring cell, a modified Stokes-Einstein equation⁸⁹ (Equation 1-2) is applied to calculate the particle size with $(x,y)^2$ as the mean-squared particle path in two dimensions, k_B as the Boltzmann's constant, T as the absolute temperature, t as the measurement time, η as the viscosity and r as the hydrodynamic radius.

$$\frac{(x, y)^2}{3\pi\eta r} = \frac{2k_B Tt}{3\pi\eta r}$$

Equation 1-2

A comprehensive comparison of NTA with DLS is given by Filipe et al.⁹⁰ An important advantage of NTA compared to DLS is the better peak resolution. Particles with diameters of only 1.5 fold difference can be distinguished in NTA⁹⁰ compared to the at least 2-3 fold difference required for DLS (see above). The lower size limit of NTA depends on the particle refractive index and can be as small as 10 nm for high refractive index particles such as gold particles, but is

usually 40 to 50 nm for low refractive index particles such as protein particles;⁹¹ the upper size limit is about 1000 nm.⁸⁹

Another benefit of NTA is the visualization of the particles as light-scattering centers providing additional information about the sample, e.g. the degree of heterogeneity. Moreover, disturbing large particles in the μm size range can immediately be seen and excluded from the analysis. Alternatively, such particles could be removed prior to analysis, e.g. by filtration or centrifugation as shown for monoclonal antibody aggregates.³¹ However, one needs to consider that the subsequent analysis of the pretreated samples then displays only a selected fraction of the sample.

In addition to the particle size, NTA provides semi-quantitative information about the particle concentration. The optimal concentration for a proper NTA measurement is between 10^7 and 10^9 particles/mL, which often requires dilution of aggregated protein samples which can potentially change the sample properties.⁹⁰ Furthermore, highly concentrated protein solutions also need to be diluted in cases when high monomer amounts confound the analysis.

NTA requires a trained operator in order to obtain reliable, reproducible results, as the adjustment of the instrument settings to the needs of the sample requires experience. If used properly NTA can be a powerful technique to gain better insight into the size distribution of the sample as shown for PEGylated vs. non-PEGylated insulin⁹² or for HSA and IgG particles.^{31,93}

3.4.4 Static light scattering / multi-angle laser light scattering

Static light scattering (SLS) can provide information about the size (molecular weight) of the analyte in the measured solution. In SLS, the time-averaged intensity of scattered laser light at a certain angle is measured as the excess scattering intensity compared to the scattering intensity of the solvent, also called excess Rayleigh's ratio. SLS is suitable for smaller analytes, i.e. molecules with a radius of gyration smaller than 1/20 of the incident wavelength, as these molecules scatter light roughly isotropically. This holds true for molecules up to a radius of gyration up to about 30 nm, which includes protein monomers, as laser wavelengths in the range of 600 to 700 nm are mostly used.⁹⁴

In multi-angle laser light scattering (MALLS), scattered light is measured at multiple angles to obtain more detailed information especially for higher molecular weight aggregates, whose scattering type is no longer isotropic.⁹⁵ The Zimm-equation⁹⁶ is used to calculate the radius of gyration and the molecular weight of the analyzed species from the angle-dependent light scattering intensities, which also depend on the concentration and the refractive index difference between analyte and solution.

When using SLS as a stand-alone method for heterogeneous samples, e.g. aggregated protein solutions, one has to be aware that only a Z-average value for the molar mass of all species present in the solution is obtained.⁹⁷ Therefore, in protein aggregation analytics, SLS and MALLS are mostly used as a detector for size exclusion chromatography (SEC)^{95,97,98} or asymmetrical flow field flow fractionation (AF4)^{66,98,99} in combination with UV and/or refractive index detection (to measure the concentration that is needed to calculate the molecular weight).^{97,100} The major benefit of SLS/MALLS in combination with separation techniques is the possibility to calculate the molecular weight and size of the individually eluting species. This makes the use of molecular weight standards, e.g. for SEC column calibration, dispensable¹⁰¹ and misinterpretation of aggregate sizes based on different elution behavior of standards and analytes can be avoided.^{80,102} Furthermore, the (Z-average) molecular weight of species eluting in the void volume of SEC can be determined by MALLS.⁹⁷ Consequently, the combination of MALLS with SEC or AF4 is the static light scattering method of choice for the analysis of protein aggregates and particles as shown as AF4-MALLS for monoclonal antibodies^{66,103} or SEC-MALLS for alpha-chymotrypsinogen⁹⁷ and monoclonal antibodies.¹⁰²

3.4.5 Fluorescence activated particle sorting

Fluorescence activated particle sorting (FAPS) is a method similar to fluorescence activated cell sorting (FACS) based on the principle of flow cytometry.⁶⁷ FAPS is able to size labeled and unlabeled particles from 100 nm to 5 μm by light scattering, but should in theory also be applicable to a size range up to 100 μm as FACS was originally developed for eukaryotic cells. Fluorescence labeling enables separation of differently labeled and/or unlabeled particles, i.e. of protein from non-protein particles in case of a protein-specific dye such as SYPRO

Orange.¹⁰⁴ Furthermore, the characterization of particles in complex media, e.g. serum, should be possible as shown for nanoparticles analyzed by fluorescence single particle tracking.⁹³ Size determination is also possible with unlabeled material based on sideward scatter (SSC) quantification and calibration with size standards. The size standards need to have a refractive index similar to the sample material which poses a challenge for protein particles as most size standards such as polystyrene beads show refractive indices much higher than protein particles. Size determination of labeled material is also possible based on the pulse width of the fluorescence signal after calibration with fluorescent size standards.¹⁰⁵ Compared to other light scattering techniques such as DLS or SLS, FAPS analyzes particles individually and therefore shows size distributions of higher resolution.⁶⁷ FAPS offers the possibility of miniaturization as only 100-200 μL sample volumes are required and measurements can be performed using a microplate autosampler.¹⁰⁴ A benefit of FAPS as a preparative separation method (based on analytical data) is that particles can be used for further processing afterwards. However, the particles are highly diluted during the measurement, so they may need to tolerate concentration procedures to be reused.

FAPS was used for size determination of polyethyleneimine (PEI) polyplexes,⁶⁷ liposomes from 100 nm to 1 μm ,¹⁰⁶ protein particles from 1 to 5 μm ¹⁰⁴ as well as for mixtures of protein particles and silicone oil droplets in the lower μm range.¹⁰⁷ Overall, the method is not yet well established for the analysis of protein particles and needs further method development.

3.5 Non-optical counting and sizing methods

3.5.1 Electrical sensing zone / Coulter counter method

The electrical sensing zone method is based on the increase in the electric resistance by particles passing an electrical sensing zone. The particles need to be suspended in a conductive electrolyte solution that enables an electric current in the measuring container between two electrodes separated by a small aperture. Each particle passing the electrical sensing zone around this aperture causes a change in the electric current that is proportional to its volume, following the so called Coulter principle. By calibration with size standards the

equivalent spherical diameter (ESD), i.e. the diameter of a sphere of the same volume as the particle, can be calculated.¹⁰⁸ Furthermore, quantification of particles is also possible by the electrical sensing zone method which is therefore also designated as Coulter counter method. Providing size and number information for particles from 0.5 to 1000 μm with concentration limits of 40,000 to 340,000 particles/mL, both depending on the aperture size, the Coulter counter method can be compared to light obscuration and flow imaging techniques. However, multiple apertures are needed to achieve this dynamic range and morphological parameters such as shape, aspect ratio or circularity are not provided by the Coulter counter method. The major benefit of a Coulter counter is the absolute and direct determination of the particle size which does not depend on optical properties such as transparency, shape or compactness – parameters that are critical for light-based methods, e.g. light obscuration or flow imaging techniques.^{25,109,110} The Coulter counter is therefore more suitable than light-based methods for the detection of particles in highly-concentrated protein solutions leading to high viscosity and low contrast between particles and solution.³² The major shortcoming of the Coulter counter method is the required suspension of the particles in an electrolyte solution if the formulation buffer itself does not show sufficient conductivity, which can trigger particle formation or disaggregation.²⁰ Higher conductivity (in the range of 150 mM NaCl) is needed for the analysis of smaller particles from 0.5 to 20 μm , whereas lower conductivity (down to 20 mM) is sufficient for the analysis of larger particles from 1 to 1000 μm (according to Beckman Coulter, the manufacturer of the Coulter counter) or for highly concentrated protein solutions as the proteins themselves can act as electrolytes. The application of the Coulter counter method for the quantification of subvisible particles in therapeutic protein formulations is relatively new. Only few examples show the successful detection of subvisible particles such as IgG particles^{25,32,111} and BSA particles.¹⁰⁹

3.5.2 Resonant mass measurement / Archimedes

Resonant mass measurement is a novel technique developed by Affinity Biosensors which is based on the Archimedes principle: the upward buoyant force acting on an object in a fluid is equal to the weight of the fluid displaced by the object.¹¹² In the Archimedes system, the sample solution is flushed through a

suspended microchannel resonator (SMR) or microcantilever which changes its resonance frequency depending on the buoyant mass of the particles passing the channel.¹¹³ Analysis of the peaks in the frequency trace enables (1) differentiation of particles into positively buoyant particles (e.g. silicone oil droplets) and negatively buoyant particles (e.g. protein particles) by the peak direction, (2) determination of the particle/droplet concentration by quantifying the number of peaks, and (3) determination of the particle/droplet size as the equivalent spherical diameter (ESD) by quantifying the height of the peak.¹¹⁴ Particles/droplets from about 50 nm to about 6 μm (depending on the sensor and the particle type) can be analyzed by RMM in a concentration range from about 10^5 to 10^7 particles/mL (depending on the applied measurement time). The major benefit of RMM is the straightforward measurement principle enabling the differentiation of silicone oil droplets and protein particles. Furthermore, particles are analyzed individually and the coincidence rate (if two peaks are located too closely together) is indicated by the system in case of high concentrations enabling corrective actions such as sample dilution. This is in contrast to optical methods where the coincidence of two particles is not noticed during the measurement and the user needs to trust the results as long as the concentration is within the specified range. The major shortcoming of RMM is the very low flow rate of the system (around 15 nL/min) leading to a very low sampling efficiency. This in turn requires extended measurement times (up to several hours) especially for low concentration samples if sufficient particle numbers should be counted to achieve statistically sound results.¹¹³ As a further limitation, the calculation of the particle/droplet size requires the density of the fluid and of the particles/droplets as input parameters although the density of protein particles is often not known. The limited experience with this novel technique represents a further challenge. In the available studies, RMM was applied for the characterization of various microspheres, silicone oil droplets and protein particles in a technical evaluation of the system¹¹³ and the differentiation of droplets and particles in pharmaceutical products.¹¹⁵

3.6 Separation methods

3.6.1 Size exclusion chromatography

In size exclusion chromatography (SEC) proteins are separated by their hydrodynamic volume. SEC is usually used to quantify protein monomer, fragments, oligomers, and small soluble aggregates.^{100,103} Large aggregates and particles either elute with the void volume or accumulate at the column top or pre-column. For the analysis of protein particles by SEC, there are in principle two possibilities: (1) SEC can be used to indirectly estimate the fraction of insoluble aggregates and protein particles as a loss in the total peak area^{36,48} or (2) SEC columns of higher cut-off up to 200,000 kDa (e.g. Tosoh Bioscience, Tokyo, Japan) can be used to analyze particles. The latter method comes along with low resolution between fragments, monomer and smaller aggregates. UV, fluorescence or refractive index detectors are typically used to monitor the elution process and estimate the protein content; light scattering detectors can be used to determine the molecular weight of the protein monomer and aggregates. Shortcomings of SEC are changes of the analyte properties by dilution in the mobile phase or interaction with the column material, which is especially the case for hydrophobic proteins and/or aggregates.^{116,117} Low required sample volumes and high sensitivity and robustness represent major benefits of SEC. However, for the analysis of protein particles, SEC is mostly used as an indirect method to correlate the loss of the total peak area with the amount of particles as mentioned above.^{36,48}

3.6.2 Centrifugation

Centrifugation techniques use sedimentation to separate solid matter in a suspension according to particle size or density. Following Stokes' law,¹¹⁸ the sedimentation velocity v depends on the density difference of particle and fluid ($\rho_p - \rho_f$), the hydrodynamic radius of the particle r and the viscosity of the fluid η with g being the gravitational force (Equation 1-3).

$$v = \frac{2 (\rho_p - \rho_f) g r^2}{9 \eta}$$

Equation 1-3

Thus, centrifugation methods are suitable to determine the size of particles in a suspension. The most commonly used centrifugation method for the analysis of protein particles is disk centrifugation. Analytical ultracentrifugation (AUC) is described only briefly here for the sake of completeness and is reviewed in detail in the literature.¹¹⁹⁻¹²¹ It has only been reported for small protein aggregates in the size range up to 2000 kDa¹²¹ and seems to be not suitable for particles larger than 100 nm⁶ due to scattering effects and rapid sedimentation of large particles hampering the detection. Approaches with reduced centrifugation speed to analyze protein particles are currently under development.

Disk centrifugation, also called differential centrifugal sedimentation (DCS), applies rotation speeds up to 24000 rpm. The centrifuge in the form of a disk, filled with a density gradient fluid, e.g. sucrose or glycerin solutions, is orientated in a vertical direction for analytical purposes.¹²² The sample is diluted in a fluid of a lower density and injected into the disk center. Thereby, sample fluid and disk fluid are not mixed and only the particles sediment from the disk center to the edge where they are detected by a light extinction/scattering detector allowing concentration determination by Mie theory. This detection principle leads to a wider size range of DCS compared to AUC where light absorption is measured. The size of the particles is calculated following Stokes' Law which requires knowledge (or at least an estimate) of the particle density. Depending on the used instrument particles from 5 nm to 75 μm (Chemical Process Specialists, Gorham, ME) or 10 nm to 30 μm (BI-DCP Disk Centrifuge Particle Size Analyzer, Brookhaven Instruments Corporation, Holtsville, NY) can be analyzed. However, suspension of the particles in the density gradient fluid can change sample properties. Particle size determination by DCS is not absolute, so external or internal calibration standards are required.¹²³ DCS was used to analyze size distributions of particles in cytokine-HSA formulations,⁶⁸ but is mainly found as analytical method to characterize nanoparticles, e.g. interacting with protein.¹²⁴

3.6.3 Asymmetrical flow field flow fractionation

Asymmetrical flow field flow fractionation (AF4), like SEC and centrifugation methods, separates protein aggregates and particles by hydrodynamic size.¹²⁵ For a detailed description of the technique including application examples the reader is referred to the literature.^{99,126-132} In brief, the sample is injected into a

channel of a height in the μm range and transported by a mobile phase in the direction of the channel. Simultaneously, a cross flow perpendicular to the channel flow is induced, which transports the particles towards a semipermeable membrane. Due to the parabolic flow shape in the channel direction, smaller particles, diffusing faster back to the channel center than larger particles, will elute earlier than larger particles which will stay closer to the membrane where the channel flow is slower. The elution of the particles is monitored by similar detectors as used for SEC, i.e. UV, fluorescence, refractive index, and/or light scattering detectors.

Major advantages of particle characterization by AF4 compared to SEC are the lack of a stationary phase that could interact with the sample, as well as the larger separation range from 1 nm up to 100 μm , depending on the channel diameter and measurement settings.^{6,125} Little sample preparation and low sample amounts are further benefits of the technique.¹²⁸ However, dilution and concentration effects during the measurement, as well as solution viscosity due to high protein concentration and potential interactions of the analyte with the membrane can influence the separation. Parameters such as membrane material, molecular weight cut-off and the interplay between channel flow and cross flow rate need to be chosen carefully. Considering these factors, AF4 can typically provide complementary results to AUC and SEC. In some cases AF4 was even more suitable for the analysis of protein particles than AUC or SEC, as shown for submicron antibody particles.^{99,103} However, while the technique is well established for nanoparticles and smaller protein aggregates,¹³⁰⁻¹³² further method development is needed for the analysis of protein particles. These particles follow the principle of steric elution, elute directly after the focusing step is finished, and can in most cases be evaluated only qualitatively.

3.7 Spectroscopic methods

Spectroscopic methods provide qualitative insight into particle structure, conformation and/or identity.

3.7.1 Circular dichroism spectroscopy

Circular dichroism (CD) describes the unequal absorption of right-handed and left-handed circularly polarized light by chiral molecules.¹³³ The underlying principles of CD spectroscopy are outlined in detail within the literature.¹³⁴⁻¹³⁶ Far-UV CD spectroscopy operates in a wavelength range of ca. 170-250 nm and provides information about the secondary structure of a protein,¹³⁷ near-UV CD spectroscopy covers a wavelength range of ca. 250-350 nm and allows assessments of the tertiary structure.¹³⁸ The technique is especially sensitive to α -helix determination and is therefore complementary to the β -sheet sensitive technique of FT-IR spectroscopy (see below). The major shortcoming of CD spectroscopy is its limitation to only monomeric and oligomeric protein and aggregates, as sedimentation and light scattering of protein particles disturbs the analysis.⁶ Currently, methods enabling CD spectroscopy of protein immobilized on particles are under development which use a rotating cylindrical sample cell to avoid sedimentation and a small distance between sample cell and detector to minimize light scattering.¹³⁹ This approach may also be suitable for the characterization of particles in protein formulations.

3.7.2 Fourier-transform infrared spectroscopy

Infrared (IR) spectroscopy measures the absorption of light due to vibrations of the molecule in the wavelength range from 0.8 μm to 1000 μm (described as wavenumbers from 12500 cm^{-1} to 10 cm^{-1}). MIR (middle infrared spectroscopy, 4000 – 400 cm^{-1}) is mostly used to analyze protein secondary structure as vibrations of functional groups such as amide groups are observed in this region.¹⁴⁰ Detailed information about the application of IR spectroscopy for proteins is reviewed in the literature.^{140,141}

As a main benefit, FT-IR spectroscopy can be applied both on liquid samples (solutions and dispersions) and on solid samples (e.g. lyophilizates).¹⁴² Also the analysis of highly aggregated protein formulations and particle containing protein formulations is possible. For this purpose mainly attenuated total reflectance (ATR) FT-IR spectroscopy is used, where the incoming light is reflected several times at the interface between an IR transparent crystal and the sample thereby generating an evanescent wave at the reflection points. The interaction of this

evanescent wave with the sample reduces the amount of reflected light reaching the detector and provides the IR spectroscopic information of the sample.^{140,141}

As a challenge of FT-IR spectroscopy, the amide I band of protein often appears in the spectrum as a broad peak which contains multiple underlying peaks originating from intramolecular secondary structures, but also intermolecular β -sheets.¹⁴³ To extract secondary structure information from the amide I band, spectral processing, e.g. by performing the 2nd derivative, is required which provides the relative percentages of the different secondary structures. The technique can also differentiate between subtypes of β -sheets such as parallel and anti-parallel β -sheets or native β -sheets and amyloid structures. Therefore, it is a complementary technique to CD spectroscopy which is especially sensitive for α -helix determination (see above). FT-IR spectroscopy was applied for IgG particles both in suspension⁶⁶ or as a pellet after centrifugation.^{33,48}

IR microscopy enables visualization and identification of particles in therapeutic protein solutions.¹⁴⁴ The technique is suitable for particles larger than 20 μm using the reflection-absorption spectroscopy mode: the particles are isolated on a filter, preferably a metal-coated membrane or a gold filter, which allows light that has passed the sample to be reflected by the metal surface and pass through the sample again.²⁷ The main benefit of IR microscopy is the possibility not only to distinguish between non-proteinaceous and proteinaceous particles, but also to identify the source of the non-proteinaceous particles. This was shown for a therapeutic protein formulation containing one single particle composed of butyl rubber, talc, and silica which was identified by a combination of IR microscopy and Raman microscopy.¹⁴⁴ In another example, IgG particles were shown to contain silicone oil via analysis by IR microscopy and SEM-EDS.²⁷

3.7.3 Raman spectroscopy

Raman spectroscopy is based on (inelastic) Raman scattering, which was first described in 1928.^{145,146} When illuminated by a laser, molecules absorb energy and emit it as a photon of lower energy/frequency than the absorbed photon. A good overview of Raman spectroscopy for therapeutic proteins is given by Wen.¹⁴⁷

Two types of information can be gained from a Raman spectrum: (1) The presence and position of bands in the fingerprint region ($2000 - 400 \text{ cm}^{-1}$) enables the chemical identification of the analyzed material by comparison with a database of Raman spectra.¹⁴⁸ This principle is also used in Raman microscopy.²⁶ (2) The exact wavenumber ($= 1/\lambda$) of distinct bands in protein samples gives information about the environment of the peptide bond, i.e. the secondary structure of the protein,^{147,149} or aromatic side chains and disulfide bonds, providing hints about changes in the tertiary structure.¹⁵⁰

Benefits of Raman spectroscopy include easy sample handling as analysis can be performed with samples in any physical state¹⁴⁹ and even in original closed containers.¹⁴⁸ As a drawback, fluorescence is often disturbing in Raman spectroscopy, as the fluorescence signal is clearly stronger than the Raman signal. Raman spectroscopy brings the advantage that the wavelength of the incident light can be selected according to the requirements of the sample. Thus, using an NIR laser wavelength for excitation can reduce this phenomenon as these long wavelengths usually do not contain absorption bands relevant for fluorescence and the light intensity is usually too low to induce fluorescence.^{147,149} However, Raman signals are in general low as compared to IR signals (see above) and Raman spectroscopy therefore requires sufficient protein quantities and very sensitive detectors.¹⁴⁹ In the field of therapeutic proteins, changes in the secondary structure have been analyzed by Raman spectroscopy to monitor the aggregation process.¹⁵¹⁻¹⁵³ Analysis of proteinaceous and non-proteinaceous particles by Raman spectroscopy mostly involves Raman microscopy, an emerging technique combining visualization and identification of particles.

In Raman microscopy particles in solution or isolated particles are visualized by optical microscopy with the possibility to record Raman spectra of individual particles. For particle isolation, gold-coated filters are often used to prevent background signals from the filter material. Particles larger than $5 \mu\text{m}$ (for some applications even down to $0.5 \mu\text{m}$) can be identified by comparing the recorded spectra with a reference database, e.g. by the technique of rap.ID (rap.ID Particle Systems GmbH, Berlin, Germany).²⁶

As an example, a single particle composed of butyl rubber, talc, and silica was analyzed first by Raman spectroscopy in the original container and afterwards by IR microscopy of the isolated particle.¹⁴⁴ Raman microscopy of isolated particles was shown to differentiate between protein particles and protein-silicone oil particles.²⁶ The identification of particles by Raman microscopy in a protein formulation can be of great benefit as it helps to decide whether the formulation needs to be improved or the particles originate from other sources, e.g. from silicone oil coating in prefilled syringes or contamination sources. Expensive equipment, time-consuming measurements and the risk of “burning” protein particles by high laser power are among the shortcomings of this technique. In general, this method is still an emerging technique and needs to prove its value for the analysis of particles in therapeutic protein formulations.

3.7.4 Fluorescence methods

Fluorescence occurs when the energy of a photon absorbed by a molecule is partly emitted as a photon of a lower frequency/energy. In contrast to Raman scattering (see above), fluorescence is restricted to distinct absorption bands triggering a transition of the fluorophore to an excited state. The resulting photon emission from the excited state is also restricted to distinct emission bands. A good overview of fluorescence spectroscopy for proteins is given in the literature.^{154,155}

Protein fluorescence is analyzed to monitor changes in the tertiary structure and the environment of the fluorescent amino acids, mainly tryptophan. Measurements are originally performed in cuvettes where incident light beam and detector are orientated at right angle.^{154,155} However, if high amounts of aggregates or particles are present in the sample the emitted light does not fully reach the detector due to multiple scattering (inner filter effect). For this case, front face measurements with cuvettes rotated to a measurement angle of ideally 34° or 56° are the better option.¹⁵⁶ These set-ups have also been used to measure protein adsorbed to beads^{157,158} and are in principle also possible for protein particles even though applications for protein particles are still lacking. Whereas the protein concentration should be adjusted to show an absorbance at the excitation wavelength not higher than 0.1 in normal fluorescence measurements because of the inner filter effect, this is less critical for front face

measurements. Another possibility to analyze protein particles is the measurement in a plate reader where excitation and detection are both vertical and higher protein concentrations are possible.¹⁵⁹

Intrinsic protein fluorescence is induced by tryptophan, tyrosine, and phenylalanine as fluorophores with fluorescence intensities decreasing in this order. The absorption / emission maxima in aqueous solution are located at 280 nm / 350 nm for tryptophan, 275 nm / 304 nm for tyrosine, and 258 nm / 282 nm for phenylalanine. Tryptophan is mostly the fluorophore of choice as it shows the strongest fluorescence and is selectively excitable at wavelengths between 295 and 300 nm. As tryptophan fluorescence depends on the polarity of the environment, tryptophan fluorimetry is used to monitor changes in protein structure and the formation of aggregates.^{160,161} However, fluorescence is only suitable to detect relative structural changes, not to determine the absolute tertiary structure.

In addition to intrinsic fluorescence, fluorescent dyes can also be used to probe the conformation and other properties of protein aggregates. Fluorescent dyes can be covalently or non-covalently attached to the protein of interest. For detailed information about fluorescent dyes for the analysis of therapeutic proteins, the reader is referred to the literature.^{28,155} Covalently attached fluorescent dyes can be used to analyze protein aggregates and particles in complex buffers or directly in serum.^{93,162} Non-covalent fluorescent dyes that bind by hydrophobic or electrostatic interactions are typically more interesting for the study of therapeutic protein aggregates and particles. The fluorescence intensity of non-covalent dyes such as ANS (8-Anilino-1-naphthalenesulfonate), Bis-ANS (4,4'-Dianilino-1,1'-binaphthyl-5,5'-disulfonate), SYPRO orange or Nile Red depends on the polarity of the environment, e.g. the exposure of hydrophobic protein regions by unfolding and aggregation. Fluorescent molecular rotors like DCVJ (9-(2,2-dicyanovinyl)-julolidine) and CCVJ (9-(2-carboxy-2-cyanovinyl)-julolidine) also interact with hydrophobic parts on the protein, whereas their fluorescence properties are sensitive to the microviscosity of the binding environment.¹⁶³ Extrinsic dyes can provide information about structural changes and/or the formation of aggregates, as well as the properties of the formed aggregates.^{164,165} However, fluorescent dyes are often prepared in

organic solvents and one should consider control measurements to exclude induction or suppression of aggregation by the organic solvent or by the fluorescent dye itself.⁴²⁻⁴⁴ As an example ANS was used to detect changes in the tertiary structure of a monoclonal antibody,⁵³ Bis-ANS proved to bind strongly to heat stressed IgG,¹⁶⁶ ANS and SYPRO orange were applied to analyze the surface hydrophobicity of monoclonal antibody aggregates³¹ and ANS fluorescence was analyzed to monitor the aggregation process of concanavalin A.¹⁶⁴ In case of protein particles, fluorescent dyes are mostly used for visualization in fluorescence microscopy or for FAPS analysis (see above).

3.7.5 Energy dispersive X-ray spectroscopy

Energy dispersive X-ray spectroscopy (EDS or EDX) is used to determine the chemical composition of a sample. The irradiation of the sample by an electron beam causes the loss of inner shell electrons in the atoms of the sample. The replacement of the lost electrons by electrons of lower energy shells enables the release of free energy in the form of X-rays. The energy level of these emitted X-rays is specific for each atomic element and thereby provides information about the chemical identity.^{167,168} An energy dispersive X-ray spectrometer is often coupled with a scanning electron microscope (SEM) to combine optical and chemical characterization of protein particles or to identify particulate contaminants in pharmaceutical products. For example, IgG particles were shown to contain silicone oil by IR microscopy and SEM-EDS.²⁷ In another study, the identity of three different materials present in one particle, determined by IR microscopy and Raman microscopy, was confirmed by SEM-EDS.¹⁴⁴

4 Conclusion

The number of analytical methods for the quantification and characterization of protein particles has continuously increased during the last few years. Numerous characteristics of particles in therapeutic protein formulations, such as size (distribution), shape, chemical composition or structure, can be determined based on different measurement principles. However, no single method is capable of providing information on all desired parameters for the complete size range, which makes a combination of several methods based on different measurement principles necessary for a comprehensive characterization.²¹ For data analysis, one needs to consider that in most cases two methods will not show exactly the same result for one parameter due to a different underlying measurement principle. In this regard, for the comparison of different analytical methods, more proteinaceous particle standards rather than the hitherto used polystyrene beads would be valuable. As therapeutic proteins can form various types of aggregates and particles, the appropriate analytical methods need to be selected case by case and general recommendations for the analysis of protein particles are difficult to give.

5 References

1. <http://www.accessdata.fda.gov/scripts/cder/drugsatfda/index.cfm?fuseaction=Reports.Rep>, accessed on 11/19/2011:
2. Walsh G 2010. Biopharmaceutical benchmarks 2010. *Nat Biotechnol* 28:917-924.
3. Reubsaet JL, Beijnen JH, Bult A, van Maanen RJ, Marchal JA, Underberg WJ 1998. Analytical techniques used to study the degradation of proteins and peptides: chemical instability. *J Pharm Biomed Anal* 17:955-978.
4. Reubsaet JL, Beijnen JH, Bult A, van Maanen RJ, Marchal JA, Underberg WJ 1998. Analytical techniques used to study the degradation of proteins and peptides: physical instability. *J Pharm Biomed Anal* 17:979-984.
5. Carpenter J, Cherney B, Lubinecki A, Ma S, Marszal E, Mire-Sluis A, Nikolai T, Novak J, Ragheb J, Simak J 2010. Meeting report on protein particles and immunogenicity of therapeutic proteins: filling in the gaps in risk evaluation and mitigation. *Biologicals* 38:602-611.
6. den Engelsman J, Garidel P, Smulders R, Koll H, Smith B, Bassarab S, Seidl A, Hainzl O, Jiskoot W 2011. Strategies for the assessment of protein aggregates in pharmaceutical biotech product development. *Pharm Res* 28:920-933.
7. Cao S, Jiao N, Jiang Y, Mire-Sluis A, Narhi LO 2009. Sub-visible particle quantitation in protein therapeutics. *Pharmeur Bio Sci Notes* 2009:73-79.
8. Carpenter JF, Randolph TW, Jiskoot W, Crommelin DJA, Middaugh CR, Winter G, Fan Y-X, Kirshner S, Verthelyi D, Kozlowski S, Clouse KA, Swann PG, Rosenberg A, Cherney B 2009. Overlooking subvisible particles in therapeutic protein products: gaps that may compromise product quality. *J Pharm Sci* 98:1201-1205.
9. Singh SK, Afonina N, Awwad M, Bechtold-Peters K, Blue JT, Chou D, Cromwell M, Krause H-J, Mahler H-C, Meyer BK, Narhi L, Nesta DP, Spitznagel T 2010. An industry perspective on the monitoring of subvisible particles as a quality attribute for protein therapeutics. *J Pharm Sci* 99:3302-3321.
10. Narhi LO, Schmit J, Bechtold-Peters K, Sharma D 2012. Classification of protein aggregates. *J Pharm Sci* 101:493-498.
11. Ph.Eur. 2.9.19, Pharmacopoea europaea, 6th ed. 2008. Particulate contamination: Sub-visible particles. European Directorate For The Quality Of Medicine (EDQM).
12. Ph.Eur. 2.9.20, Pharmacopoea europaea, 6th ed. 2008. Particulate contamination: Visible particles. European Directorate For The Quality Of Medicine (EDQM).
13. USP<788>, United States Pharmacopeia, USP33, 2009. Particulate matter in injections. United States Pharmacopeial Convention.
14. Rosenberg AS 2006. Effects of protein aggregates: an immunologic perspective. *AAPS J* 8:E501-507.
15. Jiskoot W, van Schie RMF, Carstens MG, Schellekens H 2009. Immunological risk of injectable drug delivery systems. *Pharm Res* 26:1303-1314.
16. Fradkin AH, Carpenter JF, Randolph TW 2011. Glass particles as an adjuvant: A model for adverse immunogenicity of therapeutic proteins. *J Pharm Sci* 100:4953-4964.
17. Van Beers MMC, Gilli F, Schellekens H, Randolph TW, Jiskoot W 2011. Immunogenicity of recombinant human interferon beta interacting with particles of glass, metal, and polystyrene. *J Pharm Sci* 101:187-199.
18. Philo JS 2009. A critical review of methods for size characterization of non-particulate protein aggregates. *Curr Pharm Biotechnol* 10:359-372.
19. Mahler H-C, Friess W, Grauschopf U, Kiese S 2009. Protein aggregation: pathways, induction factors and analysis. *J Pharm Sci* 98:2909-2934.
20. Narhi LO, Jiang Y, Cao S, Benedek K, Shnek D 2009. A critical review of analytical methods for subvisible and visible particles. *Curr Pharm Biotechnol* 10:373-381.
21. Narhi LO, Cao S, Jiang Y 2011. Particles in therapeutic protein formulations - Part II. Application examples. *J Pharm Sci*, in preparation.
22. USP<1>, United States Pharmacopeia, USP33, 2009. Injections / General requirements. United States Pharmacopeial convention.
23. Kishore RSK, Kiese S, Fischer S, Pappenberger A, Grauschopf U, Mahler H-C 2011. The degradation of polysorbates 20 and 80 and its potential impact on the stability of biotherapeutics. *Pharm Res* 28:1194-1210.
24. Chi EY, Weickmann J, Carpenter JF, Manning MC, Randolph TW 2005. Heterogeneous nucleation-controlled particulate formation of recombinant human platelet-activating factor acetylhydrolase in pharmaceutical formulation. *J Pharm Sci* 94:256-274.

25. Tyagi AK, Randolph TW, Dong A, Maloney KM, Hitscherich C, Carpenter JF 2009. IgG particle formation during filling pump operation: a case study of heterogeneous nucleation on stainless steel nanoparticles. *J Pharm Sci* 98:94-104.
26. Lankers M, Munhall J, Valet O 2008. Differentiation between foreign particulate matter and silicone oil induced protein aggregation in drug solutions by automated raman spectroscopy. *Microscopy and Microanalysis* 14:1612-1613.
27. Wuchner K, Büchler J, Spycher R, Dalmonte P, Volkin DB 2010. Development of a microflow digital imaging assay to characterize protein particulates during storage of a high concentration IgG1 monoclonal antibody formulation. *J Pharm Sci* 99:3343-3361.
28. Hawe A, Sutter M, Jiskoot W 2008. Extrinsic fluorescent dyes as tools for protein characterization. *Pharm Res* 25:1487-1499.
29. Sharma DK, King D, Oma P, Merchant C 2010. Micro-flow imaging: flow microscopy applied to sub-visible particulate analysis in protein formulations. *AAPS J* 12:455-464.
30. Strehl R, Rombach-Riegraf V, Diez M, Egodage K, Bluemel M, Jeschke M, Koulov AV 2012. Discrimination between silicone oil droplets and protein aggregates in biopharmaceuticals: a novel multiparametric image filter for sub-visible particles in microflow imaging analysis. *Pharm Res* 29:594-602.
31. Joubert MK, Luo Q, Nashed-Samuel Y, Wypych J, Narhi LO 2011. Classification and characterization of therapeutic antibody aggregates. *J Biol Chem* 286:25118-25133.
32. Demeule B, Messick S, Shire SJ, Liu J 2010. Characterization of particles in protein solutions: reaching the limits of current technologies. *AAPS J* 12:708-715.
33. Kiese S, Pappenberger A, Friess W, Mahler H-C 2010. Equilibrium studies of protein aggregates and homogeneous nucleation in protein formulation. *J Pharm Sci* 99:632-644.
34. Knapp JZ, Kushner HK 1980. Generalized methodology for evaluation of parenteral inspection procedures. *J Parenteral Drug Assoc* 34:14-61.
35. Deutscher Arzneimittel Codex (DAC), 2006. DAC-Probe 5. ed.: Govi Verlag. p 1-4.
36. Eppler A, Weigandt M, Hanefeld A, Bunjes H 2010. Relevant shaking stress conditions for antibody preformulation development. *Eur J Pharm Biopharm* 74:139-147.
37. Li B, Flores J, Corvari V 2007. A simple method for the detection of insoluble aggregates in protein formulations. *J Pharm Sci* 96:1840-1843.
38. Demeule B, Gurny R, Arvinte T 2007. Detection and characterization of protein aggregates by fluorescence microscopy. *Int J Pharm* 329:37-45.
39. White JG, Amos WB, Fordham M 1987. An evaluation of confocal versus conventional imaging of biological structures by fluorescence light microscopy. *J Cell Biol* 105:41-48.
40. Amos WB, White JG 2003. How the confocal laser scanning microscope entered biological research. *Biol Cell* 95:335-342.
41. Demeule B, Lawrence MJ, Drake AF, Gurny R, Arvinte T 2007. Characterization of protein aggregation: the case of a therapeutic immunoglobulin. *Biochimica et Biophysica Acta* 1774:146-153.
42. Ali V, Prakash K, Kulkarni S, Ahmad a, Madhusudan KP, Bhakuni V 1999. 8-anilino-1-naphthalene sulfonic acid (ANS) induces folding of acid unfolded cytochrome c to molten globule state as a result of electrostatic interactions. *Biochemistry-US* 38:13635-13642.
43. Fu X, Zhang X, Chang Z 2005. 4,4'-Dianilino-1,1'-binaphthyl-5,5'-sulfonate, a novel molecule having chaperone-like activity. *Biochem Biophys Res Commun* 329:1087-1093.
44. Sereikaite J, Bumelis V-A 2006. Congo red interaction with alpha-proteins. *Acta Biochimica Polonica* 53:87-92.
45. Brown L 2007. Rapid Particle Size and Shape Characterization Using Continuous Digital Imaging. Proceedings of the PMCA 61st Annual Production Conference.
46. <http://www.malvern.com/common/downloads/MRK652.pdf>, accessed on 11/19/2011
47. <http://www.fluidimaging.com/products-particle-imaging-analyzer.htm>, accessed on 11/19/2011
48. Barnard JG, Singh S, Randolph TW, Carpenter JF 2011. Subvisible particle counting provides a sensitive method of detecting and quantifying aggregation of monoclonal antibody caused by freeze-thawing: insights into the roles of particles in the protein aggregation pathway. *J Pharm Sci* 100:492-503.
49. Huang C-T, Sharma D, Oma P, Krishnamurthy R 2009. Quantitation of protein particles in parenteral solutions using micro-flow imaging. *J Pharm Sci* 98:3058-3071.
50. Lochmann A, Nitzsche H, von Einem S, Schwarz E, Mäder K 2010. The influence of covalently linked and free polyethylene glycol on the structural and release properties of rhBMP-2 loaded microspheres. *J Control Release* 147:92-100.
51. McKinlay KJ, Allison FJ, Scotchford CA, Grant DM, Oliver JM, King JR, Wood JV, Brown PD 2004. Comparison of environmental scanning electron microscopy with high vacuum scanning electron microscopy as applied to the assessment of cell morphology. *J Biomed Mater Res Part A* 69:359-366.

52. Kuntsche J, Horst JC, Bunjes H 2011. Cryogenic transmission electron microscopy (cryo-TEM) for studying the morphology of colloidal drug delivery systems. *Int J Pharm* 417(1-2):120-137.
53. Demeule B, Palais C, Machaidze G, Gurny R, Arvinte T 2009. New methods allowing the detection of protein aggregates: a case study on trastuzumab. *mAbs* 1:142-150.
54. Taboada P, Barbosa S, Castro E, Mosquera V 2006. Amyloid fibril formation and other aggregate species formed by human serum albumin association. *J Phys Chem* 110:20733-20736.
55. Allison DP, Mortensen NP, Sullivan CJ, Doktycz MJ 2010. Atomic force microscopy of biological samples. *Wiley interdisciplinary rev Nanomedicine and nanobiotechnology* 2:618-634.
56. Müller DJ, Dufrêne YF 2008. Atomic force microscopy as a multifunctional molecular toolbox in nanobiotechnology. *Nat Nanotechnol* 3:261-269.
57. Lee H, Kirchmeier M, Mach H 2011. Monoclonal antibody aggregation intermediates visualized by atomic force microscopy. *J Pharm Sci* 100:416-423.
58. Jansen R, Dzwolak W, Winter R 2005. Amyloidogenic self-assembly of insulin aggregates probed by high resolution atomic force microscopy. *Biophys J* 88:1344-1353.
59. Stirpe A, Pantusa M, Rizzuti B, Sportelli L, Bartucci R, Guzzi R 2011. Early stage aggregation of human serum albumin in the presence of metal ions. *Int J Biol Macromol* 49(3):337-342.
60. Hawe A, Schaubhut F, Geidobler R, Wiggenghorn M, Friess W, Winter G, Jiskoot W, Rast M, De Muynck C 2010. Reduced sample expenditure for the detection of sub-visible particles in therapeutic protein preparations using an optimized light obscuration protocol based on the USP/Ph.Eur. method. AAPS Annual Meeting and Exposition, New Orleans, Louisiana.
61. Cao S, Jiang Y, Narhi L, Resources A 2010. A Light-obscuration Method Specific for Quantifying Subvisible Particles in Protein Therapeutics. *Pharmacopeial Forum*:824-834.
62. Sharma DK, Oma P, Pollo MJ, Sukumar M 2010. Quantification and characterization of subvisible proteinaceous particles in opalescent mAb formulations using micro-flow imaging. *J Pharm Sci* 99:2628-2642.
63. Kiese S, Pappenberg A, Friess W, Mahler H-C 2008. Shaken, not stirred: mechanical stress testing of an IgG1 antibody. *J Pharm Sci* 97:4347-4366.
64. Mahler H-C, Müller R, Friess W, Delille A, Matheus S 2005. Induction and analysis of aggregates in a liquid IgG1-antibody formulation. *Eur J Pharm Biopharm* 59:407-417.
65. van Maarschalkerweerd A, Wolbink G-J, Stapel SO, Jiskoot W, Hawe A 2011. Comparison of analytical methods to detect instability of etanercept during thermal stress testing. *Eur J Pharm Biopharm* 78(2):213-221.
66. Hawe A, Kasper JC, Friess W, Jiskoot W 2009. Structural properties of monoclonal antibody aggregates induced by freeze-thawing and thermal stress. *Eur J Pharm Sci* 38:79-87.
67. van Gaal EVB, Spierenburg G, Hennink WE, Crommelin DJA, Mastrobattista E 2010. Flow cytometry for rapid size determination and sorting of nucleic acid containing nanoparticles in biological fluids. *J Control Release* 141:328-338.
68. Hawe A, Friess W 2007. Stabilization of a hydrophobic recombinant cytokine by human serum albumin. *J Pharm Sci* 96:2987-2999.
69. Ph.Eur. 2.2.1, Pharmacopoea europaea, 6th ed. 2008. Clarity and degree of opalescence of liquids. European Directorate For The Quality Of Medicine (EDQM).
70. USP<851>, United States Pharmacopeia, USP33, 2009. Spectrophotometry and light-scattering. United States Pharmacopeial convention.
71. Salinas BA, Sathish HA, Bishop SM, Harn N, Carpenter JF, Randolph TW 2010. Understanding and modulating opalescence and viscosity in a monoclonal antibody formulation. *J Pharm Sci* 99:82-93.
72. Le Ru EC, Etchegoin PG. 2009. Scattering processes. *Principles of Surface-enhanced Raman Spectroscopy and related plasmonic effects*, 1st ed., Amsterdam: Elsevier. p 42-43.
73. Arakawa T, Philo J, Ejima D, Tsumoto K, Arisaka F 2007. Aggregation analysis of therapeutic proteins, part 2: Analytical ultracentrifugation and dynamic light scattering. *Bioprocess International* 5:36-47.
74. Lomakin A, Teplow DB, Benedek GB 2005. Quasielastic light scattering for protein assembly studies. *Methods Mol Biol* 299:153-174.
75. Svedberg T 1906. Über die Eigenbewegung der Teilchen in kolloidalen Lösungen. *Zeitschrift für Elektrochemie und angewandte physikalische Chemie* 12:853-860.
76. Einstein A 1908. Elementare Theorie der Brownschen Bewegung. *Zeitschrift für Elektrochemie und angewandte physikalische Chemie* 14:235-239.
77. Nobbmann U, Connah M, Fish B, Varley P, Gee C, Mulot S, Chen J, Zhou L, Lu Y, Shen F, Yi J, Harding SE 2007. Dynamic light scattering as a relative tool for assessing the molecular integrity and stability of monoclonal antibodies. *Biotechnol Genetic Eng Rev* 24:117-128.

78. <http://www.malvern.com/malvern/kbase.nsf/allfaqbyno/KB001102>, accessed on 11/19/2011
79. <http://www.malvern.com/common/downloads/campaign/MRK656-01.pdf>, accessed on 11/19/2011
80. Philo JS 2006. Is any measurement method optimal for all aggregate sizes and types? *AAPS J* 8:E564-571.
81. Ahrer K, Buchacher A, Iberer G, Josic D, Jungbauer A 2003. Analysis of aggregates of human immunoglobulin G using size-exclusion chromatography, static and dynamic light scattering. *J Chromatogr A* 1009:89-96.
82. http://www.malvern.com/LabEng/technology/dynamic_light_scattering/nibs.htm, accessed on 11/19/2011
83. http://www.bic.com/products/particle_sizing/p_PS_FOQELS.html, accessed on 11/19/2011
84. Bloomfield VA. 1985. Biological applications. In Pecora R, editor *Dynamic light scattering*, 1st ed., New York: Springer. p 363-380.
85. Ahrer K, Buchacher A, Iberer G, Jungbauer A 2006. Thermodynamic stability and formation of aggregates of human immunoglobulin G characterised by differential scanning calorimetry and dynamic light scattering. *J Biochem Bioph Meth* 66:73-86.
86. Bermudez O, Forciniti D 2004. Aggregation and denaturation of antibodies: a capillary electrophoresis, dynamic light scattering, and aqueous two-phase partitioning study. *J Chromatogr B Anal Technol Biomed Life Sci* 807:17-24.
87. Zhao H, Graf O, Milovic N, Luan X, Bluemel M, Smolny M, Forrer K 2010. Formulation development of antibodies using robotic system and high-throughput laboratory (HTL). *J Pharm Sci* 99:2279-2294.
88. Hawe A, Hulse WL, Jiskoot W, Forbes RT 2011. Taylor dispersion analysis compared to dynamic light scattering for the size analysis of therapeutic peptides and proteins and their aggregates. *Pharm Res* 28(9):2302-2310.
89. <http://www.nanosight.com/appnotes/M110B%20Application%20Review%20NTA%20April%202009.pdf>, accessed on 11/19/2011
90. Filipe V, Hawe A, Jiskoot W 2010. Critical evaluation of Nanoparticle Tracking Analysis (NTA) by NanoSight for the measurement of nanoparticles and protein aggregates. *Pharm Res* 27:796-810.
91. <http://www.nanosight.com/faq#Size-range>, accessed on 11/19/2011
92. Torosantucci R, Kukrer B, Mero A, Winsen MV, Tantipolphan R, Jiskoot W 2011. Plain and mono-pegylated recombinant human insulin exhibit similar stress-induced aggregation profiles. *J Pharm Sci* 100:2574-2585.
93. Filipe V, Poole R, Kutscher M, Forier K, Braeckmans K, Jiskoot W 2011. Fluorescence single particle tracking for the characterization of submicron protein aggregates in biological fluids and complex formulations. *Pharm Res* 28(5):1112-1120.
94. Demeester J, De Smedt SS, Sanders NN, Hastraete J. 2005. Light scattering. In Jiskoot W, Crommelin DJA, editors. *Methods for structural analysis of protein pharmaceuticals*, 1st ed., Arlington: American Association of Pharmaceutical Scientists. p 245-275.
95. Sharma VK, Kalonia DS. 2010. Experimental detection and characterization of protein aggregates. In Wang W, Roberts CJ, editors. *Aggregation of therapeutic proteins*, 1st ed., Hoboken, New Jersey: John Wiley & Sons, Inc. p 205-256.
96. Zimm BH 1946. Application of the Methods of Molecular Distribution to Solutions of Large Molecules. *J Chem Phys* 14:164.
97. Li Y, Weiss WF, Roberts CJ 2009. Characterization of high-molecular-weight nonnative aggregates and aggregation kinetics by size exclusion chromatography with inline multi-angle laser light scattering. *J Pharm Sci* 98:3997-4016.
98. Pavišić R, Dodig I, Horvatić A, Mijić L, Sedić M, Linarić MR, Sovulj IG, Preočanin T, Krajačić MB, Cindrić M 2010. Differences between reversible (self-association) and irreversible aggregation of rHuG-CSF in carbohydrate and polyol formulations. *Eur J Pharm Biopharm* 76:357-365.
99. Cao S, Pollastrini J, Jiang Y 2009. Separation and characterization of protein aggregates and particles by field flow fractionation. *Curr Pharm Biotechnol* 10:382-390.
100. Wen J, Arakawa T, Philo JS 1996. Size-exclusion chromatography with on-line light-scattering, absorbance, and refractive index detectors for studying proteins and their interactions. *Anal Biochem* 240:155-166.
101. Knobloch JE, Shaklee PN 1997. Absolute molecular weight distribution of low-molecular-weight heparins by size-exclusion chromatography with multiangle laser light scattering detection. *Anal Biochem* 245:231-241.
102. Ye H 2006. Simultaneous determination of protein aggregation, degradation, and absolute molecular weight by size exclusion chromatography-multiangle laser light scattering. *Anal Biochem* 356:76-85.

103. Gabrielson JP, Brader ML, Pekar AH, Mathis KB, Winter G, Carpenter JF, Randolph TW 2007. Quantitation of aggregate levels in a recombinant humanized monoclonal antibody formulation by size-exclusion chromatography, asymmetrical flow field flow fractionation, and sedimentation velocity. *J Pharm Sci* 96:268-279.
104. Mach H, Bhambhani A, Meyer BK, Burek S, Davis H, Blue JT, Evans RK 2011. The use of flow cytometry for the detection of subvisible particles in therapeutic protein formulations. *J Pharm Sci* 100:1671-1678.
105. Hoffman R. 2009. Pulse width for particle sizing. In Robinson JP, editor *Current protocols in cytometry*, 1st ed., Pittsburgh, PA, USA: John Wiley & Sons, Inc. p 1.23.21 - 1.23.17.
106. Vorauer-Uhl K, Wagner A, Borth N, Katinger H 2000. Determination of liposome size distribution by flow cytometry. *Cytometry* 39:166-171.
107. Ludwig DB, Trotter JT, Gabrielson JP, Carpenter JF, Randolph TW 2010. Flow cytometry: A promising technique for the study of silicone oil-induced particulate formation in protein formulations. *Anal Biochem* 410:191-199.
108. Grover NB, Naaman J, Ben-Sasson S, Doljanski F 1969. Electrical sizing of particles in suspensions. I. Theory. *Biophys J* 9:1398-1414.
109. Rhyner MN 2011. The Coulter principle for analysis of subvisible particles in protein formulations. *AAPS J* 13(1):54-58.
110. Thirumangalathu R, Krishnan S, Ricci MS, Brems DN, Randolph TW, Carpenter JF 2009. Silicone oil- and agitation-induced aggregation of a monoclonal antibody in aqueous solution. *J Pharm Sci* 98:3167-3181.
111. Barnard JG, Rhyner MN, Carpenter JF 2011. Which particle counting technique is most suitable for protein solutions? Coulter Method, micro-flow imaging, or light obscuration? Colorado Protein Stability Conference, Breckenridge, CO, 07/20/2011
112. Burg TP, Godin M, Knudsen SM, Shen W, Carlson G, Foster JS, Babcock K, Manalis SR 2007. Weighing of biomolecules, single cells and single nanoparticles in fluid. *Nature* 446:1066-1069.
113. Patel AR, Lau D, Liu J 2012. Quantification and characterization of micrometer and submicrometer subvisible particles in protein therapeutics by use of a suspended microchannel resonator. *Anal Chem* 84:6833-6840.
114. Weinbuch D, Zölls S, Wiggernhorn M, Friess W, Winter G, Jiskoot W, Hawe A 2013. Micro-Flow Imaging and resonant mass measurement (Archimedes) – Complimentary methods to quantitatively differentiate protein particles and silicone oil droplets. *J Pharm Sci* 102:2152-2165.
115. Barnard JG, Babcock K, Carpenter JF 2012. Characterization and Quantitation of Aggregates and Particles in Interferon- β Products : Potential Links Between Product Quality Attributes and Immunogenicity. *J Pharm Sci* 102:915-928.
116. Carpenter JF, Randolph TW, Jiskoot W, Crommelin DJA, Middaugh CR, Winter G 2010. Potential inaccurate quantitation and sizing of protein aggregates by size exclusion chromatography: essential need to use orthogonal methods to assure the quality of therapeutic protein products. *J Pharm Sci* 99:2200-2208.
117. Arakawa T, Ejima D, Li T, Philo JS 2010. The critical role of mobile phase composition in size exclusion chromatography of protein pharmaceuticals. *J Pharm Sci* 99:1674-1692.
118. Lamb H. 1932. *Hydrodynamics*. 6th ed., Cambridge: Cambridge University Press.
119. Lebowitz J, Lewis MS, Schuck P 2002. Modern analytical ultracentrifugation in protein science: a tutorial review. *Protein Sci* 11:2067-2079.
120. Schuck P 2000. Size-distribution analysis of macromolecules by sedimentation velocity ultracentrifugation and lamm equation modeling. *Biophys J* 78:1606-1619.
121. Philo JS. 2005. Analytical ultracentrifugation. In Jiskoot W, Crommelin DJA, editors. *Methods for structural analysis of protein pharmaceuticals*, 1st ed., Arlington: American Association of Pharmaceutical Scientists. p 379-412.
122. Laidlaw I, Steinmetz M. 2005. Introduction to Differential Sedimentation. In Scott DJ, Harding SE, Rowe AJ, editors. *Analytical ultracentrifugation: techniques and methods*, 1st ed., Cambridge: The Royal Society of Chemistry. p 270-290.
123. Thomas JC, Middelberg AP, Hamel JF, Snoswell MA 1991. High-resolution particle size analysis in biotechnology process control. *Biotechnol Prog* 7:377-379.
124. Monopoli MP, Walczyk D, Campbell A, Elia G, Lynch I, Bombelli FB, Dawson Ka 2011. Physical-chemical aspects of protein corona: relevance to in vitro and in vivo biological impacts of nanoparticles. *J Am Chem Soc* 133:2525-2534.
125. Giddings JC 1993. *Field-Flow Fractionation: Analysis of Macromolecular, Colloidal, and Particulate Materials*. *Science* 260:1456-1465.
126. Caldwell KD. 2005. Field-flow fractionation. In Jiskoot W, Crommelin DJA, editors. *Methods for structural analysis of protein pharmaceuticals*, 1st ed., Arlington: American Association of Pharmaceutical Scientists. p 413-434.

127. Arakawa T, Philo JS, Ejima D, Sato H, Tsumoto K 2007. Aggregation Analysis of therapeutic proteins, part 3: Principles and optimization of field-flow fractionation (FFF). *Bioprocess International* 5:52-70.
128. Liu J, Andya JD, Shire SJ 2006. A critical review of analytical ultracentrifugation and field flow fractionation methods for measuring protein aggregation. *AAPS J* 8:E580-589.
129. Fraunhofer W, Winter G 2004. The use of asymmetrical flow field-flow fractionation in pharmaceuticals and biopharmaceutics. *Eur J Pharm Biopharm* 58:369-383.
130. Yohannes G, Jussila M, Hartonen K, Riekkola M-L 2011. Asymmetrical flow field-flow fractionation technique for separation and characterization of biopolymers and bioparticles. *J Chromatogr A* 1218:4104-4116.
131. Zillies JC, Zwioerek K, Winter G, Coester C 2007. Method for quantifying the PEGylation of gelatin nanoparticle drug carrier systems using asymmetrical flow field-flow fractionation and refractive index detection. *Anal Chem* 79:4574-4580.
132. Lang R, Winter G, Vogt L, Zurcher A, Dorigo B, Schimmele B 2009. Rational design of a stable, freeze-dried virus-like particle-based vaccine formulation. *Drug Dev Ind Pharm* 35:83-97.
133. Beychok S 1966. Circular dichroism of biological macromolecules. *Science* 154:1288-1299.
134. Kelly SM, Jess TJ, Price NC 2005. How to study proteins by circular dichroism. *Biochimica et Biophysica Acta* 1751:119-139.
135. Fasman GD. 1996. Circular dichroism and the conformation analysis of biomolecules. 1st ed., New York: Plenum Press.
136. Bloemendal M, Jiskoot W. 2005. Circular dichroism spectroscopy. In Jiskoot W, Crommelin DJA, editors. *Methods for structural analysis of protein pharmaceuticals*, 1st ed., Arlington: American Association of Pharmaceutical Scientists. p 83-130.
137. Whitmore L, Wallace Ba 2008. Protein secondary structure analyses from circular dichroism spectroscopy: methods and reference databases. *Biopolymers* 89:392-400.
138. Greenfield NJ 1999. Applications of circular dichroism in protein and peptide analysis. *Trends Anal Chem* 18:236-244.
139. Ganesan A, Price NC, Kelly SM, Petry I, Moore BD, Halling PJ 2006. Circular dichroism studies of subtilisin Carlsberg immobilised on micron sized silica particles. *Biochimica et Biophysica Acta* 1764:1119-1125.
140. van de Weert M, Hering JA, Haris PI. 2005. Fourier transform infrared spectroscopy. In Jiskoot W, Crommelin DJA, editors. *Methods for structural analysis of protein pharmaceuticals*, 1st ed., Arlington: American Association of Pharmaceutical Scientists. p 131-166.
141. Barth A 2007. Infrared spectroscopy of proteins. *Biochimica et Biophysica Acta* 1767:1073-1101.
142. Li CH, Li T 2009. Application of vibrational spectroscopy to the structural characterization of monoclonal antibody and its aggregate. *Curr Pharm Biotechnol* 10:391-399.
143. van de Weert M, Hoehstetter J, Hennink WE, Crommelin DJ 2000. The effect of a water/organic solvent interface on the structural stability of lysozyme. *J Control Release* 68:351-359.
144. Cao X, Masatani P, Torraca G, Wen Z-Q 2010. Identification of a mixed microparticle by combined microspectroscopic techniques: a real forensic case study in the biopharmaceutical industry. *Appl Spectrosc* 64:895-900.
145. Raman CV, Krishnan KS 1928. A new type of secondary radiation. *Nature* 121:501-502.
146. Landsberg G, Mandelstam L 1928. Eine neue Erscheinung bei der Lichtzerstreuung in Krystallen. *Naturwissenschaften* 16:557-558.
147. Wen Z-Q 2007. Raman spectroscopy of protein pharmaceuticals. *J Pharm Sci* 96:2861-2878.
148. McCreery RL, Horn aJ, Spencer J, Jefferson E 1998. Noninvasive identification of materials inside USP vials with Raman spectroscopy and a Raman spectral library. *J Pharm Sci* 87:1-8.
149. Nielsen OF. 2005. Raman spectroscopy. In Jiskoot W, Crommelin DJA, editors. *Methods for structural analysis of protein pharmaceuticals*, 1st ed., Arlington: American Association of Pharmaceutical Scientists. p 167-198.
150. Yu NT 1974. Comparison of protein structure in crystals, in lyophilized state, and in solution by laser Raman scattering. 3. Alpha-Lactalbumin. *J Am Chem Soc* 96:4664-4668.
151. Sane SU, Wong R, Hsu CC 2004. Raman spectroscopic characterization of drying-induced structural changes in a therapeutic antibody: correlating structural changes with long-term stability. *J Pharm Sci* 93:1005-1018.
152. Tattini V, Parra DF, Polakiewicz B, Pitombo RNM 2005. Effect of lyophilization on the structure and phase changes of PEGylated-bovine serum albumin. *Int J Pharm* 304:124-134.

153. Forbes RT, Barry BW, Elkordy Aa 2007. Preparation and characterisation of spray-dried and crystallised trypsin: FT-Raman study to detect protein denaturation after thermal stress. *Eur J Pharm Sci* 30:315-323.
154. Lakowicz JR. 2006. Fluorescence spectroscopy. Principles of fluorescence spectroscopy, 3rd ed., New York: Springer. p 27-60.
155. Jiskoot W, Visser AJWG, Herron JN, Sutter M. 2005. Fluorescence spectroscopy. In Jiskoot W, Crommelin DJA, editors. Methods for structural analysis of protein pharmaceuticals, 1st ed., Arlington: American Association of Pharmaceutical Scientists. p 27-82.
156. Eisinger J, Flores J 1979. Front-face fluorometry of liquid samples. *Anal Biochem* 94:15-21.
157. Hoehne M, Samuel F, Dong A, Wurth C, Mahler H-C, Carpenter JF, Randolph TW 2010. Adsorption of monoclonal antibodies to glass microparticles. *J Pharm Sci* 100:123-132.
158. Bee JS, Chiu D, Sawicki S, Stevenson JL, Chatterjee K, Freund E, Carpenter JF, Randolph TW 2009. Monoclonal antibody interactions with micro- and nanoparticles: adsorption, aggregation, and accelerated stress studies. *J Pharm Sci* 98:3218-3238.
159. Capelle MAH, Gurny R, Arvinte T 2007. High throughput screening of protein formulation stability: practical considerations. *Eur J Pharm Biopharm* 65:131-148.
160. Tanaka N, Nishizawa H, Kunugi S 1997. Structure of pressure-induced denatured state of human serum albumin: a comparison with the intermediate in urea-induced denaturation. *Biochimica et Biophysica Acta* 1338:13-20.
161. Jiskoot W, Bloemendal M, van Haeringen B, van Grondelle R, Beuvery EC, Herron JN, Crommelin DJ 1991. Non-random conformation of a mouse IgG2a monoclonal antibody at low pH. *Eur J Biochem/FEBS* 201:223-232.
162. Demeule B, Shire SJ, Liu J 2009. A therapeutic antibody and its antigen form different complexes in serum than in phosphate-buffered saline: a study by analytical ultracentrifugation. *Anal Biochem* 388:279-287.
163. Hawe A, Filipe V, Jiskoot W 2010. Fluorescent molecular rotors as dyes to characterize polysorbate-containing IgG formulations. *Pharm Res* 27:314-326.
164. Vetri V, Canale C, Relini A, Librizzi F, Militello V, Gliozzi A, Leone M 2007. Amyloid fibrils formation and amorphous aggregation in concanavalin A. *Biophys Chem* 125:184-190.
165. Lindgren M, Sörgjerd K, Hammarström P 2005. Detection and characterization of aggregates, prefibrillar amyloidogenic oligomers, and protofibrils using fluorescence spectroscopy. *Biophys J* 88:4200-4212.
166. Hawe A, Rispens T, Herron JN, Jiskoot W 2010. Probing bis-ANS binding sites of different affinity on aggregated IgG by steady-state fluorescence, time-resolved fluorescence and isothermal titration calorimetry. *J Pharm Sci* 100:1294-1305.
167. Goldstein J, Newbury D, Joy D, Lyman C, Echlin P, Lifshin E, Sawyer L, Michael J. 2003. Scanning electron microscopy and x-ray microanalysis. 3rd ed., New York: Springer US.
168. D'Alfonso AJ, Freitag B, Klenov D, Allen LJ 2010. Atomic-resolution chemical mapping using energy-dispersive x-ray spectroscopy. *Phys Rev B* 81:2-5.

Chapter 2

Evaluation of novel techniques for protein particle analysis

Abstract

The aim of this study was a critical evaluation of novel techniques for protein particle analysis. The performance of these techniques (flow imaging microscopy (Sysmex FPIA-3000 and Occhio FC200S+), electrical sensing zone (Coulter counter Multisizer 4), resonant mass measurement (Archimedes), and image directed Raman spectroscopy (rapID)) was compared to the performance of more established analytical methods (Micro-Flow Imaging (MFI), light obscuration (LO), dynamic light scattering (DLS), and nanoparticle tracking analysis (NTA)). The studies demonstrated that flow imaging microscopy results strongly depend on the used system, that the non-optical particle counting techniques ESZ and RMM provide good sizing and counting performance, and that the identification of particles by image directed Raman spectroscopy shows difficulties in the detection of protein particles, but appears to be an interesting approach for non-proteinaceous particles. Taken together, novel techniques need to be evaluated carefully case by case before their implementation for routine analysis.

1 Introduction

Aggregates and particles need to be characterized during formulation development, production, and release of therapeutic protein formulations not only due to regulatory requirements¹⁻⁴ and the potential risk of immunogenicity,⁵ but also to get the best possible insight into product properties.⁶ The number of analytical techniques for protein aggregate and particle analysis available for this purpose is constantly increasing.^{7,8} This includes on the one hand established techniques which are used for a different purpose, and on the other hand methods which apply completely new measurement principles. As an example for the first group, some flow imaging microscopy systems were not originally designed for the analysis of protein particles, but for application in the industrial production of inks, construction materials or food. For protein particle analysis, those techniques are valuable as they combine quantification and characterization of particles captured on the images. Two such systems, the Sysmex FPIA-3000 and the Occhio FC200S+, were evaluated in this study. The principle of electrical sensing zone (ESZ) analysis as applied by the Coulter counter was originally intended for cell counting and is still the major technique for this purpose.^{9,10} Only some years ago, the technique was introduced for the analysis of protein particles as a non optical particle counting technique¹¹ and only few studies about this application are available.¹²⁻¹⁴

In contrast to those “recycled” measurement principles, resonant mass measurement (RMM) reflects a new approach which is based on the frequency change of a resonating cantilever by particles passing a microchannel within the cantilever.¹⁵ The main strength of this technique is the differentiation of protein particles and silicone oil droplets which was evaluated thoroughly in other studies.¹⁶⁻¹⁸ Further identification of particles in pharmaceutical products by chemical or physical approaches may be necessary for root-cause analysis. Typically, Fourier-transform infrared (FT-IR) and Raman microscopy or scanning electron microscopy coupled with energy-dispersive X-ray spectroscopy (SEM-EDS) are used for this purpose.¹⁹ The recently introduced image directed Raman spectroscopy²⁰ combines particle quantification by automated microscopy and identification by Raman spectroscopy.

The aim of this study was a critical evaluation of novel techniques for protein particle analysis, either techniques from other fields of application or completely new measurement principles. Techniques evaluated were flow imaging microscopy (Sysmex FPIA-3000 and Occhio FC200S+), ESZ (Coulter counter Multisizer 4), RMM (Archimedes), and image directed Raman spectroscopy (rapID). These methods were compared to more established techniques such as Micro-Flow Imaging (MFI), light obscuration (LO), dynamic light scattering (DLS), and nanoparticle tracking analysis (NTA) with respect to particle detection, quantification, sizing or identification.

2 Materials and methods

2.1 Materials

Infliximab (Remicade[®], lots no. 7GD9301402, 7FD8701601, 7RMKA81402, pooled) and rituximab (MabThera[®], lot no. B6082) were provided by local hospitals. Polystyrene particle standards were purchased from Duke Scientific (through Thermo Scientific, Fremont, CA) and diluted in water for analysis.

Infliximab solution at a concentration of 1 mg/mL was prepared by dilution of 10 mg/mL infliximab commercial product in 100 mM phosphate buffer (pH 7.2). Rituximab solution at a concentration of 1 mg/mL was prepared by dilution of 10 mg/mL rituximab commercial product in 25 mM citrate buffer (pH 6.5) containing 154 mM NaCl and 0.07% polysorbate 80. All protein formulations were filtered using a 0.2 µm cellulose acetate syringe filter (Minisart[®], Sartorius Stedim Biotech, Aubagne, France) for further use.

Freeze-thaw-stressed infliximab was prepared by subjecting 1.5 mL (for FPIA) or 1 mL (for rapID) of the formulation to 5 (for FPIA) or 7 (for rapID) freeze-thawing cycles of 30 minutes in a -80 °C freezer and 10 minutes in a 25 °C water bath in a 1.5 mL low protein binding reaction tube (Eppendorf, Hamburg, Germany). Stir-stressed infliximab was prepared by stirring 8 mL of the formulation in a 10R glass vial with a 18 mm Teflon[®]-coated stir bar at 250 rpm at room temperature on a magnetic stirrer (MR Hei-Standard, Heidolph, Schwabach, Germany) for 2 hours (for FPIA) or 24 hours (for ESZ and RMM) or by stirring 6 mL of the formulation for 1.5 hours (for rapID). Heat-stressed rituximab was prepared by incubating 1.5 mL of the formulation for 30 minutes at 71 °C in a 1.5 mL reaction tube in a thermomixer (Eppendorf, Hamburg, Germany).

Sodium hydroxide, di-sodium hydrogenphosphate dihydrate and sodium dihydrogenphosphate dihydrate were purchased from Merck KGaA (Darmstadt, Germany). Sodium chloride, sodium citrate dihydrate and polysorbate 80 were from VWR (Darmstadt, Germany). The water used in this study was highly purified water (Advantage A10 purification system, Millipore, Newark, NJ).

2.2 Light obscuration (LO)

Subvisible particles in a size range between 1 and 200 μm were analyzed by LO using a PAMAS SVSS-C (Partikelmess- und Analysesysteme GmbH, Rutesheim, Germany) equipped with an HCB-LD-25/25 sensor. Particle suspensions were diluted with the according buffer (filtered by a 0.22 μm cellulose acetate/nitrate membrane filter, MF-Millipore[®], Millipore, Newark, NJ) or water in order to adhere to the concentration limit of the system of 120,000 particles/mL $> 1 \mu\text{m}$. Three measurements of a volume of 0.3 mL of each sample were performed with a pre-run volume of 0.5 mL at a fixed fill rate, emptying rate and rinse rate of 10 mL/min and the mean particle concentration per mL was reported by the system. Samples were measured in triplicates and mean and standard deviation were calculated.

2.3 Micro-Flow Imaging (MFI)

Subvisible particles in a size range between 1 and 70 μm were analyzed by MFI using an MFI4100 (ProteinSimple, Santa Clara, CA) equipped with a high-resolution 100 μm flow cell. Particle suspensions were diluted with the according buffer (filtered by a 0.22 μm cellulose acetate/nitrate membrane filter) or water in order to adhere to the concentration limit of the system of 1,200,000 particles/mL $> 0.75 \mu\text{m}$. Samples were analyzed with a sample volume of 0.65 mL and a pre-run volume of 0.3 mL at a flow rate of 0.1 mL/min. Prior to each sample run the respective diluting buffer was flushed through the system to provide a clean flow cell and to perform optimize illumination. Particles stuck to the flow cell wall were only counted once and edge particles were ignored for analysis. Samples were measured in triplicates and mean and standard deviation were calculated. Results were analyzed using the MFI view application software version 1.2 (ProteinSimple).

2.4 Flow particle image analysis (FPIA)

Subvisible particles in a size range between 1 and 300 μm were analyzed by flow particle image analysis (FPIA) using a Sysmex FPIA-3000 system (Malvern, Herrenberg, Germany) operated in high power field (HPF) with a 10x magnification lens. Particle suspensions were diluted with the according buffer

(filtered by a 0.22 μm cellulose acetate/nitrate membrane filter) or water in the same dilution as for MFI. Samples were analyzed directly in "particle sheath liquid" (containing detergents, exact composition is not disclosed by the manufacturer) in which the sample solution is "sandwiched" in order to enable a regular liquid flow and the orientation of particles parallel to the flow direction. Results were analyzed using the FPIA software version 13 (Malvern).

2.5 Flow imaging microscopy analysis (Occhio)

Subvisible particles in a size range between 1 and 100 μm were analyzed by flow imaging microscopy using an Occhio FC200S+ system (Occhio, Angleur, Belgium) equipped with a 50 μm spacer. Particle suspensions were diluted with the according buffer (filtered by a 0.22 μm cellulose acetate/nitrate membrane filter) in the same dilution as for MFI. Results were analyzed using the Callisto software (Occhio).

2.6 Flow imaging microscopy analysis (FlowCAM VS1)

Subvisible particles in a size range between 2 and 50 μm were analyzed by flow imaging microscopy using a FlowCAM VS1 Benchtop B3 system (Fluid Imaging, Yarmouth, ME) equipped with a 50 μm single-use cell and a 20x magnification lens. Samples were analyzed with a sample volume of 0.5 mL with a pre-run volume of 0.5 mL (primed manually into the flow cell) with a flow rate of 0.07 mL/min and a camera rate of 20 frames/s. Prior to each sample run the system was flushed with 1 mL purified water at a flow rate of 0.5 mL/min and flow cell cleanliness was checked visually. Samples were measured in triplicates and mean and standard deviation were calculated. Results were analyzed using the VisualSpreadsheet software version 3.1.10 (Fluid Imaging).

2.7 Electrical sensing zone (ESZ, Coulter counter)

Subvisible particles in a size range between 1 and 30 μm were analyzed by ESZ using a Multisizer 4 system (Beckman Coulter, Fullerton, CA) equipped with a 50 μm aperture tube. The system was filled with the appropriate buffer for analyzing protein particles or Isoton II (solution supplied by Beckman Coulter containing 154 mM NaCl as well as detergents, exact composition is not disclosed

by the manufacturer) for analyzing polystyrene standards. All diluents were filtered by a 0.22 μm cellulose acetate/nitrate membrane filter. The system was calibrated three times with 5 μm polystyrene standards (supplied by Beckman Coulter) in the respective diluent and the mean calibration factor was used for further analysis. Each day before the first sample measurement, the calibration was verified with the same standards and performed again, if necessary. Particle suspensions were diluted with the according buffer or Isoton II in the same dilution as for LO. Samples were analyzed with a total sample volume of 10 mL in a 20 mL Accuvette[®] sample container (Beckman Coulter) for polystyrene standards or 2.4 mL in a 5 mL sample container (Nalgene[®], distributed by VWR) for protein particles. Three runs of a volume of 0.1 mL were performed per measurement and the mean particle concentration per mL was reported by the system. In order to remove air bubbles the aperture tube was flushed with the respective diluent before the first run. Samples were measured in triplicates and mean and standard deviation were calculated. Results were analyzed using the Multisizer 4 software (Beckman Coulter).

2.8 Resonant mass measurements (RMM, Archimedes)

RMM was performed using the Archimedes particle metrology system (Affinity Biosensors, Santa Barbara, CA) equipped with a Micro sensor (size range 0.3 μm to 4 μm) calibrated with 1 μm polystyrene standards. Before each measurement, the system was filled with sample and the lower size limit of detection was determined three times in automatic mode. The mean value was set as a fixed limit of detection for the measurement. The buffer density was determined for each sample. The particle density for negatively buoyant particles was set to 1.05 g/mL for polystyrene standards and 1.32 g/mL for proteinaceous particles according to the recommendation of the manufacturer. Particle suspensions were diluted with the according buffer (filtered by a 0.22 μm cellulose acetate/nitrate membrane filter) or water to achieve a coincidence rate (indicated by the system) below 10%. Measurements were performed in triplicates and the sensor was filled with fresh sample for each measurement. The measured volume was 0.15 μL and the overall sample volume for triplicate measurements was 600 μL . Between triplicate measurements, the system was rinsed with water. Results

were analyzed using the ParticleLab software (v1.8.570, Affinity Biosensors) with a size bin step of 10 nm.

2.9 Dynamic light scattering (DLS)

Submicron aggregates and particles were analyzed by DLS using a DynaPro plate reader (Wyatt Technology Europe, Dernbach, Germany) at 25 °C. If possible samples were measured in the original state without sample preparation. However, in the presence of large protein particles which impeded the measurement due to extensive light scattering, samples were centrifuged for 10 minutes at 7,000 g to remove those large particles. Three measurements per sample of 200 µL each were performed in a Corning 96-well plate using a manual mode of 10 runs of 5 or 10 s per measurement. Results were analyzed using the Dynamics software (version 6.12.03, Wyatt Technology Europe).

2.10 Nanoparticle tracking analysis (NTA)

Submicron aggregates and particles were analyzed by nanoparticle tracking analysis (NTA) using a NanoSight LM20 (NanoSight, Amesbury, United Kingdom) equipped with a 405 nm blue laser. Particle suspensions were diluted with the according buffer (filtered by a 0.22 µm cellulose acetate/nitrate membrane filter) or water to achieve particle concentrations between 10^7 and 10^9 particles/mL. Samples were loaded into the measurement cell using a 1 mL syringe. Movements of the particles in the samples were recorded as videos for 60 seconds at room temperature using the NTA 2.1 software (NanoSight). Shutter and gain values were chosen manually to achieve an optimal particle resolution. The extended dynamic range mode, which allows different settings for two populations in one measurement, was applied for polydisperse samples. The recorded videos were analyzed using the NTA 2.1 software (NanoSight).

2.11 Image directed Raman spectroscopy (rapID)

Subvisible particles in a size range between 2 and 100 µm were analyzed by image directed Raman spectroscopy (rapID) using a liquid particle explorer (LPE, rapID Particle Systems, Berlin, Germany) or a single particle explorer (SPE, rapID Particle Systems) system.

Particle suspensions were filtered onto a gold coated membrane (pore size 0.8 μm) under laminar air flow conditions and the filter was inserted into the LPE or SPE system. Particles larger than 2 μm were counted by automated optical microscopy in both systems and then identified by the SPE system by image directed Raman spectroscopy by comparison of the obtained Raman spectra for individual particles to a database (provided by rapID Particle Systems). Samples were analyzed in triplicates and mean and standard deviation were calculated if feasible due to long measurement times of several hours per sample.

3 Results and discussion

3.1 Flow imaging techniques

Flow imaging microscopy techniques are a valuable method to simultaneously count and visualize particles in therapeutic protein formulations and several different instruments are available which were comparatively evaluated for their suitability for protein particle analysis. The most common flow imaging microscopy instruments are MFI and FlowCAM which were comparatively evaluated in detail in a separate study (see Chapter 4). The systems evaluated in this study were originally developed for a different purpose and have entered the field of protein particle analysis only recently.

The first flow imaging microscopy system evaluated in this study is the Sysmex FPIA-3000 system. In this instrument the sample is passed through a flow cell "sandwiched" between "particle sheath liquid", particles are illuminated by a stroboscopic light source and images are captured by a charge-coupled device (CCD) camera. The particle sheath liquid technology is specific for this instrument and should ensure a preferential orientation of particles with their largest side towards the camera. This is in contrast to other flow imaging microscopy systems such as MFI or FlowCAM where the vertical flow presumably also ensures an orientation with the longest side, but not necessarily with the broadest side of the particle towards the camera. The image resolution is very high at the expense of sampling efficiency due to the small focus area connected to a very low analyzed volume of less than 1 μL .

Polystyrene size standards were analyzed to assess size accuracy by FPIA as compared to MFI as a standard flow imaging microscopy technique and LO as the commonly used compendial technique for subvisible particle analysis (Figure 2-1). The analysis of 5 μm size standards revealed a very narrow peak for FPIA, but at a too large size (around 6 μm), whereas analysis by MFI provided a slightly broader peak at the correct size. LO analysis showed a very broad peak due to the larger size channels in this instrument. For 10 μm size standards, all systems showed good size accuracy with again the FPIA system providing the sharpest peak. In contrast, the quantification of polystyrene count standards

(5 μm count standard, certified concentration 3000 \pm 300 particles/mL > 3 μm) revealed clear differences among the systems: whereas the MFI system slightly overestimated the concentration (3488 particles/mL) and LO provided the correct concentration (3046 particles/mL), the FPIA system clearly undercounted the particles (952 particles/mL). This might be due to the very low analyzed volume in FPIA of less than 1 μL which is not representative of a sample of such a comparatively low concentration.

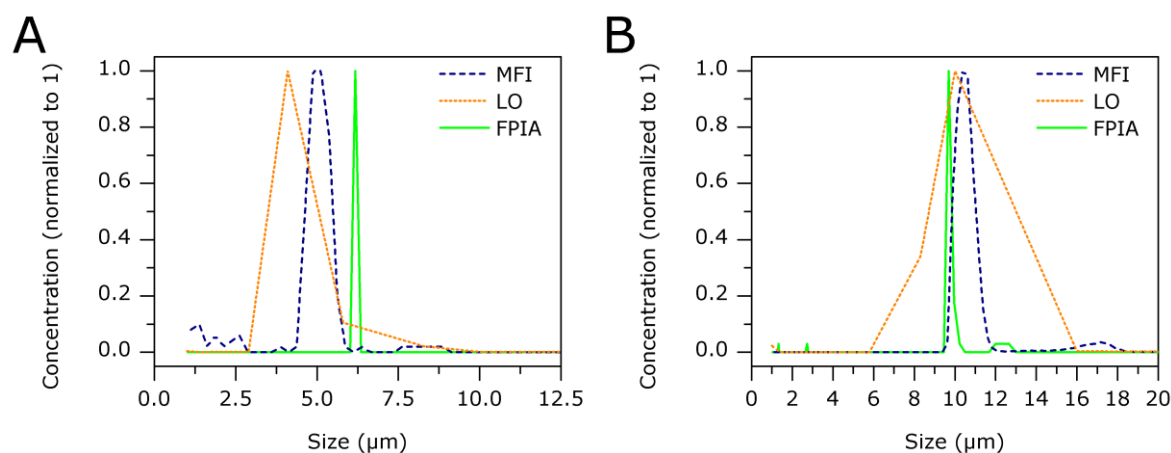


Figure 2-1: Size accuracy of FPIA, MFI, and LO for (A) 5 μm and (B) 10 μm polystyrene size standards.

The concentration of protein particles detected was clearly lower for FPIA as compared with MFI and LO (Figure 2-2). The determined concentration for FPIA as compared with MFI was about 10-15x lower for freeze-thaw-stressed (Figure 2-2A) and about 3-4x lower for stir-stressed infliximab (Figure 2-2B), both for particles from 1 to around 8 μm . For freeze-thaw stressed infliximab, the number of particles above 8 μm was too low to draw significant conclusions. For stir-stressed infliximab, the concentration for particles above 8 μm was higher for FPIA as compared with MFI. This could be due to the orientation of particles induced by the particle sheath liquid which becomes more important for larger particles with a clearly detectable shape as compared with small particles which appear rather spherical in general due to limitations in image resolution. However, the difference was not significant and this is more likely a minor effect. Above 10 μm the overall concentration of particles was too low to draw significant conclusions for both particle types. As compared with LO, MFI

detected about 2-3x higher concentrations as observed also in other studies.^{11,21-23}

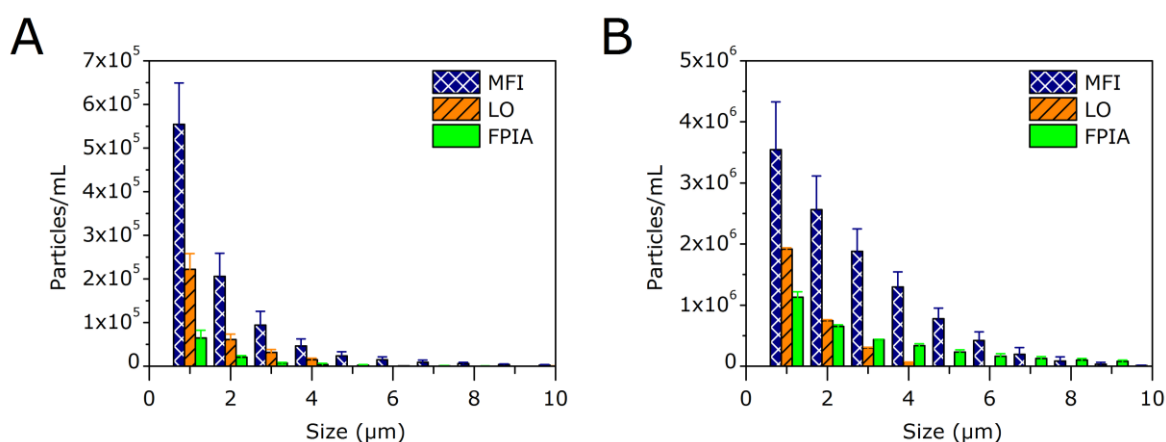


Figure 2-2: Protein particle concentrations for (A) freeze-thaw-stressed or (B) stir-stressed infliximab as determined by MFI, LO, and FPIA (cumulative size distribution). Error bars represent standard deviations from triplicate measurements.

In addition to the technical differences in image capture between FPIA and MFI, the contact of the sample with the particle sheath liquid might also contribute to the observed differences in detected particle concentration. This might on the one hand lead to a dilution effect of the sample which is not exactly known and cannot be quantified, and on the other hand to a direct dissolution or generation of particles, e.g. by the contained detergents and other non-disclosed ingredients. To assess the second possibility, IgG particles were diluted in formulation buffer and in particle sheath liquid with the same dilution factor and analyzed by MFI (Figure 2-3). Interestingly, clear differences could be observed depending on the type of stress. IgG particles generated by freeze-thawing stress were not affected by dilution in particle sheath liquid and showed the same concentration in both diluents (Figure 2-3A). In contrast, IgG particles generated by stirring stress showed an about 1.5x higher concentration in formulation buffer for small particles below 10 μm, but higher concentrations in particle sheath liquid for particles above 10 μm (Figure 2-3B). This indicates on the one hand that small particles could indeed be partially dissolved by the sheath liquid, however only to a small extent as the difference between concentrations in the two liquids is not significant. The opposite effect for particles above 10 μm on the

other hand points towards potentially enhanced aggregation caused by the particle sheath liquid, but the difference was again not significant.

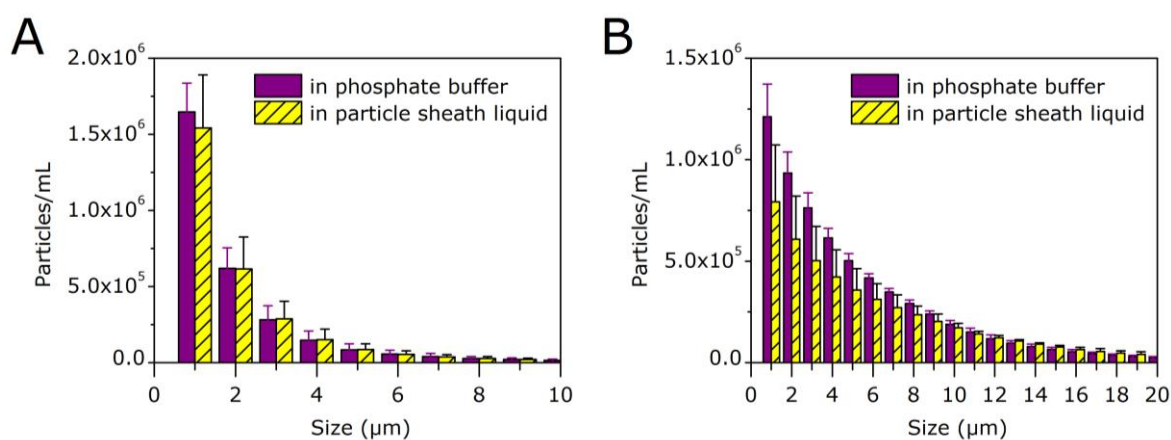


Figure 2-3: Protein particle concentrations for (A) freeze-thaw-stressed or (B) stir-stressed infliximab after dilution in formulation buffer or particle sheath liquid as determined by MFI (cumulative size distribution). Error bars represent standard deviations from triplicate measurements.

Another flow imaging microscopy system evaluated in this study is the Occhio FC200S+ system. This system uses an LED light source for particle illumination in a glass flow cell. The official size range starts already at 0.4 μm although image analysis in this size range is rather questionable. According to the manufacturer, this is possible as every recorded pixel of a particle is subsequently divided into 4 parts which can be analyzed separately. Various possibilities to change the optical settings allow the user to adjust the measurement parameters to the specific sample, but at the same time carry the risk of incorrect concentration and size determination due to non-optimal settings for threshold, shutter or gain. The evaluated Occhio FC200S+ system detected clearly (up to 17x) more protein particles (heat-stressed rituximab) than MFI, mainly in the lower size range below 5 μm, whereas lower concentrations were detected above 5 μm (Figure 2-4). A clear overestimation of small particles together with an underestimation of larger particles in flow imaging microscopy points towards image fragmentation - as suspected for the instrument by the division of one pixel into four parts after the analysis - which could potentially be addressed by the adjustment of the optical measurement settings. However, due to limited availability of the system, the sample could only be measured n=1 and further experiments to analyze or prevent potential image fragmentation could

not be performed. The phenomenon of image fragmentation in flow imaging microscopy is further described in Chapter 4.

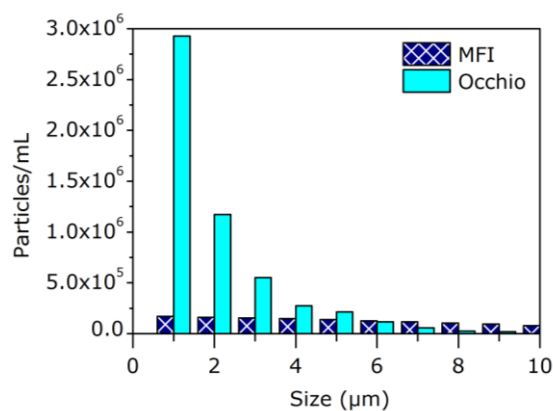
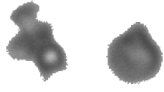
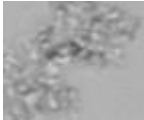
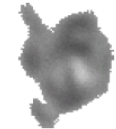
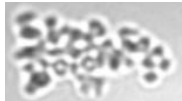
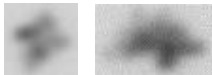
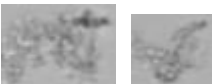
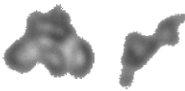


Figure 2-4: Protein particle concentrations for heat-stressed rituximab as determined by MFI and Occhio (cumulative size distribution).

The image quality is an important parameter in flow imaging microscopy for the correct size determination and for characterization of particle transparency or shape supporting particle identification. Images of protein particles captured by the flow imaging microscopy techniques clearly differ (Table 2-1). Images from FPIA show the most details and the highest resolution due to the small focus area / analyzed volume. This confirms again that this instrument is very suitable for detailed particle morphology characterization as needed for example for the analysis of raw materials in odontology,^{24,25} at the expense of a reliable quantification. Images from the FlowCAM VS1 system show a similar image quality. The FlowCAM VS1 is listed only exemplarily here for a comparison of the image quality (see Chapter 4 for a detailed evaluation of this system). Images from MFI appear rather blurry as described also in Chapter 4, whereas particle images from Occhio are difficult to judge as they are displayed cropped at the particle border hampering also the evaluation of potential image fragmentation as described above. To our knowledge, neither the FPIA system nor the Occhio system has been applied for the characterization of protein particles in published studies.

Table 2-1: Representative protein particle images in a size range of about 5-20 μm of stir-stressed infliximab (MFI, FPIA) or heat-stressed rituximab (Occhio, FlowCAM VS1).

Instrument	MFI	FPIA	Occhio	FlowCAM VS1
Protein particles (5-20 μm)				
				
				

3.2 Non-optical particle analysis

Non-optical techniques can be a promising alternative to light-based particle analysis. ESZ analysis is based on the increase of the electrical resistance caused by a particle passing an electrical field between two electrodes which is proportional to the non-conductive volume of the particle.¹² The determined volume is then used to calculate the equivalent spherical diameter (ESD) assuming spherical shape. In RMM the change of the resonance frequency of a microchannel caused by a particle is proportional to the buoyant mass of the particle over the surrounding fluid which is then calculated also into the ESD provided that the density of the fluid and the particle is known. This instrument was introduced only a few years ago and is taking its first steps in the field of particle analysis. A detailed evaluation of RMM for its main application, the differentiation of silicone oil droplets and protein particles, is described in a separate study²⁶ (see Chapter 3). In this chapter, ESZ and RMM were evaluated regarding sizing and counting performance for polystyrene standards and protein particles.

Size accuracy in the μm size range was evaluated using 2 μm polystyrene size standards (Figure 2-5A). The standards were detected at exactly the correct size with a very narrow distribution by RMM. Also ESZ determined the particle size correctly with a marginally broader distribution. In contrast, particles were sized clearly below 2 μm by MFI which is probably due to the limited image resolution in this low size range. LO showed a very broad size distribution due to the larger size channels as discussed above.

Concentration linearity was evaluated with different dilutions of 2 μm (for MFI, LO, and RMM) or 5 μm standards (for ESZ) over a wide range from about 3×10^3 to 1×10^6 particles/mL, based on LO (Figure 2-5B). The particle concentration measured by LO (as the established, compendial technique) was used as the theoretical concentration. For concentrations above the coincidence limit of LO (120,000 particles/mL), the theoretical concentration was calculated based on the concentration measured by LO below the coincidence limit.

Up to a theoretical concentration of 1×10^5 particles/mL, all techniques showed very good linearity (Figure 2-5B, insert). This is in accordance with the literature for MFI, LO, and ESZ.¹³ Between 1×10^5 and 3×10^5 particles/mL, all techniques showed still good linearity with ESZ slightly overcounting and RMM slightly undercounting the particles (LO is only possible up to 1.2×10^5 particles/mL due to the coincidence limit of the system). Concentrations above 3×10^5 particles/mL could only be analyzed by MFI and RMM. Here, MFI provided good linearity whereas RMM clearly underestimated the concentration. This is due to coincidence of two particles. Those particles are not identified as coincidence, but simply counted as one particle in MFI, LO, and ESZ. In RMM, two particles detected too closely together are identified as coincidence, but as a consequence excluded completely from the analysis and not counted at all by the system. This means that the impact of concentration underestimation due to coincidence is in theory two times higher in RMM. However, the advantage of the RMM system is that the coincidence level is indicated by the system and it is recommended to dilute a sample if a coincidence level of 10% or higher is detected to avoid strong concentration underestimation.

Furthermore, RMM data was affected by higher standard deviations as compared with the other techniques as described earlier¹⁶ due to the low analyzed volume (only 150 nL per measurement in this study). An increase of the analyzed volume would come along with very long measurement times (due to the very low flow rate of the system) which potentially changes sample properties in case of protein particles. Thus, the low sampling efficiency of RMM, which can lead to measurement times of several hours for very clean samples in order to count a sufficient number of particles, is a clear shortcoming of this technique.

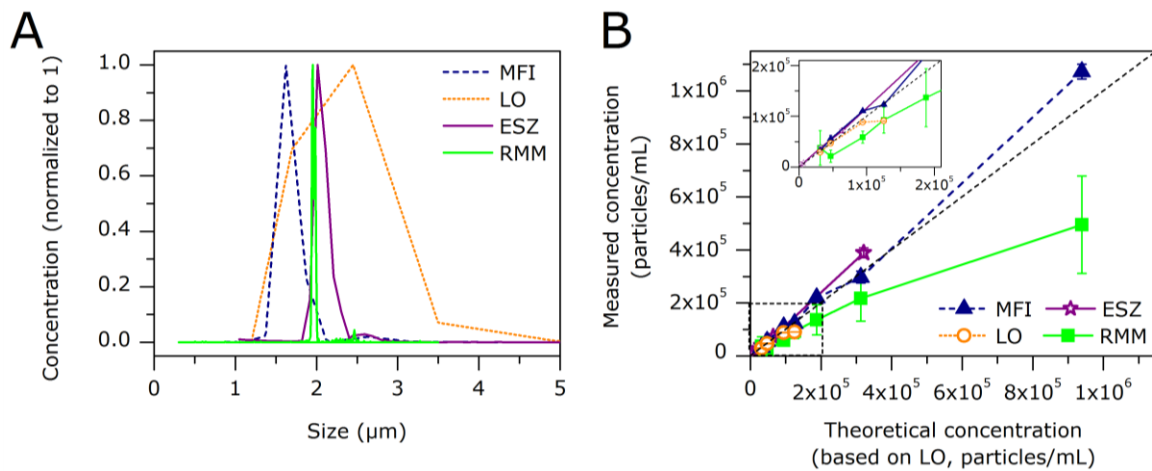


Figure 2-5: (A) Size accuracy of 2 μm polystyrene size standards and (B) linearity of 2 μm polystyrene size standards analyzed by MFI, LO, and RMM and 5 μm polystyrene size standards analyzed by ESZ. The insert in (B) shows a zoom into low concentrations. Error bars represent standard deviations from triplicate measurements.

Size accuracy and resolution were further evaluated for ESZ as compared with LO using 2 μm, 5 μm, and 10 μm polystyrene size standards analyzed separately and as a mix (Figure 2-6). ESZ provided very good size accuracy and narrow size distributions for all sizes and also very clear resolution between the sizes (Figure 2-6A). LO showed good size accuracy as well together with broader distributions as discussed above, but also acceptable separation between the different standards (Figure 2-6B).

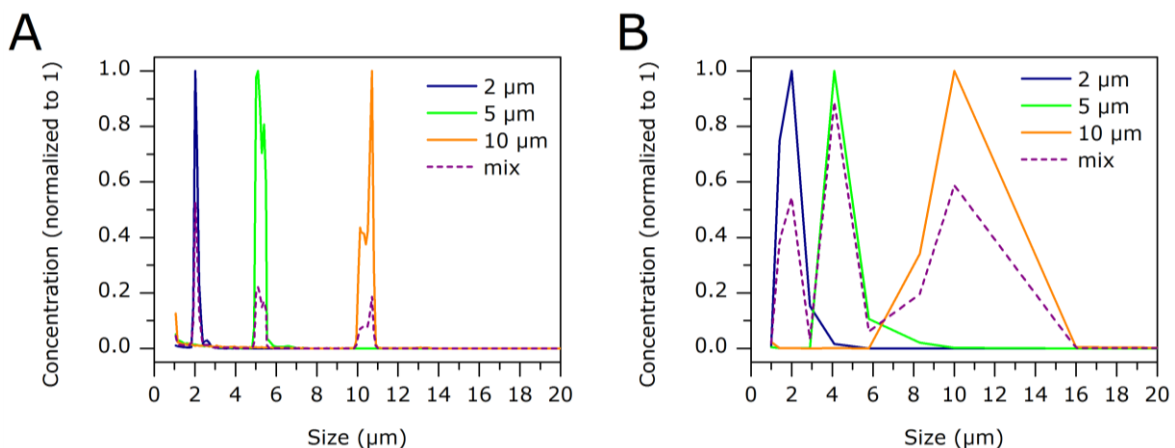


Figure 2-6: Size accuracy of polystyrene size standards of different sizes analyzed separately and as a mix by (A) ESZ and (B) LO.

Size accuracy of RMM, DLS, and NTA in the nm size range was evaluated using 500 nm polystyrene size standards analyzed separately and as a mix together with 200 nm and 800 nm polystyrene size standards (Figure 2-7). RMM showed the best size accuracy for 500 nm standards whereas NTA slightly undersized the standards and DLS showed a broader distribution (Figure 2-7A). For the mix of 200, 500, and 800 nm standards, RMM showed two distinct populations at the correct sizes of 500 and 800 nm (Figure 2-7B). The 200 nm standards were below the size range of the micro sensor used in this study and were therefore not detected. This result shows that the smaller 200 nm particles do not disturb the analysis of the larger particles. This is an important consideration for the analysis of protein samples which often contain large amounts of small particles below the measurement range. For NTA, it was not possible to analyze all three sizes with one single measurement setting. Thus, two measurements were performed with settings either optimized for larger or for smaller particles. Settings for larger particles enabled the detection of 500 and 800 nm standards at the correct size. Settings for smaller particles led to the detection of 200 and 500 nm standards, however with diminished size accuracy especially for the 200 nm standards. With DLS, only one population at about 500 nm was detected. These observations are in accordance with earlier studies about DLS and NTA²⁷ and show the benefit of single particle analysis as applied by NTA and RMM which enables excellent size resolution, especially by RMM, as compared with batch analysis as by DLS.

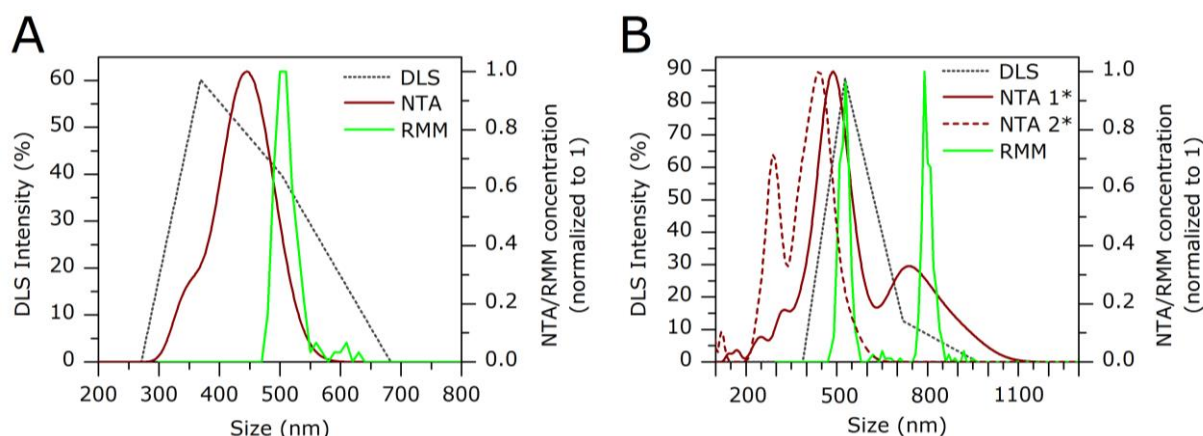


Figure 2-7: Size accuracy of (A) 500 nm polystyrene size standards and (B) a mix of 200, 500, and 800 nm polystyrene size standards (number ratio 1:1:1) analyzed by DLS, NTA, and RMM. NTA 1* indicates a measurement with settings optimized for larger particles and NTA 2* for smaller particles.

Size accuracy was further evaluated for RMM with different concentrations of 500 nm polystyrene size standards (Figure 2-8). The total particle concentration had a clear influence on the size accuracy as a second population was detected for higher particle concentrations (Figure 2-8A). A total particle concentration of 1.5×10^6 particles/mL led to the best size accuracy with a size mode at 503 nm and was therefore used as the basis for the calculation of the theoretical particle concentration in the other samples. The second population appeared at around 600 nm for theoretical total particle numbers of 7.5×10^6 and 1.5×10^7 particles/mL (representing the concentration range recommended by the manufacturer). The determined concentrations for those samples were only 4×10^6 and 9×10^6 particles/mL indicating clear undercounting due to the high particle concentration as seen also for particles in the μm size range (Figure 2-5B). For the highest evaluated concentration (theoretical concentration of 7.5×10^7 particles/mL), a population at around 700 nm was detected as the only population. The total particle concentration in this case was determined as only 1×10^7 particles/mL. This is mainly due to the high coincidence level of 16% which indicates that $2 \times 16\% = 32\%$ of all particles were excluded from the analysis as the peaks were located too closely together. This confirms again the coincidence level as an important measurement parameter for RMM which should be monitored carefully. Coincidence levels above 10% lead not only to clear underestimation of the particle load, but also to incorrect particle sizing (Figure 2-8B) and should therefore be avoided. On the other hand, a minimum particle

load of at least around 3×10^5 particles/mL (with the described measurement settings) is necessary to achieve a sufficient number of measured particles together with reasonable measurement times. This is due to the very low analyzed volume and the very low flow rate. As an example, an analyzed volume as small as 150 nL requires a measurement time of 10 minutes.

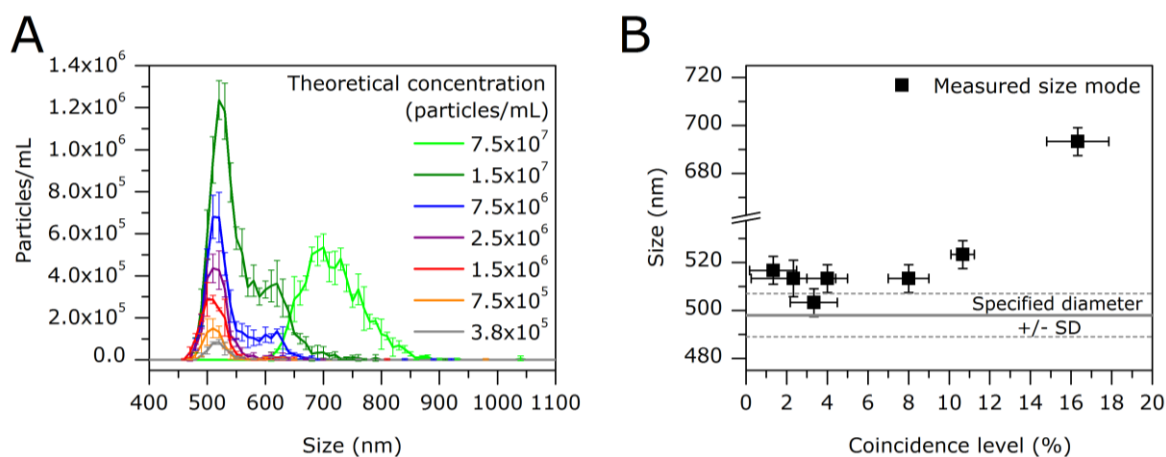


Figure 2-8: Size accuracy for 500 nm polystyrene size standards (A) depending on the theoretical particle concentration (based on a theoretical concentration of 1.5×10^6 particles/mL for the sample which showed the best size accuracy) and (B) connected to the coincidence level in RMM.

Protein particles were analyzed by ESZ and RMM as novel techniques as compared to MFI, LO, DLS, and NTA (Figure 2-9). Samples for the μm -range were diluted for ESZ, MFI, and LO with the same dilution factor whereas a lower dilution factor could be applied for RMM. The obtained concentrations were calculated back to the original concentration in the sample to ensure comparability (Figure 2-9A). In the overlapping size range of 1-4 μm , ESZ detected a higher number of particles than MFI and LO which is in agreement with the literature.^{11,13} It is unclear whether this is due to an increased sensitivity of ESZ for protein particles or the underlying measurement principle. ESZ applies a three-dimensional size calculation as a particle “fits” completely into the aperture area and thus completely contributes to the electric signal. This is in contrast to the two-dimensional particle sizing by MFI and LO which is based on the image (MFI) or the shadow (LO) and only considers a cross section of the particle. ESZ detects those parts of a protein particle which block the electric current and converts this detected volume to the diameter of an equivalent

sphere. Buffer parts within the particle but also the protein itself might partially carry the electric current in ESZ and might thus be excluded from the calculated particle size. A clear disadvantage of ESZ is the requirement for sufficient buffer conductivity. In this case, the particles could be analyzed in the original buffer solution (100 mM phosphate buffer) as this buffer showed sufficient ionic strength for the used aperture tube (50 μm). However, in many cases, the ionic strength of the original formulation buffer is not sufficient and needs to be increased for the measurement which can then affect the particle properties.

RMM detected for this specific sample similar particle concentrations as LO, clearly less than MFI and ESZ, in all size ranges. The difference to MFI may be again connected to the different underlying measurement principle as particle analysis by RMM is influenced by the particle density (see also Chapter 5 for further results and discussion of this topic).

Samples for the nm range could be analyzed by DLS and NTA only after a centrifugation step to remove intensively scattering large particles (Figure 2-9B). In contrast, the sample could be analyzed in its original state by RMM (Figure 2-9B, insert) enabling RMM to be applied in the "submicron size gap".^{6,28} However, a difficulty with RMM for highly-aggregated samples is potential clogging of the sensor which was not observed for this specific sample, but occurred for samples in other studies (data not shown). A major drawback of RMM is the small analyzed volume leading to a high multiplication factor for the calculation of the particle concentration per mL and causing high standard deviations. Taken together, RMM is a promising technique due to the light-independent novel measurement principle, but quantitative data must be evaluated carefully and the technique might be more suitable for qualitative differentiation between two particle types. RMM was further evaluated in a separate study with the focus on the differentiation of silicone oil droplets and protein particles as its main area of application (see Chapter 3).

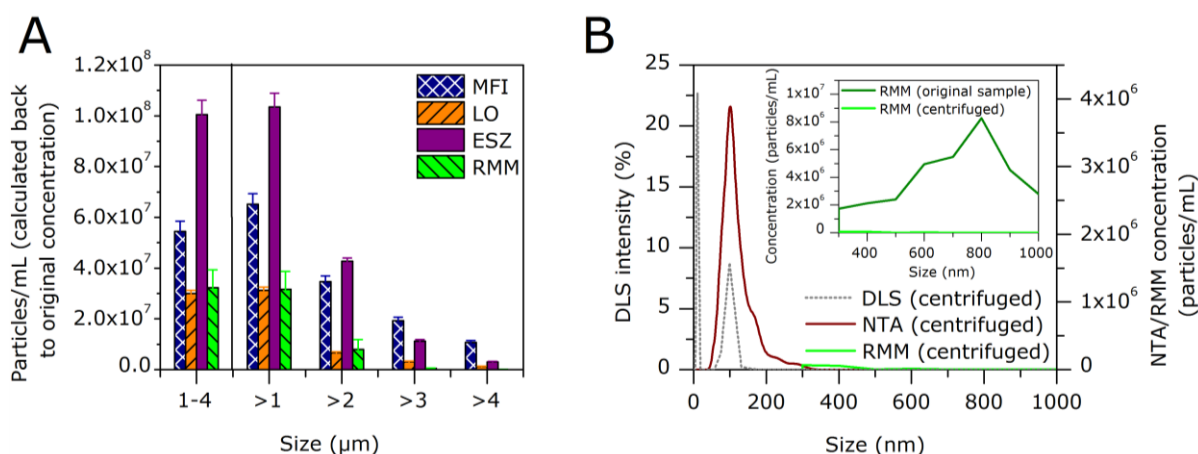


Figure 2-9: Protein particles (stir-stressed infliximab) analyzed by (A) MFI, LO, ESZ, and RMM for the μm size range and (B) DLS, NTA, and RMM for the nm size range. The insert shows results from RMM for the nm size range for the original sample and a sample after centrifugation. Error bars represent standard deviations from triplicate measurements.

3.3 Particle identification techniques

Characterization and identification are required for the root cause analysis about the origin of particles detected in therapeutic protein formulations. Also the authorities do not only require quantification, but also characterization and identification of particles as far as possible starting already at a particle size of $2\ \mu\text{m}$.²⁹ Several techniques are available for particle identification such as Raman and FT-IR microscopy or SEM-EDS⁷ (see Chapter 1). Image directed Raman spectroscopy, e.g. by rapID Particle Systems, combines automated light microscopy after filtration onto a gold-coated filter for quantification and Raman spectroscopy for identification by comparison of the obtained spectra of selected particles to a database. The difference to conventional Raman spectroscopy is that after the digital image analysis by light microscopy, the particle population can be filtered in the software e.g. by size, shape, or other parameters. Specific populations can then be selected for identification by Raman spectroscopy.

To evaluate the quantification performance of image directed Raman spectroscopy, protein particle samples (freeze-thaw-stressed and stir-stressed infliximab) were analyzed by rapID LPE, a system specialized on quantification, and rapID SPE, a system specialized on identification. The obtained concentrations were compared to MFI and LO as established techniques (Figure

2-10). As expected from previous experiments, clearly more particles were detected by MFI as compared with LO. Clearly less particles as compared with LO were detected for freeze-thaw-stressed infliximab by both rapID LPE and SPE whereas similar concentrations as for LO were detected for stir-stressed infliximab. The results show that particle quantification by light microscopy after filtration may miss particles probably mainly due to the low contrast.³⁰ Furthermore, especially small, but also large particles may end up after the filtration as very thin protein layers on the filter due to their high liquid content and low compactness. This might be more critical in the case of freeze-thaw stressed samples as this stress induced many small and few large particles (Figure 2-2). Concentrations determined by rapID LPE were higher than those determined by rapID SPE for both particle types which was expected due to the specialization of the instruments.

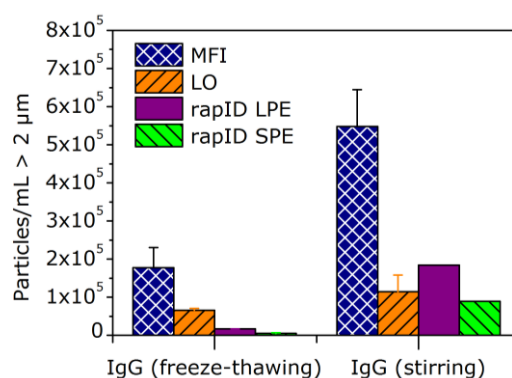


Figure 2-10: Protein particles (freeze-thaw-stressed or stir-stressed infliximab) analyzed by MFI, LO, rapID LPE, and rapID SPE. Error bars represent standard deviations from triplicate measurements for all techniques for freeze-thaw-stressed infliximab and MFI and LO for stir-stressed infliximab.

Particle identification was performed by automated comparison of the recorded Raman spectra of 250 particles > 2 μm per sample to a database (Figure 2-11). In the stressed protein samples, only few particles were identified as protein particles (Figure 2-11A). The Raman spectra of the particles did not show sufficient quality and resolution to draw further conclusions. Very few particles were determined as cellulose and glass particles. In total, only 10% of all particles could be identified.

For samples of protein particles spiked with polystyrene size standards, the instrument was able to identify 10 μm polystyrene standards well whereas 5 μm polystyrene standards were hardly detected (Figure 2-11B). For 10 μm polystyrene standards, the obtained ratio of protein particles to polystyrene standards was 1:50 whereas a ratio of 8:1 was expected from the sample preparation. This underlines again the difficulty of the system for the detection of protein particles as the original purpose of this system is to identify non-proteinaceous, extrinsic particles. The technique was successfully applied in literature to identify particles containing both protein and silicone oil larger than 10 μm .²⁰ A potential reason for the low performance in this study could be the size distribution of the protein particles with many small and few large particles. The filtration process for the rapID system should furthermore be improved to minimize contaminations, e.g. by single-use filtration units directly attached to the instrument.

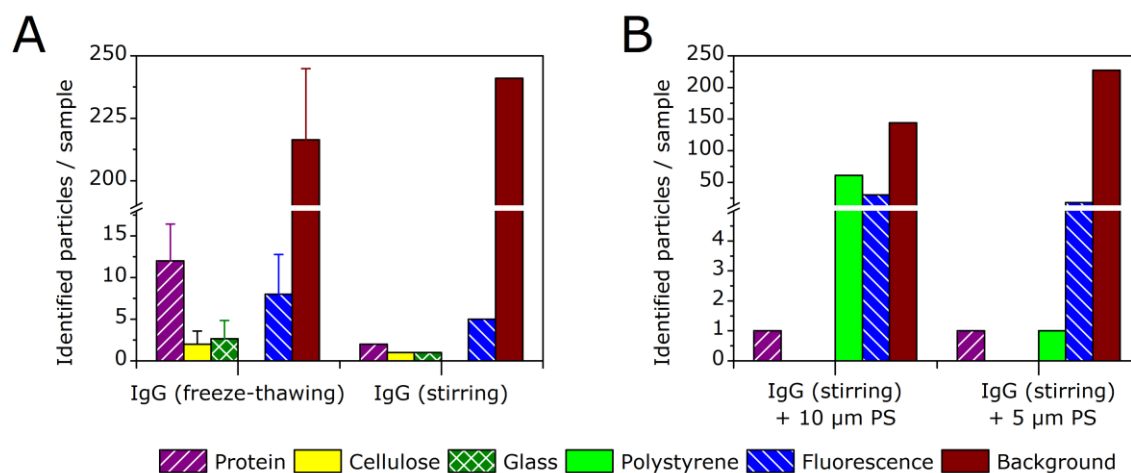


Figure 2-11: Particle identification by image directed Raman spectroscopy (rapID LPE system) for (A) samples prepared to contain only protein particles (freeze-thaw-stressed or stir-stressed infliximab) and (B) samples of protein particles (stir-stressed infliximab) spiked with polystyrene size standards. Error bars represent standard deviations from triplicate measurements for freeze-thaw-stressed infliximab.

4 Conclusion

This study showed that a critical evaluation of novel analytical techniques for the specific purpose of application is crucial to judge the suitability for protein particle analysis. Table 2-2 provides an overview of the systems evaluated in this study including the most important benefits and shortcomings which were observed. Flow imaging microscopy provided varying results depending on the used instrument: The FPIA system showed its strength in capturing images of high resolution enabling a profound particle characterization, but its weakness in particle quantification. The Occhio system determined a clearly different particle size distribution as compared to MFI pointing towards strong dependency on the optical measurement settings for this instrument. Thus, the more established flow imaging microscopy techniques for the analysis of protein particles are to be preferred. The non-optical particle counting techniques ESZ and RMM displayed both good sizing and counting performance. Analysis by RMM demonstrated clear benefits for highly polydisperse samples, especially in the high nm size range, which enables this technique to be applied in the "submicron size gap". However, the main application of this technique is the differentiation of silicone oil droplets and protein particles. The identification of particles in therapeutic protein formulations by image directed Raman spectroscopy appeared as an interesting approach with the need for further technical improvements. Taken together, techniques and systems which were originally developed for other purposes and also novel measurement principles might be beneficial for protein particle analysis, but need to be evaluated carefully case by case.

Table 2-2: Overview of the properties as well as benefits and shortcomings of the systems evaluated in this study.

Technique	Principle	Purpose	Instrument	Size range	Benefits	Shortcomings
Flow imaging microscopy	Image analysis of digital particle images captured in a flow cell	Size and count information, characterization of particle transparency, shape, identity (limited)	Sysmex FPIA-3000	1-300 μm	High image resolution	Very low analyzed volume \rightarrow limited quantification performance
			Occhio FC200 S+	1-100 μm	-	Large difference to concentration in MFI (reason unclear, potentially image fragmentation)
			FlowCAM VS1	2-50 μm	High image resolution	n.a. ^a
Electrical sensing zone	Increase of the electrical resistance in an electrical field proportional to particle size	Size and count information	Coulter counter Multisizer 4	1-30 μm	Non-optical measurement principle	Sufficient buffer conductivity required
Resonant mass measurement	Frequency shift of a resonating cantilever proportional to buoyant mass of particles in the cantilever	Size and count information, differentiation between particles of different density ^b	Archimedes	0.3-4 μm	Non-optical measurement principle, suitable for the analysis in the submicron size gap	Very low analyzed volume \rightarrow low sampling efficiency, potential clogging of the sensor by large particles
Image directed Raman spectroscopy	Image analysis after filtration followed by Raman spectroscopy on selected particles	Identification of extrinsic particles	rapID LPE rapID SPE	2-100 μm	Additional information about particle identity	Difficulties for the detection of protein particles probably due to shrinkage during filtration

^a see Chapter 4 for a detailed evaluation of this instrument; ^b see Chapter 3 for a detailed evaluation of this application

5 References

1. Ph.Eur. 2.9.19, Pharmacopoea europaea, 7th ed. 2010. Particulate contamination: Sub-visible particles. European Directorate For The Quality Of Medicine (EDQM).
2. Ph.Eur. 2.9.20 Pharmacopoea europaea, 7th ed. 2010. Particulate contamination: Visible particles. European Directorate For The Quality Of Medicine (EDQM).
3. USP<788>, United States Pharmacopeia, USP35-NF30, 2012. Particulate matter in injections. United States Pharmacopeial convention.
4. USP<1>, United States Pharmacopeia, USP35-NF30, 2012. Injections / General requirements. United States Pharmacopeial convention.
5. Rosenberg AS 2006. Effects of protein aggregates: an immunologic perspective. *AAPS J* 8:E501-507.
6. Carpenter J, Cherney B, Lubinecki A, Ma S, Marszal E, Mire-Sluis A, Nikolai T, Novak J, Ragheb J, Simak J 2010. Meeting report on protein particles and immunogenicity of therapeutic proteins: filling in the gaps in risk evaluation and mitigation. *Biologicals* 38:602-611.
7. Zölls S, Tantipolphan R, Wiggenhorn M, Winter G, Jiskoot W, Friess W, Hawe A 2012. Particles in therapeutic protein formulations, Part 1: Overview of analytical methods. *J Pharm Sci* 101:914-935.
8. den Engelsman J, Garidel P, Smulders R, Koll H, Smith B, Bassarab S, Seidl A, Hainzl O, Jiskoot W 2011. Strategies for the assessment of protein aggregates in pharmaceutical biotech product development. *Pharm Res* 28:920-933.
9. Grover NB, Naaman J, Ben-Sasson S, Doljanski F 1969. Electrical sizing of particles in suspensions. I. Theory. *Biophys J* 9:1398-1414.
10. Robinson JP 2013. Wallace H. Coulter: Decades of invention and discovery. *Cytometry A* 83:424-438.
11. Demeule B, Messick S, Shire SJ, Liu J 2010. Characterization of particles in protein solutions: reaching the limits of current technologies. *AAPS J* 12:708-715.
12. Rhyner MN 2011. The Coulter principle for analysis of subvisible particles in protein formulations. *AAPS J* 13:54-58.
13. Barnard JG, Rhyner MN, Carpenter JF 2012. Critical evaluation and guidance for using the coulter method for counting subvisible particles in protein solutions. *J Pharm Sci* 101:140-153.
14. Mück C 2002. Analytik von Proteinaggregation mittels Coulter-Prinzip : Vergleich mit der Lichtblockade-Messung. Diploma thesis, Ludwig-Maximilians-Universität München / FH Albstadt-Sigmaringen.
15. Burg TP, Godin M, Knudsen SM, Shen W, Carlson G, Foster JS, Babcock K, Manalis SR 2007. Weighing of biomolecules, single cells and single nanoparticles in fluid. *Nature* 446:1066-1069.
16. Dextras P, Burg TP, Manalis SR 2009. Integrated measurement of the mass and surface charge of discrete microparticles using a suspended microchannel resonator. *Anal Chem* 81:4517-4523.
17. Strehl R, Rombach-Riegraf V, Diez M, Egodage K, Bluemel M, Jeschke M, Koulov AV 2012. Discrimination between silicone oil droplets and protein aggregates in biopharmaceuticals: a novel multiparametric image filter for sub-visible particles in microflow imaging analysis. *Pharm Res* 29(2):594-602.
18. Patel AR, Lau D, Liu J 2012. Quantification and characterization of micrometer and submicrometer subvisible particles in protein therapeutics by use of a suspended microchannel resonator. *Anal Chem* 84(15):6833-6840.
19. Cao X, Masatani P, Torraca G, Wen Z-Q 2010. Identification of a mixed microparticle by combined microspectroscopic techniques: a real forensic case study in the biopharmaceutical industry. *Appl Spectrosc* 64:895-900.
20. Lankers M, Munhall J, Valet O 2008. Differentiation between foreign particulate matter and silicone oil induced protein aggregation in drug solutions by automated raman spectroscopy. *Microscopy and Microanalysis* 14:1612-1613.
21. Zölls S, Gregoritz M, Tantipolphan R, Wiggenhorn M, Winter G, Friess W, Hawe A 2013. How subvisible particles become invisible-relevance of the refractive index for protein particle analysis. *J Pharm Sci* 102:1434-1446.
22. Wuchner K, Büchler J, Spycher R, Dalmonte P, Volkin DB 2010. Development of a microflow digital imaging assay to characterize protein particulates during storage of a high concentration IgG1 monoclonal antibody formulation. *J Pharm Sci* 99:3343-3361.

23. Huang C-T, Sharma D, Oma P, Krishnamurthy R 2009. Quantitation of protein particles in parenteral solutions using micro-flow imaging. *J Pharm Sci* 98:3058-3071.
24. Komabayashi T, Spångberg LSW 2008. Comparative analysis of the particle size and shape of commercially available mineral trioxide aggregates and Portland cement: a study with a flow particle image analyzer. *J Endodont* 34:94-98.
25. Komabayashi T, D'souza RN, Dechow PC, Safavi KE, Spångberg LSW 2009. Particle size and shape of calcium hydroxide. *J Endodont* 35:284-287.
26. Weinbuch D, Zöls S, Wiggerhorn M, Friess W, Winter G, Jiskoot W, Hawe A 2013. Micro-Flow Imaging and resonant mass measurement (Archimedes) – Complimentary methods to quantitatively differentiate protein particles and silicone oil droplets. *J Pharm Sci* 102:2152-2165.
27. Filipe V, Hawe A, Jiskoot W 2010. Critical evaluation of Nanoparticle Tracking Analysis (NTA) by NanoSight for the measurement of nanoparticles and protein aggregates. *Pharm Res* 27:796-810.
28. Carpenter JF, Randolph TW, Jiskoot W, Crommelin DJA, Middaugh CR, Winter G, Fan Y-X, Kirshner S, Verthelyi D, Kozlowski S, Clouse KA, Swann PG, Rosenberg A, Cherney B 2009. Overlooking subvisible particles in therapeutic protein products: gaps that may compromise product quality. *J Pharm Sci* 98:1201-1205.
29. Kirshner S Regulatory expectations for analysis of aggregates and particles. Talk at Workshop on Protein Aggregation and Immunogenicity, Breckenridge, Colorado, 07/12/12.
30. Narhi LO, Jiang Y, Cao S, Benedek K, Shnek D 2009. A critical review of analytical methods for subvisible and visible particles. *Curr Pharm Biotechno* 10:373-381.

Chapter 3

Micro-Flow Imaging and resonant mass measurement (Archimedes) – Complementary methods to quantitatively differentiate protein particles and silicone oil droplets

Abstract

Our study aimed to comparatively evaluate Micro-Flow Imaging (MFI) and the recently introduced technique of resonant mass measurement (Archimedes, RMM) as orthogonal methods for the quantitative differentiation of silicone oil droplets and protein particles. This distinction in the submicron and micron size range is highly relevant for the development of biopharmaceuticals, in particular for products in prefilled syringes. Samples of artificially generated silicone oil droplets and protein particles were quantified individually and in defined mixtures to assess the performance of the two techniques. The built-in MFI software solution proved to be suitable to discriminate between droplets and particles for sizes above 2 μm at moderate droplet/particle ratios (70:30 – 30:70). A customized filter developed specifically for this study greatly improved the results and enabled reliable discrimination also for more extreme mixing ratios (95:5 – 15:85). RMM showed highly accurate discrimination in the size range of about 0.5 to 2 μm independent of the ratio, provided that a sufficient number of particles (> 50 counted particles) were analyzed. We recommend applying both techniques for a comprehensive analysis of biotherapeutics potentially containing silicone oil droplets and protein particles in the submicron and micron size range.

The following chapter was published as a research article in the Journal of Pharmaceutical Sciences and appears in this thesis with the journal's permission:

D. Weinbuch, S. Zölls*, M. Wiggerhorn, W. Friess, G. Winter, W. Jiskoot, A. Hawe: "Micro-Flow Imaging and resonant mass measurement (Archimedes) – complementary methods to quantitatively differentiate protein particles and silicone oil droplets"; J Pharm Sci 102(7):2152-2165 (2013); *joint first authors*

1 Introduction

Protein aggregates can be classified according to their size as visible ($>100\ \mu\text{m}$), micron ($1\text{-}100\ \mu\text{m}$), submicron ($100\ \text{nm}\text{-}1000\ \text{nm}$) and nanometer particles ($<100\ \text{nm}$).¹ Especially aggregates in the micron and submicron size range raise concerns as they are potentially immunogenic,^{2,3} could coalesce to form larger particles over time or function as nuclei for further aggregation.⁴ Even though the United States Pharmacopeia (USP) and the European Pharmacopoeia (Ph. Eur.) currently define concentration limits in parenteral solutions only for particles larger than $10\ \mu\text{m}$, regulatory authorities increasingly expect quantitative characterization of micron particles from 1 to $10\ \mu\text{m}$ and qualitative characterization of submicron particles from $100\ \text{nm}$ to $1000\ \text{nm}$ already in early stages of the development phase.⁵⁻⁷ In many cases substantial amounts of particles below $10\ \mu\text{m}$ are often present in formulations that meet the limits of the pharmacopoeias for larger particles.⁸⁻¹⁰

In general, particles of all sizes can be proteinaceous or non-proteinaceous. Among the group of non-proteinaceous particles, silicone oil droplets, which are also quantified as particles by routine methods like light obscuration, play a major role. This is especially important for products in prefilled syringes or cartridges, where silicone oil droplets are introduced into the product deriving from the lubrication of the glass barrel and the plunger. In a case study, silicone oil droplets were identified inside the eyes of patients after intravitreal injection, likely originating from the siliconized glass syringes.¹¹ In earlier studies, silicone oil droplets were detected in insulin syringes and associated with loss of insulin efficacy.^{12,13} Furthermore, silicone oil droplets were present in Interferon products in prefilled syringes.¹⁴ Even though silicone oil itself is not necessarily harmful to the patient,¹⁵ it has been described to induce aggregation of monoclonal antibodies¹⁶ and various other proteins^{17,18} and the formation of protein-silicone oil complexes^{18,19} which might potentially be immunogenic.²⁰ From a manufacturing perspective, elevated concentrations of (silicone) oil droplets can indicate problems during the production process, e.g. improper siliconization of syringes or contamination from leaking components during lyophilization. These factors make an analytical differentiation of the total particle load into protein particles and silicone oil droplets necessary.

Among the various techniques for particle analysis,²¹ scanning electron microscopy coupled with energy dispersive X-ray spectroscopy (SEM-EDS),²² Fourier-transformed infrared (FT-IR)²² and Raman microscopy,²³ asymmetrical flow field flow fractionation,²⁴ electrical sensing zone as well as flow cytometry²⁵ are in principle able to differentiate silicone oil droplets and protein particles. However, mainly flow imaging microscopy techniques and the recently introduced resonant mass measurement (RMM) technique are designed for the differentiation of these particles in a higher throughput and without cumbersome sample preparation (e.g. staining or fixation). Micro-Flow Imaging (MFI) has received major attention for the analysis of protein particles^{22,26-28} but has also been applied for the identification of silicone oil droplets.²⁹ Silicone oil droplets were successfully differentiated from protein particles on MFI images on the basis of their spherical shape³⁰ and, more efficiently, by employing a multi-parametric filter.³¹

The recently introduced Archimedes system employs the novel principle of RMM for the analysis of submicron and micron particles.³² The sample solution is flushed through a microchannel inside a resonating cantilever (also designated as suspended microchannel resonator (SMR)) which changes its frequency depending on the mass of the particles passing the channel. Importantly, positively buoyant particles (e.g. silicone oil droplets) and negatively buoyant particles (e.g. protein particles) can be clearly discriminated as they increase and decrease the frequency of the cantilever, respectively.³³ With a theoretical size range from about 50 nm up to about 6 μm (depending on the sensor and the particle type), RMM aims to bridge the "submicron size gap"^{15,34} between on the one hand flow imaging microscopy and light obscuration, which cover the micrometer size range, and on the other hand nanoparticle tracking analysis and dynamic light scattering, which allow analysis in the nanometer size range. Literature on RMM is still very limited. Patel *et al.*³⁵ presented a first study on the principle of RMM using various microspheres as well as silicone oil droplets and protein particles for a technical evaluation of the system. Barnard *et al.*¹⁴ applied RMM to analyze protein particles and silicone oil droplets in marketed Interferon-beta products. However, the accuracy of the differentiation between these two particle types was not investigated in those studies and remains to be elucidated.

The aim of our study was to evaluate MFI and RMM as orthogonal tools for the quantitative discrimination between silicone oil droplets and proteinaceous particles in the micron and submicron range. For this purpose, defined mixtures of silicone oil droplets and protein particles were prepared at various ratios on the basis of the distributions expected in marketed biopharmaceutical products in prefilled syringes. The optical discrimination of silicone oil droplets from protein particles in MFI by (i) the built-in software solution “find similar” and (ii) a new customized data filter developed in this study was compared to the physical discrimination principle of RMM.

2 Materials and methods

2.1 Materials

Etanercept (Enbrel[®], prefilled syringe, lot no. 31576, exp. 12/2008; lot no. 32411, exp. 09/2009), adalimumab (Humira[®], prefilled syringe, lot no. 292209A05, exp. 10/2006; lot no. 430989A04, exp. 02/2008), rituximab (MabThera[®], vial, lot no. B6073, exp. 12/2013) and infliximab (Remicade[®], vial, lot no. 7GD9301402, 7FD8701601, 7RMKA81402, pooled) were donated by local hospitals. Sucrose, mannitol, sodium chloride, trisodium citrate dihydrate and polysorbate 80 were purchased from VWR (Darmstadt, Germany), disodium hydrogenphosphate dihydrate and sodium dihydrogenphosphate dihydrate were purchased from Merck KGaA (Darmstadt, Germany). Silicone oil with a viscosity of 1000 cSt (same viscosity as used in other studies^{15,16,25} and as listed in the Ph.Eur. monography for silicone oil as a lubricant³⁶), citric acid and arginine hydrochloride were purchased from Sigma Aldrich (Steinheim, Germany).

2.2 Preparation of protein samples

Etanercept solution at a concentration of 5 mg/mL was prepared by dilution of 50 mg/mL etanercept (removed from the prefilled syringe through the needle) in 25 mM phosphate buffer (pH 6.3) containing 100 mM NaCl, 25 mM arginine hydrochloride and 1% sucrose. Adalimumab solution at a concentration of 5 mg/mL was prepared by dilution of 50 mg/mL adalimumab in 15 mM phosphate/citrate buffer (pH 5.2) containing 105 mM NaCl, 1.2% mannitol and 0.1% polysorbate 80.

Rituximab solution at a concentration of 1 mg/mL was prepared by dilution of 10 mg/mL rituximab commercial product in 25 mM citrate buffer (pH 6.5) containing 154 mM NaCl and 0.07% polysorbate 80 (formulation buffer). The formulation was filtered using a 0.2 µm polyethersulfone syringe filter (Sartorius, Göttingen, Germany) and kept at 2-8 °C for a maximum of one week. Heat-stressed rituximab was prepared by incubating 1.5 mL of the 1 mg/mL rituximab solution for 30 minutes at 71 °C in a thermomixer (Eppendorf, Hamburg, Germany). Stir-stressed rituximab was prepared by incubating 3 mL of the 1 mg/mL rituximab solution in a 5R glass vial using a 12 mm Teflon[®]-coated stir

bar at 1000 rpm for 24 hours at room temperature on a magnetic stirrer (Heidolph MR 3001K, Heidolph, Schwabach, Germany). Stressed rituximab at 1 mg/mL (protein particle stock suspension) was stored at 2-8 °C until the measurement.

Infliximab solution at a concentration of 1 mg/mL was prepared by dilution of 10 mg/mL infliximab commercial product in 100 mM phosphate buffer (pH 7.2). The formulation was filtered using a 0.2 µm polyethersulfone syringe filter. Heat-stressed infliximab was prepared by incubating 0.5 mL of the 1 mg/mL infliximab solution for 30 minutes at 60 °C in a thermomixer. Stir-stressed infliximab was prepared by incubating 8 mL of the 1 mg/mL infliximab solution in a 10R glass vial using a 18 mm Teflon[®]-coated stir bar at 250 rpm for 24 hours at room temperature on a magnetic stirrer (Heidolph MR Hei-Standard).

2.3 Preparation of silicone oil emulsion

Pure silicone oil was added to filtered formulation buffer (0.2 µm polyethersulfone syringe filter) in a particle-free 15 mL conical tube (VWR) to a final concentration of 2% (w/v) to generate a pure emulsion without additives. After vortexing briefly, silicone oil droplet formation was induced by sonication in a water bath (Sonorex, Brandelin, Berlin, Germany) for 10 minutes. Fresh silicone oil emulsion (silicone oil droplet stock emulsion) was prepared on the day of the measurement and kept at room temperature.

2.4 Preparation of individual and mixed samples of silicone oil droplets and protein particles

Silicone oil droplet stock emulsion and/or protein particle stock suspension (heat-stressed rituximab) was diluted in unstressed protein solution or filtered formulation buffer for the preparation of mixed and individual samples. Unless stated otherwise, samples were prepared to a final protein concentration of 0.5 mg/mL. Mixed samples were prepared to cover ratios of silicone oil droplets to protein particles of 95:5 to 15:85 based on particle counts > 1 µm determined by MFI. Individual samples were prepared to contain the same amount of silicone oil droplets and protein particles, respectively, as in the mixed samples and were

referred to as the theoretical concentration. The samples were gently mixed with a pipette, kept at room temperature and measured on the day of preparation.

2.5 Micro-Flow Imaging (MFI)

An MFI DPA4100 series A system (ProteinSimple, Santa Clara, CA) equipped with a 100 μm flow cell, operated at high magnification (14x) and controlled by the MFI View software version 6.9 was used. The system was flushed with 5 mL purified water at maximum flow rate and flow cell cleanliness was checked between measurements. Unstressed and filtered rituximab or the appropriate formulation buffer was used to perform “optimize illumination” prior to each measurement. Samples of 0.65 mL with a pre-run volume of 0.3 mL were analyzed at a flow rate of 0.1 mL/min ($n=3$). MVAS version 1.2 was used for data analysis.

2.6 Development of a customized filter for MFI

The MVAS software of the MFI system enables the discrimination of particles based on optical parameters of the generated images through the “find similar” operation. For our study, a minimum of 20 particles above 5 μm clearly recognizable as silicone oil droplets was selected for the discrimination. In addition to this, a customized filter was developed specifically for the heat-stressed rituximab samples of this study. In detail, the new filter was based on four customized size-specific cut-offs for particle parameters of silicone oil droplets provided by MFI (Figure 3-1), which proved to be suitable to discriminate silicone oil droplets and protein particles. This approach is a modification of previous work by Strehl *et al.*³¹ The four parameters used for our filter were intensity mean (Figure 3-1A), intensity minimum (Figure 3-1B), intensity standard deviation (Figure 3-1C) and aspect ratio (Figure 3-1D). The first three parameters are based on the intensity of the particle image, which is directly proportional to the transparency of the particle.²⁷ The intensity mean describes the mean intensity value over all pixels within one particle; the intensity minimum describes the intensity of the darkest pixel of a particle; and the intensity standard deviation describes differences between higher and lower intensity values within the same particle. The aspect ratio defines the shape of a particle with “1” for an absolutely spherical particle and “0” for a needle with an

infinite length. For each of the four particle parameters, the individual distributions for silicone oil droplets and protein particles from heat-stressed rituximab were compared as a function of size.

Cut-offs were defined at the mean value of the 95% confidence intervals between the two populations (Figure 3-2). A polynomial function was automatically fitted to these points from 1 to 11 μm and applied for particles from 1 to 9 μm . Above 11 μm , the number of counts acquired was not sufficient for this statistical approach; therefore, the fit was adjusted manually in this larger size range. The automated and the manual fit were overlapped in the size range from 9 to 11 μm to ensure a smooth transition. Since the silicone oil droplet population was more homogeneous than the protein particle population, the customized filter was set to identify objects as silicone oil droplets only when they fulfilled all four cut-off fit criteria. Particles showing values below the cutoff for intensity mean and minimum (Figure 3-1A and B) and at the same time above the cutoff for intensity standard deviation and aspect ratio (Figure 3-1C and D) were marked as silicone oil droplets by the algorithm. Particles fulfilling less than four of these criteria were assigned as non-silicone oil particles, which means in our case protein particles.

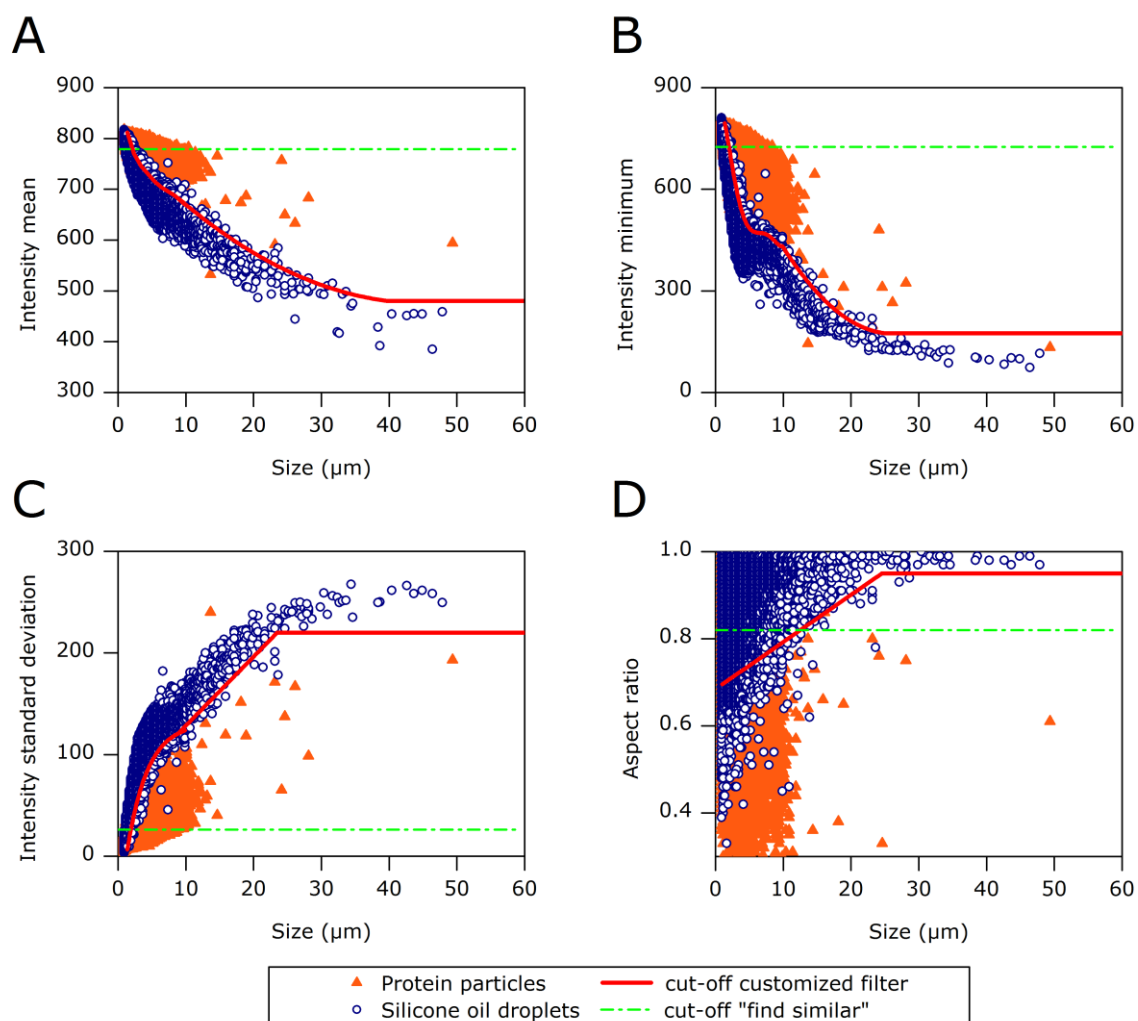


Figure 3-1: Scatter plots of particle parameters (A) intensity mean, (B) intensity minimum, (C) intensity standard deviation, and (D) aspect ratio for individual samples containing only protein particles (heat-stressed rituximab) or only silicone oil droplets analyzed separately by MFI and merged into one graph per particle parameter. The solid red lines illustrate cutoffs as a function of size, generated by our customized fit for the discrimination between silicone oil droplets and protein particles. The dash-dotted green lines illustrate linear cutoffs used by the MVAS software for the "find similar" operation.

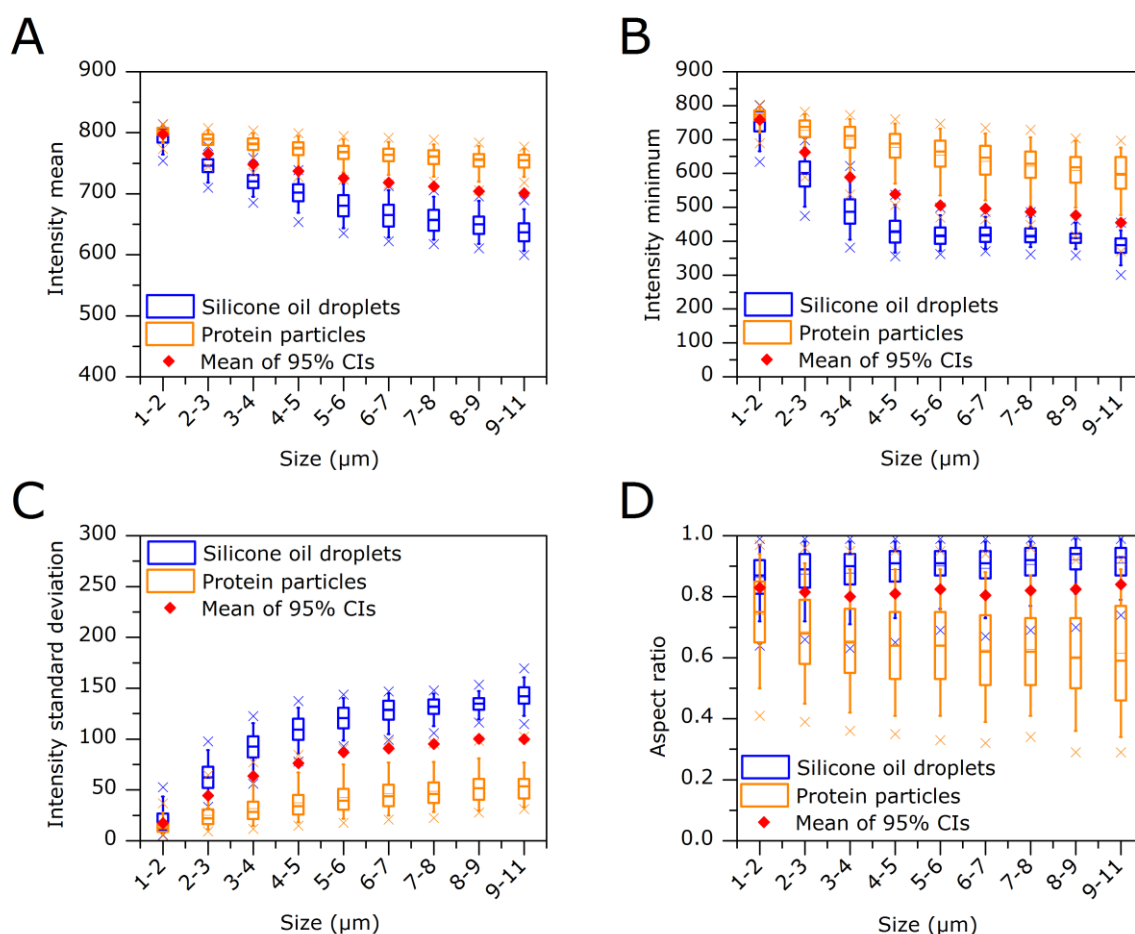


Figure 3-2: Distribution of the MFI particle parameters (A) intensity mean, (B) intensity minimum, (C) intensity standard deviation and (D) aspect ratio for individual samples of silicone oil droplets and protein particles (heat-stressed rituximab). Box plots show 25/75% (box) and 5/95% percentiles (whisker) as well as minimum and maximum values (X). The mean values of the 95% confidence intervals (CI) were used as a basis to fit the function for the customized filter.

2.7 Resonant mass measurement (RMM)

An Archimedes system (Affinity Biosensors, Santa Barbara, CA) was equipped with a Hi-Q Micro Sensor and controlled by the ParticleLab software version 1.8. The sensor was flushed for 60 seconds with purified water prior to analysis. Subsequently, possible impurities in the system were removed by two “sneeze” operations (liquid in the sensor is pushed into both directions) and the system was flushed again for 60 seconds with purified water. The sample solution was then loaded for 45 seconds. Prior to analysis, the limit of detection (LOD) was determined three times in automatic LOD mode. The mean value was then set

fixed for each measurement. Samples of 150 nL were analyzed (n=3) and fresh sample solution was loaded for each of the triplicate measurements.

Size determination of particles by RMM is based on the frequency shift f which is proportional to the buoyant mass M_B and depending on the sensitivity S of the resonator (Equation 3-1).

$$M_B = \Delta f * S$$

Equation 3-1

The conversion of buoyant mass M_B into dry mass M (Equation 3-2) and diameter D (Equation 3-3) is then based on the density of the particle, ρ_{particle} (1.32 g/mL for protein particles, based on the density estimation of pure protein³⁷ and the recommendation of the manufacturer; 0.97 g/mL for silicone oil, according to the supplier) and the density of the fluid, ρ_{fluid} (calculated based on the sensor frequency relative to the frequency and the density of water as a reference).

$$M = \frac{M_B}{1 - \rho_{\text{fluid}} / \rho_{\text{particle}}}$$

Equation 3-2

$$D = \sqrt[3]{\frac{6M}{\pi\rho_{\text{particle}}}}$$

Equation 3-3

3 Results and discussion

3.1 Silicone oil droplets in prefilled syringes

Expired prefilled syringes of etanercept and adalimumab were available for the study and analyzed in order to gain insight into relevant levels and size distributions of silicone oil droplets in marketed products as a worst case scenario. Four and six years after expiration, respectively, MFI determined for both products about 4×10^5 particles/mL above $1 \mu\text{m}$. Based on the images generated by MFI, about 80% of the particles above $5 \mu\text{m}$ in both products could be identified as silicone oil droplets using the “find similar” operation provided by the MVAS software. RMM determined 3.2×10^6 particles/mL larger than $0.5 \mu\text{m}$ for etanercept and 2.0×10^6 particles/mL for adalimumab, of which 51% and 97%, respectively, could be attributed to silicone oil. Three and four years after expiration, RMM determined for both analyzed products lower concentrations of protein particles and of silicone oil droplets when compared to products four and six years after expiration, respectively (Table 3-1). This implies that total particle concentrations as well as the ratio between silicone oil droplets and protein particles can vary substantially between products, lots, and age of the product.

Table 3-1: Total particle and silicone oil droplet concentrations of expired marketed products in prefilled syringes determined by RMM.

Product	Total particle concentration per mL (> $0.5 \mu\text{m}$)	Identified as silicone oil droplets per mL (> $0.5 \mu\text{m}$)
Etanercept		
lot 32411, exp. 09/2009	1.50×10^6	1.46×10^6
lot 31576, exp. 12/2008	3.25×10^6	1.68×10^6
Adalimumab		
lot 430989A04, exp. 02/2008	1.74×10^6	1.61×10^6
lot 292209A05, exp. 10/2006	2.01×10^6	1.94×10^6

3.2 Determination of total particle concentrations (without discrimination)

For the evaluation of MFI and RMM, silicone oil droplets were artificially generated, which appeared similar to those found in etanercept and adalimumab prefilled syringes with respect to their shape, optical properties (Figure 3-3) and

size distribution (Figure 3-4). The concentrations used in our study (0.003% to 0.025% (w/v) silicone oil) provided droplet concentrations similar to those identified in the expired etanercept and adalimumab prefilled syringes and are in agreement with other studies suggesting the presence of up to 0.03% of silicone oil in prefilled syringes.^{38,39}

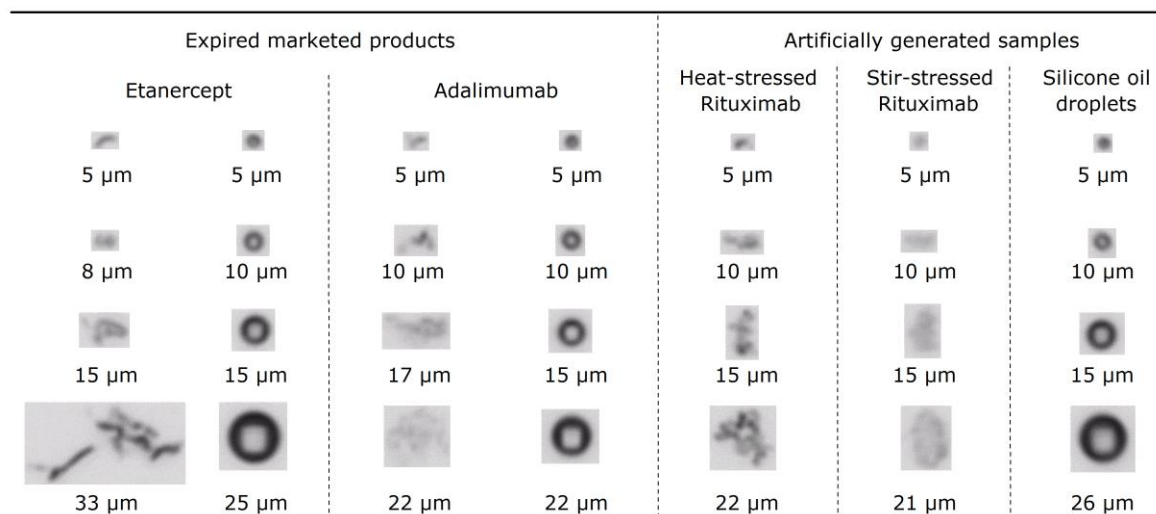


Figure 3-3: Examples of MFI images of protein particles and silicone oil droplets detected in marketed products and artificially generated samples.

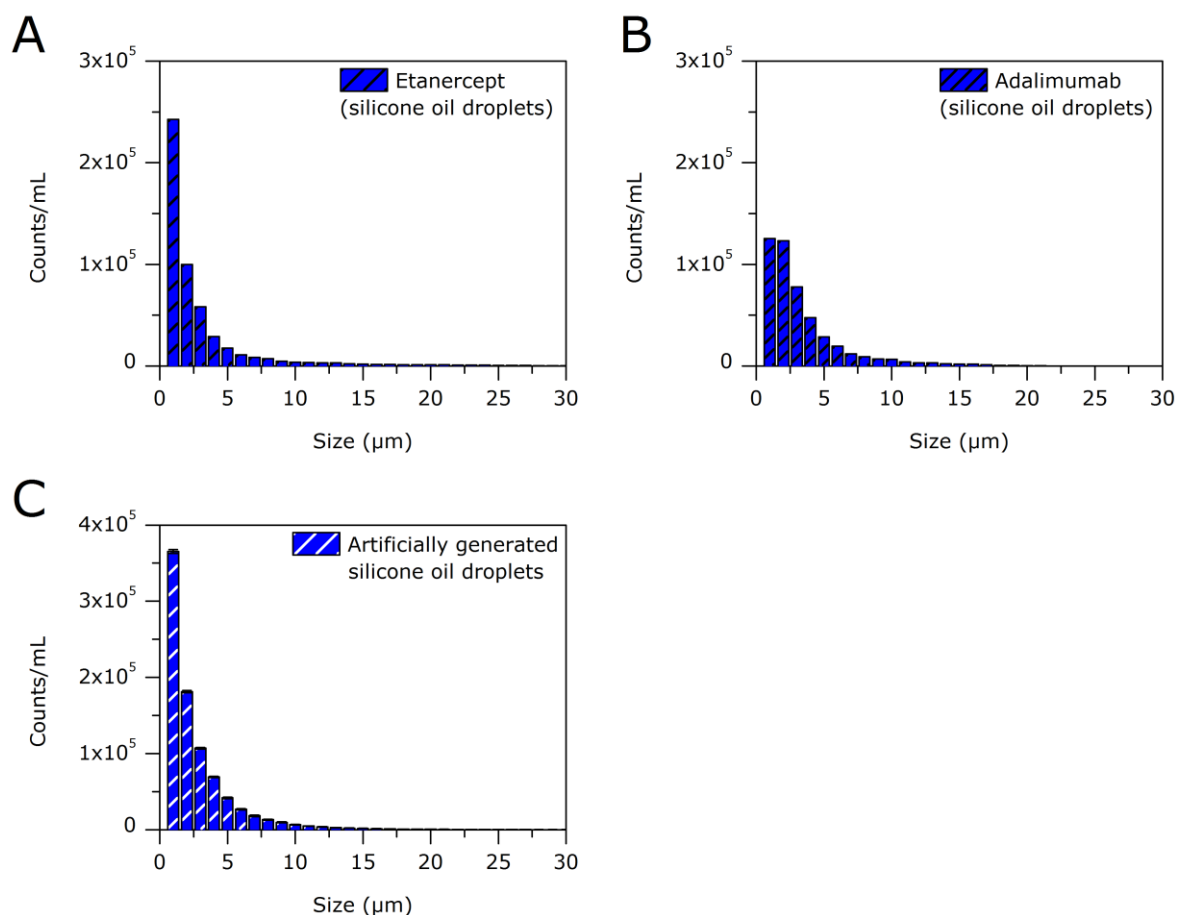


Figure 3-4: Cumulative size distributions of silicone oil droplets determined by MFI and identified by the “find similar” operation in (A) etanercept prefilled syringes, (B) adalimumab prefilled syringes, (C) a sample containing only artificially generated silicone oil droplets. Error bars represent standard deviations from triplicate measurements.

A heat-stress method was developed using rituximab as a model for the generation of particles with a similar appearance to protein particles in etanercept prefilled syringes. A stir-stress method was developed for the generation of particles similar to those in adalimumab prefilled syringes (Figure 3-3). All protein samples showed comparable particle size distributions with the smaller particles representing the largest fraction (Figure 3-5). Protein particles in concentrations from 1×10^5 to 5×10^5 particles/mL above 1 μm (according to MFI) were combined with silicone oil droplets in concentrations from 1×10^5 to 3×10^5 particles/mL above 1 μm (according to MFI). Using MFI and RMM, several samples with varying concentrations of protein particles and silicone oil droplets

were analyzed, both individually and as mixtures at various defined droplet/particle ratios.

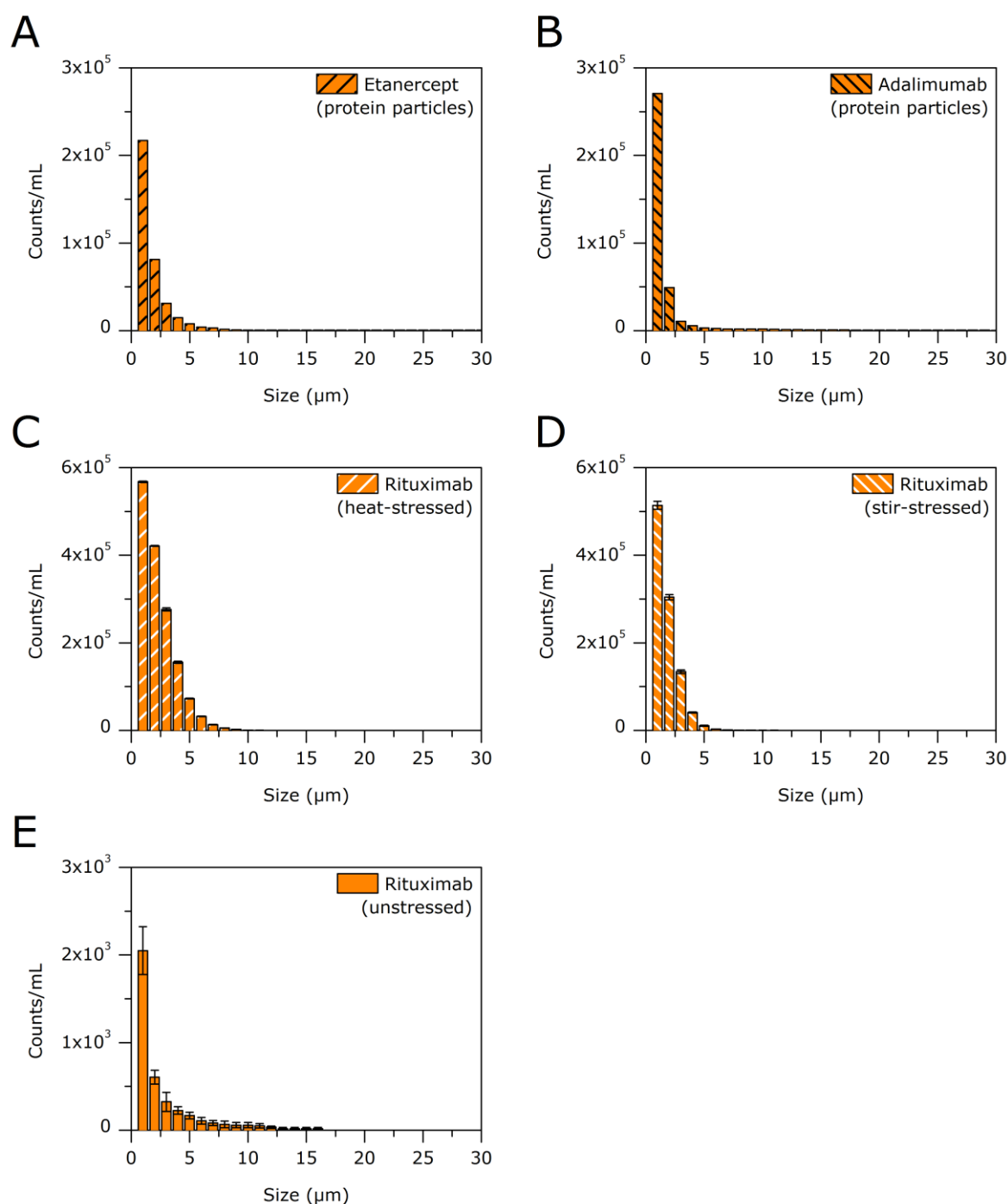


Figure 3-5: Cumulative size distributions of protein particles determined by MFI and identified by the “find similar” operation for silicone oil droplets (protein particles are identified as the inverse population) in (A) etanercept prefilled syringes, (B) adalimumab prefilled syringes, (C) heat-stressed rituximab, (D) stir-stressed rituximab, (E) unstressed rituximab. Error bars represent standard deviations from triplicate measurements.

First, the particle concentrations for individual samples containing either only silicone oil droplets or only protein particles were determined by MFI and RMM. One combination is shown as a representative example in Figure 3-6 for the overlapping measurement size range of both techniques (1-4 μm). Overall, the results indicate that particle counts and size distributions by MFI and RMM are in general agreement. However, certain differences were observed depending on the type of sample and the ratio of protein particles and silicone oil droplets: For samples containing only silicone oil, RMM detected slightly more droplets of 1 to 4 μm as compared to MFI, while MFI detected more droplets in the size range from 2 to 4 μm (Figure 3-6A). This trend was reproducible for all silicone oil droplet samples, with an up to twofold higher silicone oil droplet count in the size range of 1 to 4 μm detected by RMM as compared to MFI.

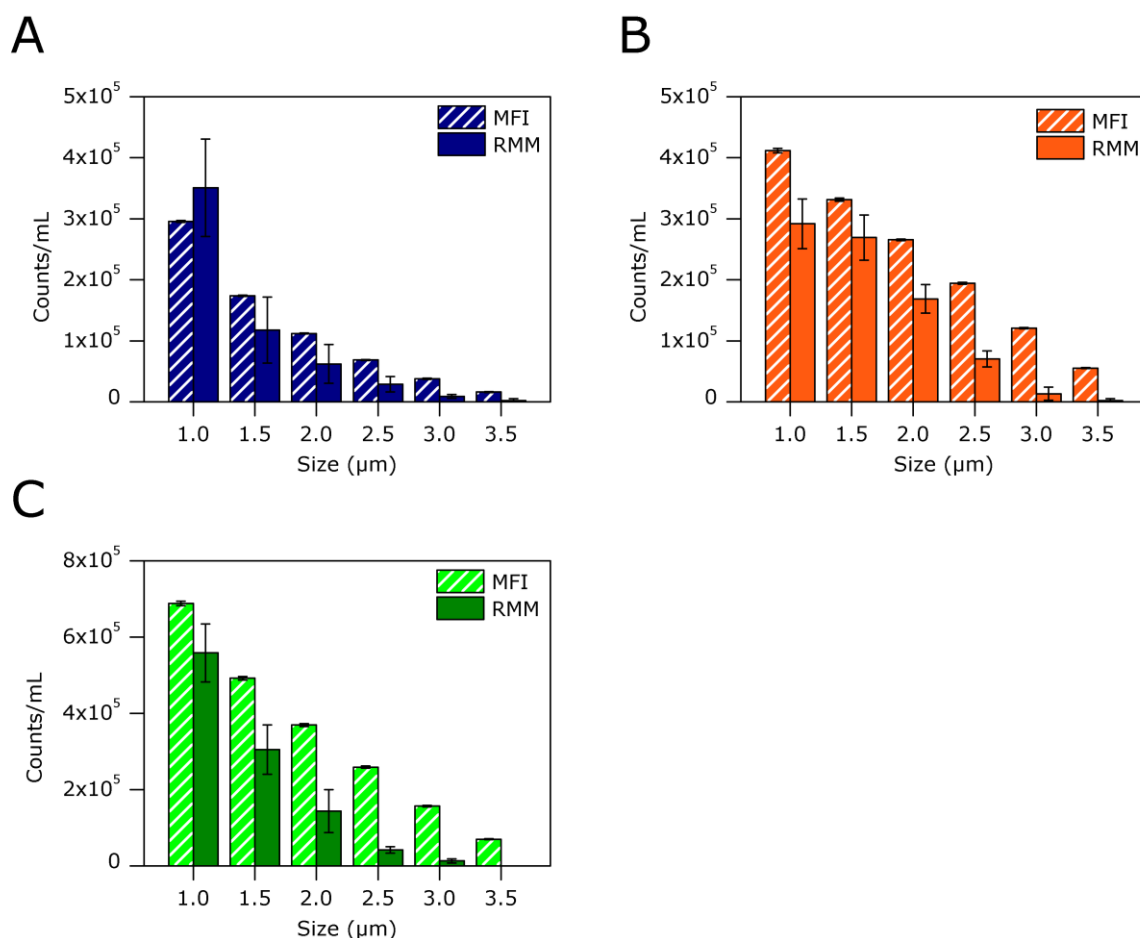


Figure 3-6: Cumulative size distributions in the size range of 1-4 μm of (A) a sample containing only silicone oil droplets, (B) a sample containing only protein particles (heat-stressed rituximab), and (C) the corresponding mixture (droplet/particle ratio 40:60 for particles $> 1 \mu\text{m}$ based on MFI) as determined by MFI and RMM. Error bars represent standard deviations from triplicate measurements.

This difference might be due to two major reasons:

(i) Silicone oil droplets of sizes up to $50 \mu\text{m}$ were identified by MFI, which are much larger than the microchannel diameter of RMM ($8 \mu\text{m}$). Those particles larger than $8 \mu\text{m}$ represent only 4% of all silicone oil droplets in the sample detected by MFI by number; however, they contain 72% of the total mass of all silicone oil droplets in the sample detected by MFI (mass was calculated based on droplet counts at the respective diameter and the density of silicone oil of 0.97 g/mL). These observations led us to the hypothesis that larger silicone oil droplets might be fragmented into smaller ones by shear forces inside the microchannels and capillaries of the RMM system. This would result in an

increased number of smaller silicone oil droplets in RMM. Our hypothesis was supported by MFI data from a sample containing only silicone oil, which was analyzed before RMM and collected after an RMM measurement. In this case, an increase in silicone oil droplet concentration between 1 and 2 μm with a concomitant decrease above 2 μm was observed when comparing particle concentrations before and after the RMM measurement (Figure 3-7A). It could be shown that this was clearly an effect of the RMM measurement itself and not of the dilution of the sample during the RMM measurement (Figure 3-7B). A decreased flow rate during sample analysis might reduce this fragmentation effect but would further increase the already long measurement time of RMM.

(ii) Additionally, small particles near the detection limit of MFI could be “overlooked” by the software, as suggested also by others,⁴⁰ further enhancing the differences between MFI and RMM for small (1 μm) silicone oil droplet counts.

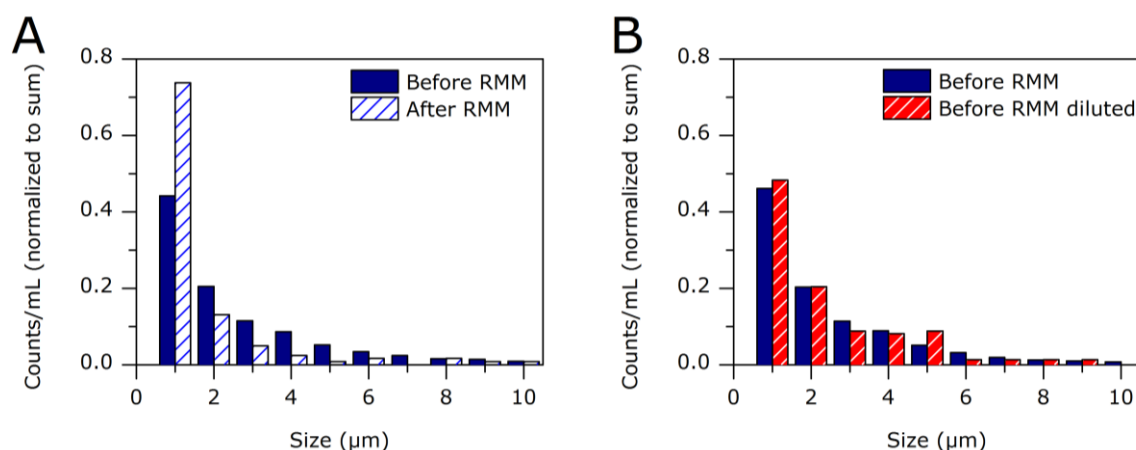


Figure 3-7: Differential size distribution of a sample containing only silicone oil droplets (0.04% (w/v)) analyzed by MFI (A) before RMM and collected after RMM analysis and (B) before and after dilution according to the dilution factor of 218 of the sample during RMM analysis. Counts were normalized to the total particle count.

In contrast to the results from silicone oil samples, RMM detected consistently less protein particles than MFI in individual samples over the entire 1 to 4 μm size range (Figure 3-6B). This was also observed in another study by our group.⁴¹ This difference is suggested to occur for two reasons:

(i) MFI and RMM apply fundamentally different measurement principles (Figure 3-8): MFI captures 2D microscopic particle images (Figure 3-8A) and size determination of particles by MFI is performed according to their spatial dimension on the images defined by the outer boundary of the particle. The differentiation of protein particles and silicone oil droplets is based on morphological parameters such as particle shape and transparency. In contrast, RMM detects particles as distinct positive or negative peaks in the frequency trace caused by the physical parameter of particle buoyancy (Figure 3-8B). However, protein particles may vary in density and contain substantial amounts of liquid.⁴² This is not included into the size calculation by RMM, causing a potential underestimation of particle sizes in RMM as compared to MFI, which includes liquid inside the particle in the size calculation. This in turn would lead to an apparent shift of the complete particle size distribution in RMM towards smaller particle sizes resulting in lower concentrations detected for the respective size bins in RMM as compared to MFI.

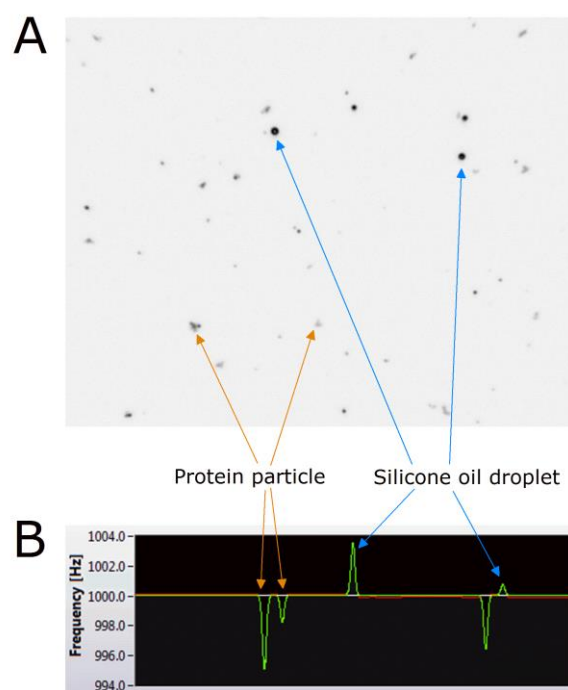


Figure 3-8: Raw data of an exemplary mixed sample containing protein particles (heat-stressed rituximab) and silicone oil droplets from (A) MFI (image-based discrimination) and (B) RMM (frequency-based discrimination).

(ii) As a second reason, the micron-sized capillaries and channels of the RMM sensor are vulnerable to clogging by particles at or above the upper size limit of the system. Even though RMM offers several tools to remove stuck particles, clogging cannot always be avoided. Thus, large stuck particles could hinder other particles from reaching the sensor. This could explain why the concentration discrepancy between RMM and MFI is more pronounced at larger particle sizes, because smaller particles will pass a clogged site more easily, whereas larger particles, although still in the measurement range, are more likely to be excluded from the analysis. Altogether, this will result in lower apparent protein particle concentrations in RMM. A possible solution would be sample preparation for highly aggregated samples, e.g. filtration or centrifugation, which can however potentially change sample properties.

Total particle concentrations for mixed samples containing both silicone oil droplets and protein particles also revealed slight differences between MFI and RMM for the overlapping size range of 1 to 4 μm (Figure 3-6C). For moderate ratios (silicone oil droplets/protein particles 40:60 based on MFI shown as a representative sample), RMM detected less particles than MFI, likely due to the underestimation of protein particles as described before. However, in mixed samples of higher silicone oil content (silicone oil droplets/protein particles 80:20 or 95:5 based on MFI) similar concentrations were determined by the two techniques. In those samples, the overestimation of silicone oil droplets by RMM was balanced out by the underestimation of protein particles by RMM leading to similar total particle counts in MFI and RMM. For all samples, RMM showed higher standard deviations than MFI. This is probably mainly due to the small analyzed volume in RMM (about 0.15 μL) as compared to MFI (about 35 μL).

It was further investigated whether the presence of both silicone oil droplets and protein particles within the same sample influenced the accuracy of MFI or RMM to determine total particle concentrations. For MFI, the concentration determined for mixed samples of silicone oil droplets and protein particles from heat-stressed rituximab matched very closely the sum of the concentrations determined for the corresponding individual samples (Figure 3-9A). For RMM, the concentration for the mixed sample reasonably matched the sum of the individual samples for the main size classes (Figure 3-9B). These observations were consistent for different

ratios and also for protein particles from stir-stressed rituximab mixed with silicone oil droplets. This justified the use of particle counts of individual samples as the theoretical concentrations for mixed samples.

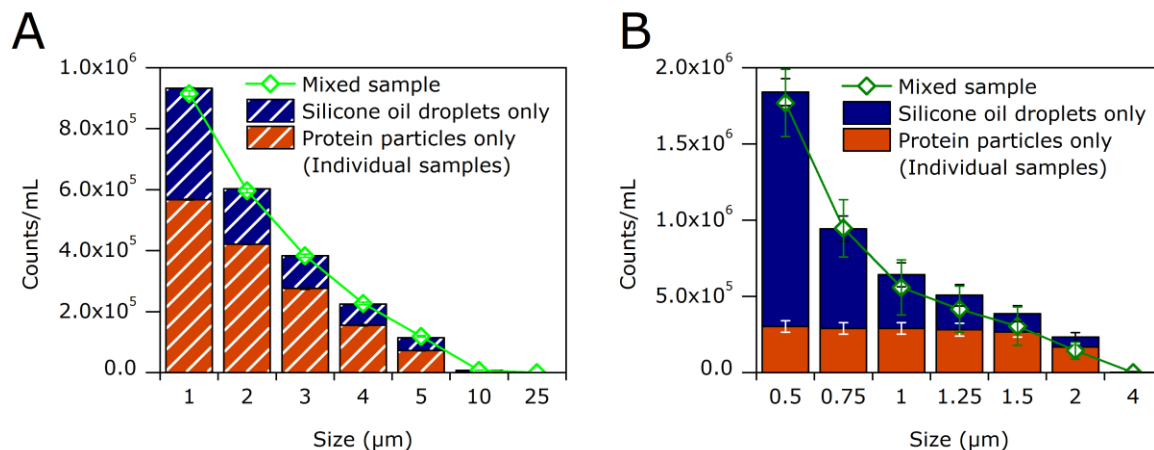


Figure 3-9: Cumulative size distributions in individual samples of silicone oil droplets and protein particles (heat-stressed rituximab) and the corresponding mixture analyzed by (A) MFI and (B) RMM. Error bars represent standard deviations from triplicate measurements.

3.3 Discrimination between silicone oil droplets and protein particles

The discrimination between silicone oil droplets and protein particles by MFI and RMM is based on clearly different mechanisms (see above and Figure 3-8). The optical discrimination by MFI bears the potential risk of false classification due to optically similar silicone oil droplets and protein particles in the lower size range, especially near the detection limit. In contrast, the discrimination by RMM based on the physical parameter of particle buoyancy enables a clear discrimination with minimal risk of false classification. In this case, the difference in density between silicone oil droplets and protein particles is beneficial.

3.3.1 Discrimination between droplets and particles by MFI

In the present paper, the performance of MFI was assessed using the built-in software solution “find similar” and a customized data filter developed specifically for this study. To evaluate the reliability of our customized filter, the following

control experiments were performed: the filter was applied on samples containing only silicone oil droplets and the number of objects falsely marked as protein particles was determined and vice versa. Our customized filter marked less than 3% of the counts in the samples containing only silicone oil droplets (3×10^5 particles/mL $> 1 \mu\text{m}$ based on MFI) falsely as protein particles ($> 2 \mu\text{m}$) and less than 8% of the counts in the samples containing only protein particles (4×10^5 particles/mL $> 1 \mu\text{m}$ based on MFI) falsely as silicone oil droplets ($> 2 \mu\text{m}$). These controls illustrate the capability of our filter to properly discriminate protein particles and silicone oil droplets. The requirement that all four criteria of particle parameters need to be fulfilled at the same time is the main difference of our filter compared to the filter previously developed by Strehl *et al.*³¹, which used the product of four particle parameters as criterion for particle classification. In this case, extreme values in one parameter could shift the product to the side of one particle type although the other three parameters would classify it clearly as the other particle type. Thus, their filter led to errors of 10% to 12% ($> 2 \mu\text{m}$) for silicone oil droplets classified falsely as protein particles; the error for protein particles classified falsely as silicone oil droplets depended strongly on the type of protein particles and varied between 2% and 42% in their study.³¹ In contrast, our filter applies more strict criteria for silicone oil droplet identification as particles fulfilling only three out of four criteria are not marked as silicone oil droplets leading to lower errors as discussed above. However, for protein particles generated from a different monoclonal IgG (influximab) by heat stress or stir stress the customized filter marked up to 40% ($> 2 \mu\text{m}$) falsely as silicone oil droplets. This was most likely due to the lower intensity (lower transparency) of particle images of this IgG, which makes a misclassification as silicone oil droplets of similarly low transparency more likely. This is in agreement with the literature, where large variations were also observed by Strehl *et al.*³¹ when their filter was applied to different types of protein particles. The MVAS software filter could not be tested on these protein samples as it was based on manual selection of silicone oil droplet images which were not present in these pure protein samples.

The “find similar” operation of the MVAS software as well as the customized filter were both used to categorize particles from mixed samples into silicone oil droplets and non-silicone oil particles. Non-silicone oil particles were defined as

protein particles in our case. The obtained concentrations were compared to the theoretical concentrations based on the analysis of the individual samples, which were used to assess the accuracy of both methods (Figure 3-10A,C, Figure 3-11). For moderate droplet/particle number ratios from 30:70 to 70:30 based on MFI, both the selection by “find similar” and the customized filter were able to determine the correct concentrations within acceptable deviations for particles $> 2 \mu\text{m}$. This was observed for samples containing silicone oil droplets and protein particles from heat-stressed rituximab (Figure 3-10A exemplarily shows the results for a sample with a droplet/particle ratio of 40:60 based on MFI). For stir-stressed rituximab (Figure 3-10C) the customized filter for MFI showed superior discrimination compared to the “find similar” method for particles $> 2 \mu\text{m}$, even though the customized filter was designed based on heat-stressed rituximab particles. The even higher intensity of MFI particle images of stir-stressed rituximab compared to those of heat-stressed rituximab (Figure 3-3) likely contributes to this: since three out of four parameters of the customized filter are based on the particle intensity, it facilitates discrimination from the lower intensity silicone oil droplets. Furthermore, the customized filter was superior for samples with more extreme droplet/particle number ratios (see Figure 3-11A, B for representative examples) and for samples based on original, undiluted rituximab solution (Figure 3-11C).

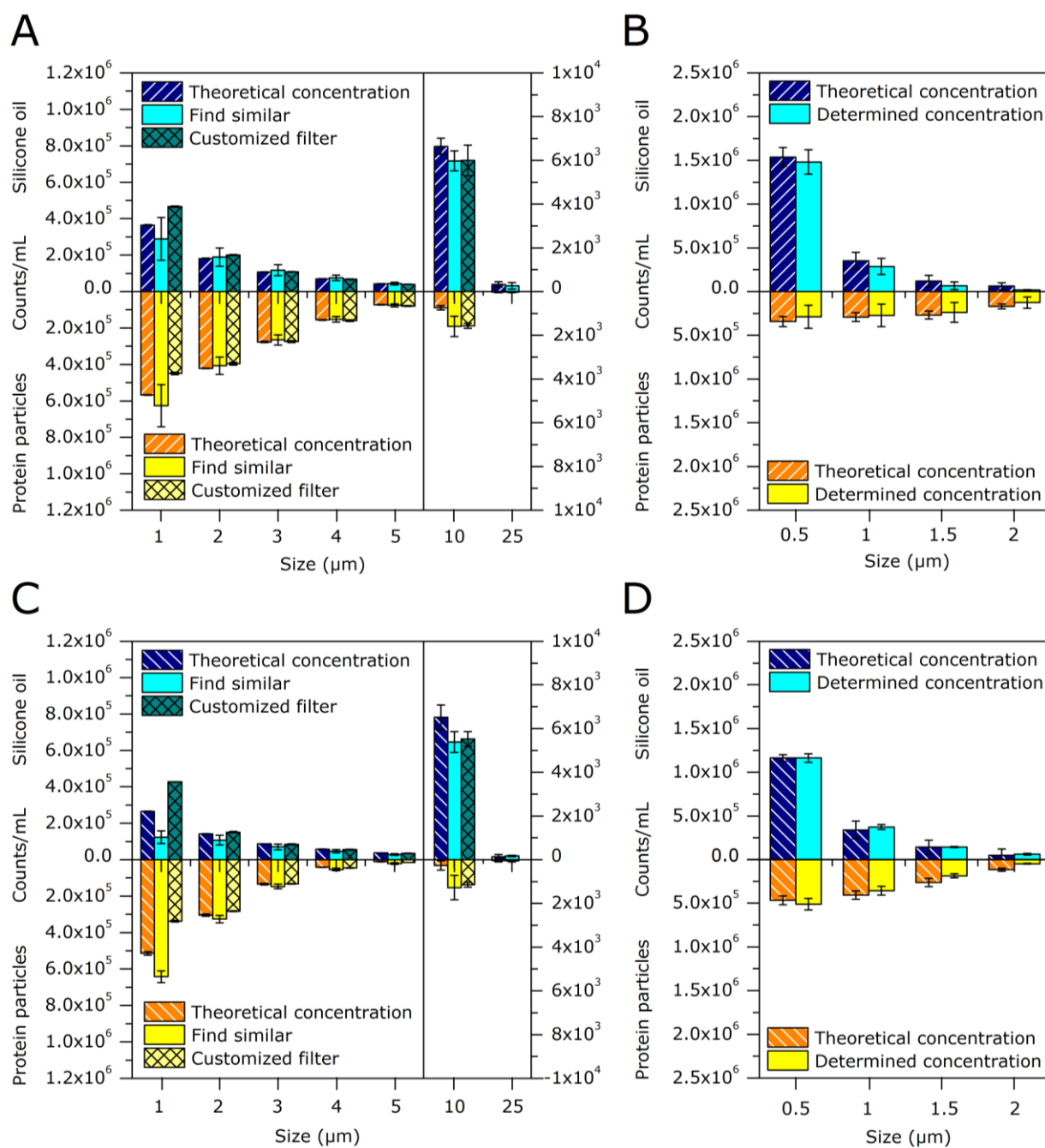


Figure 3-10: Results from MFI (A and C) or RMM (B and D) for the discrimination between silicone oil droplets and protein particles. Histograms comparing the theoretical concentrations (based on individual samples) and determined concentrations of silicone oil droplets and protein particles (A and B, heat-stressed rituximab; C and D, stir-stressed rituximab) in mixed samples with moderate ratios (droplet-particle ratio 40:60 based on MFI). Error bars represent standard deviations from triplicate measurements.

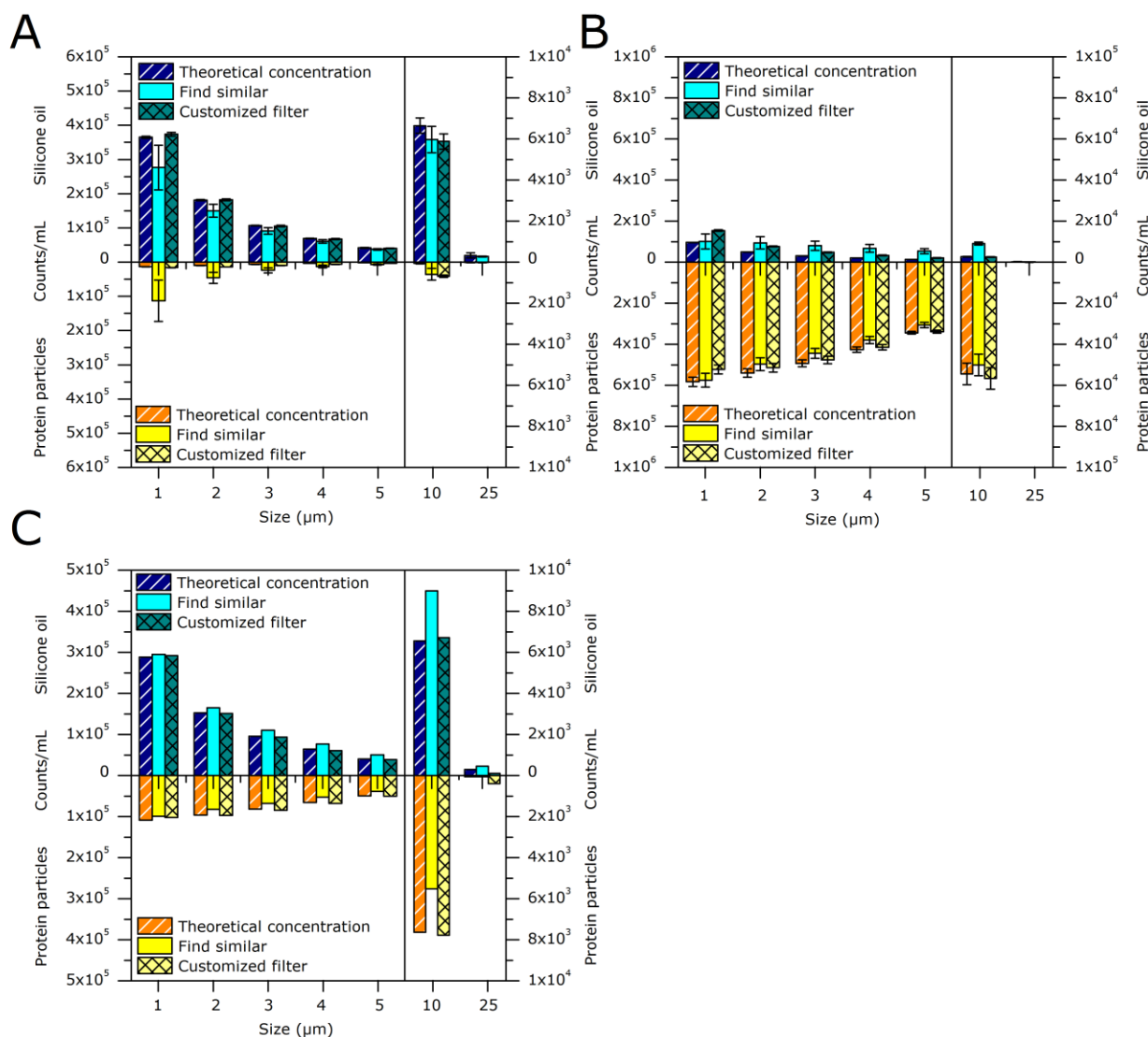


Figure 3-11: MFI cumulative counts comparing theoretical concentrations (based on individual samples) and determined concentrations of silicone oil droplets and protein particles (heat-stressed rituximab) in droplet/particle ratios of (A) 95:5 and (B) 15:85 in samples containing 0.5 mg/mL rituximab as well as (C) 60:40 in a sample containing undiluted rituximab (10 mg/mL). Error bars (A and B) represent standard deviations from triplicate measurements.

Thus, for particles between 2 μm and 25 μm , the development of a customized filter is useful for an accurate discrimination by MFI. For particles with a size below 2 μm , discrimination by an alternative method is recommended (e.g. RMM, as discussed later) as both “find similar” and the customized filter were not reliably capable of determining the correct concentration. For particles larger than 25 μm , due to usually low particle numbers in this size range, manual classification of the MFI images might be preferred over the built-in software

solution or a customized filter. Those particles can usually be identified easily by visual evaluation of the images.

3.3.2 Discrimination between droplets and particles by RMM

As described for MFI, RMM was evaluated with respect to an accurate discrimination between silicone oil droplets and protein particles in mixed samples (Figure 3-10B,D, Figure 3-12). For moderate particle/droplet ratios, RMM was consistently able to discriminate particles correctly with small deviations from the theoretical concentrations for heat-stressed (Figure 3-10B) and stir-stressed rituximab (Figure 3-10D). Large deviations of 20% or more from the theoretical concentration were only observed if the discrimination was based on less than 50 counted particles (corresponding in this case to total concentrations (droplets + particles) $< 3 \times 10^5$ particles/mL) and thus statistical representation of the sample population was limited. This was for example the case for particles larger than $2 \mu\text{m}$ (Figure 3-10B,D). Increasing the analyzed sample volume would compensate for the limited reliability of RMM to quantify low particle concentrations, as also reported by others.³⁵ However, it needs to be considered that very long measurement times associated with large analyzed volumes could also provoke changes in sample properties. In contrast, fairly high concentrations of protein particles $> 2 \times 10^6$ particles/mL caused high standard deviations potentially due to the increased probability of coinciding particles and also blockage of the channel by particles (Figure 3-12A). However, extreme droplet/particle ratios with high amounts of silicone oil droplets provided moderate standard deviations and also fairly accurate determination of the theoretical concentration (Figure 3-12B exemplarily displays results for a droplet/particle ratio of 95:5 based on RMM). Those results provide evidence that RMM discrimination is reliable for particles below $2 \mu\text{m}$.

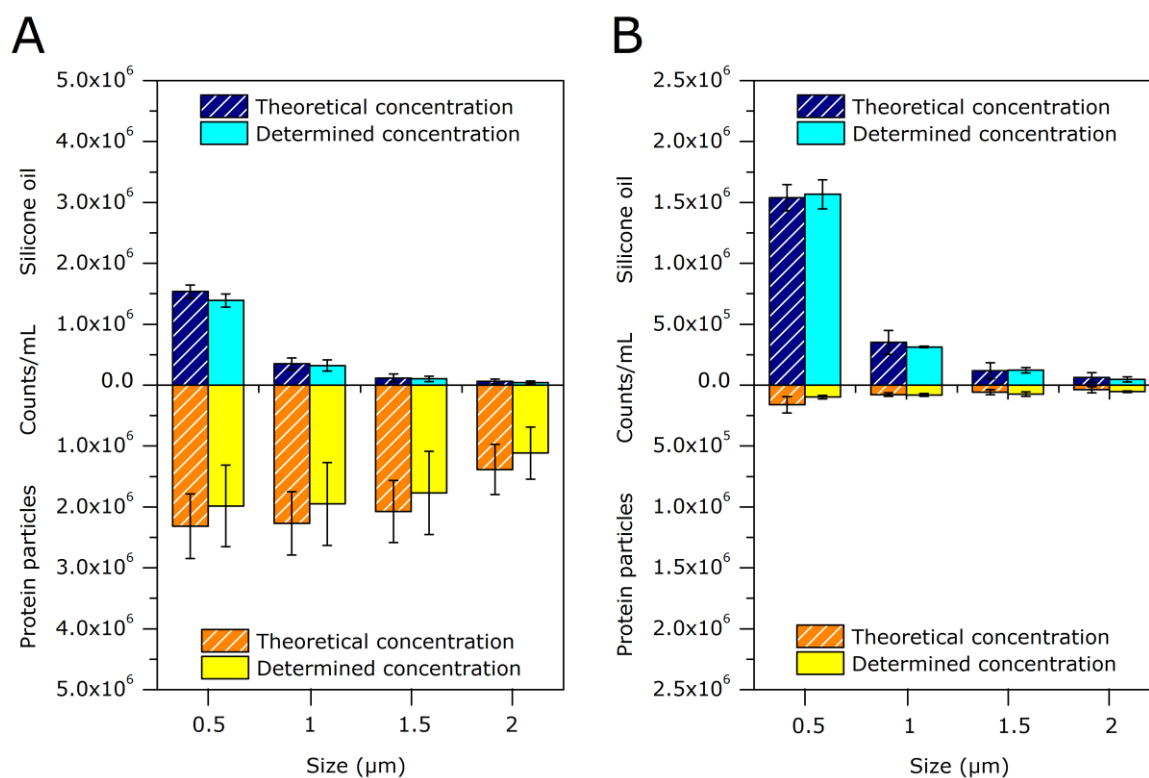


Figure 3-12: RMM cumulative counts comparing theoretical concentrations (based on individual samples) and determined concentrations of silicone oil droplets and protein particles (heat-stressed rituximab) in droplet/particle ratios of (A) 40:60 and (B) 95:5. Error bars represent standard deviations from triplicate measurements.

3.4 Comparison of results for MFI and RMM

For a final evaluation of MFI and RMM regarding the discrimination of silicone oil droplets and protein particles, results for the same sample were compared between the two techniques. For silicone oil droplets and heat-stressed rituximab (Figure 3-10A,B, droplet/particle ratio 40:60) as well as stir-stressed rituximab (Figure 3-10C,D, droplet/particle ratio 40:60), RMM detected a higher fraction of silicone oil droplets as compared to MFI for the sizes above 1 μm already in the individual samples. This originated foremost from the differences in total concentration determination as discussed earlier: RMM detected in general more silicone oil droplets than MFI, whereas MFI detected in general more protein particles than RMM (see also Figure 3-6). However, in this size range, RMM results for the mixed samples are considered more reliable as RMM differentiation was shown to be highly accurate (Figure 3-10B,D). MFI differentiation suffered from low image resolution in the lower size range leading to large deviations for

both the “find similar” operation and the customized filter (Figure 3-10A,C). With increasing particle size, the ratios between MFI and RMM in the individual samples converged and similar ratios for individual samples were obtained for particles $> 2 \mu\text{m}$ (Figure 3-10A,B shows a droplet/particle ratio of 30:70 for particles $> 2 \mu\text{m}$ in individual samples for both MFI and RMM). For mixed samples, the concentration obtained by MFI is suggested to be more reliable for sizes above $2 \mu\text{m}$ as the discrimination between droplets and particles was highly accurate, especially when the customized filter was applied (Figure 3-10A,C). RMM analysis of objects with a size above $2 \mu\text{m}$ was based on small numbers of counts, questioning the reliability of the determined concentrations (Figure 3-10B,D) in our study.

4 Recommendations and conclusions

Table 3-2 summarizes properties as well as pros and cons during the application of MFI and RMM which were identified in our study. For MFI, the customized filter was shown to provide correct results for moderate and extreme ratios between silicone oil droplets and protein particles. The filter was developed using heat-stressed rituximab particles, but was also found applicable for rituximab particles generated by stir stress and for samples containing rituximab solution in high concentrations (10 mg/mL). In contrast, the application for infliximab particles generated by either heat or stir stress resulted in large errors. These results emphasize the necessity of customizing the filter to each specific protein, the formulation, and the particle type / stress method of interest. Thus, the development of a customized filter for quality control of protein therapeutics in prefilled syringes with comparable manufacturing conditions can be considered reasonable. In contrast, the implementation during formulation development with varying conditions should be critically evaluated case by case. The separation by the MVAS software was acceptably accurate especially for moderate ratios of silicone oil droplets and protein particles. It could still be applied in those cases, when costs and time for the development of a customized filter would exceed the benefit of a more accurate discrimination. However, the differentiation by “find similar” showed clearly higher standard deviations as compared to the customized filter. This higher variation of the “find similar” operation originated most likely from the underlying sample and operator dependent manual selection of the particle images. For both MFI-based solutions it is important to consider that the separation is based on the identification of silicone oil droplets, whereas the remaining particles, identified only as “non-silicone oil particles”, are simply equated with protein particles by the operator.

Table 3-2: Summarizing comparison of MFI and RMM for the analysis of silicone oil droplets and protein particles.

	MFI (MFI4100, HighMag settings)	RMM (Archimedes, Micro sensor)
Properties of the techniques		
Principle	Flow imaging microscopy with digital image analysis Sizing based on optical particle boundary	Mass determination by quantification of frequency shift Sizing based on particle density
Size range	1-70 μm	0.3-4 μm
Differentiation of protein particles and silicone oil droplets	Based on morphological parameters (shape, transparency...) of particle images Differentiation may be time-consuming (esp. development of customized filter)	Based on particle buoyancy (density) Differentiation during the measurement without additional time consumption
Concentration range	Up to 1×10^6 particles/mL (coincidence not indicated by the system)	3×10^5 to 1×10^7 particles/mL (coincidence indicated by the system)
Reproducibility	Higher reproducibility	Lower reproducibility (due to lower analyzed volume)
Status of the technique	Established R&D and cGMP technique	Novel R&D technique
Pros and Cons during application		
Protein particles	Clear visualization of larger particles	Clogging by larger particles possible
Silicone oil droplets	Detection of larger droplets without fragmentation	Fragmentation of larger droplets possible
Samples containing protein particles and silicone oil droplets	2-10 μm : good differentiation by built-in software filter or (preferably) customized filter >10 μm : easy identification by visual evaluation of particle images	0.5-2 μm : unambiguous differentiation due to physical detection principle
Complexes of protein particles and silicone oil droplets	Potential identification of larger complexes (> about 5-10 μm)	Potential misclassification, miscalculation of particle size or no detection
More than one particle type of higher density (e.g. protein and rubber, steel, glass)	Potential differentiation according to optical appearance (refractive index or shape)	No differentiation possible

For RMM, the discrimination was very accurate for different types of protein particles and different ratios as long as sufficiently high numbers of particles were detected. The high accuracy of RMM is due to the straightforward categorization of particles and droplets according to buoyant mass. This makes

RMM a very robust technique for exactly this task. It needs to be considered that RMM can only discriminate one type of positively buoyant from one type of negatively buoyant particles. Thus, if a sample contains protein particles as well as other particles of higher density than the buffer, e.g. particles shed from filling pumps or rubber stoppers, RMM is not able to discriminate them. Here, methods such as SEM-EDS, FT-IR or Raman microscopy⁴³ could be used as orthogonal methods to further identify these “non-silicone oil” particles. Furthermore, complexes consisting of both protein and silicone oil can pose a challenge for the technique of RMM: The reported size of those complexes may be incorrect due to the simultaneous influence of both material densities on the density of the complex. As a worst case the complexes might be missed entirely as the higher density of protein is compensated by the lower density of silicone oil, eliminating a clear density difference between particle and formulation. Those complexes might be detectable by MFI (given that they are large enough) as shown for an IgG particle containing silicone oil.²² In our study, only very few of those complexes were observed in MFI, because protein particles and silicone oil droplets were prepared separately to avoid interactions of protein and silicone oil during the particle formation process.

Taken together, the robust detection principle of RMM has brought significant benefit to the field of protein product characterization, especially for the discrimination of silicone oil droplets and protein particles. RMM differentiation is recommended for particles below 2 μm , provided that sufficient particle quantities are detected. MFI differentiation is recommended above 2 μm , preferably using a customized filter. In order to cover a size range as broad as possible, both techniques should be applied in parallel for a comprehensive analysis of samples potentially containing silicone oil droplets and protein particles in the size range from 500 nm to 70 μm .

5 References

1. Narhi LO, Schmit J, Bechtold-Peters K, Sharma D 2012. Classification of protein aggregates. *J Pharm Sci* 101:493-498.
2. Carpenter J, Cherney B, Lubinecki A, Ma S, Marszal E, Mire-Sluis A, Nikolai T, Novak J, Ragheb J, Simak J 2010. Meeting report on protein particles and immunogenicity of therapeutic proteins: filling in the gaps in risk evaluation and mitigation. *Biologicals* 38:602-611.
3. Rosenberg AS 2006. Effects of protein aggregates: an immunologic perspective. *AAPS J* 8:E501-507.
4. Chi EY, Krishnan S, Randolph TW, Carpenter JF 2003. Physical stability of proteins in aqueous solution: mechanism and driving forces in nonnative protein aggregation. *Pharm Res* 20:1325-1336.
5. USP<788>, United States Pharmacopeia, USP35-NF30. 2012. Particulate matter in injections. United States Pharmacopeial convention.
6. Ph.Eur. 2.9.19, Pharmacopoea europaea, 7th ed. 2010. Particulate contamination: Sub-visible particles. European Directorate For The Quality Of Medicine (EDQM).
7. Kirshner S 2012. Regulatory expectations for analysis of aggregates and particles. Talk at Workshop on Protein Aggregation and Immunogenicity, Breckenridge, Colorado, 07/12/2012.
8. Kerwin BA, Akers MJ, Apostol I, Moore-Einsel C, Etter JE, Hess E, Lippincott J, Levine J, Mathews AJ, Revilla-Sharp P, Schubert R, Looker DL 1999. Acute and long-term stability studies of deoxy hemoglobin and characterization of ascorbate-induced modifications. *J Pharm Sci* 88:79-88.
9. Hawe A, Friess W 2007. Stabilization of a hydrophobic recombinant cytokine by human serum albumin. *J Pharm Sci* 96:2987-2999.
10. Tyagi AK, Randolph TW, Dong A, Maloney KM, Hitscherich C, Carpenter JF 2009. IgG particle formation during filling pump operation: a case study of heterogeneous nucleation on stainless steel nanoparticles. *J Pharm Sci* 98:94-104.
11. Freund KB, Laud K, Eandi CM, Spaide RF 2006. Silicone oil droplets following intravitreal injection. *Retina* 26:701-703.
12. Chantelau E, Berger M 1985. Pollution of insulin with silicone oil, a hazard of disposable plastic syringes. *The Lancet* June:1459.
13. Chantelau E, Berger M, Böhken B 1986. Silicone oil released from disposable insulin syringes. *Diabetes Care* 9:672-673.
14. Barnard JG, Babcock K, Carpenter JF 2012. Characterization and Quantitation of Aggregates and Particles in Interferon- β Products : Potential Links Between Product Quality Attributes and Immunogenicity. *J Pharm Sci* 102:915-928.
15. Felsovalyi F, Janvier S, Soukiassian H, Mangiagalli P 2012. Silicone-oil-based subvisible particles: Their detection, interactions, and regulation in prefilled container closure systems for biopharmaceuticals. *J Pharm Sci* 101:4569-4583.
16. Thirumangalathu R, Krishnan S, Ricci MS, Brems DN, Randolph TW, Carpenter JF 2009. Silicone oil- and agitation-induced aggregation of a monoclonal antibody in aqueous solution. *J Pharm Sci* 98:3167-3181.
17. Jones LS, Kaufmann A, Middaugh CR 2005. Silicone oil induced aggregation of proteins. *J Pharm Sci* 94:918-927.
18. Ludwig DB, Carpenter JF, Hamel J-B, Randolph TW 2010. Protein adsorption and excipient effects on kinetic stability of silicone oil emulsions. *J Pharm Sci* 99:1721-1733.
19. Britt KA, Schwartz DK, Wurth C, Mahler H-C, Carpenter JF, Randolph TW 2012. Excipient effects on humanized monoclonal antibody interactions with silicone oil emulsions. *J Pharm Sci* 101:4419-4432.
20. Kossovsky N, Heggors JP, Robson MC 1987. Experimental demonstration of the immunogenicity of silicone-protein complexes. *J Biomed Mater* 21:1125-1133.
21. Zöls S, Tantipolphan R, Wiggenghorn M, Winter G, Jiskoot W, Friess W, Hawe A 2012. Particles in therapeutic protein formulations, Part 1: Overview of analytical methods. *J Pharm Sci* 101:914-935.
22. Wuchner K, Büchler J, Spycher R, Dalmonte P, Volkin DB 2010. Development of a microflow digital imaging assay to characterize protein particulates during storage of a high concentration IgG1 monoclonal antibody formulation. *J Pharm Sci* 99:3343-3361.

23. Lankers M, Munhall J, Valet O 2008. Differentiation between foreign particulate matter and silicone oil induced protein aggregation in drug solutions by automated raman spectroscopy. *Microscopy and Microanalysis* 14:1612-1613.
24. Fraunhofer W, Winter G 2004. The use of asymmetrical flow field-flow fractionation in pharmaceuticals and biopharmaceuticals. *Eur J Pharm Biopharm* 58:369-383.
25. Ludwig DB, Trotter JT, Gabrielson JP, Carpenter JF, Randolph TW 2011. Flow cytometry: a promising technique for the study of silicone oil-induced particulate formation in protein formulations. *Anal Biochem* 410:191-199.
26. Sharma DK, King D, Oma P, Merchant C 2010. Micro-flow imaging: flow microscopy applied to sub-visible particulate analysis in protein formulations. *AAPS J* 12:455-464.
27. Sharma DK, Oma P, Pollo MJ, Sukumar M 2010. Quantification and characterization of subvisible proteinaceous particles in opalescent mAb formulations using micro-flow imaging. *J Pharm Sci* 99:2628-2642.
28. Demeule B, Messick S, Shire SJ, Liu J 2010. Characterization of particles in protein solutions: reaching the limits of current technologies. *AAPS J* 12:708-715.
29. Liu L, Ammar DA, Ross LA, Mandava N, Kahook MY, Carpenter JF 2011. Silicone oil microdroplets and protein aggregates in repackaged bevacizumab and ranibizumab: effects of long-term storage and product mishandling. *IOVS* 52:1023-1034.
30. Sharma D, Oma P, Krishnan S 2009. Silicone Microdroplets in Protein Formulations - Detection and Enumeration. *Pharm Tech* 33:74-79.
31. Strehl R, Rombach-Riegraf V, Diez M, Egodage K, Bluemel M, Jeschke M, Koulov AV 2012. Discrimination between silicone oil droplets and protein aggregates in biopharmaceuticals: a novel multiparametric image filter for sub-visible particles in microflow imaging analysis. *Pharm Res* 29:594-602.
32. Burg TP, Godin M, Knudsen SM, Shen W, Carlson G, Foster JS, Babcock K, Manalis SR 2007. Weighing of biomolecules, single cells and single nanoparticles in fluid. *Nature* 446:1066-1069.
33. Dextras P, Burg TP, Manalis SR 2009. Integrated measurement of the mass and surface charge of discrete microparticles using a suspended microchannel resonator. *Anal Chem* 81:4517-4523.
34. Rosenberg AS, Verthelyi D, Cherney BW 2012. Managing uncertainty: A perspective on risk pertaining to product quality attributes as they bear on immunogenicity of therapeutic proteins. *J Pharm Sci* 101:3560-3567.
35. Patel AR, Lau D, Liu J 2012. Quantification and characterization of micrometer and submicrometer subvisible particles in protein therapeutics by use of a suspended microchannel resonator. *Anal Chem* 84:6833-6840.
36. Ph.Eur. 3.1.8, Pharmacopoea europaea, 7th ed. 2010. Silicone oil used as a lubricant. European Directorate For The Quality Of Medicine (EDQM).
37. Fischer H, Polikarpov I, Craievich AF 2004. Average protein density is a molecular-weight-dependent function. *Protein Sci* 13:2825-2828.
38. Majumdar S, Ford BM, Mar KD, Sullivan VJ, Ulrich RG, D'souza AJM 2011. Evaluation of the effect of syringe surfaces on protein formulations. *J Pharm Sci* 100:2563-2573.
39. Chantelau E 1989. Silicone oil contamination of insulin. *Diabetic Med* 6:278.
40. Pedersen JS 2012. Statistical evaluation of MFI dataset quality for high-throughput analysis. Talk at Protein Simple User Meeting, Basle, Switzerland, 07/04/2012.
41. Zöls S, Gregoritz M, Tantipolphan R, Wiggenhorn M, Winter G, Friess W, Hawe A 2013. How subvisible particles become invisible - Relevance of the refractive index for protein particle analysis. *J Pharm Sci* 102:1434-1446.
42. Ripple DC, Wayment JR, Carrier MJ 2011. Standards for the optical detection of protein particles. *APR (July/August)*:90-96.
43. Cao X, Masatani P, Torraca G, Wen Z-Q 2010. Identification of a mixed microparticle by combined microspectroscopic techniques: a real forensic case study in the biopharmaceutical industry. *Appl Spectrosc* 64:895-900.

Chapter 4

Flow imaging microscopy for protein particle analysis – a comparative evaluation of four different analytical instruments

Abstract

Flow imaging microscopy was introduced as a technique for protein particle analysis a few years ago and has strongly gained in importance ever since. The aim of the present study was a comparative evaluation of four of the most relevant flow imaging microscopy systems for biopharmaceuticals on the market: MFI4100, MFI5200, FlowCAM VS1, and FlowCAM PV. The performance was critically assessed regarding particle quantification, characterization, image quality, differentiation of protein particles and silicone oil droplets, and handling of the systems. The FlowCAM systems, especially the FlowCAM VS1, showed high resolution images. The FlowCAM PV system provided the most precise quantification of particles of therapeutic monoclonal antibodies, also under impaired optical conditions by an increased refractive index of the formulation, and furthermore, the most accurate differentiation of protein particles and silicone oil droplets could be achieved with this instrument. The MFI systems provided excellent size and count accuracy (evaluated with polystyrene standards), especially the MFI5200 system. This instrument also showed very good performance for protein particles, also in case of an increased refractive index of the formulation. Both MFI systems were easier to use and appeared more standardized regarding measurement and data analysis as compared to the FlowCAM systems. Our study shows that the selection of the appropriate flow imaging microscopy system depends strongly on the main output parameters of interest and it is recommended to decide based on the intended application.

The following chapter was accepted for publication as a research article in The AAPS Journal:

S. Zölls, D. Weinbuch*, M. Wiggerhorn, G. Winter, W. Friess, W. Jiskoot, A. Hawe: "Flow imaging microscopy for protein particle analysis – a comparative evaluation of four different analytical instruments"; The AAPS Journal (accepted); *joint first authors*

1 Introduction

Protein aggregates and particles are important quality attributes of therapeutic protein formulations.¹⁻³ Especially micron sized aggregates (subvisible protein particles)⁴ are considered as critical due to their potential risk of enhancing an immunogenic response.⁵ Quantification of (not necessarily proteinaceous) subvisible particles larger than 10 μm and 25 μm in parenterals is required by the pharmacopoeias, and is commonly performed using light obscuration (LO) techniques.^{6,7} For therapeutic protein products regulatory agencies increasingly ask for quantification and characterization of particles with a size below 10 μm by an orthogonal approach.^{8,9} Furthermore, the availability of an increasing number of emerging techniques^{10,11} extends the spectrum of particle analysis tools and enables a more detailed characterization of the particles counted. These factors inspired the development of a new educational chapter USP<1787> entitled "Measurement of Subvisible Particulate Matter in Therapeutic Protein Injections".¹² It is currently being discussed whether this chapter should include particle analysis starting already from 2 μm as well as the use of additional techniques, such as flow imaging microscopy. Flow imaging microscopy has already been used extensively in research and development¹³⁻¹⁹ and more recently also for quality control/routine testing (own experiences).

Flow imaging microscopy uses a CCD camera with high magnification to capture images of the sample solution passing a thin flow cell. The flow cell is illuminated and particles with a different refractive index (RI) than the solution decrease the light intensity compared to the background and can be detected on the captured images.^{20,21} Particle size and count information is then generated based on image analysis. Besides quantification, the digital particle images allow for subsequent morphological characterization including size, shape and optical parameters. This, however, requires sufficiently high image quality to draw reliable conclusions.²¹ A prominent application example is the differentiation of silicone oil droplets and protein particles in prefilled syringes and cartridges. For this approach, flow imaging microscopy has been successfully applied in several studies.²²⁻²⁴ In general, flow imaging microscopy tends to be more sensitive than LO for small transparent protein particles and therefore usually detects higher particle numbers.^{13,15,25} An increased RI of the formulation, leading to a

decreased RI difference between particles and formulation, can impede a correct detection of protein particles by light-based techniques. Compared to LO, MFI was shown to be slightly more robust against such a decreased RI difference.^{13,26}

There are several flow imaging microscopy instruments available on the market provided by different suppliers. Those are, for example, Sysmex Flow Particle Image Analyzer (FPIA) 3000 by Malvern Instruments (Worcestershire, UK), various Occhio Flowcell systems by Occhio (Angleur, Belgium), the MicroFlow Particle Sizing System by JM Canty (Buffalo, NY), several Micro-Flow Imaging (MFI) systems by Protein Simple (Santa Clara, CA), and various Flow Cytometer And Microscope (FlowCAM) systems by Fluid Imaging (Yarmouth, ME). In this study, MFI and FlowCAM systems with different settings were evaluated (Table 4-1). Both systems are often used for the analysis of subvisible particles in research and development and partly also for routine testing in a QC environment. A short general article about the handling of MFI and FlowCAM is available,²⁷ but no comprehensive report about a direct comparison of the four systems has been published until now.

Here we present the first study thoroughly challenging four of the most relevant flow imaging microscopy systems for biopharmaceuticals on the market: MFI4100 and MFI5200 as well as FlowCAM VS1 and FlowCAM PV. By that we want to provide a basis for the increasing use of such systems in QC and support industry and authorities in their efforts towards new standards in the field of subvisible particle characterization.

Table 4-1: Overview of technical parameters and settings of the systems evaluated in this study.

Parameter	Effect on	MFI4100	MFI5200	FlowCAM VS1	FlowCAM PV
Magnification (combination of camera and lens magnification)	Image resolution	14x	5x	200x	100x
Flow cell depth (depth of field)	Sample volume, flow rate, measurement time	100 µm	100 µm	50 µm	80 µm
Focus adjustment	Size accuracy	By screw driver (supported by software)		By turning knob (evaluated optically) ^a	By manufacturer (not adjustable by user)
Size range	-	0.75 – 70 µm	1 – 70 µm	2 – 50 µm ^b	2 – 80 µm ^b
Flow rate	Sampling efficiency, measurement time	Fixed (0.1 mL/min)	Fixed (0.17 mL/min)	Adjustable (0.005-200 mL/min) ^c (0.07 mL/min in this study)	Adjustable (0.005-20 mL/min) ^c (0.04 mL/min in this study)
Image capture rate		Fixed to maximize efficiency and to minimize image overlaps		Adjustable (1-22 frames/sec) (20 frames/s in this study)	Adjustable (1-22 frames/sec) (21 frames/s in this study)
Sampling efficiency	Statistical relevance of the data	Fixed (5-8%)	Fixed (80-85%)	Adjustable (5-8% in this study)	Adjustable (80-85% in this study)
CFR21 part 11 compatibility	GMP suitability	No	Yes	No	Yes

^a support by software available in the newest generation of the FlowCAM VS1 according to the manufacturer; ^b official size range as indicated by the manufacturer, lower size limit could be extended to 1 µm in this study; ^c depending on the syringe size

2 Materials and methods

2.1 Materials

Infliximab (Remicade[®], lots no. 7GD9301402, 7FD8701601, 7RMKA81402, pooled) and rituximab (MabThera[®], lot no. B6082) were provided by local hospitals. Polystyrene particle standards were purchased from Duke Scientific (through Thermo Scientific, Fremont, CA) and diluted in water for analysis.

Sucrose, sodium hydroxide, di-sodium hydrogenphosphate dihydrate and sodium dihydrogenphosphate dihydrate were purchased from Merck KGaA (Darmstadt, Germany). Sodium chloride, sodium citrate dihydrate and polysorbate 80 were from VWR (Darmstadt, Germany). Silicone oil with a viscosity of 1000 cSt was purchased from Sigma Aldrich (Steinheim, Germany). The water used in this study was highly purified water (Advantage A10 purification system, Millipore, Newark, NJ).

Sucrose solutions were prepared by dilution (w/w) of a 70% (w/w) solution, filtered using a 0.2 µm cellulose acetate syringe filter (Minisart[®], Sartorius Stedim Biotech, Aubagne, France) and air bubbles were removed by centrifugation for 5 minutes at 7,000 g (Centrifuge 5810R, Eppendorf, Hamburg, Germany) prior to use.

2.2 Preparation of protein samples

Rituximab solution at a concentration of 1 mg/mL was prepared by dilution of 10 mg/mL rituximab commercial product in 25 mM citrate buffer (pH 6.5) containing 154 mM NaCl and 0.07% polysorbate 80 (formulation buffer). The formulation was filtered using a 0.2 µm polyethersulfone syringe filter (Sartorius, Göttingen, Germany) and kept at 2-8 °C for a maximum of one week. Heat-stressed rituximab was prepared by incubating 1.5 mL of the 1 mg/mL rituximab solution for 30 minutes at 71 °C in a thermomixer (Eppendorf, Hamburg, Germany). Stressed rituximab at 1 mg/mL (protein particles stock suspension) was stored at 2-8 °C until the measurement.

Infliximab solution at a concentration of 1 mg/mL was prepared by dilution of 10 mg/mL infliximab commercial product in 100 mM phosphate buffer (pH 7.2). The formulation was filtered through a 0.2 µm polyethersulfone syringe filter. Stir-stressed infliximab was prepared by incubating 8 mL of the 1 mg/mL infliximab solution in a 10R glass vial using a 18 mm Teflon[®]-coated stir bar at 250 rpm for 24 hours at room temperature on a magnetic stirrer (MR Hei-Standard, Heidolph, Schwabach, Germany).

For analysis of protein samples, stressed protein solution was diluted in the appropriate buffer (filtered through a 0.22 µm cellulose acetate/nitrate membrane filter, MF-Millipore[®], Millipore), sucrose solution or water.

2.3 Preparation of silicone oil emulsion

Silicone oil was added to filtered formulation buffer in a particle-free 15 mL conical tube to a final concentration of 2% (w/v) to generate an emulsion without additives. After vortexing briefly, silicone oil droplet formation was induced by sonication in a water bath (Sonorex, Brandelin, Berlin, Germany) for 10 min. Fresh silicone oil emulsion (silicone oil droplet stock emulsion) was prepared on the day of the measurement and kept at room temperature.

2.4 Preparation of individual and mixed samples of silicone oil droplets and protein particles

Silicone oil droplet stock emulsion and/or protein particles stock suspension was diluted in unstressed protein solution or filtered formulation buffer for the preparation of mixed and individual samples. Mixed samples were prepared in a number ratio of 10:90 based on particle counts > 2 µm determined by MFI4100. Individual samples were prepared to contain the same number of silicone oil droplets and protein particles, respectively, as in the mixed samples and are referred to as the theoretical concentration. All samples were prepared to a final protein concentration of 0.5 mg/mL rituximab. The samples were gently mixed with a pipette, kept at room temperature and measured on the day of preparation.

2.5 Refractive index determination

Refractive indices of sucrose solutions were determined using an Abbé refractometer (Carl Zeiss, Oberkochen, Germany). Measurements were performed in triplicate at a wavelength of 589 nm at room temperature and the mean value was calculated.

2.6 Light obscuration (LO)

Polystyrene standards were analyzed by LO using a PAMAS SVSS-C (Partikelmess- und Analysesysteme, Rutesheim, Germany) equipped with an HCB-LD-25/25 sensor in order to obtain a reference value for linearity evaluation with polystyrene standards of MFI4100, MFI5200, FlowCAM VS1, and FlowCAM PV. Samples were diluted to a concentration of approx. 10^3 particles/mL as a reference point for the flow imaging microscopy instruments. Three measurements of a volume of 0.3 mL for each sample were performed with a pre-run volume of 0.5 mL at a fixed fill rate, emptying rate and rinse rate of 10 mL/min and the mean particle concentration per mL was reported by the system. Samples were measured in triplicate and mean and standard deviation were calculated.

2.7 Micro-Flow Imaging (MFI)

2.7.1 MFI4100

An MFI4100 system (ProteinSimple) equipped with a 100 μ m flow cell, operated at high magnification (14x) and controlled by the MFI View software version 6.9 was used. The system was flushed with 5 mL purified water at maximum flow rate and flow cell cleanliness was checked visually between measurements. Water, the appropriate sucrose solution, filtered unstressed rituximab formulation (0.5 mg/mL) or the appropriate formulation buffer was used to perform "optimize illumination" prior to each measurement to ensure correct thresholding of the MFI system. Samples of 0.65 mL with a pre-run volume of 0.3 mL were analyzed at a flow rate of 0.1 mL/min and a fixed camera rate (not adjustable by the user) leading to a sampling efficiency of about 5-8%. Samples were measured in triplicate and mean and standard deviation were calculated.

2.7.2 MFI5200

An MFI5200 system (ProteinSimple) equipped with a 100 μm flow cell and controlled by the MFI View System Software (MVSS) version 2-R2.6.1.20.1915 was used. The system was flushed with 10 mL purified water at maximum flow rate and flow cell cleanliness was checked visually between measurements. "Optimize illumination" prior to each measurement was done comparably to MFI4100. Samples of 0.5 mL with a pre-run volume of 0.2 mL were analyzed at a flow rate of 0.17 mL/min and a fixed camera rate (not adjustable by the user) leading to a sampling efficiency of about 80-85%. Samples were measured in triplicate and mean and standard deviation were calculated.

2.7.3 Particle data analysis MFI

For both systems, MFI View Analysis Suite (MVAS) version 1.2 was used for data analysis. Particles stuck to the flow cell wall were only counted once and edge particles were excluded from analysis. Particle size was evaluated as the diameter of a circle with the same projected area as the particle (designated as ECD, equivalent circular diameter, in the MFI software). For the discrimination of silicone oil droplets and protein particles, a minimum of 20 particles (MFI4100) or 50 particles (MFI5200) above 5 μm clearly recognizable as silicone oil droplets was selected for the "find similar" operation in the MVAS software.

2.8 FlowCAM analysis

2.8.1 FlowCAM VS1

A FlowCAM VS1 Benchtop B3 system (Fluid Imaging Technologies) was equipped with a 50 μm single-use cell, a 20x magnification lens and controlled by the VisualSpreadsheet software version 3.1.10. The system was flushed with 1 mL purified water at a flow rate of 0.5 mL/min and flow cell cleanliness was checked visually. 0.5 mL sample solution with a pre-run volume of 0.5 mL (primed manually into the flow cell) was analyzed with a flow rate of 0.07 mL/min and a camera rate of 20 frames/s leading to a sampling efficiency of about 5-8%. Only dark pixels were selected for particle size determination at the preset default threshold value of 20. Particle size was evaluated as the diameter of a circle with the same projected area as the particle (designated as ABD, area based

diameter, in the FlowCAM software). For the discrimination of silicone oil droplets and protein particles, a filter can be developed and the parameters can be saved in the software. However, to ensure comparability with the MFI systems and to represent the analysis of a single sample as good as possible, the selection of silicone oil droplets in this study was performed on a sample-by-sample basis. A minimum of 20 particles above 5 μm clearly recognizable as silicone oil droplets was selected for the "find similar as selected" function. Samples were measured in triplicate and mean and standard deviation were calculated.

2.8.2 FlowCAM PV

A FlowCAM PV-100 Benchtop system (Fluid Imaging Technologies) was equipped with a 80 μm multi-use cell, a 10x magnification lens and controlled by the VisualSpreadsheet software version 3.4.2. The system was flushed with 5x1 mL purified water by the flushing function in the software and flow cell cleanliness was accepted if less 10 particles were counted in 0.02 mL water in the "autoimage mode (no save)". 0.5 mL sample solution with a pre-run volume of 0.2 mL (primed manually into the flow cell) was analyzed with a flow rate of 0.04 mL/min and a camera rate of 21 frames/s leading to a sampling efficiency of about 80-85%. Dark and bright pixels were selected for particle size determination at the preset default threshold value of 30. Particle size was evaluated as the diameter of a circle with the same projected area as the particle (designated as ABD, area based diameter, in the FlowCAM software). For the discrimination of silicone oil droplets and protein particles through the "find similar" operation, a minimum of 100 particles above 5 μm clearly recognizable as silicone oil droplets was selected to generate a library. The complete particle population was filtered by the "find similar as library" function. The resulting particle population was sorted by filter score and particles with filter scores of 0 to 5 (with 0 describing images which the highest match to the images in the library) were defined as silicone oil droplets. This procedure was necessary as the software was not able to perform the same "find similar as selected function" as applied for the FlowCAM VS1 which was probably due to the clearly higher number of particles images captured by the FlowCAM PV. Samples were measured in triplicate and mean and standard deviation were calculated.

2.9 Performance evaluation

Critical performance parameters (e.g. image quality, size accuracy, and several other factors as described below) were ranked relatively within the evaluated systems. The system with the strongest performance for one specific parameter was scored as "4" (++++), the system with the weakest performance in this parameter was scored as "1" (+). In detail, the performance was quantified as follows: The image quality parameters were evaluated by eye. Polystyrene sizing and counting performance was judged with respect to the specifications by the manufacturer (NIST-traceable), linearity was evaluated based on the deviation from the theoretical concentration expected from the dilution factor and the linearity of the obtained concentrations (assessed by the R^2 value). For the robustness towards RI influences, the relative decrease in the measured protein particle concentration in formulations with a higher RI was used for the ranking. The differentiation of silicone oil droplets and protein particles was evaluated based on the match with the theoretical concentration within the system (based on individual samples) and the standard deviation, defined as precision.

3 Results and discussion

3.1 Count and size performance with polystyrene standards

The four systems MFI4100, MFI5200, FlowCAM VS1, and FlowCAM PV were first evaluated regarding their size and count performance with monodisperse certified polystyrene standards. All systems determined the correct concentration of a 5 μm polystyrene count standard with 3000 ± 300 particles/mL $> 3 \mu\text{m}$ (Table 4-2).

Table 4-2: Results of polystyrene standard measurements with MFI4100, MFI5200, FlowCAM VS1, and FlowCAM PV.

Standard type	Specification	MFI4100	MFI5200	FlowCAM VS1	FlowCAM PV
5 μm count standard	3000 ± 300 part./mL ^a	2906 ± 324 part./mL ^c	3203 ± 116 part./mL ^c	2779 ± 162 part./mL ^c	2974 ± 184 part./mL ^c
2 μm size standard	$1.999 \pm 0.020 \mu\text{m}$ ^b	$1.74 \pm 0.28 \mu\text{m}$ ^d	$1.95 \pm 0.35 \mu\text{m}$ ^d	$3.20 \pm 1.39 \mu\text{m}$ ^d	$2.38 \pm 0.90 \mu\text{m}$ ^d
5 μm size standard	$4.993 \pm 0.040 \mu\text{m}$ ^b	$5.10 \pm 0.80 \mu\text{m}$ ^d	$5.12 \pm 0.57 \mu\text{m}$ ^d	$5.94 \pm 1.61 \mu\text{m}$ ^d	$4.66 \pm 1.52 \mu\text{m}$ ^d
10 μm size standard	$10.00 \pm 0.08 \mu\text{m}$ ^b	$10.56 \pm 1.22 \mu\text{m}$ ^d	$10.16 \pm 1.16 \mu\text{m}$ ^d	$10.71 \pm 2.41 \mu\text{m}$ ^d	$9.66 \pm 1.43 \mu\text{m}$ ^d

^a based on light obscuration for particles $> 3 \mu\text{m}$; ^b based on microscopy; ^c standard deviation from three measurements; ^d full peak width at half of the maximum height

Concentration linearity was evaluated with different dilutions of 5 μm polystyrene size standards over a wide range from about 4×10^2 to 8×10^6 particles/mL. The obtained concentrations for particles $> 3 \mu\text{m}$ (as specified for the 5 μm count standard) were compared to the theoretical concentration as determined by LO in the low concentration range (4056 particles/mL for the second highest dilution) and calculated for the higher concentrations (Figure 4-1). All systems showed good overall linearity, but underestimated the particle number at high concentrations (Figure 4-1A) probably due to coincidence of particles, meaning that two particles which are located very closely next to or behind each other are detected as one particle. For the highest concentration of theoretically 8×10^6 particles/mL, a measurement was only possible with the MFI4100 and FlowCAM VS1. MFI5200 and FlowCAM PV were not able to handle such high particle

concentrations as the measurements were automatically aborted at 1×10^6 and 5×10^5 captured particles, respectively. This is due to a software setting limiting the number of captured particles to 500,000 per analysis to ensure proper data handling. The limit can be increased, but this would slow down data processing by the software. For the sample with a theoretical concentration of 4×10^6 particles/mL, MFI4100, MFI5200, and FlowCAM VS1 underestimated the particle concentration by less than 10%, whereas the FlowCAM PV system detected 25% less particles than actually expected. In the medium concentration range of theoretically 4×10^3 to 1×10^6 particles/mL, all systems showed good results (Figure 4-1B,C). Whereas the FlowCAM systems slightly underestimated the concentration, the MFI4100 system overestimated the concentration in the case of theoretically 4×10^5 particles/mL. The MFI5200 system constantly showed deviations from the theoretical concentration of less than 2%. For the lowest concentration of theoretically 406 particles/mL, MFI4100, MFI5200 and FlowCAM PV showed large deviations of 11-28% and only the FlowCAM VS1 system detected the theoretical concentration within 1% (Figure 4-1C). All systems showed large relative standard deviations in the low concentration range below 4×10^3 particles/mL (8% for MFI5200, 18% and more for the other systems).

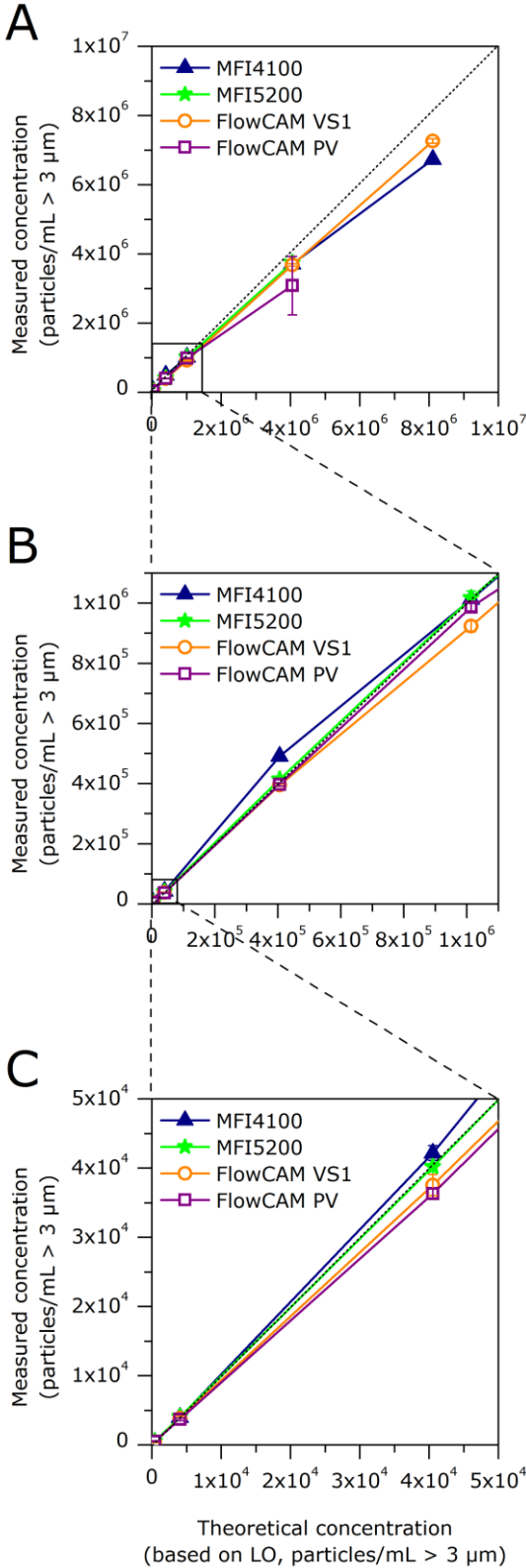


Figure 4-1: Linearity of particle concentration measurements by MFI4100, MFI5200, FlowCAM VS1, and FlowCAM PV. 5 μm PS standards measured at various dilutions. The theoretical concentrations are based on the counts of the second highest dilution obtained by LO (result: 4056 particles/mL). (A) Full concentration range, (B) zoom into medium concentrations, (C) zoom into low concentrations. Error bars represent standard deviations from triplicate measurements.

Size accuracy was evaluated with monodisperse polystyrene size standards of 2, 5, and 10 μm . Overall, the MFI systems rendered images of poorer resolution, but better size accuracy as compared with the FlowCAM systems evaluated in this study (Table 4-2 and Figure 4-2). The MFI4100 system underestimated the size of the 2 μm polystyrene standards due to resolution limitations for those small particles, but showed satisfying size accuracy for 5 μm and 10 μm as well as a narrow distribution for all sizes (Figure 4-2A). MFI5200 was the only system that determined all sizes accurately and with a high precision (Figure 4-2B). The images of size standards obtained by the MFI systems appeared rather blurry, but comparable in size and optical appearance, leading to the observed good size accuracy and precision. In contrast, the images obtained by the FlowCAM systems showed high resolution and sharpness, but also a large variability in size and optical appearance. Especially the FlowCAM VS1 system showed clear deviations from the correct size (Table 4-2) and also a broad size distribution with apparently more than one population per analyzed size standard (Figure 4-2C). This is particularly striking for the 10 μm polystyrene standard, for which two apparent populations around 10 μm and 12 μm were detected. The 10 μm peak particles appear to be captured in focus, whereas the 12 μm peak particles appear out of focus as indicated by the concentric rings. Although the FlowCAM software VisualSpreadsheet is theoretically able to exclude out-of-focus particles, this was not performed as it would compromise the accuracy of the particle concentration and does therefore not represent a suitable option for real protein sample analysis. The FlowCAM PV rendered images of slightly lower resolution, but in return better size homogeneity leading to better size accuracy and precision (Figure 4-2D). For a mixed sample of 2, 5, and 10 μm polystyrene size standards, the described differences in image quality and homogeneity led to a better separation between the sizes in the MFI systems as compared with the FlowCAM systems (Figure 4-2A-D, lower panels). The underlying reasons for the differing image quality and homogeneity are assumed to be (i) the magnification and (ii) the depth of focus (Table 4-1). Furthermore, the threshold value in the FlowCAM systems influences the size accuracy as there is always a trade-off between size accuracy and image fragmentation.

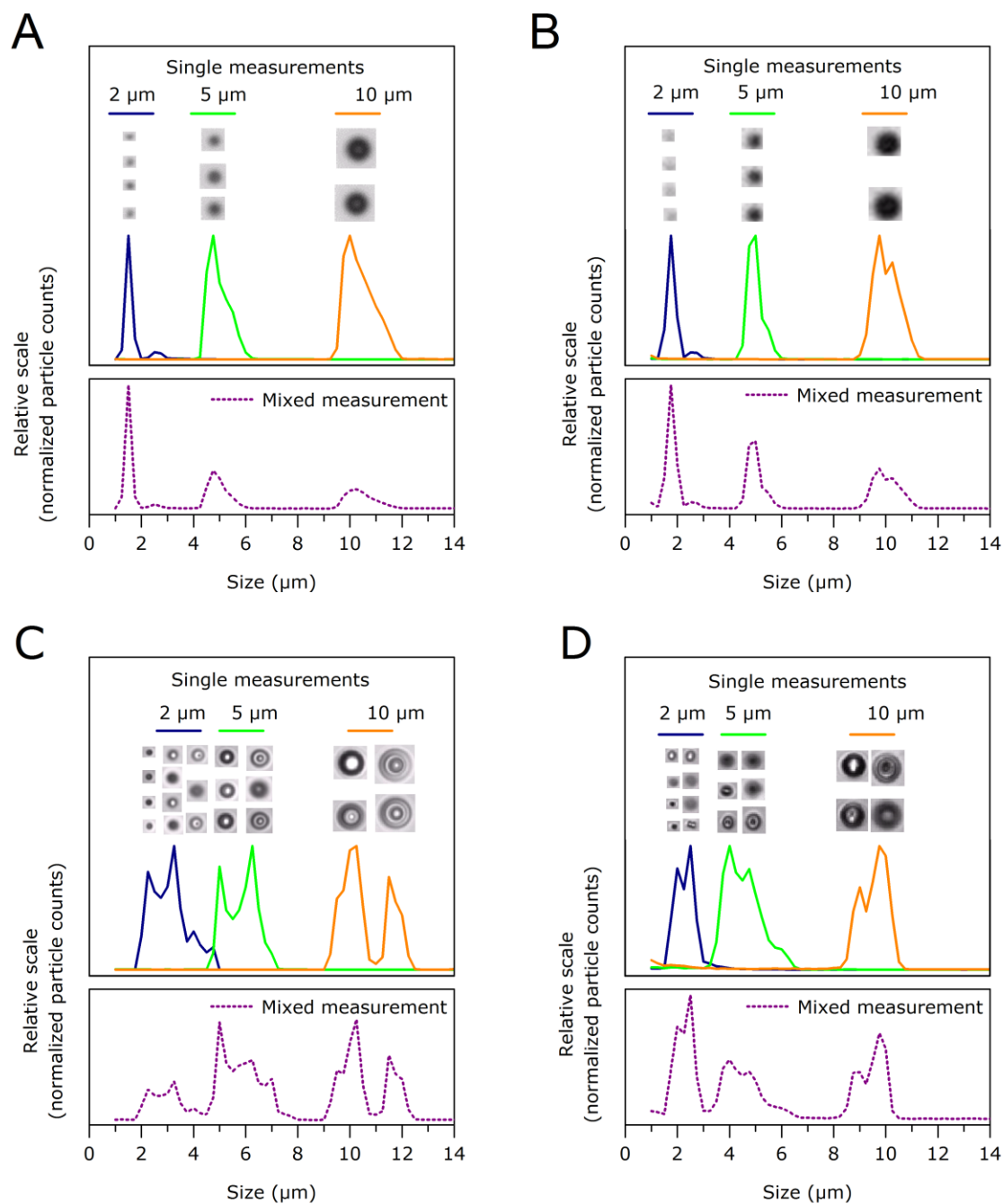


Figure 4-2: Size accuracy and precision of 2 μm , 5 μm and 10 μm PS size standards measured separately (upper panels) and as a mix (lower panels) by (A) MFI4100, (B) MFI5200, (C) FlowCAM VS1, and (D) FlowCAM PV. Representative images are shown above the corresponding peak of the size distribution.

3.2 Image properties

As discussed above, differences in the image properties and especially in the image homogeneity lead to divergences in size determination. Furthermore, the image quality is a crucial parameter for morphological analysis and for a reliable discrimination of different particle types, e.g. proteinaceous vs. non-proteinaceous particles. Therefore, we compared images of polystyrene standards, artificially generated silicone oil droplets, and protein particles (heat-stressed rituximab) (Figure 4-3). In general, images provided by the FlowCAM systems appeared sharper and of higher resolution than images captured by the MFI systems. This is mainly due to the smaller focus area and higher magnification of the FlowCAM optics. Thus, many morphological details were already visible on particles as small as 5 μm in size, especially for the FlowCAM VS1 system. However, the small focus area caused particles of the same type to appear optically different, which could be well observed on images for polystyrene standards and silicone oil droplets. Dark particles with a bright halo as well as bright particles with a dark edge and several nuances in between were detected within one sample. For protein particles, images captured by the FlowCAM systems appeared more uniform regarding the optical contrast than for polystyrene standards and silicone oil droplets. The MFI4100 system provided comparable images of protein particles. In contrast the images captured by the MFI5200 system appeared more variable, presumably due to its larger view window which results in different illumination of particles depending on their location within the view window. For protein particles, this can lead to a high diversity in the optical appearance due to diffraction patterns within those heterogeneous particles.²¹ However, it is difficult to judge which instrument displays the real heterogeneity of protein particles as this is not known. The difference in sharpness and resolution between MFI systems and FlowCAM systems was particularly obvious for protein particles with sizes of about 5 μm and 10 μm . Here, FlowCAM images provide more morphological details, whereas MFI images appear rather blurry. Furthermore, the MFI systems capture only pixels of the particle which are darker than the background. In contrast, the FlowCAM systems use a different background calibration procedure allowing the additional depiction of pixels brighter than the background which probably result from specific diffraction patterns.²¹ This contributes to the enhanced visibility of

morphological details but also leads to the heterogeneity in FlowCAM images. Within the brands, the MFI4100 and FlowCAM VS1 captured better images than the MFI5200 and FlowCAM PV.

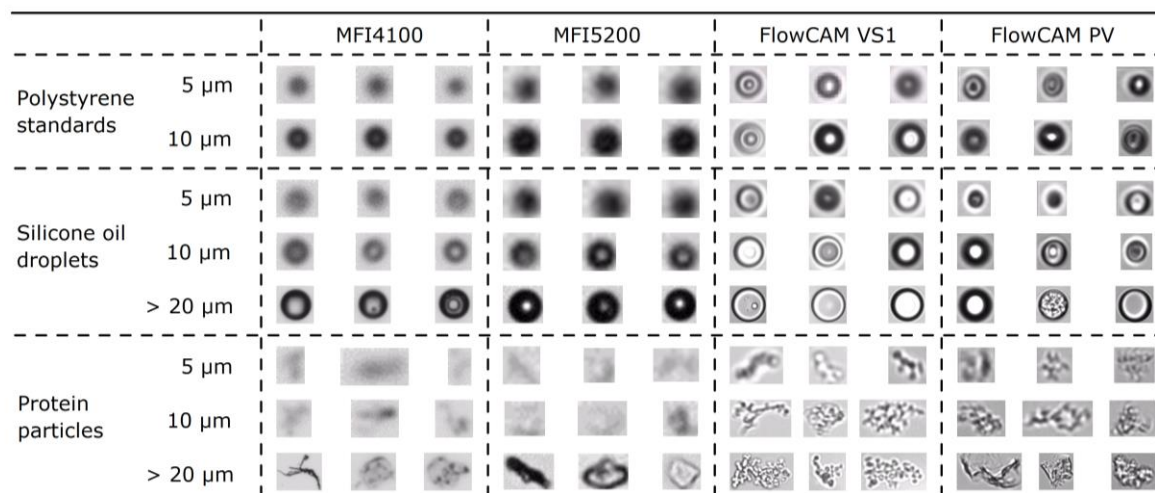


Figure 4-3: Representative images of polystyrene standards, silicone oil droplets, and protein particles (heat-stressed rituximab) of different particle sizes scaled to the same image size.

An additional cause of image variability in the FlowCAM systems for polystyrene standards and silicone oil droplets might be the illumination of the flow cell. While the background of an MFI flow cell appears uniformly grey (Figure 4-4A,B), the background of a FlowCAM flow cell seems to be less evenly illuminated, especially for the FlowCAM VS1 system (Figure 4-4C,D). This can affect the overall brightness of an image depending on where within the flow cell it was captured. According to the manufacturer, this feature is currently under development for the FlowCAM systems.

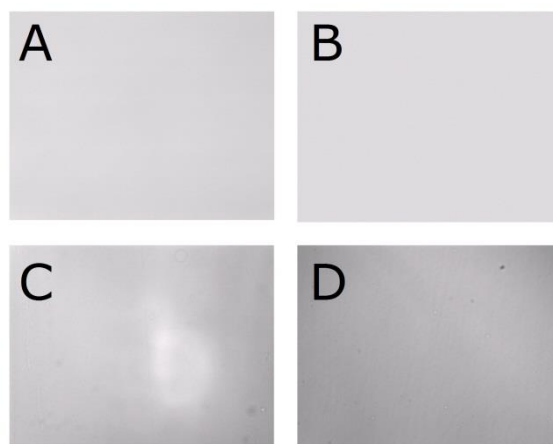


Figure 4-4: Images of a clean flow cell (purged with water) in (A) MFI4100, (B) MFI5200, (C) FlowCAM VS1, and (D) FlowCAM PV.

3.3 Quantification of protein particles

Because the captured particle images form the basis for particle analysis, a potential correlation between image quality and detected particle numbers was investigated. To this end, protein particles were generated by heating a rituximab formulation and analyzed by the four systems. Due to the time-shifted availability of the FlowCAM systems, the exact same sample could not be analyzed in parallel by all four systems. Instead, one sample was analyzed in parallel by the MFI4100 and FlowCAM VS1 (Figure 4-5A). Another sample, prepared later under the same conditions, was analyzed in parallel by the MFI5200 and FlowCAM PV as well as by MFI4100 for comparison (Figure 4-5B). Thus, the difference in the cumulative size distribution between Figure 4-5A and Figure 4-5B can be attributed to the variability in the sample preparation. System-dependent differences can only be evaluated within Figure 4-5A or within Figure 4-5B. Although the image resolution for particles below 2 μm was poor and the official lower size limit of the FlowCAM systems is 2 μm , counting of particles could be performed for particles $> 1 \mu\text{m}$ with satisfying data quality for all systems. For the same sample, the FlowCAM VS1 system detected more particles below 3 μm but fewer particles above 3 μm , particularly above 10 μm , as compared with the MFI4100 system (Figure 4-5A).

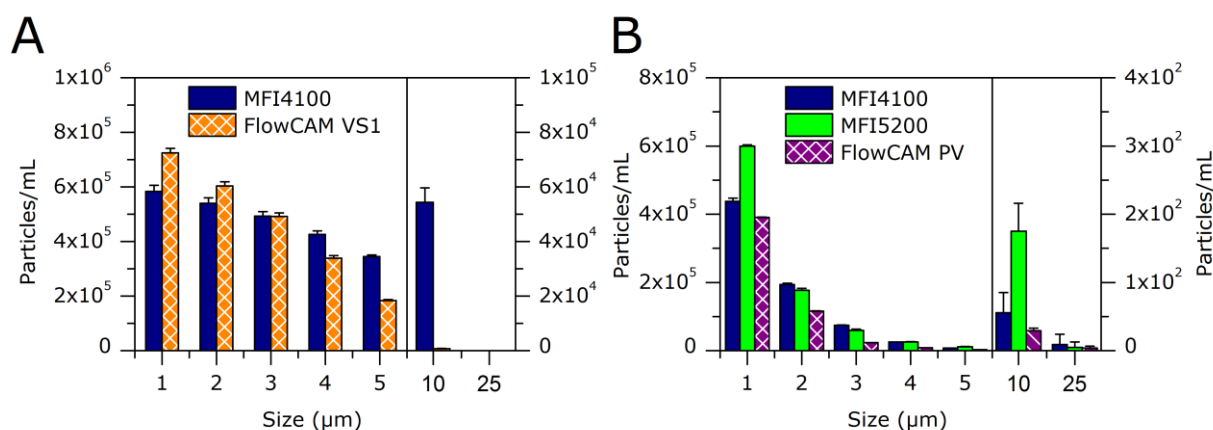


Figure 4-5: Cumulative particle counts for protein particles of heat-stressed rituximab analyzed by (A) MFI4100 and FlowCAM VS1 and (B) MFI4100, MFI5200, and FlowCAM PV. Error bars represent standard deviations from triplicate measurements.

A possible reason for this might be image fragmentation which was observed for the FlowCAM VS1 when using the setting “only dark particles” (Figure 4-6). It seems that bright parts of particles were detected as the particle boundary by the software. This effect was observed for particles larger than 10 μm. Although image fragmentation might also have occurred for smaller particles it could not be confirmed by optical evaluation of the images due to resolution limitations. Changing the settings to “dark & bright” might have decreased this effect but, as discussed earlier, failed to provide the correct size for polystyrene size standards and was therefore not chosen. This shows again that the user has to accept a certain trade-off between good size accuracy and robustness against image fragmentation for the FlowCAM systems which on the one hand brings along certain user-dependency and data variability. On the other hand, those many adjustable settings in the FlowCAM systems enable the handling of a specific problem. In contrast, the MFI systems require the trust of the user in the predefined settings which cannot be changed. For the other systems evaluated in this study image fragmentation was not observed for the same samples. However, for an IgG-containing sample from a different study image fragmentation was observed for the MFI4100 system (data not shown due to confidentiality).

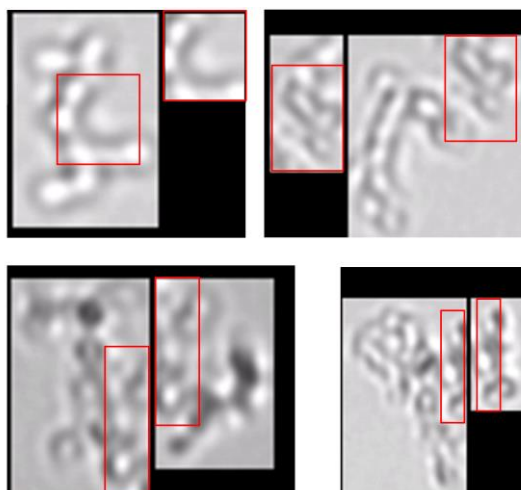


Figure 4-6: Images of protein particles around 10 μm (heat-stressed rituximab) captured by the FlowCAM VS1 system. Red boxes indicate overlapping or doubly imaged regions in two separate images due to image fragmentation.

For the second sample analyzed, MFI5200 and FlowCAM PV detected similar size distributions with slightly less particles detected by the FlowCAM PV system (Figure 4-5B). Clearly more small particles larger than 1 μm were detected by the MFI5200 system, pointing on the one hand towards a better sensitivity for small transparent particles, on the other hand potentially also towards undetected image fragmentation. For the FlowCAM PV system it needs to be considered that the official size range of this system starts only at 2 μm and was extended consciously in this study. For total particle concentrations larger than 2 μm , similar concentrations were detected by all three systems. The difference for particles larger than 10 μm is probably due to the low total number in this size range causing higher standard deviations. In general, the MFI5200 and FlowCAM PV showed lower standard deviations for total particle counts larger than 1 μm as compared with the MFI4100 and FlowCAM VS1, as could be expected from the differences in the analyzed volume.

It was shown earlier that light-based quantification of protein particles is influenced by the RI of both, particles and surrounding formulation and that this effect is partly system dependent.²⁶ Therefore, the robustness of MFI4100, MFI5200, and FlowCAM PV towards RI influences was determined by quantifying protein particles larger than 1 μm (stir-stressed infliximab) in the same

concentration in formulations of increasing RI, adjusted by addition of sucrose (Figure 4-7). The FlowCAM VS1 system was not available at the time of these experiments. Particle concentrations obtained by MFI4100 were rather sensitive to an increase in RI of the formulation. In 20% sucrose (RI 1.36), 80% of the original particle concentration was still detected whereas in 50% sucrose (RI 1.42), only 25% could be detected. MFI5200 and FlowCAM PV were both more robust towards RI influences: in 20% sucrose, 93% and 89% of the original particle concentration, respectively, were still detected and in 50% sucrose the apparent concentration decreased only to 54% and 69% with MFI5200 and FlowCAM PV, respectively. The reason for the superior performance of MFI5200 and FlowCAM PV is potentially connected to optimized optical settings of these newer systems. Two different control experiments in a previous study have shown that the particle concentration was not affected directly by the high sucrose concentration, e.g. by dissolution or generation of particles.²⁶ Instead, the decreased RI difference between particles and surrounding formulation reduced the apparent particle concentration. The RI of a 20% sucrose solution (1.36) represents pharmaceutically relevant conditions, e.g. at high protein concentration or a combination of excipients such as sucrose and high protein concentration.²⁶

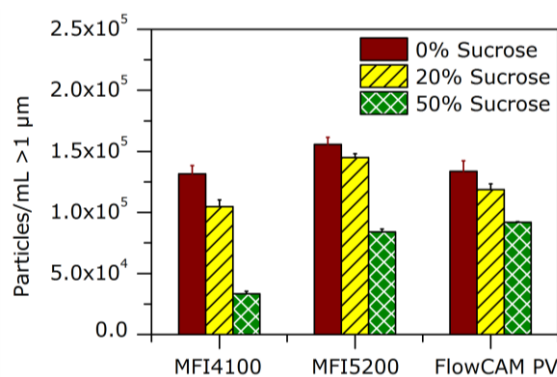


Figure 4-7: Total particle counts for protein particles of stir-stressed infliximab for fixed particle concentrations in sucrose solutions of varying concentration and thus RI. Error bars represent standard deviations from triplicate measurements.

3.4 Differentiation of silicone oil droplets and protein particles

A major advantage of flow imaging microscopy as compared with other analytical techniques for subvisible particles, e.g. LO or electrical sensing zone analysis, is the possibility to characterize particles based on images.¹⁰ Parameters such as shape and transparency can be used to differentiate between different particle types.^{22,23} In this context, the discrimination of silicone oil droplets and protein particles is especially relevant due to the increasing application of prefilled syringes. Similar to a previous study,²² protein particles (heat-stressed rituximab) and silicone oil droplets were analyzed by MFI4100, MFI5200, FlowCAM VS1, and FlowCAM PV as individual samples (to obtain the theoretical concentration within the same system) and in controlled mixtures. The “find similar” algorithm in the respective software was used to differentiate between silicone oil droplets and protein particles. Due to the time-shifted availability of the FlowCAM systems, the exact same sample could not be analyzed in parallel by all four systems. Instead, one group of samples was analyzed in parallel by the MFI4100 and FlowCAM VS1 (Figure 4-8A,C). Another group of samples which was prepared later under the same conditions was analyzed in parallel by the MFI5200 and FlowCAM PV (Figure 4-8B,D). The concentration was adjusted in such a way that similar total particle counts larger than 1 μm were obtained for both groups of samples with the MFI4100 as the bridging instrument. However, the relative size distribution for protein particles differed clearly between the two sample groups. Thus, the differentiation performance was evaluated within the systems, but not between the systems. The evaluation was based on the match of the detected concentration (in mixed samples) and the theoretical concentration (in individual samples) within each system. The theoretical concentration may differ from system to system and is only valid for the mixed samples analyzed by the same system. Although an optical discrimination of silicone oil droplets and protein particles based on the particle images, which is the basis for the “find similar” operation, was only reasonable for particles of 5 μm and larger, the “find similar” function of the software was able to differentiate particles down to 2 μm .

The FlowCAM PV system showed the best match with the theoretical concentration, thus the best differentiation of silicone oil droplets and protein particles (Figure 4-8D). The MFI5200 and FlowCAM PV (Figure 4-8B,D) showed a higher precision than the MFI4100 and FlowCAM VS1 (Figure 4-8A,C). However, the differences were rather small and results might depend on the specific sample properties. In conclusion, all systems proved to be suitable for the differentiation of silicone oil droplets and protein particles from 2 to 10 μm . For particles below 2 μm , alternative techniques such as resonant mass measurement (RMM) can be beneficial.²² For particles larger 10 μm , it is recommended independently of the system to differentiate particles by optical evaluation of the images rather than by applying the “find similar” function. This approach is feasible due to the clear images and usually low particle counts in this size range.

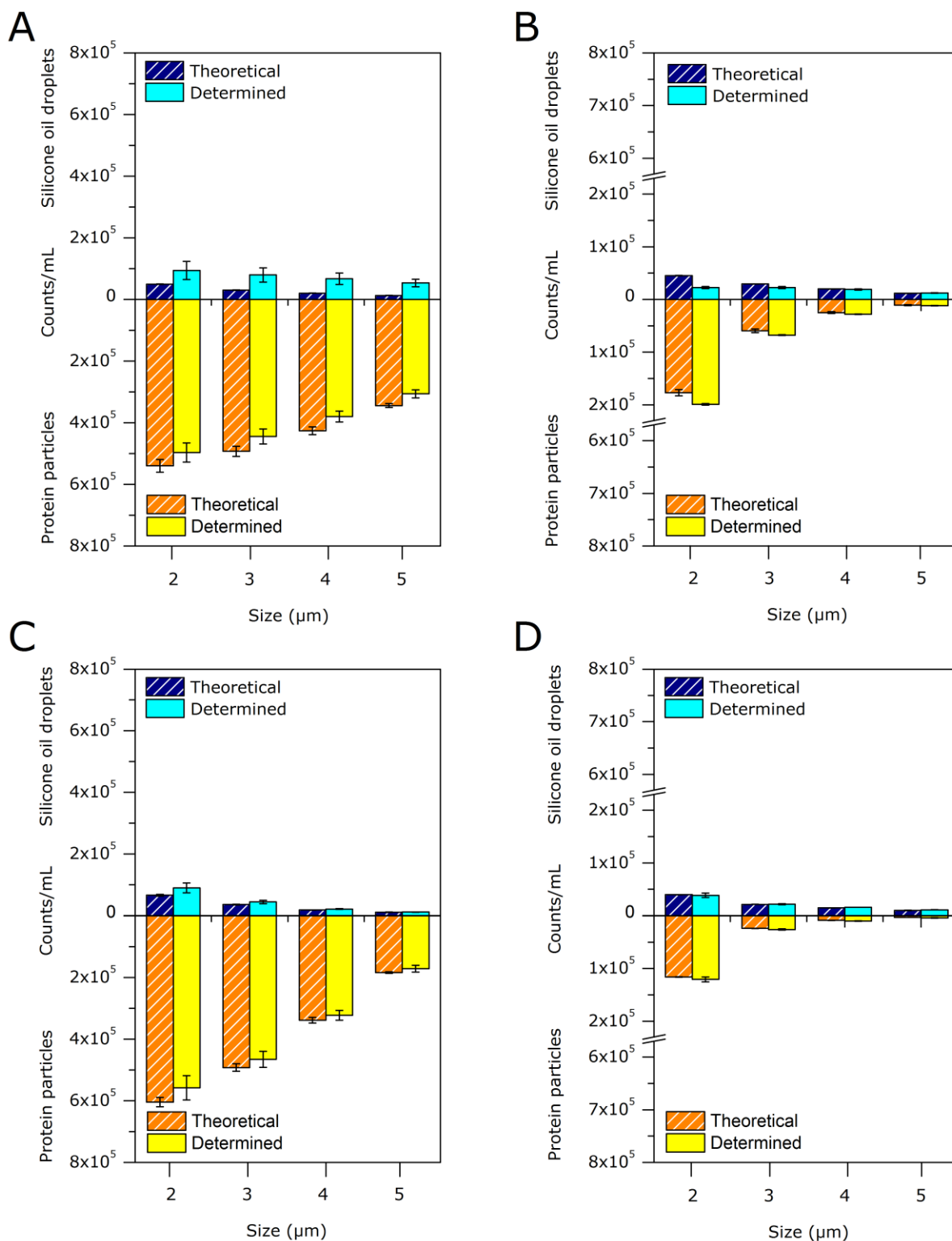


Figure 4-8: Cumulative particle counts comparing theoretical concentrations (based on individual samples measured with the corresponding instrument) and determined concentrations (mixed samples) of artificially generated silicone oil droplets and protein particles (heat-stressed rituximab) in a droplet/particle ratio of 10:90 (based on particle counts $> 2 \mu\text{m}$ with MFI4100). (A) MFI4100, (B) MFI5200, (C) FlowCAM VS1, (D) FlowCAM PV. Error bars represent standard deviations from triplicate measurements.

3.5 Handling of the systems

Concerning the hardware, MFI systems only allow the adjustment of the sample volume. This ensures standardized, user-independent measurements and repeatable results, but requires full trust in the settings predefined by the manufacturer, which cannot be customized to specific needs or samples. In contrast, the FlowCAM systems allow changes in optical settings (e.g. threshold, shutter, and gain) or technical settings (flow rate, image capture rate) offering customization of the analysis to specific needs for experienced users, but impede comparability between samples analyzed by different operators, at different times or even by different instruments of the same type.

The exchange of a flow cell, which requires the adjustment of the focus as a critical parameter for image-based particle analysis, is straightforward and unambiguous for the MFI systems. For the FlowCAM systems, especially the FlowCAM VS1, this process was found to be cumbersome but this is currently being improved by the manufacturer. Furthermore, the MFI systems use a peristaltic pump enabling high flow rates and large volumes which is useful for an efficient cleaning step, but the flow rate needs to be calibrated regularly. The FlowCAM systems for small volumes (as applicable for protein samples) are typically equipped with a syringe pump, which does not require calibration by the user, but is restricted in volume and speed limited by the flow cell diameter. Thus, cleaning cycles with FlowCAM need to be performed several times with low volume and flow rate, especially in case of small syringe sizes.

Concerning the software, the MFI systems use different software types for the measurement (MFI View software for MFI4100, MVSS for MFI5200) and the data analysis (MVAS), whereas the FlowCAM systems apply the same software for both steps (VisualSpreadsheet). While the latter allows the analysis of the particle population, regarding size distribution and cropped images, already during the measurement as a real time analysis, this data becomes available only after the measurement for the MFI systems. However, the MVAS software includes an essential function to "remove stuck particles" (particles stuck to the flow cell wall which would otherwise be counted on every image they were captured on). This option is not yet available for VisualSpreadsheet but is

currently under development. In both software solutions, particle data can be exported in many different ways and the raw data of every single particle (e.g. shape or transparency values) is available. MVAS enables export of single particle images, whereas VisualSpreadsheet offers collages of particle images. Regarding the differentiation of silicone oil droplets and protein particles, the analysis of a single sample is simpler in MVAS, while VisualSpreadsheet enables the generation of libraries from selected particles, which can be used to build a filter for future samples. In addition, VisualSpreadsheet offers the possibility to sort the resulting population of similar particles by “filter score”, i.e. by similarity to the selected particles. Taken together, MFI systems are more standardized, whereas FlowCAM systems are designed for more flexibility for the user, concerning both hardware and software.

4 Conclusion

Our study showed that the selection of the appropriate flow imaging microscopy system depends strongly on the main output parameters of interest and the intended application. Each system shows its strengths and weaknesses in different aspects (Table 4-3). The four systems evaluated in this study can be categorized based on the technical data and the results obtained in this study into high-resolution systems (MFI4100 and FlowCAM VS1) and high-efficiency systems (MFI5200 and FlowCAM PV). The best images were obtained by the FlowCAM VS1 system, which was seen as the best system among the high-resolution instruments. The best performance regarding particle counting accuracy and precision was achieved by the MFI5200 system, which appeared to be the preferred system among the high-efficiency instruments. The MFI4100 and the FlowCAM PV system were observed as all-round systems which might be a good compromise between the other two systems that are more biased towards particle counting (MFI5200) or particle imaging (FlowCAM VS1).

Table 4-3: Summarizing assessment of important analysis factors for MFI4100, MFI5200, FlowCAM VS1, and FlowCAM PV.

Parameter	MFI4100	MFI5200	FlowCAM VS1	FlowCAM PV	
Image properties	Resolution	++	+	++++	+++
	Contrast within the particle	+	++	++++	+++
	Image consistency (standards)	++++	++++	+	+
Polystyrene size	Accuracy	+++	++++	+	++
	Precision	+++	++++	+	++
Polystyrene count	Accuracy	+++	++	+	++++
	Precision	+	++++	+++	++
	Linearity	++	++++	++++	+
Protein particle quantification	Precision	+	+++	+	++++
	Robustness against RI influences	++	+++	n.a.	++++
Differentiation of silicone oil droplets and protein particles	Match with the theoretical concentration	+	++	+++	++++
	Precision	+	+++	++	++++
Handling	Hardware	+++	++++	+	++
	Software for measurement	++++	+++	+	++
	Software for data analysis		++++		+++

++++ = strongest performance; +++ = second strongest performance; ++ = third strongest performance; + = weakest performance; all criteria were judged only relatively among the evaluated systems.

5 References

1. Carpenter JF, Randolph TW, Jiskoot W, Crommelin DJA, Middaugh CR, Winter G, Fan Y-X, Kirshner S, Verthelyi D, Kozlowski S, Clouse KA, Swann PG, Rosenberg A, Cherney B 2009. Overlooking subvisible particles in therapeutic protein products: gaps that may compromise product quality. *J Pharm Sci* 98:1201-1205.
2. Carpenter J, Cherney B, Lubinecki A, Ma S, Marszal E, Mire-Sluis A, Nikolai T, Novak J, Ragheb J, Simak J 2010. Meeting report on protein particles and immunogenicity of therapeutic proteins: filling in the gaps in risk evaluation and mitigation. *Biologicals* 38:602-611.
3. Hawe A, Wiggenhorn M, van de Weert M, Garbe JHO, Mahler H-C, Jiskoot W 2012. Forced degradation of therapeutic proteins. *J Pharm Sci* 101:895-913.
4. Narhi LO, Schmit J, Bechtold-Peters K, Sharma D 2012. Classification of protein aggregates. *J Pharm Sci* 101:493-498.
5. Rosenberg AS 2006. Effects of protein aggregates: an immunologic perspective. *AAPS J* 8:E501-507.
6. USP<788>, United States Pharmacopeia, USP35-NF30. 2012. Particulate matter in injections. United States Pharmacopeial convention.
7. Ph.Eur. 2.9.19, Pharmacopoea europaea, 7th ed. 2010. Particulate contamination: Sub-visible particles. European Directorate For The Quality Of Medicine (EDQM).
8. Kirshner S Regulatory expectations for analysis of aggregates and particles. Talk at Workshop on Protein Aggregation and Immunogenicity, Breckenridge, Colorado, 07/12/12.
9. U.S. Food and Drug Administration, 2013. Guidance for Industry - Immunogenicity Assessment for Therapeutic Protein Products (draft guidance). FDA, Silver Spring, Maryland.
10. Zölls S, Tantipolphan R, Wiggenhorn M, Winter G, Jiskoot W, Friess W, Hawe A 2012. Particles in therapeutic protein formulations, Part 1: Overview of analytical methods. *J Pharm Sci* 101:914-935.
11. Burg TP, Godin M, Knudsen SM, Shen W, Carlson G, Foster JS, Babcock K, Manalis SR 2007. Weighing of biomolecules, single cells and single nanoparticles in fluid. *Nature* 446:1066-1069.
12. Narhi LO 2012. AAPS update on USP expert committee for Sub visible particle analysis. Newsletter of the AAPS Aggregation and Biological Relevance Focus Group 3(2).
13. Demeule B, Messick S, Shire SJ, Liu J 2010. Characterization of particles in protein solutions: reaching the limits of current technologies. *AAPS J* 12:708-715.
14. Sharma DK, Oma P, Pollo MJ, Sukumar M 2010. Quantification and characterization of subvisible proteinaceous particles in opalescent mAb formulations using micro-flow imaging. *J Pharm Sci* 99:2628-2642.
15. Wuchner K, Büchler J, Spycher R, Dalmonte P, Volkin DB 2010. Development of a microflow digital imaging assay to characterize protein particulates during storage of a high concentration IgG1 monoclonal antibody formulation. *J Pharm Sci* 99:3343-3361.
16. Joubert MK, Luo Q, Nashed-Samuel Y, Wypych J, Narhi LO 2011. Classification and characterization of therapeutic antibody aggregates. *JBC* 286:25118-25133.
17. Barnard JG, Babcock K, Carpenter JF 2012. Characterization and Quantitation of Aggregates and Particles in Interferon- β Products : Potential Links Between Product Quality Attributes and Immunogenicity. *J Pharm Sci* 102:915-928.
18. Barnard JG, Singh S, Randolph TW, Carpenter JF 2011. Subvisible particle counting provides a sensitive method of detecting and quantifying aggregation of monoclonal antibody caused by freeze-thawing: insights into the roles of particles in the protein aggregation pathway. *J Pharm Sci* 100:492-503.
19. Patel AR, Lau D, Liu J 2012. Quantification and characterization of micrometer and submicrometer subvisible particles in protein therapeutics by use of a suspended microchannel resonator. *Anal Chem* 84(15):6833-6840.
20. Sharma DK, King D, Oma P, Merchant C 2010. Micro-flow imaging: flow microscopy applied to sub-visible particulate analysis in protein formulations. *AAPS J* 12:455-464.
21. Brown L 2011. Characterizing Biologics Using Dynamic Imaging Particle Analysis. *BioPharm Int*:s1-8.
22. Weinbuch D, Zölls S, Wiggenhorn M, Friess W, Winter G, Jiskoot W, Hawe A 2013. Micro-Flow Imaging and resonant mass measurement (Archimedes) – Complimentary methods to quantitatively differentiate protein particles and silicone oil droplets. *J Pharm Sci* 102:2152-2165.

23. Strehl R, Rombach-Riegraf V, Diez M, Egodage K, Bluemel M, Jeschke M, Koulov AV 2012. Discrimination between silicone oil droplets and protein aggregates in biopharmaceuticals: a novel multiparametric image filter for sub-visible particles in microflow imaging analysis. *Pharm Res* 29(2):594-602.
24. Sharma D, Oma P, Krishnan S 2009. Silicone Microdroplets in Protein Formulations - Detection and Enumeration. *Pharm Tech* 33:74-79.
25. Huang C-T, Sharma D, Oma P, Krishnamurthy R 2009. Quantitation of protein particles in parenteral solutions using micro-flow imaging. *J Pharm Sci* 98:3058-3071.
26. Zölls S, Gregoritz M, Tantipolphan R, Wiggerhorn M, Winter G, Friess W, Hawe A 2013. How subvisible particles become invisible-relevance of the refractive index for protein particle analysis. *J Pharm Sci* 102:1434-1446.
27. Wilson GA, Manning MC 2013. Flow imaging: Moving toward best practices for subvisible particle quantitation in protein products. *J Pharm Sci* 102:1133-1134.

Chapter 5

Material screening and investigation of particle density for the development of standardized protein-like particles

Abstract

The aim of this study was the identification of suitable materials and preparation methods for the development of standardized protein-like particles. In the first part, a material screening based on optical particle properties was performed. Proteinaceous (human serum albumin (HSA)-starch particles, spray-dried HSA, gelatin particles, and zein) and non-proteinaceous materials (chitosan and polytetrafluoroethylene (PTFE)) were compared to HSA particles generated by heat stress as a representative model for protein particles in therapeutic formulations. The particle properties size, size distribution, shape, transparency, and stability were assessed by light obscuration (LO) and Micro-Flow Imaging (MFI). As a result, gelatin and PTFE particles reflected the most relevant optical properties (shape and transparency) of protein particles and were regarded as promising candidates for the development of standardized protein-like particles for light-based techniques. In the second part, the density of protein particles in aqueous formulations as a further crucial property was investigated. Two different methods based on resonant mass measurement (RMM) were developed to determine (i) the density of pure protein and (ii) the apparent density of protein particles including entrapped liquid. The first method provided a density around 1.4 g/mL for pure protein, which complied with theoretically calculated values. The second method was only applicable for particles showing a clear maximum in the size distribution and yielded an apparent density of around 1.1 g/mL for protein particles including entrapped liquid. Based on these parameters, PTFE particles were regarded as suitable standard material especially for light-based techniques, whereas gelatin particles could be used for both light-based and weight-based methods.

1 Introduction

The analysis of particles in therapeutic protein formulations requires calibration of the instruments with certified particle standards. Mostly polystyrene particle standards are used for this purpose, although these standards do not represent optical and morphological properties of protein particles.¹ Thus, novel standards are more and more claimed by academia and industry²⁻⁴ which should be applied mainly for comparison and evaluation of results acquired by different techniques or instruments and if possible also for instrument calibration. These novel standards should reflect protein particle properties (size, size distribution, optical and morphological parameters), should be stable as an aqueous suspension, and should behave similar to protein particles in the commonly applied analytical techniques regarding measurement performance and data evaluation. This could involve the direct use of raw material powder or preparation of particles from raw materials. Proteinaceous and non-proteinaceous materials are theoretically suitable for both alternatives. Proteinaceous materials bring the benefit of high similarity, but might bear the risk of low stability, especially at ambient conditions in solution. Non-proteinaceous materials have the advantages of easier handling and potentially increased stability, but might face the problem of low conformity with protein particles as known for polystyrene standards.

Proteinaceous materials evaluated in this study include human serum albumin (HSA)-starch particles, which were originally developed as particles with an irregular and rough surface structure for mucosal delivery of vaccines,⁵ spray-dried HSA and gelatin particles prepared by desolvation, both stabilized by a cross-linker, and the hydrophobic water insoluble protein zein as the raw material powder. Non-proteinaceous raw material powders screened for their suitability as standardized protein-like particles were the polysaccharide chitosan and the synthetic fluoropolymer polytetrafluoroethylene (PTFE). The application purpose of the novel standards are light obscuration (LO) and Micro-Flow Imaging (MFI) as the workhorses of protein particle analysis. Therefore, the focus was set on the similarity of particle properties relevant for those techniques: Size, size distribution, shape, and transparency for the novel materials were compared to those of HSA particles generated by heat stress as a

representative for particles of therapeutic proteins. Furthermore, the stability in an aqueous suspension was assessed.

The density of protein particles is a crucial parameter for protein particle analysis which has not been characterized well up to now.⁶ Light-based techniques like LO and MFI determine the particle size based on the optical signal which is caused by the combination of protein parts and entrapped liquid within a particle. The novel technique of resonant mass measurement (RMM) detects the buoyant mass which is only influenced by protein parts within the particle and the size calculation depends on the particle density as an input parameter. Thus, the techniques consider the particle density in different ways and a deeper understanding of protein particle density is valuable for data evaluation and therefore also the development of protein-like standards. RMM was applied in this study to investigate (i) the density of pure protein and (ii) the density of protein particles including entrapped liquid and the results were compared to the density of the screened materials.

2 Materials and methods

2.1 Materials

5 μm polystyrene particle size standards were purchased from Duke Scientific (through Thermo Scientific, Fremont, CA) and diluted in water for analysis. Dry borosilicate glass particle standards (5 μm) were purchased from Duke Scientific, suspended in water containing a minimum amount of isopropanol (according to the instructions by the manufacturer), sonicated for 1.5 h and vortexed directly before analysis. 5 μm silica particle size standards were purchased from microparticles GmbH (Berlin, Germany) and diluted in water for analysis.

Rituximab (MabThera[®], lot no. B6082) was provided by local hospitals, diluted to 1 mg/mL in 25 mM citrate buffer (pH 6.5) containing 154 mM NaCl and 0.07% polysorbate 80 and filtered (0.2 μm polyethersulfone syringe filter, Sartorius, Göttingen, Germany) for further use. HSA was purchased from Sigma-Aldrich (Steinheim, Germany), formulated at 1 mg/mL in 50 mM citrate buffer (pH 4.8) or at 5% (m/v) in water and filtered (0.2 μm cellulose acetate syringe filter, Minisart[®], Sartorius Stedim Biotech, Aubagne, France) for further use. Gelatin from porcine skin (type A, medium gel strength, 170-190 g Bloom, for microbiology) was purchased from Sigma-Aldrich. Chitosan (poly-(D-glucosamine) deacetylated chitin, >75% deacetylated, coarse ground flakes and powder) was obtained from Sigma-Aldrich and suspended in water for analysis. Zein F 4000 was obtained as a gift from capol GmbH (Elmshorn, Germany), sieved through a 100 μm mesh and suspended in 10% polysorbate 80 in water. PTFE (Microdispers 8000 from Polysciences Inc., Warrington, PA) was suspended at a concentration of 50 mg/mL in 0.5% polysorbate 80 using an Ultra Turrax dispersing system (T10 basic, IKA[®] Werke, Staufen, Germany) for 3 minutes. Larger agglomerates were removed by filtration through a coarse tea filter (dm, Karlsruhe, Germany).

Dimethylsulfoxide (DMSO, for synthesis) was purchased from Merck Schuchardt (Hohenbrunn, Germany). Rape oil was obtained from A&P (Kaiser's Tengelmann, Mühlheim an der Ruhr, Germany). Glutaraldehyde (technical, 50% in water, 5.6 M) and hydrochloric acid were purchased from Sigma-Aldrich. White soluble

potato starch (GR for analysis), sucrose, acetone for analysis, citric acid monohydrate, and sodium hydroxide were purchased from Merck KGaA (Darmstadt, Germany). Polysorbate 80 and tri-sodium citrate dehydrate were from VWR (Darmstadt, Germany). The water used in this study was highly purified water (Advantage A10 purification system, Millipore, Newark, NJ).

2.2 Particle preparation

Rituximab particles were prepared by incubating 1.5 mL of the 1 mg/mL rituximab solution for 30 minutes at 71 °C in a thermomixer (Eppendorf, Hamburg, Germany). HSA particles were generated by heating 50 mL of the 1 mg/mL formulation in a 50 mL tube (Greiner bio-one, Frickenhausen, Germany) for 30 minutes at 70 °C in a water bath (HSA (heating)) or by spray-drying 50 mL of the 5% formulation using a Büchi Mini Spray-Dryer B-290 (HSA spray-dried (Mini)) or Büchi Nano Spray-Dryer B-90 (HSA spray-dried (Nano)) (Büchi Labortechnik, Flawil, Switzerland) with subsequent cross-linking. For the Mini Spray-Dryer, process parameters were chosen based on previous studies by Schüle⁷ and Fuhrherr⁸: inlet temperature (T_{in}) 130 °C, outlet temperature (T_{out}) 60-70 °C, liquid feed flow rate 3 mL/min (9%), atomizing air volumetric flow rate 670 L/min (40 mmHg), aspirator flow rate 35 m³/h (100%), cooled two-fluid nozzle (0.7 mm). For the Nano Spray-Dryer, the following process parameters were applied: T_{in} 55 °C, T_{out} 25 °C, gas flow 115 L/min, pressure 37 hPa, pump mode 1, spray cap diameter 5.5 µm, spray head temperature 33 °C, spray rate 100%, spray angle 45°. After the spray-drying process, 150 mg of the particles generated by the two different approaches were suspended in 30 mL acetone and cross-linked by the addition of 500 µL glutaraldehyde (8%) under stirring at 400 rpm (Heidolph MR 3001K, Schwabach, Germany). After stirring for additional 30 minutes at 400 rpm, the suspensions were centrifuged for 10 minutes at 7,000 g (centrifuge 5810 R, Eppendorf AG, Hamburg, Germany) and the supernatants were discarded. Subsequently, the sediments were resuspended in 4 mL water and filtered through a coarse tea filter to remove large agglomerates.

Gelatin microparticles were prepared by a two-step desolvation method, which was originally developed for preparing nanoparticles.⁹ The first precipitation was triggered by the addition of 25 mL acetone at 500-600 rpm to 25 mL of a 5%

gelatin solution at room temperature with a precipitation time of 2 minutes. The supernatant was discarded and the deposit was redissolved in 25 mL water at 50 °C. The pH was adjusted to 3.9 with 1 M HCl. The second precipitation was initiated by adding 50 mL acetone at about 9-10 mL/min using a burette. After 10 minutes of stirring at 500-600 rpm, 500 µL glutaraldehyde (8%) were added as a cross-linker and the suspension was stirred for another 30 minutes. The particles were harvested by centrifugation at 10,000 g for 10 minutes at room temperature. The supernatant was discarded and the pellet was resuspended in 5 mL water and filtered through a coarse tea filter to remove large agglomerates.

For the evaluation of particle density, the preparation process was optimized to maximize the number of particles in the target size range of 2-8 µm. The cross-linking time with glutaraldehyde was extended to 40 minutes and the centrifugation speed for particle harvesting was decreased to 5,000 g. After filtration through a coarse tea filter to remove large agglomerates an additional purification step was introduced to minimize the number of particles below 2 µm: The pH of the filtrate was adjusted to pH 3 to provoke electrostatic repulsion between the particles prior to an additional centrifugation step (200 g, 20 minutes). The pellet was discarded and the supernatant was used.

HSA starch particles were produced by an emulsion-based process according to previous studies by Heritage *et al.*⁵ 1 g starch was dissolved in 2 mL DMSO under stirring at 85 °C, cooled down to room temperature and subsequently 1 mL 10% (w/v) aqueous HSA solution was added drop-wise. This solution was emulsified drop-wise in 20 mL rape oil under stirring at 1250 rpm (Heidolph MR 3001K) and sonication. Afterwards this emulsion was added drop-wise to 400 mL acetone containing 0.5 mL polysorbate 80, again under stirring at 1250 rpm. The generated microparticles were then collected by filtration (0.22 µm Durapore[®] (PVDF) membrane filter, Millipore) under vacuum, washed with 1 L acetone, and dried on the filter by vacuum. The powder was sieved through a 100 µm mesh to exclude large agglomerates and the particles were stored under desiccation at 5±3 °C. 30 mg of the particles were suspended in 4 mL water for analysis.

2.3 Light obscuration (LO)

Subvisible particles in a size range between 1 and 200 μm were analyzed by LO using a PAMAS SVSS-C (Partikelmess- und Analysesysteme GmbH, Rutesheim, Germany) equipped with an HCB-LD-25/25 sensor. Particle suspensions were diluted with the according buffer (filtered by a 0.22 μm cellulose acetate/nitrate membrane filter, MF-Millipore[®]) or water in order to adhere to the concentration limit of the system of 120,000 particles/mL $> 1 \mu\text{m}$. Three measurements of a volume of 0.3 mL of each sample were performed with a pre-run volume of 0.5 mL at a fixed fill rate, emptying rate and rinse rate of 10 mL/min and the mean particle concentration per mL was reported by the system. Samples were measured in triplicates and mean and standard deviation were calculated.

2.4 Micro-Flow Imaging (MFI)

Subvisible particles in a size range between 1 and 70 μm were analyzed by MFI using an MFI4100 (ProteinSimple, Santa Clara, CA) equipped with a high-resolution 100 μm flow cell. Particle suspensions were diluted with the according buffer (filtered by a 0.22 μm cellulose acetate/nitrate membrane filter) or water in order to adhere to the concentration limit of the system of 1,200,000 particles/mL $> 0.75 \mu\text{m}$. Samples were analyzed with a sample volume of 0.65 mL and a pre-run volume of 0.3 mL at a flow rate of 0.1 mL/min. Prior to each sample run the appropriate diluting buffer was flushed through the system to provide a clean flow cell and to perform "optimize illumination". Particles stuck to the flow cell wall were only counted once and edge particles were ignored for analysis. Samples were measured in triplicates and mean and standard deviation were calculated. Results were analyzed using the MFI view application software (version 1.2, ProteinSimple).

2.5 Resonant mass measurements (RMM)

RMM was performed using the Archimedes particle metrology system (Affinity Biosensors, Santa Barbara, CA) equipped with a Micro sensor (size range 0.3 μm to 4 μm) calibrated with 1 μm polystyrene standards. Before each measurement, the system was filled with sample and the lower size limit of detection was determined three times in automatic mode. The mean value was set as a fixed

limit of detection for the measurement. The buffer density was determined for each sample based on the sensor frequency relative to the frequency and the density of water as a reference. The density of the solid part of a particle (pure protein in case of protein particles) was determined by quantifying the buoyant mass (sum of all particles in the sample) in aqueous buffer and two liquids of higher density (20% and 40% sucrose). The buoyant mass decreases with the decreasing density difference between particles and liquid and was extrapolated to a buoyant mass of zero which indicates a density match between particles and surrounding liquid. The density of the solution was then set as the density of the solid part of the particle (liquid parts within the particle do not contribute to the buoyant mass as they possess the same density as the surrounding liquid). The apparent density of protein particles including entrapped liquid was determined by adjusting the particle density input in the software from 1.37 g/mL (as used in another RMM study¹⁰) to smaller values until the size distributions determined by RMM and MFI for the same sample overlapped (defined by the same location of the maximum). Measurements were performed in triplicates and the sensor was filled with fresh sample for each measurement. The measured volume was 0.15 μL and the overall sample volume for triplicate measurements was 600 μL . Between triplicate measurements, the system was rinsed with water. Results were analyzed using the ParticleLab software (v1.8.570, Affinity Biosensors) with a size bin step of 250 nm.

3 Results and discussion

3.1 Comparison of current standards to protein particles by LO and MFI

HSA particles generated by heat stress were analyzed as a representative for protein particles in general to determine typical properties of protein particles regarding size, size distribution, shape, and transparency in order to derive target specifications for novel standardized protein-like particles. The size distribution of HSA particles generated by heat stress appeared polydisperse with small particles representing the largest fraction (Figure 5-1). Furthermore, it revealed 3 to 10x higher particle concentration detected by MFI compared to LO which is in agreement with the literature.^{4,11,12}

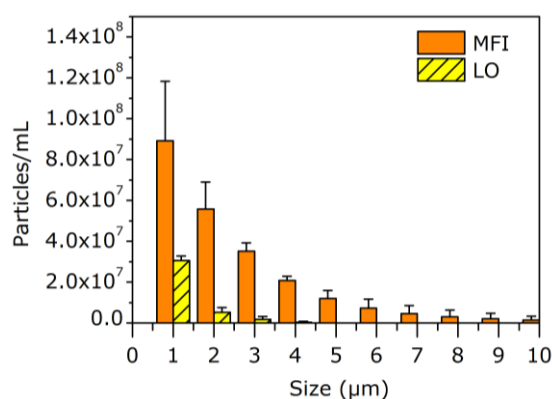


Figure 5-1: Cumulative size distribution for HSA particles generated by heat stress as determined by MFI and LO. Error bars represent standard deviations from triplicate measurements.

In contrast, 5 μm size standards made of polystyrene, glass, and silica showed a monodisperse size distribution (Figure 5-2) and identical concentrations in LO and MFI (data not shown).

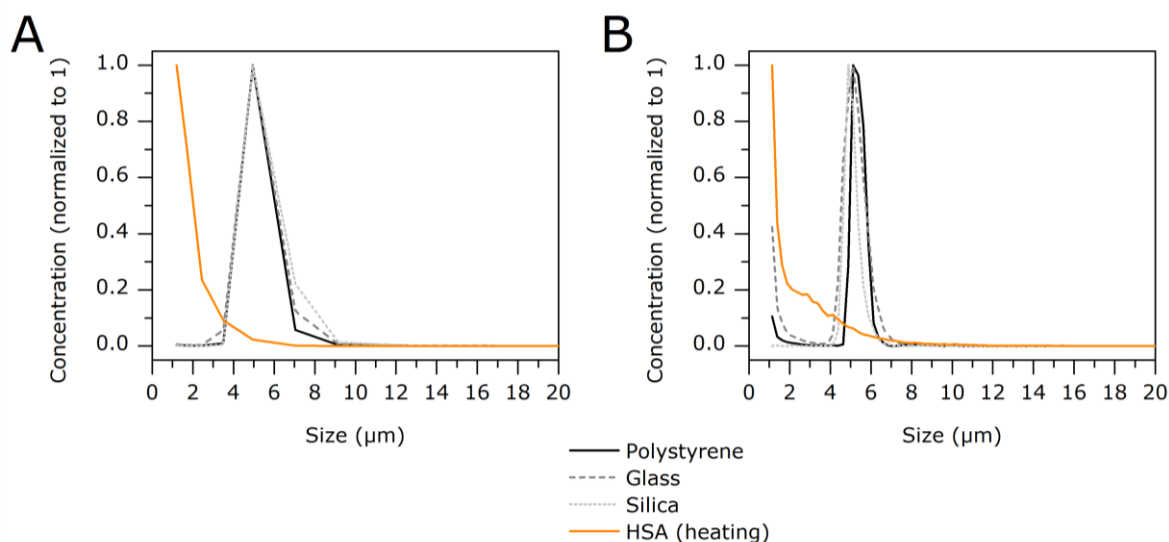


Figure 5-2: Differential size distribution of 5 μm polystyrene, glass, and silica particle size standards and HSA particles generated by heat stress determined by (A) LO and (B) MFI.

The optical particle properties shape and transparency are especially important for standards for the light-based techniques LO and MFI. The aspect ratio (between 1 for an absolutely spherical particle and 0 for a needle with an infinite length) of HSA (heating) particles was broadly distributed between 0.3 and 1.0 whereas the particle standards showed higher aspect ratios mainly above 0.8 (Figure 5-3A). The transparency was evaluated by the directly proportional intensity minimum which describes the darkest pixel on a particle image.¹³ As the intensity depends on the particle size¹⁴ the 2-6 μm range was used for the evaluation of the different materials (see Chapter 6 for further details). Particle standards displayed low intensity values (polystyrene standards approx. 300) corresponding to low transparency. In contrast, HSA (heating) particles are highly transparent with intensity values of about 700, which is close to the maximum intensity values of the instrument of about 850 typically (Figure 5-3B). These clear differences in shape and transparency between the current standards and protein particles are also reflected in the MFI images (Table 5-1). The results demonstrate that current standards do not represent protein particles adequately and justify a material screening in order to identify better materials for novel standardized protein-like particles.

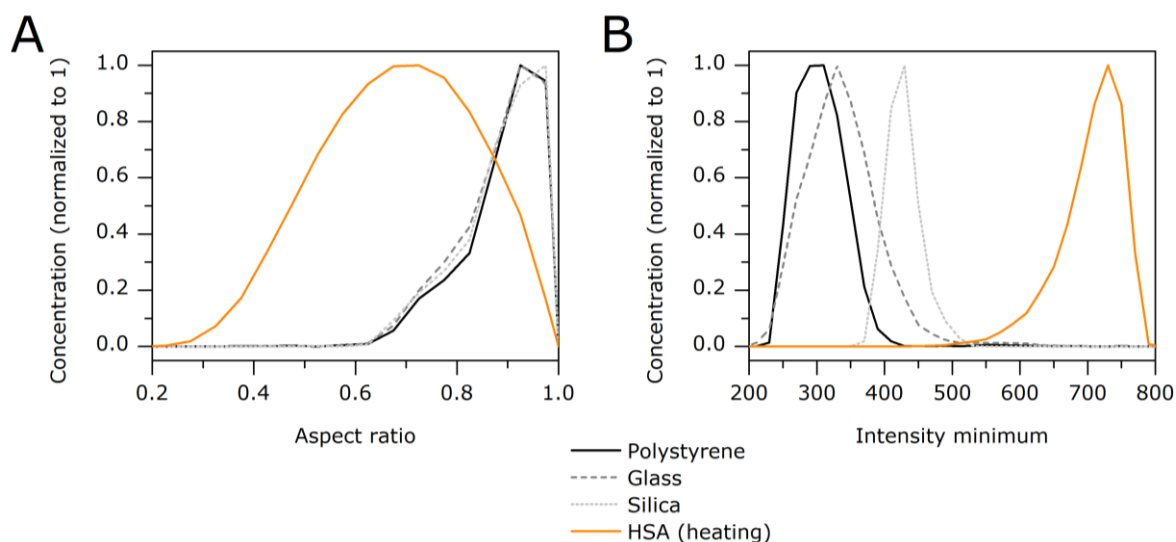


Figure 5-3: Histogram of (A) aspect ratio of all particles and (B) intensity minimum of particles in the size range of 2-6 μm for 5 μm particle size standards and HSA particles generated by heat stress determined by MFI.

Table 5-1: Representative MFI images of 5 μm particle size standards and protein particles.

Material	Polystyrene	Glass	Silica	HSA (heating)
Representative MFI images				

3.2 Evaluation of novel materials

HSA starch particles, spray-dried HSA, gelatin particles and raw powder of zein, chitosan, and PTFE were evaluated as candidates for standardized protein-like particles. In LO, only HSA-starch, gelatin, and PTFE particles displayed a similar size distribution as HSA (heating) particles, whereas spray-dried HSA and in particular chitosan and zein particles contained substantial fractions of larger particles (Figure 5-4A). These larger particles were hardly detected by MFI, presumably as they were stuck at the flow cell inlet. Overall, in MFI the size distributions of the different materials appeared rather similar (Figure 5-4B).

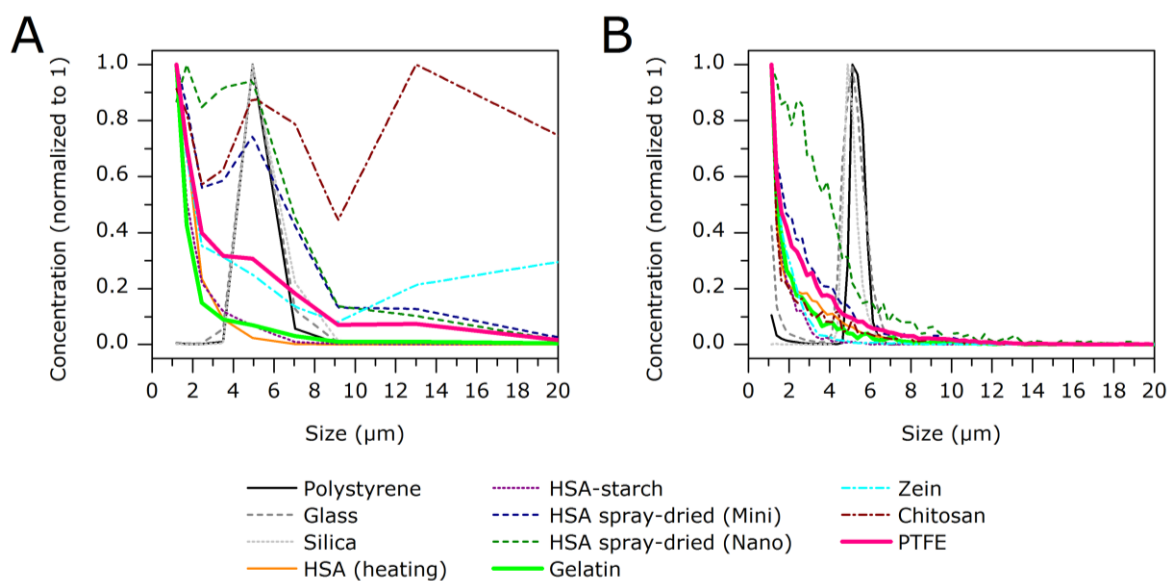


Figure 5-4: Differential size distribution (normalized) of 5 μm particle size standards and evaluated materials determined by (A) LO and (B) MFI.

With aspect ratios between 0.4 and 0.9 all evaluated particles appeared more spherical than HSA (heating) particles, but less spherical than the current particle standards (Figure 5-5A). Gelatin and PTFE particles showed higher similarity to HSA (heating) particles as compared to the other materials. The transparency as a crucial parameter was only matched by gelatin and PTFE particles whereas all other materials were clearly less transparent (Figure 5-5B). Spray-dried HSA particles were even more similar to the particle standards than to HSA (heating) particles. HSA-starch, chitosan, and zein particles showed a broad distribution in transparency with most particles in medium transparency region around 500.

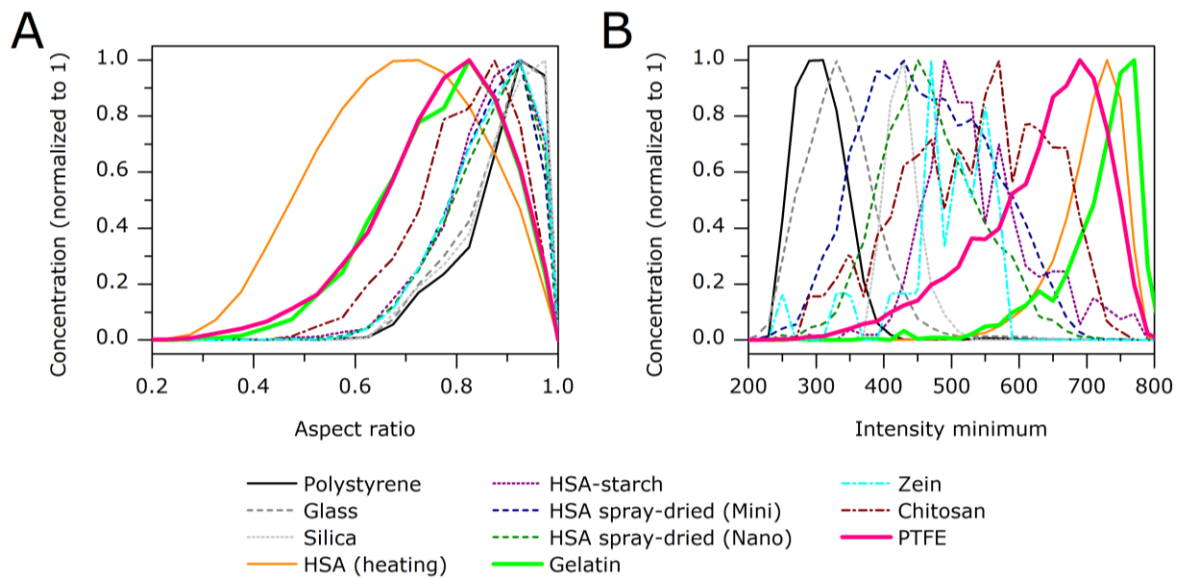


Figure 5-5: Histogram of (A) aspect ratio of all particles and (B) intensity minimum of particles in the size range of 2-6 μm for 5 μm particle size standards and evaluated materials determined by MFI.

The comparison of all evaluated parameters renders HSA starch, gelatin, and PTFE particles as most similar to HSA (heating) particles (Table 5-2). Of those three, only gelatin and PTFE particles displayed an aspect ratio mean over all particles below 0.8.

Table 5-2: Overview of results for all screened materials regarding size evaluated by MFI and LO as well as shape and transparency evaluated by MFI and representative MFI images in a size range of about 5-20 μm , scaled to the same image size. Particles most similar to HSA (heating) particles are in bold face.

Material	Size mean MFI (μm)	Size mean LO (μm)	Aspect ratio mean	Intensity minimum mean	Representative MFI images (5-20 μm)
Polystyrene	5.07	5.05	0.89	315	
Glass	4.76	5.10	0.89	356	
Silica	5.09	5.36	0.89	430	
HSA (heating)	3.09	1.67	0.68	714	
HSA-starch	1.78	1.85	0.86	651	
HSA spray-dried (Mini)	3.26	3.61	0.86	531	
HSA spray-dried (Nano)	3.65	3.55	0.86	515	
Gelatin	2.71	1.94	0.77	731	
Zein	1.87	15.5	0.86	630	
Chitosan	3.56	10.49	0.81	570	
PTFE	3.19	3.01	0.76	649	

As storage stability is an important criterion for the potential use of a material for standardized protein-like particles, HSA (heating) particles and the most promising candidates were subjected to a short stability test. Particles were stored as aqueous suspensions over 8 weeks, HSA (heating), gelatin, and HSA starch particles at 5 ± 3 °C, PTFE particles at 25 ± 2 °C. All particles showed variations in the concentration over 8 weeks (Figure 5-6). For HSA-starch particles the concentration increased significantly already after 2 days and had doubled after 8 weeks (Figure 5-6B). The concentration of PTFE particles increased clearly, but not significantly, over time (Figure 5-6D). HSA (heating) particles (Figure 5-6A) and gelatin particles (Figure 5-6C) displayed less than 40% deviation from the initial concentration.

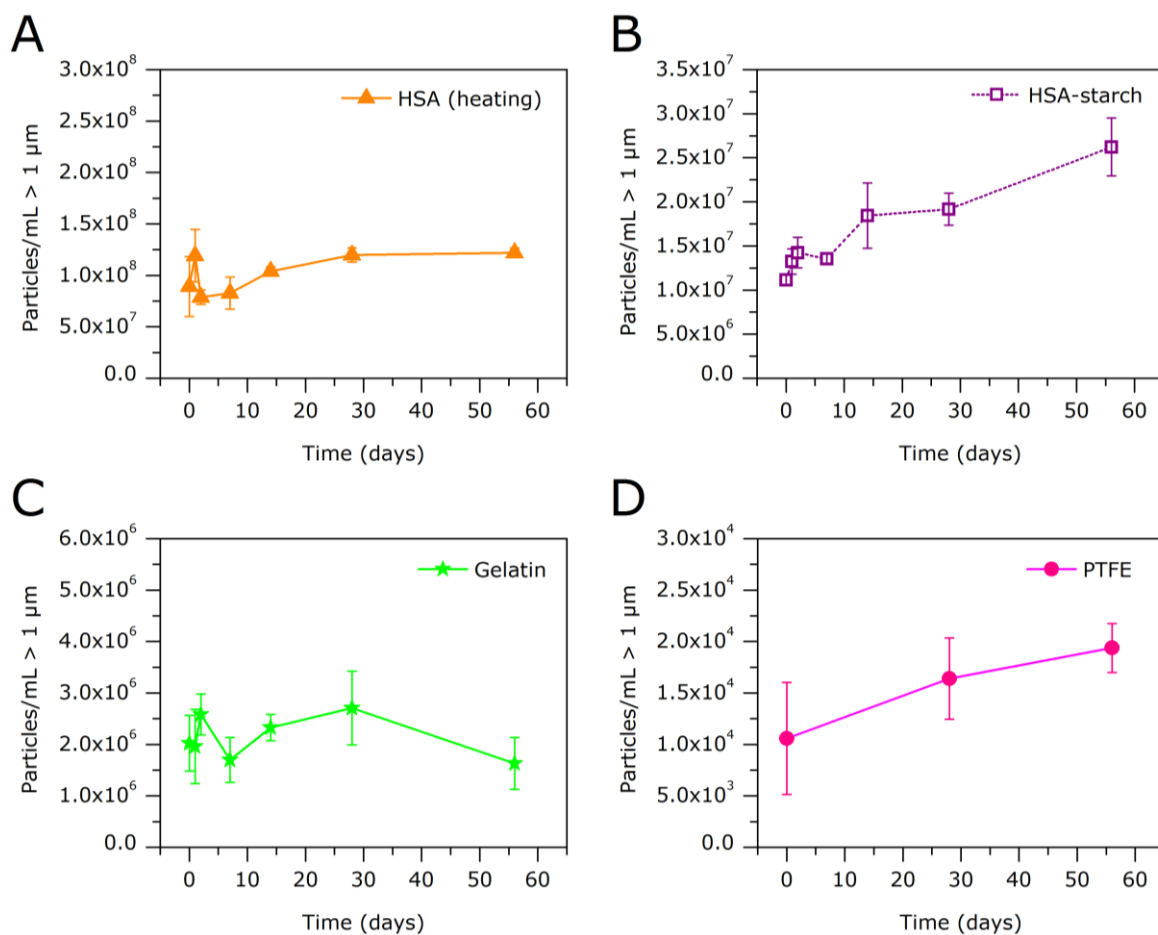


Figure 5-6: Particle concentration over time as determined by MFI for (A) HSA particles generated by heat stress, (B) HSA-starch particles, (C) gelatin particles, and (D) PTFE particles. Error bars represent standard deviations from triplicate samples.

The limited stability of HSA (heating) particles became obvious in the strong decrease in mean particle size in contrast to consistent values for HSA-starch, gelatin, and PTFE particles over storage time (Figure 5-7A). The aspect ratio varied only slightly for all materials (Figure 5-7B) and the intensity minimum mean increased slightly for all materials except gelatin particles (Figure 5-7C). Taken together, gelatin particles possessed the most constant particle properties in this stability study followed by PTFE particles. HSA-starch particles were not considered suitable due to the clear increase in concentration pointing towards particle instability.

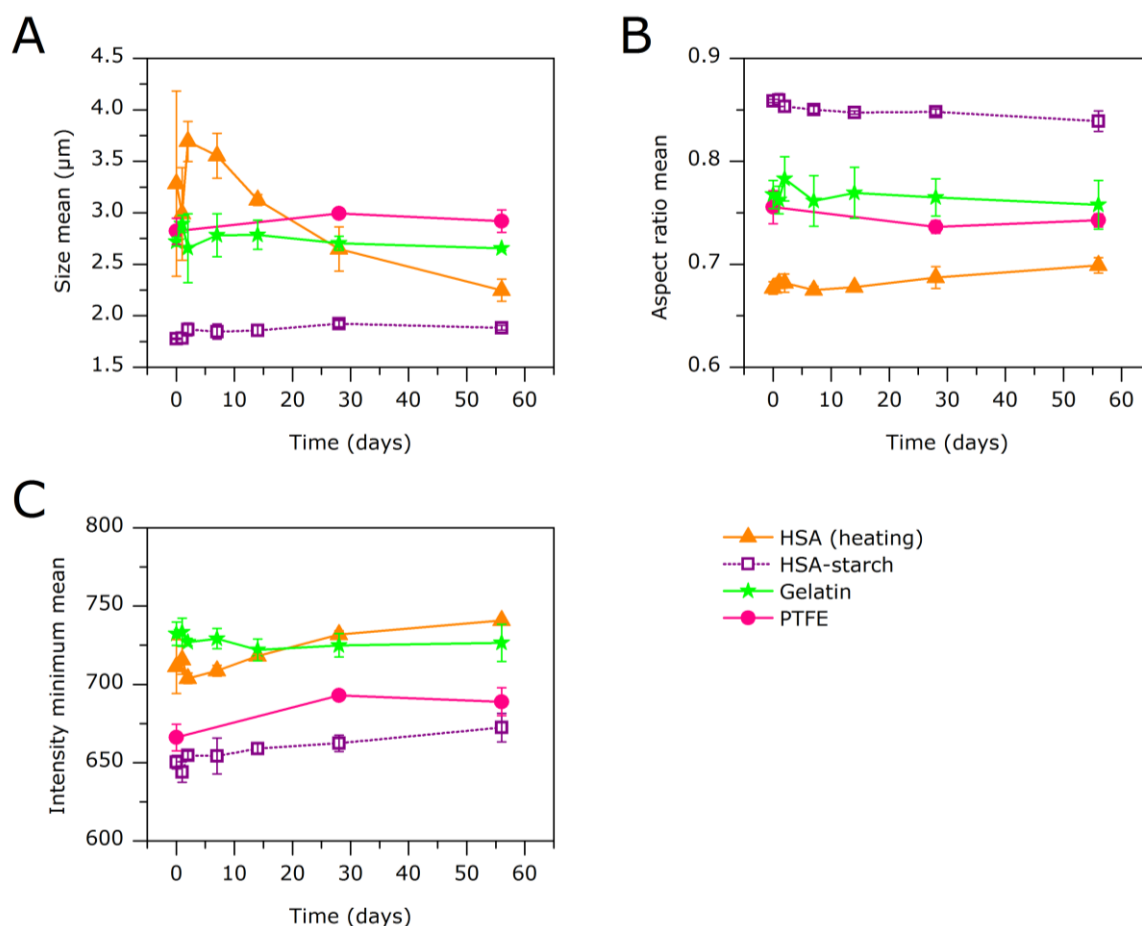


Figure 5-7: Particle properties (A) size mean, (B) aspect ratio mean, and (C) intensity minimum mean over time. Error bars represent standard deviations from triplicate samples.

3.3 Investigation of protein particle density

In addition to particle size and optical properties evaluated above, the particle density is an important criterion for particle analysis which is not yet well understood:⁶ On the one hand, a high density difference between medium and particles could influence the result by particle sedimentation or floating during the measurement. On the other hand, the non-optical technique of RMM requires knowledge of the particle density for correct size calculation. Thus, the density of protein particles is a critical property for the development of standardized protein-like particles, especially for RMM. In general, protein particles are irregularly structured and may contain substantial amounts of liquid between the solid protein parts.⁶ Therefore, two different types of density can be defined: (i) the density of only the protein part and (ii) the apparent mean density of the

complete particle including protein parts and entrapped liquid. Accordingly, methods to determine both types of density were developed in this study.

The density of only the protein part was determined based on the RMM principle.^{10,15} The buoyant mass measured by the system is converted to the particle size based on the density difference between particle and surrounding liquid. This means that if the system is not able to detect particles, the two densities must be identical making the particles “weightless”. However, an exact density match is difficult to achieve due to density variation of the particles and a viscosity limit of the system which constraints the addition of excipients for density adjustment. Alternatively, the particles can be analyzed in solutions of increasing density thereby decreasing the buoyant mass. From this data, the density at which the particles would theoretically become “weightless” can be extrapolated. As only the solid part of a particle contributes to its buoyant mass (the liquid within the particle has the same density as the surrounding liquid), only the density of the solid part is the decisive factor. This principle was used to determine the pure protein density of rituximab particles generated by heat stress and gelatin particles prepared by a two-step desolvation method.

Rituximab particles and gelatin particles were analyzed in aqueous buffer without or with 20% and 40% sucrose. Due to the broad size distribution of the particles, the sum of the buoyant mass of all particles was used for the calculation rather than the mean buoyant mass. The sum of the buoyant mass in the respective solutions was extrapolated to a buoyant mass of zero indicating a density match of particles and surrounding liquid (Figure 5-8). This method provided a density of about 1.36 g/mL and 1.42 g/mL for the solid part of rituximab (Figure 5-8A) and gelatin particles (Figure 5-8B), respectively. The results are in the range of calculated values of 1.38-1.39 g/mL for a 150 kDa antibody¹⁶ and 1.39-1.42 g/mL¹⁶ or 1.41-1.44 g/mL¹⁷ for a 40-50 kDa protein like gelatin, based on van der Waals radii and hydrodynamic volume of atomic groups (based on crystal structures of small molecules with the same atomic groups).

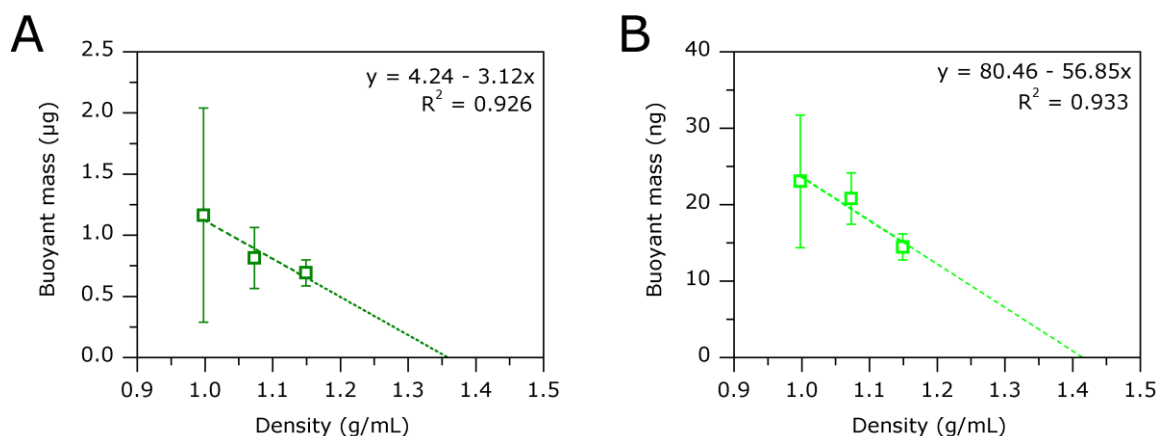


Figure 5-8: Sum of the buoyant mass over all particles determined in sucrose solutions of different density and extrapolated to the density match of particles and solution for (A) rituximab particles generated by heat stress and (B) gelatin particles. Error bars represent standard deviations from triplicate measurements.

The second type of particle density, the density of protein particles including entrapped liquid, is important for correct size determination by RMM and cross-correlation of data obtained from RMM and optical techniques. MFI and LO as light-based techniques do not consider the particle density in the size calculation. Instead, the border of the particle's image (MFI) or shadow (LO) including both solid parts and liquid parts is defined as the border of the particle. The particle size is then calculated as the equivalent circular diameter, i.e. the diameter of a circle with the same area as the particle. Thus the same particle size can only be detected by MFI/LO and RMM if the density of protein particles including liquid parts is used for the calculation in RMM. When adjusting the density value in the RMM software until the same particle size is detected in MFI/LO and RMM, i.e. the size distributions overlap, this very density reflects the density of the protein particles including liquid parts. This method requires a clear maximum in the size distribution as a reference point.

Rituximab particles generated by heat stress showed an interesting size distribution in MFI and RMM with a clear maximum (Figure 5-9) which is not typical for protein.^{4,14,18,19} Usually small particles represent the largest fraction in a protein particle size distribution as seen for example for HSA particles generated by heat stress (Figure 5-1) or other therapeutic proteins (see also Chapter 2, Chapter 3, Chapter 4, and Chapter 6). In RMM, the maximum for

rituximab particles was located at about 2.5 μm with an input density of 1.37 g/mL as used in another study for RMM¹⁰ (Figure 5-9A). In this case, the particle size represents the size of a protein particle without liquid parts. In MFI, the maximum was located at about 4.5 μm which displays the particle size including liquid parts (Figure 5-9A). The input density for size calculation in RMM was then adjusted until the size distributions from both techniques overlapped (assessed by the location of the maximum, Figure 5-9B). This suggested a particle density including liquid parts of 1.07 g/mL \pm 0.05 g/mL and indicated that a protein particle could consist of approx. 70-95% of aqueous liquid and only 5-30% of protein (calculated with 1.02 g/mL as the lowest possible and 1.12 g/mL as the highest possible density including liquid parts, 1.0 g/mL for aqueous liquid and 1.36 g/mL for pure protein as determined above).

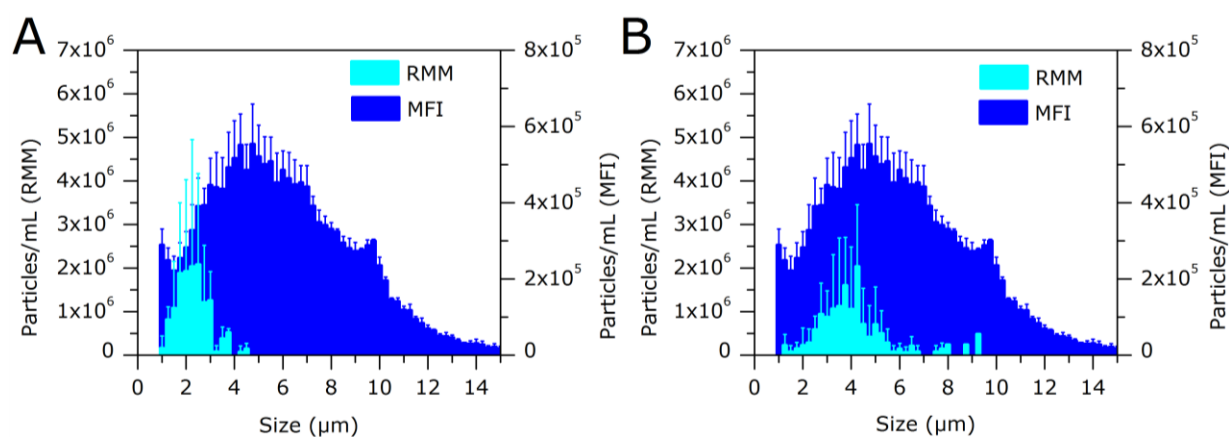


Figure 5-9: Differential size distribution of rituximab particles generated by heat stress determined by MFI and RMM using an input density of (A) 1.37 g/mL and (B) 1.07 g/mL for RMM. Error bars represent standard deviations from triplicate measurements.

For gelatin particles, density determination by this method was not possible due to a size distribution without a clear maximum of the size distribution in the μm range (Figure 5-10).

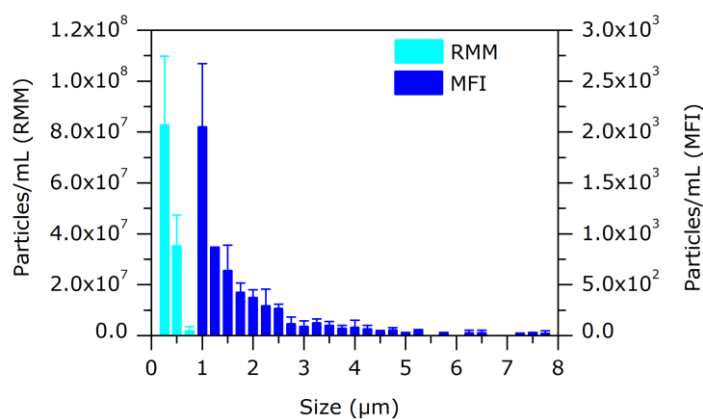


Figure 5-10: Differential size distribution of gelatin particles determined by MFI and RMM using an input density of 1.37 g/mL. Error bars represent standard deviations from triplicate measurements.

Thus, particle density is important for the development of standardized protein-like particles to be used not only in light-based methods. The density of polystyrene standards (1.05 g/mL) is very close to the density of protein particles including entrapped liquid whereas glass and silica standards show clearly higher density values (2.5 g/mL and 1.8-2.0 g/mL). Thus, polystyrene standards can be considered suitable for RMM if an input density of 1.07 g/mL is used. If the density of pure protein of around 1.4 g/mL (calculated or determined) is used, gelatin particles might be better as they showed a similar density of pure protein (calculated and determined).

4 Conclusion

This study identified gelatin particles, prepared by a two-step desolvation method with subsequent cross-linking by glutaraldehyde, and PTFE particles (raw material powder), as optically similar to particles of therapeutic proteins. Especially the particle properties shape and transparency were represented well – in contrast to polystyrene standards. This justifies the further investigation of gelatin and PTFE particles as promising candidates for the development of standardized protein-like particles especially for light-based techniques (see Chapter 6 for an application of PTFE particles). Two methods for determination of protein particle density based on RMM were developed in this study. They revealed a density of pure protein of around 1.4 g/mL, which was congruent with theoretical values, and furthermore a density of protein particles with entrapped liquid of 1.07 g/mL. Taken together, both optical properties and density are crucial for the development of novel standardized protein-like particles. PTFE particles showed useful properties especially for light-based techniques whereas gelatin particles might be suitable for both light-based and weight-based methods.

5 References

1. Sharma DK, King D, Oma P, Merchant C 2010. Micro-flow imaging: flow microscopy applied to sub-visible particulate analysis in protein formulations. *AAPS J* 12:455-464.
2. Singh SK, Afonina N, Awwad M, Bechtold-Peters K, Blue JT, Chou D, Cromwell M, Krause H-J, Mahler H-C, Meyer BK, Narhi L, Nesta DP, Spitznagel T 2010. An industry perspective on the monitoring of subvisible particles as a quality attribute for protein therapeutics. *J Pharm Sci* 99:3302-3321.
3. Carpenter J, Cherney B, Lubinecki A, Ma S, Marszal E, Mire-Sluis A, Nikolai T, Novak J, Ragheb J, Simak J 2010. Meeting report on protein particles and immunogenicity of therapeutic proteins: filling in the gaps in risk evaluation and mitigation. *Biologicals* 38:602-611.
4. Wuchner K, Büchler J, Spycher R, Dalmonte P, Volkin DB 2010. Development of a microflow digital imaging assay to characterize protein particulates during storage of a high concentration IgG1 monoclonal antibody formulation. *J Pharm Sci* 99:3343-3361.
5. Heritage PL, Loomes LM, Jianxiong J, Brook Ma, Underdown BJ, Mcdermott MR 1996. Novel polymer-grafted starch microparticles for mucosal delivery of vaccines. *Immunology* 88:162-168.
6. Ripple DC, Wayment JR, Carrier MJ 2011. Standards for the optical detection of protein particles. *APR*:90-96.
7. Schüle S 2005. Stabilization of antibodies in spray-dried powders for inhalation. Dissertation, Ludwig-Maximilians-Universität München.
8. Fuhrherr R 2005. Spray-dried antibody powders for pulmonary application. Dissertation, Ludwig-Maximilians-Universität München.
9. Zwioerek K 2006. Nanoparticles as delivery system for nucleotide based drugs. Dissertation, Ludwig-Maximilians-Universität München.
10. Patel AR, Lau D, Liu J 2012. Quantification and characterization of micrometer and submicrometer subvisible particles in protein therapeutics by use of a suspended microchannel resonator. *Anal Chem* 84(15):6833-6840.
11. Demeule B, Messick S, Shire SJ, Liu J 2010. Characterization of particles in protein solutions: reaching the limits of current technologies. *AAPS J* 12:708-715.
12. Huang C-T, Sharma D, Oma P, Krishnamurthy R 2009. Quantitation of protein particles in parenteral solutions using micro-flow imaging. *J Pharm Sci* 98:3058-3071.
13. Sharma DK, Oma P, Pollo MJ, Sukumar M 2010. Quantification and characterization of subvisible proteinaceous particles in opalescent mAb formulations using micro-flow imaging. *J Pharm Sci* 99:2628-2642.
14. Zöls S, Gregoritz M, Tantipolphan R, Wiggerhorn M, Winter G, Friess W, Hawe A 2013. How subvisible particles become invisible-relevance of the refractive index for protein particle analysis. *J Pharm Sci* 102:1434-1446.
15. Burg TP, Godin M, Knudsen SM, Shen W, Carlson G, Foster JS, Babcock K, Manalis SR 2007. Weighing of biomolecules, single cells and single nanoparticles in fluid. *Nature* 446:1066-1069.
16. Tsai J, Taylor R, Chothia C, Gerstein M 1999. The packing density in proteins: standard radii and volumes. *J Mol Biol* 290:253-266.
17. Quillin ML, Matthews BW 2000. Accurate calculation of the density of proteins. *Acta Crystallogr D* 56:791-794.
18. Barnard JG, Singh S, Randolph TW, Carpenter JF 2011. Subvisible particle counting provides a sensitive method of detecting and quantifying aggregation of monoclonal antibody caused by freeze-thawing: insights into the roles of particles in the protein aggregation pathway. *J Pharm Sci* 100:492-503.
19. Weinbuch D, Zöls S, Wiggerhorn M, Friess W, Winter G, Jiskoot W, Hawe A 2013. Micro-Flow Imaging and resonant mass measurement (Archimedes) – Complimentary methods to quantitatively differentiate protein particles and silicone oil droplets. *J Pharm Sci* 102:2152-2165.

Chapter 6

How subvisible particles become invisible – relevance of the refractive index for protein particle analysis

Abstract

The aim of the present study was to quantitatively assess the relevance of transparency and refractive index on protein particle analysis by the light-based techniques light obscuration (LO) and Micro-Flow Imaging (MFI). A novel method for determining the refractive index of protein particles was developed and provided a refractive index of 1.41 for protein particles from two different proteins. An increased refractive index of the formulation by high protein concentration and/or sugars at pharmaceutically relevant levels was shown to lead to a significant underestimation of the subvisible particle concentration determined by LO and MFI. A refractive index match even caused particles to become “invisible” for the system, i.e. not detectable anymore by LO and MFI. To determine the influence of formulation refractive index on particle measurements, we suggest the use of polytetrafluoroethylene (PTFE) particles to test a specific formulation for refractive index effects. In case of refractive index influences, we recommend also using a light-independent technique such as resonant mass measurement (Archimedes) for subvisible particle analysis in protein formulations.

The following chapter was published as a research article in the Journal of Pharmaceutical Sciences and appears in this thesis with the journal's permission:

S. Zölls, M. Gregoritz, R. Tantipolphan, M. Wiggenhorn, G. Winter, W. Friess, A. Hawe: "How subvisible particles become invisible – relevance of the refractive index for protein particle analysis"; J Pharm Sci 102(5):1434-1446 (2013)

1 Introduction

Protein aggregates and particles are an important instability product in therapeutic protein formulations, which need to be quantified and characterized due to quality requirements, potential loss of activity and the potential risk of immunogenicity.¹⁻⁴ For many years pharmacopeias have required the analysis of subvisible particles, i.e. particles below 100 μm , also designated as micron aggregates,⁵ in size classes larger than 10 μm and 25 μm .^{6,7} However, in the last few years, there has been a trend to monitor particles in the size range below 10 μm . This trend is due to regulatory interest in particle data for sizes below 10 μm as part of the analytical characterization of a new product and post marketing commitment.⁸ This resulted amongst others in the compilation of the new educational chapter USP<1787> which deals with the analysis of subvisible particles, specifically in protein formulations, also below 10 μm and will be available soon.⁹

Light-based techniques like light obscuration (LO) and flow imaging techniques, e.g. Micro-Flow Imaging (MFI), are commonly used for subvisible particle analysis.¹⁰⁻¹⁵ Light obscuration is the current compendial method but both LO and MFI will be included in the new educational chapter USP<1787>.⁹ Alternative techniques which do not rely on the interaction of particles with light are electrical sensing zone (ESZ, Coulter counter)¹⁶ or resonant mass measurements (RMM, Archimedes).¹⁷ However, ESZ requires large sample volumes and sufficient buffer conductivity which is often not feasible for protein formulations¹⁴ and experience using RMM is limited.^{18,19} Particle techniques are generally calibrated with polystyrene particle standards which have optical and morphological properties clearly different from those of protein particles.¹² Thus, researchers in the field of particle analysis from industry, regulatory agencies, and academia have emphasized the need of "proteinaceous subvisible particle standards",²⁰ "alternative particle standards with more protein-like morphology",¹⁰ or "relevant protein particulate standards".¹

One of the major differences between polystyrene particle standards and protein particles is the transparency^{12,21-23} which is in turn connected to the refractive index (RI) of the particles.²⁴ The RI is a dimensionless unit which describes the

refraction of light by a specific material.²⁵ However, the RI of protein particles has not been determined so far and is only estimated to be in the range from 1.33 to 1.4¹² or 1.4 to 1.6.¹¹ The influence of the RI on light-based techniques for particle analysis has been qualitatively studied by analyzing glass particle standards in ethylene glycol¹² and protein particles in highly-concentrated protein solutions.¹¹ Consequently, there is a need for methods for RI determination of protein particles^{24,26} as well as for the quantitative evaluation of RI effects on protein particle analysis.

Our aim was to quantitatively assess the relevance of the optical properties transparency and RI for protein particle analysis. Therefore, we set out to develop a method for RI determination of protein particles based on the immersion principle (minimized light scattering and maximized light transmission at the RI match).²⁷ The influence of the RI difference of particles and surrounding formulation on the measured particle concentration and size by LO and MFI was investigated at pharmaceutically relevant test conditions and in marketed pharmaceutical products.

2 Materials and methods

2.1 Materials

Infliximab (Remicade[®], lots no. 7GD9301402, 7FD8701601, 7RMKA81402, pooled), rituximab (MabThera[®], lot no. B6073, exp. 12/2013), adalimumab (Humira[®], lot no. 292209A05, exp. 10/2006) and etanercept (Enbrel[®], lot no. 31576, exp. 12/2008) were provided by local hospitals. Infliximab solution (IgG A) at a concentration of 1 mg/mL was prepared by dilution of 10 mg/mL infliximab in 100 mM phosphate buffer (pH 7.2). Rituximab solution (IgG B) at a concentration of 1 mg/mL was prepared by dilution of 10 mg/mL rituximab in 25 mM citrate buffer (pH 6.5) containing 154 mM NaCl and 0.07% polysorbate 80. Adalimumab solution at a concentration of 5 mg/mL was prepared by dilution of 50 mg/mL adalimumab in 15 mM phosphate/citrate buffer (pH 5.2) containing 105 mM NaCl, 1.2% mannitol and 0.1% polysorbate 80. Etanercept solutions at concentrations of 1, 2, and 5 mg/mL were prepared by dilution of 50 mg/mL etanercept in 25 mM phosphate buffer (pH 6.3) containing 100 mM NaCl, 25 mM arginine hydrochloride and 1% sucrose. Human serum albumin (HSA) was purchased from Sigma-Aldrich (Steinheim, Germany) and formulated at 1 mg/mL in a 50 mM citrate buffer (pH 4.8). All protein formulations were filtered using a 0.2 μm cellulose acetate syringe filter (Minisart[®], Sartorius Stedim Biotech, Aubagne, France) for further use.

Particles were generated by (i) stir stress, (ii) freeze-thaw stress or (iii) heat stress. For (i), 8 mL of the formulation was stirred in a 10R glass vial with a 18 mm Teflon[®]-coated stir bar at 250 rpm at room temperature on a magnetic stirrer (Heidolph MR Hei-Standard, Schwabach, Germany) for 24 hours (IgG A (stirring)). For (ii), 1 mL of the formulation in a 1.5 mL low protein binding reaction tube (Eppendorf, Hamburg, Germany) was subjected to 7 freeze-thawing cycles of 30 minutes in a -80 °C freezer and 10 minutes in a 25 °C water bath (IgG A (freeze-thawing)). For (iii), 0.5 mL of the formulation was heated for 30 minutes at 60 °C (IgG A (heating)) or 1.5 mL of the formulation was heated for 30 minutes at 71 °C (IgG B (heating)) in a 1.5 mL low protein binding reaction tube in a thermomixer (Eppendorf, Hamburg, Germany) or 50 mL of the

formulation was heated in a 50 mL tube (Greiner bio-one, Frickenhausen, Germany) for 30 minutes at 70 °C in a water bath (HSA (heating)).

Polystyrene and glass particle standards were purchased from Duke Scientific (through Thermo Scientific, Fremont, CA), silica particle standards from Microparticles GmbH (Berlin, Germany) and PTFE microparticles (Microdispers 8000) from Polysciences Inc. (Warrington, PA). Polystyrene, glass, and silica particle standards were suspended in water. PTFE particles were suspended at a concentration of 50 mg/mL in 0.5% polysorbate 80 using an Ultra Turrax dispersing system (T10 basic, IKA® Werke, Staufen, Germany) for 3 minutes. Larger agglomerates were removed by filtration through a coarse tea filter (dm, Karlsruhe, Germany).

Sucrose solutions were prepared by dilution (w/w) of a 70% (w/w) solution (prepared by dissolving sucrose in water under stirring and heating to 60 °C in a closed container). All solutions were filtered using a 0.2 µm cellulose acetate syringe filter and air bubbles were removed by centrifugation for 5 minutes at 10,400 rpm (Centrifuge 5810R, Eppendorf, Hamburg, Germany) prior to use.

Sucrose, citric acid monohydrate, sodium hydroxide, di-sodium hydrogenphosphate dihydrate and sodium dihydrogenphosphate dihydrate were purchased from Merck KGaA (Darmstadt, Germany). Sodium chloride, sodium citrate dihydrate and polysorbate 80 were from VWR (Darmstadt, Germany). The water used in this study was highly purified water (Advantage A10 purification system, Millipore, Newark, NJ).

2.2 Refractive index determination

Refractive indices of sucrose and HSA solutions as well as Humira® and Enbrel® formulations were determined using an Abbé refractometer (Carl Zeiss AG, Oberkochen, Germany). Measurements were performed in triplicates at a wavelength of 589 nm at room temperature.

For particle RI determination, the protein particle suspensions were concentrated by centrifugation and resuspension of the pellet for 5 minutes at 10,400 rpm to a final concentration between 1×10^8 particles/mL and 5×10^8 particles/mL > 1 µm as

controlled by LO (corresponding to a minimal protein concentration of about 70 µg/mL within the particles based on a minimum particle size of 1 µm and a density of protein particles of 1.32 g/mL). An overview of the procedure for particle RI determination, based on immersion, is given in Figure 6-1. Twelve different sucrose solutions, in a concentration range depending on the expected RI of the particles, e.g. from 5% to 60% in 5% steps, were pipetted into a 96 well plate (Corning Inc., Corning, NY) by an automated liquid handling station (Microlab Star[®], Hamilton Robotics, Reno, NV) in surface dispense mode (n=6, 190 µL per well with parameters optimized for highly viscous solutions). A background measurement of the sucrose solutions was performed using a Safire² plate reader (Tecan Group AG, Männedorf, Switzerland) with optimized measurement parameters. Light scattered by the sample was determined in "absorbance mode" (= scattering) and light transmitted through the sample was determined in "fluorescence mode" (= transmission), both at a wavelength of 589 nm. A pathlength correction was performed for the absorbance mode to account for the varying pathlength due to the different viscosity of the sucrose solutions according to the manufacturer's recommendation.²⁸

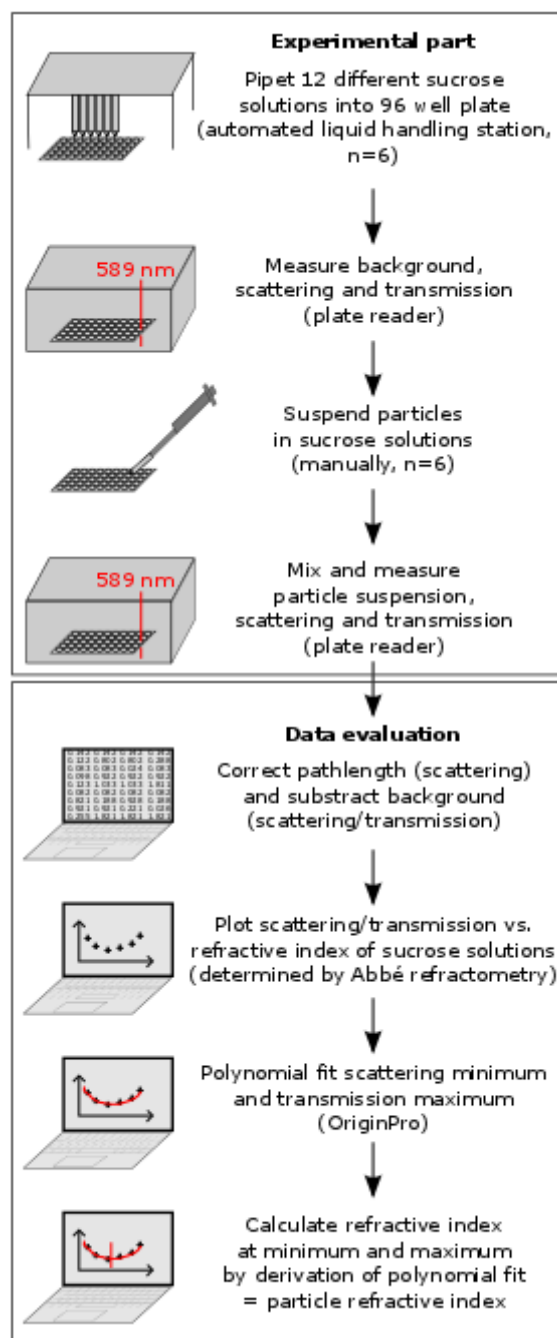


Figure 6-1: Schematic overview of the developed method for RI determination of (protein) particles based on the immersion principle.

For particle measurements, 10 μL concentrated particle suspension were added manually to each well (total volume 200 μL) and scattering and transmission were determined as described before. Mean and standard deviation for each sixuplicate were calculated, outliers were excluded from further calculation (Grubbs test, $\alpha = 0.05$) and means of scattering and transmission were plotted

against the RI of the sucrose solutions (determined by Abbé refractometry). Scattering minimum and transmission maximum (= RI match points between sucrose solution and particles) were determined by a polynomial fit (OriginPro software, version 8.5) and the particle RI was calculated as the mean from three independent experiments.

2.3 Light obscuration (LO)

Subvisible particles in a size range between 1 and 200 μm were analyzed by LO using a PAMAS SVSS-C (Partikelmess- und Analysesysteme GmbH, Rutesheim, Germany) equipped with an HCB-LD-25/25 sensor. Particle suspensions were diluted with the appropriate buffer (filtered by a 0.22 μm cellulose acetate/nitrate membrane filter, MF-Millipore[®], Millipore) or water in order to adhere to the concentration limit of the system of 120,000 particles/mL $> 1 \mu\text{m}$. Three measurements of a volume of 0.3 mL of each sample were performed with a pre-run volume of 0.5 mL at a fixed fill rate, emptying rate and rinse rate of 10 mL/min and the mean particle concentration per mL was reported by the system. Samples were measured in triplicates and mean and standard deviation were calculated.

2.4 Micro-Flow Imaging (MFI)

Subvisible particles in a size range between 1 and 70 μm were analyzed by MFI using a MFI4100 (ProteinSimple, Santa Clara, CA) equipped with a high-resolution 100 μm flow cell. Particle suspensions were diluted with the appropriate buffer (filtered by a 0.22 μm cellulose acetate/nitrate membrane filter) or water with the same dilution factor as for LO. Samples were analyzed with a sample volume of 0.65 mL and a pre-run volume of 0.3 mL at a flow rate of 0.1 mL/min. Prior to each sample run the respective diluting agent was flushed through the system to provide a clean flow cell. The "optimize illumination" procedure was performed with an appropriate diluent of the respective sample, e.g. formulation buffer, to ensure correct thresholding of the MFI system. Particles stuck to the flow cell wall were only counted once and edge particles were excluded for analysis. Samples were measured in triplicates and mean and standard deviation were calculated. Results were analyzed using the MFI view application software version (MVAS) 1.2. For samples in prefilled syringes,

protein particles and silicone oil droplets were differentiated by the “find similar” algorithm in the MVAS software (at least 20 images clearly identified as silicone oil droplets were selected manually as a basis for the automatic search function by the software).

2.5 Resonant mass measurements (RMM)

Resonant mass measurements were performed using the Archimedes particle metrology system (Affinity Biosensors, Santa Barbara, CA) equipped with a Micro sensor (size range 0.3 to 4 μm) calibrated with 1 μm polystyrene standards. Before each measurement, the system was filled with sample and the lower size limit of detection was determined three times in automatic mode. The mean value was set as a fixed limit of detection for the measurement. The buffer density was determined for each sample. The particle density was set to 1.32 g/mL for negatively buoyant particles (proteinaceous particles) according to the recommendation of the manufacturer. Measurements were performed in triplicates and the sensor was filled with fresh sample for each measurement. The measured volume was 0.15 μL and the overall sample volume for triplicate measurements was 600 μL . Between triplicate measurements, the system was rinsed with water. Results were analyzed using the ParticleLab software (v1.8.570) with a size bin step of 10 nm.

3 Results and discussion

3.1 Transparency evaluation of protein particles

Protein particles generated by freeze-thawing, stirring or heating an IgG formulation at 1 mg/mL were analyzed by MFI. Besides the particle size distribution (Figure 6-2), the optical properties of the particles, in particular the transparency, were evaluated. The transparency can be judged by means of the intensity value obtained from MFI images, which is proportional to particle transparency.²³ The intensity can vary in a unit-less theoretical range from 0 (= low transparency, "dark particles") to 1,023 (= high transparency, "bright particles"). Due to the calibration settings of the MFI system, maximum intensity values of around 850 are typically reached. The MFI system applies bright-field microscopy and thereby excludes pixels in the particle from the analysis which are brighter than the background, which are probably present due to specific diffraction patterns.²⁹ Thus, intensity parameters such as intensity mean or intensity maximum might not be representative for the real particle transparency. In contrast, the intensity minimum, which describes the transparency of the "darkest pixel" of a particle, is not influenced by pixels brighter than the background and can also be used to differentiate particles of various origins by MFI.¹² Therefore, we chose the intensity minimum for the evaluation of particle transparency in this study.

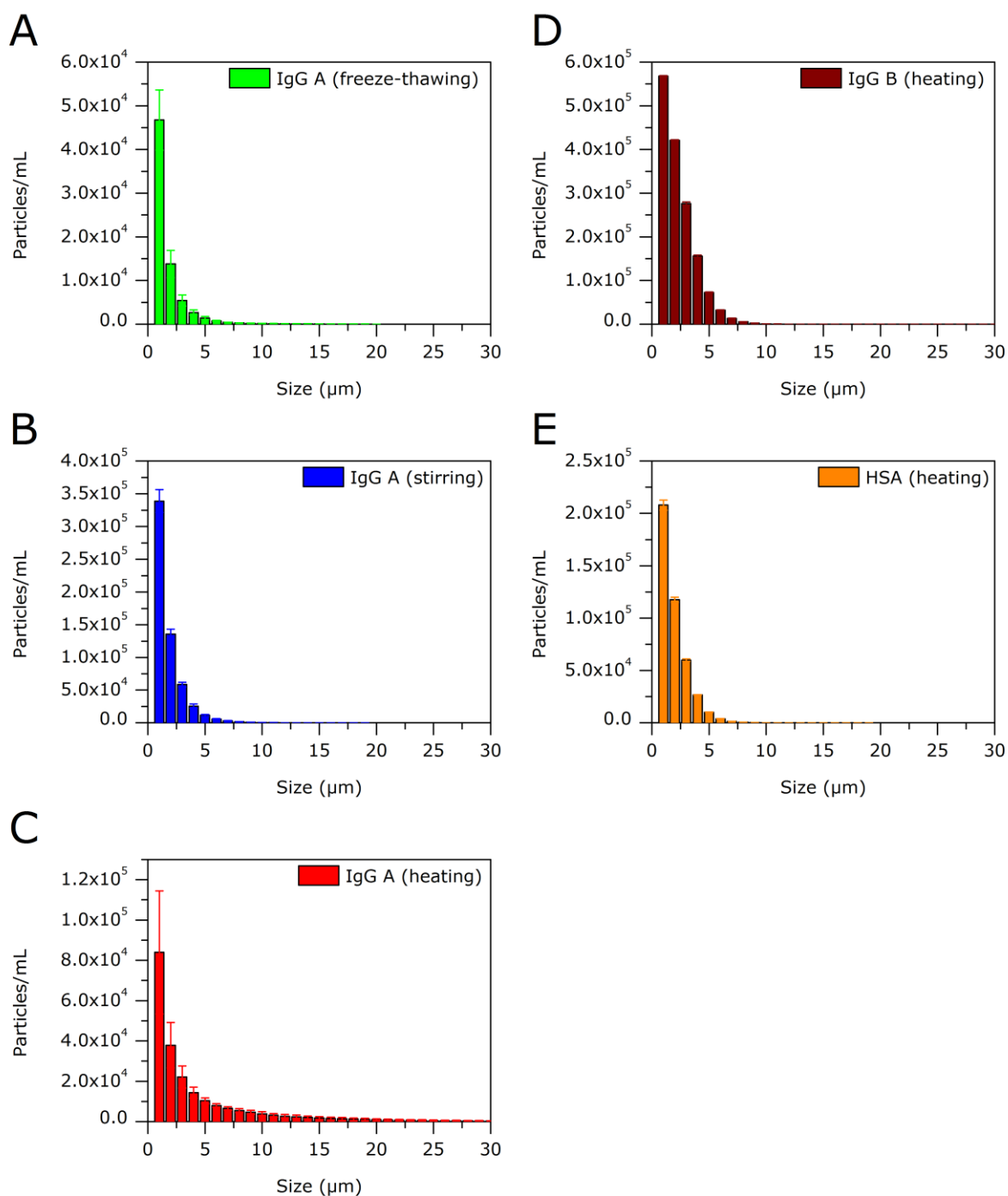


Figure 6-2: Cumulative size distributions of the different types of protein particles obtained by MFI analysis for IgG A particles generated by (A) freeze-thaw stress, (B) stir stress, (C) heat stress. (D) IgG B particles generated by heat stress, (E) HSA particles generated by heat stress.

For the protein particles generated by the three different types of stress, the intensity minimum was distributed over a broad range that was clearly influenced by the particle size (Figure 6-3A). Small particles showed high transparency, e.g.

intensity minimum values of about 700-800 for the smallest sizes of 1-2 μm , whereas larger particles appeared at lower transparency, e.g. intensity minimum values of about 300-500 for particles $> 10 \mu\text{m}$. Size-dependent differences were material-independent, as can be seen in the comparison of the particle images of protein particles and polystyrene particle standards (Figure 6-3B). The lower reported transparency values of larger particles can mainly be attributed to the longer optical path length (Z-dimension) of a larger particle which decreases the light transmission more strongly as compared to a smaller particle with a shorter optical path length. Due to the size dependence and the varying size distribution between different samples, it is reasonable to evaluate the transparency of particles in a specific size range. In this study the size range of 2-6 μm was selected for quantitative intensity evaluation, as particles in the low μm range represented the largest fraction in all samples evaluated (Figure 6-2). Below 2 μm , the image quality was insufficient to draw conclusions from intensity values. Particles larger 6 μm showed similar trends but were less representative due to lower total particle counts.

In the resulting size-specific histogram (Figure 6-3C), the intensity minimum peaks were located in very similar regions of about 600-800 for all types of protein particles. In contrast, polystyrene, glass and silica particle standards showed clearly lower intensity minimum values of about 300-400 reflecting the lower transparency of the commonly used standards. Larger particles displayed similar differences in the intensity minimum values: 300-500 for protein particles vs. about 200 for polystyrene particles of 10 μm and 200-300 for protein particles vs. about 100 for polystyrene particles of 20 μm . Differences in the transparency are also directly visible in the MFI images, as exemplarily shown for IgG A particles and polystyrene particle standards (Figure 6-3B). This confirms that transparency is an important parameter which is not represented well by current particle standards as stated by several experts in the field^{12,21-23} and explains the need for more proteinaceous particle standards.^{1,10,20} Therefore, we screened several materials in order to identify one with an intensity minimum that was more representative of protein particles. Among various proteinaceous and non-proteinaceous materials (see Chapter 5) PTFE displayed similar transparency as compared to protein particles (Figure 6-3C). Interestingly, the observed low transparency of polystyrene correlated with its high RI of 1.59

whereas the high transparency of PTFE corresponded with its lower RI of 1.35-1.38.^{30,31} This indicated a connection between RI and transparency and made the knowledge of the RI of protein particles, which has only been estimated so far,^{11,12} even more important. Consequently, we set out to develop a method for RI determination of protein particles to support the identification of a suitable reference material and to better understand the impact of the RI of both the formulation and the protein particles on the results of LO and MFI analyses.

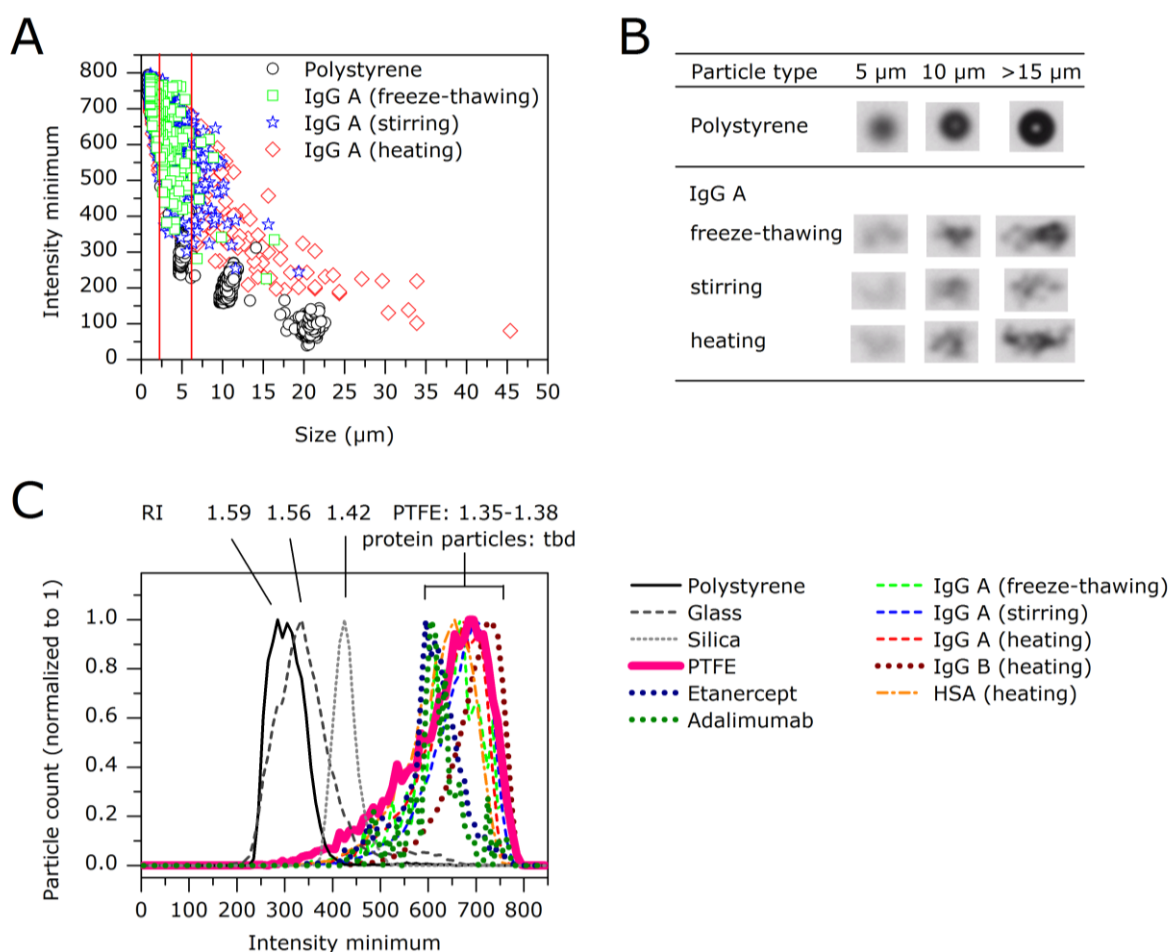


Figure 6-3: (A) Scatter plot of the intensity minimum from MFI against the particle size; the red lines indicate the size range of 2-6 μm used for further evaluation of the intensity minimum. (B) Representative particle images from MFI, scaled to the same size, indicating differences in particle transparency depending on particle size and material. (C) Histogram of the intensity minimum of particles in the size range of 2-6 μm for different materials. The RI of the respective material is indicated above the data if known. tbd = to be determined.

3.2 Refractive index determination of protein particles

A prerequisite for light scattering by an object is an RI difference between the object and the surrounding medium (usually air or liquid). In case of an RI match, light directed towards the object can pass directly through the object leading to minimized light scattering and maximized light transmission (immersion effect).²⁷ Close to the RI match, light is still scattered and transmission is still interrupted by the object. However, decreased light interaction at the edges of the object leads to decreased light scattering and increased light transmission around the absolute turning point at the RI match. Because light scattering and transmission are critical parameters in light-based particle analysis, RI determination of protein particles based on those principles is reasonable. In order to identify the RI of the protein particles, sucrose solutions of different concentrations/RIs were prepared to identify the point at which the RI of the particles and the carrier solution matched.

Light scattering and transmission of silica particle standards of known RI was first quantified for the proof of concept of the method. The obtained RI of 1.42 corresponded with the value provided by the manufacturer³² for 2 μm silica particles (Figure 6-4A) and also for 5 μm and 8 μm silica particles (Figure 6-4A, insert, only scattering mode). This shows that our method provides correct results in the lower μm size range.

For both HSA particles (heating) and IgG A particles (stirring) an RI of about 1.41 was measured. The RI of HSA particles was very uniform for scattering and transmission mode (Figure 6-4B) whereas the RI of IgG A particles was slightly higher for scattering mode as compared to transmission mode (Figure 6-4C). This value of 1.41 falls into the center of the RI estimates for protein particles in literature of 1.33 to 1.4¹² and 1.4 to 1.6.¹¹ Furthermore, a time course study revealed that the RI of HSA particles did not change significantly upon incubation in the sucrose solutions for three hours at room temperature showing that the stability of the protein particles was not compromised by the sucrose solutions.

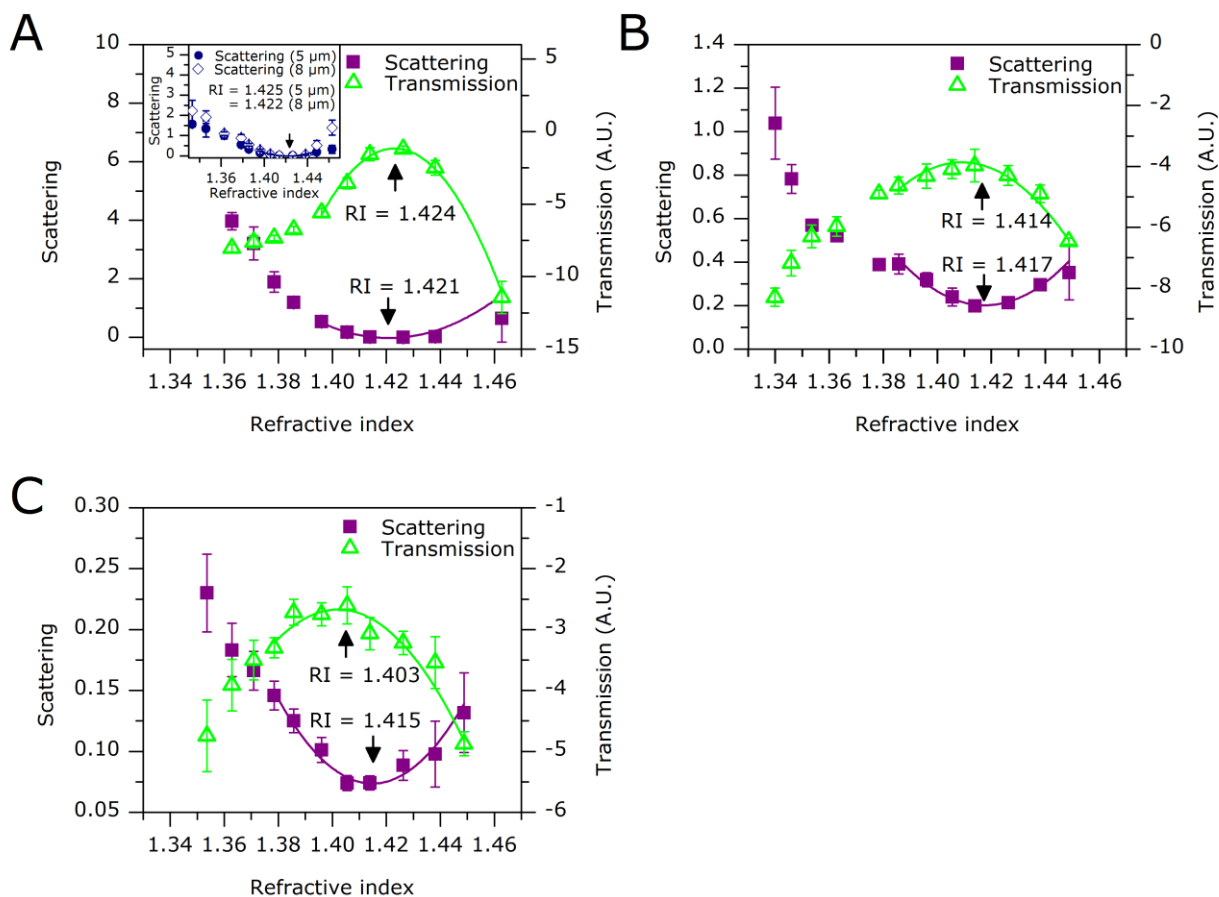


Figure 6-4: Particle RI determined by scattering or transmission for (A) silica particle standards (2 μm , the insert shows 5 μm and 8 μm) (B) HSA particles (heating), (C) IgG A particles (stirring). A polynomial fit around the extreme values is shown as a line. The RI obtained at the calculated extreme values is indicated as the mean from three independent experiments. Each graph represents one out of three independent experiments with error bars representing the standard deviation of six replicates within one experiment. A.U. = arbitrary units.

Alternative methods for RI determination of particles are turbidity measurements, which apply the same measurement principle as our method,³⁰ and digital holographic microscopy³³ and quantitative phase microscopy.³⁴ These methods were applied to spherical particles³⁰ or cells,^{33,34} but have not yet proved to be suitable for protein particles, to the best of our knowledge. Furthermore, the microscopic methods have rather low throughput as the RI of individual cells or particles is determined. In contrast, the method developed during our studies is fast, suitable to be automated and determines the mean RI of the complete particle population. One important prerequisite for the application of our method is a particle concentration of at least 1×10^8 particles/mL larger than 1 μm . Such large quantities of protein particles need to be generated either by concentration

of particles (e.g. by centrifugation) or by applying stress. Our method is probably not suitable to determine the RI of particles in a final therapeutic protein formulation with low particle numbers without further sample preparation steps.

Even though the determined RI of protein particles (1.41) was close to the RI of silica particles (1.42), the transparency of protein particles (around 700) was higher than the transparency of silica particles (around 400). Thus, as a next step we aimed to elucidate the relationship between transparency, RI, and the number of particles detected by light-based techniques.

3.3 Relevance of RI for protein particle analysis

The influence of RI on protein particle analysis was investigated by suspending protein particles or standard particles at one fixed concentration in solutions of varying RI and quantifying total particle counts larger 1 μm by LO and MFI (Figure 6-5). Because products meeting the specifications for the compendial size classes > 10 μm and > 25 μm can nonetheless contain substantial amounts of smaller particles,^{13,35,36} and the quantification of particles below 10 μm is gaining more and more importance,^{8,9} we decided to extend the evaluation of RI effects for particles to smaller size classes > 1 μm . Although the image resolution for particles below 2 μm was not sufficient to characterize particles using optical parameters such as transparency, counting of particles could be performed for particles > 1 μm with satisfying data quality. The RI of the solutions was adjusted by the addition of sucrose and/or increasing the protein concentration by adding HSA, both of which resulted in an increase in RI of the formulation. Both approaches represent pharmaceutically relevant conditions found in many therapeutic protein products. Sucrose is a common excipient with a roughly linear correlation of concentration to RI. High protein concentrations are often used for subcutaneous administration, in particular for monoclonal antibody preparations.³⁷

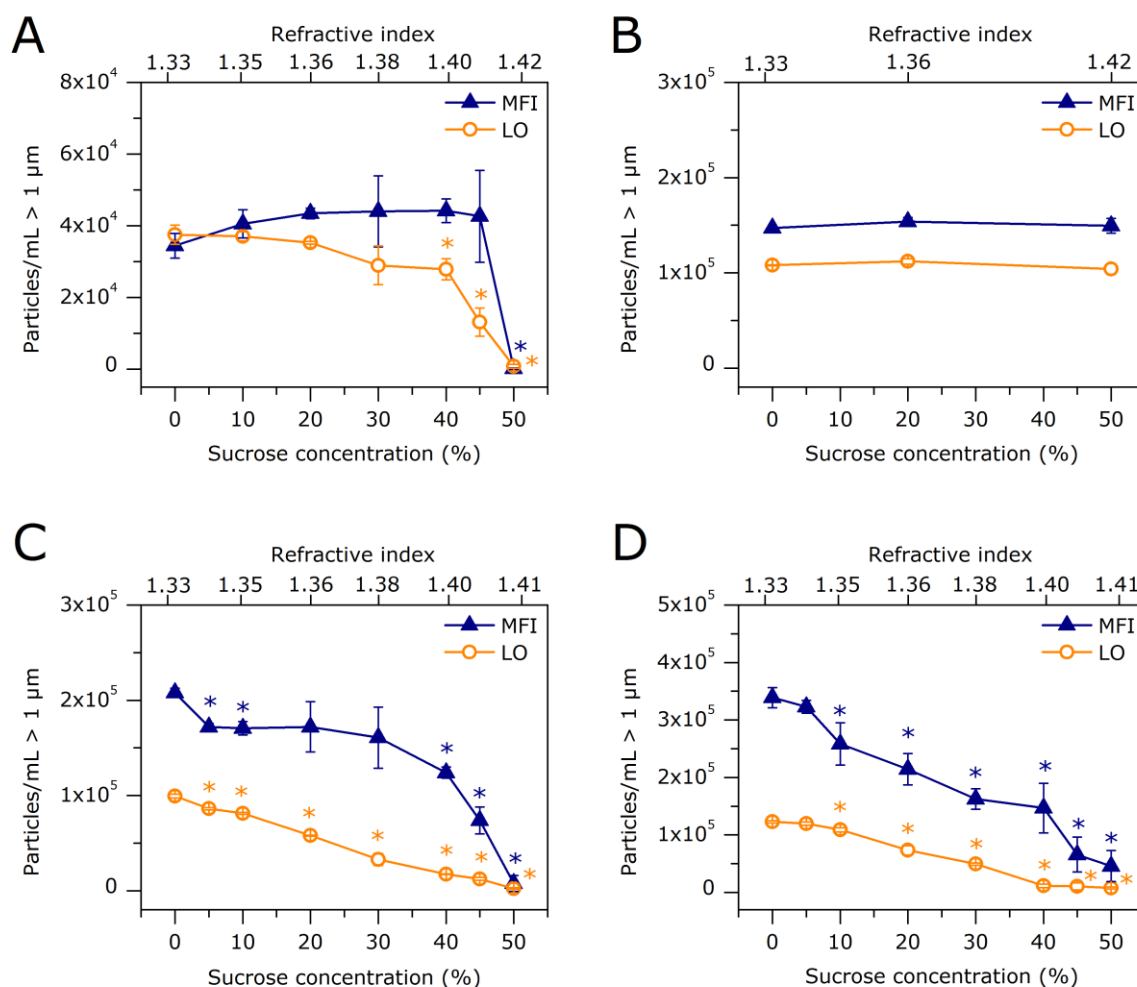


Figure 6-5: Particle counts determined by LO and MFI for fixed particle concentrations in sucrose solutions of varying RI of (A) silica particle standards (5 μm), (B) polystyrene particle standards (2 μm), (C) HSA particles (heating), (D) IgG A particles (stirring). The additional x-axis shows the RI of the respective solutions. Stars (*) indicate data points differing significantly from the initial concentration (ANOVA, $p < 0.05$). Error bars represent standard deviations from triplicate samples (dilutions were prepared in triplicates).

5 μm silica particle standards of known RI (1.42) were analyzed by LO and MFI at one fixed particle concentration in sucrose solutions of increasing concentration / RI (Figure 6-5A). The measured particle concentration (“apparent concentration”) in LO declined at higher sucrose concentrations (>40%) / RI values (>1.40) whereas particle counts in MFI stayed rather constant up to 45% sucrose / RI 1.41. Nevertheless, the particles appeared more transparent, as reflected in increasing intensity minimum values (mean of all particles) from 427 in water to 722 in 45% sucrose. Strikingly, in both techniques, silica particle standards became completely “invisible” and not detectable anymore at 50% sucrose when the RI of particles and solution matched exactly (RI 1.42).

The quantification of polystyrene particle standards by LO and MFI was not affected at all in the studied sucrose concentration range due to the high RI of polystyrene of 1.59 (Figure 6-5B) which again illustrates the need for novel more representative particle standards as claimed before.^{1,15,20} This high RI makes an RI match with sucrose solutions impossible due to the solubility limit of sucrose and the viscosity limit for LO and MFI.

Protein particles (HSA (heating) or IgG A (stirring)) were suspended in sucrose solutions of varying concentration and analyzed in the same way as the particle standards. To exclude direct effects of the high sucrose concentration, i.e. dissolution or generation of particles, two types of control experiments were performed: (1) Redilution control: high concentration sucrose samples with particles were diluted back to a lower sucrose concentration with water and the measured particle concentration was compared to the concentration measured in a particle sample directly prepared at the lower sucrose concentration. (2) Incubation control: particle concentrations were monitored before and after incubation of the protein particles in a solution of high sucrose concentration for one hour at room temperature. Both controls (1) and (2) showed no significant changes in the particle levels.

For these protein samples, significantly more particles were detected by MFI as compared to LO, which is in accordance with the literature.^{10,11,21} The measured ("apparent") concentration of HSA particles (heating) (Figure 6-5C) and IgG A particles (stirring) (Figure 6-5D) was significantly reduced at high sucrose concentrations in both techniques. This is due to the increased RI of the surrounding formulation and consequently decreased RI difference between particles and liquid. Particle counts by LO decreased nearly linearly for both particle types and showed significant differences to the initial particle concentration (at 0% sucrose) already at a sucrose concentration of 5% for HSA particles (heating) (Figure 6-5C) and 10% for IgG A particles (stirring) (Figure 6-5D). These sucrose concentrations of 5-10% are often found in (marketed) formulations of therapeutic proteins. Particle counts by MFI also decreased significantly with increasing sucrose concentration. However, the MFI system seemed to be less affected by the decreased RI difference than LO as the relative decrease in particle concentration was lower. Reasons for this might be (1) the

different measurement principle and set-up including a lower wavelength LED (470 nm) in MFI compared to a higher wavelength laser (670 nm) in LO; and (2) the “optimize illumination” process in MFI which allows the system to set the sensitivity according to the optical properties of the respective liquid.^{12,23} Strikingly, again, in both techniques, protein particles became “invisible” at the RI match of 1.41 similar to silica particles.

The transparency of protein particles shown as the intensity minimum (mean of the complete particle population of 2-6 μm) generated from MFI images increased linearly ($R^2 > 0.99$) with increasing sucrose concentration (Figure 6-6). This can also be seen in the MFI images (Figure 6-6) and explains the decrease in MFI particle counts with increasing RI of the formulation. In LO, “shadows” of the particles are projected on a light-sensitive area at the detector and the particle size is calculated proportional to the area of the shadow. Therefore, it can be assumed that increased light transmission caused by decreased RI differences, as described above in the context of the RI determination method, led to the decrease in LO counts. Similarly to the RI determination method it can be expected that particles “reappear” when the RI of the formulation is further increased exceeding the RI match point. However, those experiments were not performed due to the viscosity limit for LO and MFI.

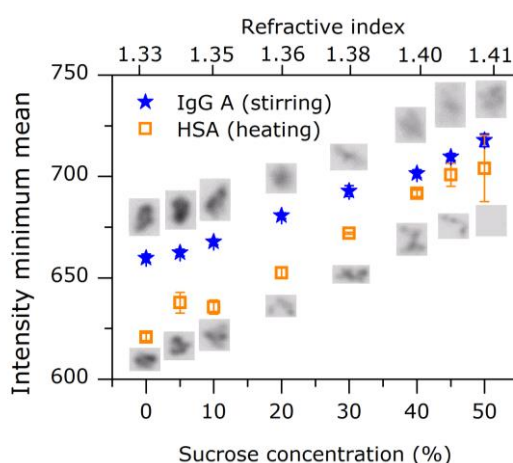


Figure 6-6: Increase in intensity minimum values from MFI (shown as the mean of the complete particle population of 2-6 μm) depending on the sucrose concentration of the solution and representative images of 10 μm particles from MFI. The additional x-axis shows the RI of the respective solutions. Error bars represent standard deviations from triplicate samples (dilutions were prepared in triplicates).

We propose the following mechanism for the phenomenon of subvisible particles becoming “invisible”: With increasing RI of the formulation, the particles get more difficult to detect by light-based techniques as the particle contour becomes blurred (also observed in MFI images of 5 μm silica particles, Figure 6-7A). For particles of uniform size and shape, this leads to a constant decrease in the apparent particle size for both LO and MFI as observed for 5 μm silica particle standards (Figure 6-7A). Nevertheless, in the case of 5 μm silica particle standards, the particles are still counted accurately as the decrease in size does not reach the detection limit of the systems until 40% sucrose with LO and 45% sucrose with MFI. Those particles only become invisible at the RI match. In the case of 2 μm silica particle standards, the particles become “invisible” at lower RI as the particle size decreases below the detection limit before the RI of particles and formulation match (Figure 6-7B). In the case of protein particles, particles become partly “invisible” at lower sucrose concentrations due to the polydisperse size distribution and the presence of smaller particles (Figure 6-2). These small particles “shrink” below the detection limit of the systems already at only slightly increased RI values, whereas larger particles are still detected and only become “invisible” when the refractive indices match. Additionally, the stronger RI influence on protein particles compared to silica particles is probably also due to other factors such as the irregular shape and surface structure, higher surface roughness and the lower compactness of protein particles which hamper the detection by light-based systems.²¹

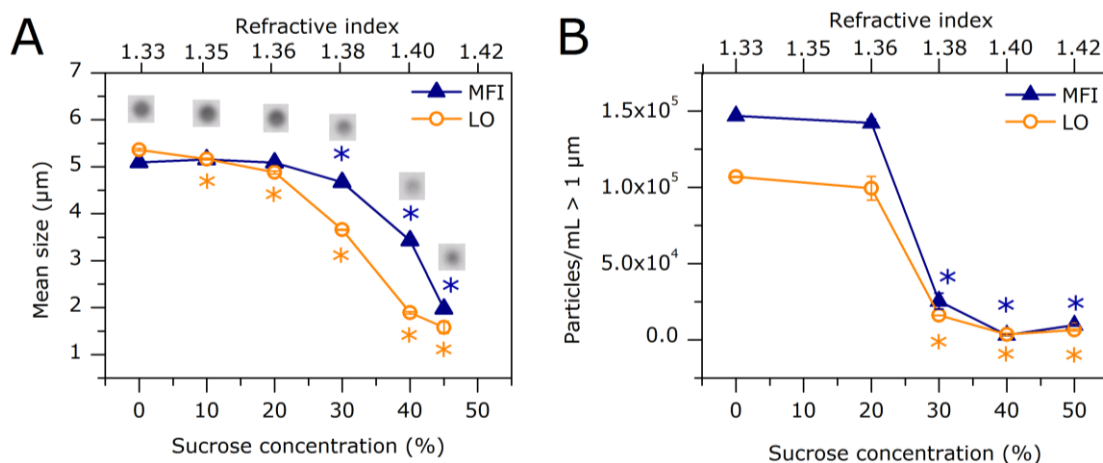


Figure 6-7: (A) Mean particle size of 5 μm silica particle standards determined by LO and MFI in sucrose solutions of varying concentration. Stars (*) indicate data points of significantly smaller particle size compared to the initial size (ANOVA, $p < 0.05$). Representative images from MFI show the softening contours of the imaged particles with increasing RI. (B) Particle counts of 2 μm silica particle standards determined by LO and MFI for a fixed particle concentration in sucrose solutions of varying concentration. Stars (*) indicate data points differing significantly from the initial concentration (ANOVA, $p < 0.05$). The additional x-axis shows the RI of the respective solutions.

Another formulation parameter that can affect RI is protein concentration. Pharmaceutically relevant protein concentrations cover a range from below 1 mg/mL up to about 200 mg/mL or even higher. Thus, the influence of RI on protein particle analysis was further evaluated with high protein concentration. Significant differences in the concentration of HSA particles (heating) were observed by LO at 100 mg/mL HSA concentration (Figure 6-8A) or 50 mg/mL HSA combined with 5% sucrose (Figure 6-8B). Both conditions represent common formulation conditions.

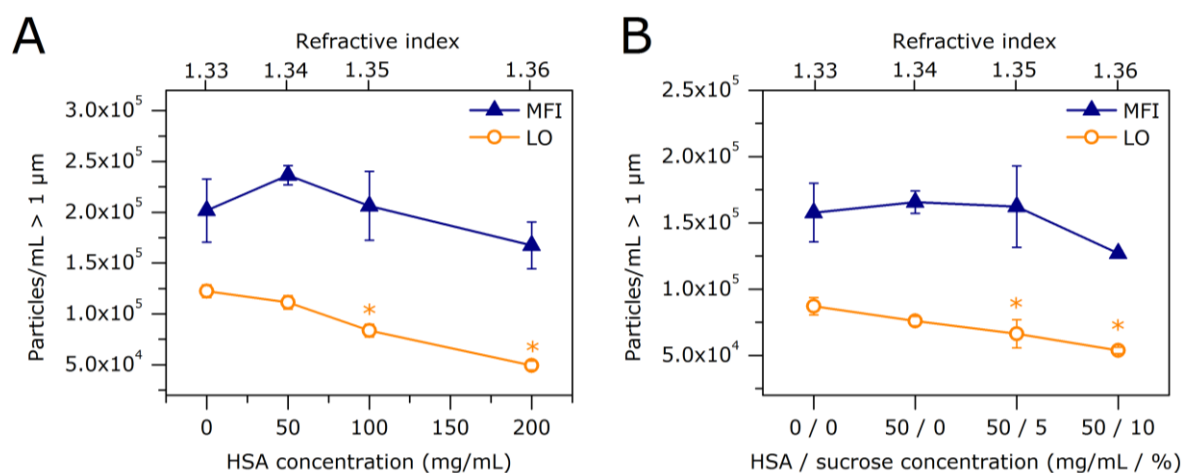


Figure 6-8: Particle counts of HSA particles (heating) at a fixed concentration determined by LO and MFI in formulations of (A) HSA and (B) HSA and sucrose. The additional x-axis shows the RI of the respective solutions. Stars (*) indicate data points differing significantly from the initial concentration (ANOVA, $p < 0.05$). Error bars represent standard deviations from triplicate samples (dilutions were prepared in triplicates).

A high protein concentration is pharmaceutically relevant especially for subcutaneous administration, for example Simponi[®] (golimumab) and Cimzia[®] (certolizumab) are formulated at 100 mg/mL and 200 mg/mL, respectively.^{38,39} Also formulations with lower protein concentration but with excipients increasing the RI are represented by our model solutions such as Humira[®] (50 mg/mL adalimumab and 1.2% mannitol)⁴⁰ and Enbrel[®] (50 mg/mL etanercept and 1% sucrose).⁴¹ For both Humira[®] and Enbrel[®] an RI of 1.35 was determined by Abbé refractometry which corresponds to the RI of formulations containing 100 mg/mL HSA or 50 mg/mL HSA with 5% sucrose. For example, the original etanercept formulation was analyzed undiluted and in several dilutions in the formulation buffer by LO and MFI (Figure 6-9). Clearly more particles (calculated back to the original concentration) were detected in diluted formulations of lower protein concentration for both LO and MFI. These results indicate that mainly LO, but also MFI might not detect the real particle load of a sample, but might instead underestimate subvisible particle numbers due to a low RI difference between particles and formulation.

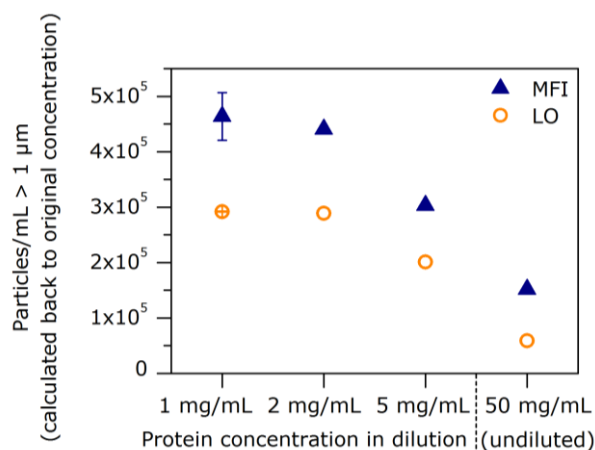


Figure 6-9: Particle counts in expired prefilled syringes of Enbrel® (etanercept) measured undiluted (50 mg/mL) and diluted in the appropriate formulation buffer by LO and MFI. The error bar for 1 mg/mL represents the standard deviation from a duplicate sample (dilution was prepared in duplicate). Formulations at 2 mg/mL, 5 mg/mL, and 50 mg/mL were analyzed only n=1 due to limited material availability.

To understand whether the obtained data are prone to error due to detection problems caused by the formulation RI we suggest two possible ways to cope with the influence of high formulation RI when using light-based techniques:

- (i) use of PTFE particles for the evaluation of the “invisible particle effect” in LO,
- (ii) use of alternative (light-independent) measurement principles.

3.4 PTFE particles for the evaluation of the “invisible particles effect” in LO

To address the question whether the RI of the formulation potentially influences the outcome of light-based subvisible particle detection methods, the formulation of interest can be tested for the “invisible particles effect” using PTFE particles. These polymeric particles in suspension show similar optical properties as protein particles (Figure 6-3) and can be spiked as a highly-concentrated suspension into the formulation of interest.

As shown in Figure 6-10A, the measured (“apparent”) concentration of PTFE particles by LO and MFI was influenced by the RI of the surrounding formulation. Decreases in PTFE particle concentration by LO were already observed at only 5% sucrose. The relative apparent particle concentrations determined by LO compared to the real concentration in the sample were very similar for protein

particles (e.g. 87%, 82%, and 58% for HSA particles and 97%, 89%, and 60% for IgG particles in 5%, 10%, and 20% sucrose, Figure 6-5C,D) and PTFE particles (88%, 72%, and 61%, Figure 6-10A). The apparent increase of the PTFE particle concentration in LO at 40% sucrose is probably due to the lower and more polydisperse RI of PTFE (RI 1.35-1.38^{30,31}) as compared to protein (RI 1.41). As the RI of 40% sucrose (RI 1.40) exceeds the RI of the particles, detection is facilitated when compared to 30% sucrose solution (RI 1.38) and particles “reappear”, due to the increase of light scattering after the RI match point (Figure 6-4). With MFI, the PTFE concentration was also affected by the RI of the sucrose solution as particle counts decreased until 10-20% sucrose. The apparent increase in PTFE particle concentration after the RI match was observed at lower sucrose concentrations compared to LO. The measured particle concentration at 40% sucrose was even higher than the initial concentration in water, presumably because of the better optical contrast of PTFE in 40% sucrose as compared to PTFE in water which is due to the low RI of PTFE.

The utility of using PTFE particles was confirmed by LO and MFI analysis of a PTFE particle suspension in a model protein formulation containing 50 mg/mL HSA and 5% sucrose (Figure 6-10B). PTFE particles were even more sensitive towards the “invisible particles effect” than protein particles. The relative apparent particle concentration by LO in the formulation containing 50 mg/mL HSA and 5% sucrose compared to the concentration in water was clearly lower for PTFE particles (53%, Figure 6-10B) as compared to HSA particles (76%, Figure 6-8B). With MFI, the apparent concentration of PTFE particles decreased to 70% in 50 mg/mL HSA and 5% sucrose whereas there was no significant effect for HSA particles. Overall, PTFE particles are recommended to test formulations for the “invisible particles effect” by LO, for an RI range up to 1.38. This range covers protein formulations with protein concentrations up to at least 150 mg/mL IgG (RI 1.37¹¹) or 200 mg/mL HSA and 10% sucrose (RI 1.38, own results).

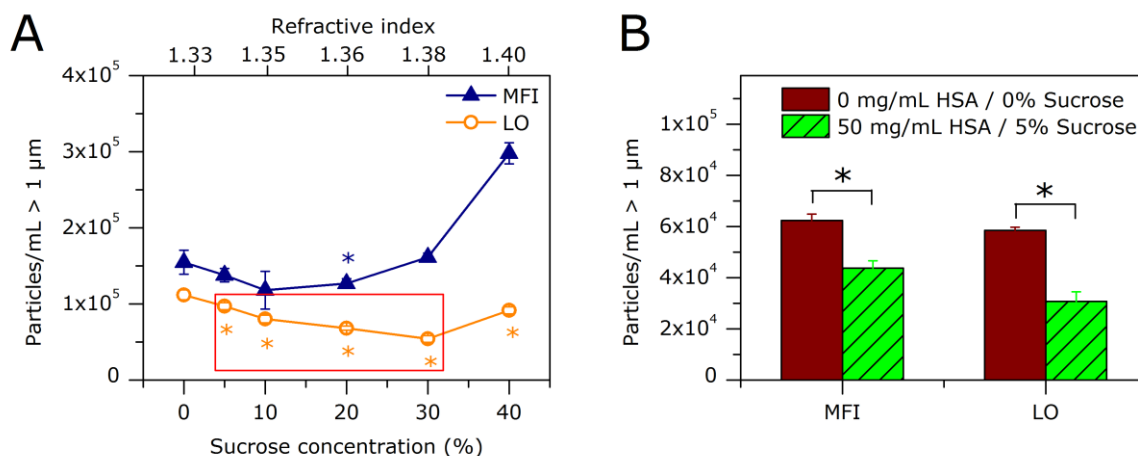


Figure 6-10: (A) Particle counts of PTFE particles at a fixed concentration determined by LO and MFI in sucrose solutions of varying RI. The red box indicates the range in which PTFE particles could be used to test specific formulations for the “invisible particles effect”. The additional x-axis shows the RI of the respective solutions. Stars (*) indicate data points differing significantly from the initial concentration (ANOVA, $p < 0.05$). (B) Particle counts of PTFE determined by LO and MFI in a solution containing HSA and sucrose in pharmaceutically relevant concentrations for an application test of PTFE particles as model particles. Stars (*) indicate significant differences between data points (ANOVA, $p < 0.05$). Error bars represent standard deviations from triplicate samples (dilutions were prepared in triplicates).

A group from the National Institute of Standards and Technology (NIST) also aimed to develop more proteinaceous particle standards and identified ethylenetetrafluoroethylene (ETFE) as a proper material.²⁶ This supports the general suitability of fluorinated polymers as protein particle-like materials and encourages searching for potentially even better fitting candidates within this class of materials.

In order to examine the formulation of interest for the “invisible particles effect” by means of PTFE particles, we suggest the following procedure: spike the same amount of a highly-concentrated PTFE particle suspension into water and into the formulation of interest, to achieve a final concentration similar to that expected in the protein formulation to be analyzed. Determine the apparent particle concentration of PTFE particles in both solutions by LO. A significant difference points towards a potential “invisible particles effect” for the analysis of protein particles in the formulation of interest. In this case, we recommend including orthogonal analytical techniques, preferably techniques with light-independent underlying principles such as ESZ or RMM (see below).

PTFE particles might furthermore serve as a protein particle surrogate material for the comparison of different analytical techniques or instruments. This could help to explain and bridge differing results for particle concentrations obtained from different instruments.

3.5 Orthogonal techniques for protein particle analysis to cope with RI influences

Difficulties with subvisible particle analysis due to RI influences can be addressed by using techniques with other underlying measurement principles. An example of a light-independent particle counting technique is the ESZ method (e.g. Coulter counter) which was originally developed for cell counting, but has recently also been applied for the analysis of protein particles.^{11,36,42-44} Drawbacks of ESZ are the large required sample volume and that the sample needs to be suspended in a conductive solution if the sample buffer does not have sufficient conductivity.

Another non-optical technique for particle counting and sizing that has recently become commercially available is the Archimedes system. In this technique, the principle of RMM is applied using a suspended microchannel resonator (SMR) or microcantilever, which resonates mechanically and changes its frequency depending on the buoyant mass of particles passing the channel.¹⁷⁻¹⁹ The buoyant mass is converted to absolute mass and then to particle size based on the density of both particle and fluid. We evaluated RMM as an orthogonal technique to LO and MFI for IgG A particles (stirring) in phosphate buffer containing 0% or 20% sucrose and compared apparent particle concentrations in the overlapping size range of 1-4 μm (Figure 6-11). The IgG particle concentration in phosphate buffer determined by RMM was in a similar range as determined by LO. In 20% sucrose, significantly less particles were detected by LO and MFI as compared to phosphate buffer (similar as in Figure 6-5D). In contrast, no significant difference was found for the same conditions by RMM. This emphasizes the suitability of light-independent techniques for the analysis of particles in therapeutic protein formulations and it can be recommended that they be included in an analytical package. This is especially important for formulations containing high protein concentration and/or excipients that

increase the RI of the formulation such as sugars. Otherwise, by applying only light-based methods particle counts in therapeutic protein formulations may be significantly underestimated.

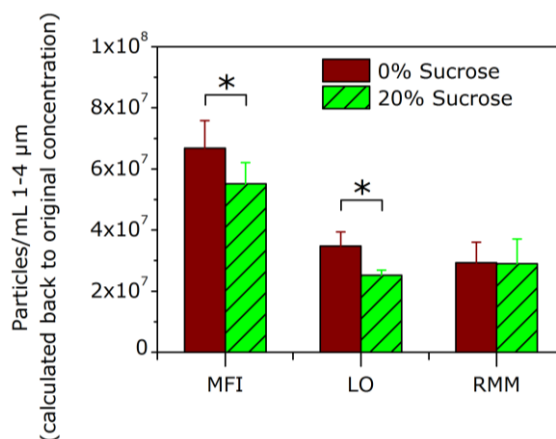


Figure 6-11: Particle counts of IgG A particles (stirring) at a fixed concentration determined by LO, MFI, and RMM in pure phosphate buffer (0% sucrose) and phosphate buffer containing 20% sucrose in the overlapping size range between the three systems. Results were calculated back to the original concentration as samples were analyzed in different dilutions due to different concentration limits of the systems. Stars (*) indicate significant differences between data points (ANOVA, $p < 0.05$). Error bars represent standard deviations from triplicate samples (dilutions were prepared in triplicates) for MFI and LO and for a triplicate measurement for RMM.

4 Conclusion

Our study showed that transparency, which is related to the RI of both particles and formulation, is an important parameter for protein particle analysis by light-based techniques. A fast batch method for RI determination of protein particles developed in this study provided an RI of 1.41 for protein particles generated by heat as well as mechanical stress. We envision the use of the method for research purposes in the development phase to get an insight into the RI of the particles of a certain protein and to judge the suitability of light-based methods for detecting subvisible particles suspended in a specific formulation. The RI difference between protein particles and surrounding formulation has a strong influence on the performance of LO and MFI. At pharmaceutically relevant sucrose concentrations (5%) and protein concentrations (100 mg/mL), the particle concentrations were clearly underestimated by LO and MFI. An RI match even caused particles to become “invisible” for the system, i.e. not detectable anymore by LO and MFI. Therefore, increased attention is required in the evaluation of subvisible particle analysis in formulations of high protein concentration and/or sugars. To address the influence of the RI, we recommend two alternatives: (1) Use of PTFE particles as model particles to test specific formulations for an RI influence in LO, because these particles have similar optical properties to protein particles. (2) Include light-independent techniques, e.g. RMM (Archimedes), in the analytical package as RMM was not affected at all by increased RI in the formulation. These procedures should help to avoid significant underestimation of the particle concentration in therapeutic protein formulations due to RI influences; which is critical for both development and release.

5 References

1. Carpenter J, Cherney B, Lubinecki A, Ma S, Marszal E, Mire-Sluis A, Nikolai T, Novak J, Ragheb J, Simak J 2010. Meeting report on protein particles and immunogenicity of therapeutic proteins: filling in the gaps in risk evaluation and mitigation. *Biologicals* 38:602-611.
2. Rosenberg AS 2006. Effects of protein aggregates: an immunologic perspective. *AAPS J* 8:E501-507.
3. Jiskoot W, van Schie RMF, Carstens MG, Schellekens H 2009. Immunological risk of injectable drug delivery systems. *Pharm Res* 26:1303-1314.
4. Fradkin AH, Carpenter JF, Randolph TW 2011. Glass particles as an adjuvant: A model for adverse immunogenicity of therapeutic proteins. *J Pharm Sci* 100:4953-4964.
5. Narhi LO, Schmit J, Bechtold-Peters K, Sharma D 2012. Classification of protein aggregates. *J Pharm Sci* 101:493-498.
6. USP<788>, United States Pharmacopeia, USP35-NF30, 2012. Particulate matter in injections. United States Pharmacopeial convention.
7. Ph.Eur. 2.9.19, Pharmacopoea europaea, 7th ed. 2010. Particulate contamination: Sub-visible particles. European Directorate For The Quality Of Medicine (EDQM).
8. Kirshner S 2012. Regulatory expectations for analysis of aggregates and particles. Talk at Workshop on Protein Aggregation and Immunogenicity, Breckenridge, Colorado, 07/12/2012.
9. Narhi LO 2012. AAPS update on USP expert committee for Sub visible particle analysis. Newsletter of the AAPS Aggregation and Biological Relevance Focus Group 3(2).
10. Wuchner K, Büchler J, Spycher R, Dalmonte P, Volkin DB 2010. Development of a microflow digital imaging assay to characterize protein particulates during storage of a high concentration IgG1 monoclonal antibody formulation. *J Pharm Sci* 99:3343-3361.
11. Demeule B, Messick S, Shire SJ, Liu J 2010. Characterization of particles in protein solutions: reaching the limits of current technologies. *AAPS J* 12:708-715.
12. Sharma DK, King D, Oma P, Merchant C 2010. Micro-flow imaging: flow microscopy applied to sub-visible particulate analysis in protein formulations. *AAPS J* 12:455-464.
13. Barnard JG, Singh S, Randolph TW, Carpenter JF 2011. Subvisible particle counting provides a sensitive method of detecting and quantifying aggregation of monoclonal antibody caused by freeze-thawing: insights into the roles of particles in the protein aggregation pathway. *J Pharm Sci* 100:492-503.
14. Narhi LO, Jiang Y, Cao S, Benedek K, Shnek D 2009. A critical review of analytical methods for subvisible and visible particles. *Curr Pharm Biotechnol* 10:373-381.
15. Zöls S, Tantipolphan R, Wiggernhorn M, Winter G, Jiskoot W, Friess W, Hawe A 2012. Particles in therapeutic protein formulations, Part 1: Overview of analytical methods. *J Pharm Sci* 101:914-935.
16. Grover NB, Naaman J, Ben-Sasson S, Doljanski F 1969. Electrical sizing of particles in suspensions. I. Theory. *Biophys J* 9:1398-1414.
17. Burg TP, Godin M, Knudsen SM, Shen W, Carlson G, Foster JS, Babcock K, Manalis SR 2007. Weighing of biomolecules, single cells and single nanoparticles in fluid. *Nature* 446:1066-1069.
18. Patel AR, Lau D, Liu J 2012. Quantification and characterization of micrometer and submicrometer subvisible particles in protein therapeutics by use of a suspended microchannel resonator. *Anal Chem* 84(15):6833-6840.
19. Barnard JG, Babcock K, Carpenter JF 2012. Characterization and Quantitation of Aggregates and Particles in Interferon- β Products : Potential Links Between Product Quality Attributes and Immunogenicity. *J Pharm Sci* 102:915-928.
20. Singh SK, Afonina N, Awwad M, Bechtold-Peters K, Blue JT, Chou D, Cromwell M, Krause H-J, Mahler H-C, Meyer BK, Narhi L, Nesta DP, Spitznagel T 2010. An industry perspective on the monitoring of subvisible particles as a quality attribute for protein therapeutics. *J Pharm Sci* 99:3302-3321.
21. Huang C-T, Sharma D, Oma P, Krishnamurthy R 2009. Quantitation of protein particles in parenteral solutions using micro-flow imaging. *J Pharm Sci* 98:3058-3071.
22. Sharma DK, King D, Merchant C 2011. Reference material development for calibration and verification of image-based particle analyzers. *Int J Pharm* 416:293-295.
23. Sharma DK, Oma P, Pollo MJ, Sukumar M 2010. Quantification and characterization of subvisible proteinaceous particles in opalescent mAb formulations using micro-flow imaging. *J Pharm Sci* 99:2628-2642.

24. Ripple DC, Dimitrova MN 2012. Protein particles: What we know and what we do not know. *J Pharm Sci* 101:3568-3579.
25. Huygens C. 1690. *Traité de la Lumière*. 1st ed., Leiden, The Netherlands: Pieter van der Aa.
26. Ripple DC, Wayment JR, Carrier MJ 2011. Standards for the optical detection of protein particles. *APR*:90-96.
27. Ojena SM, de Forest PR 1972. Precise refractive index determination by the immersion method, using phase contrast stage microscopy and the Mettler hot stage. *J Forensic Sci Soc* 12:315-329.
28. Tecan 2001. Determination of the light absorption pathlength in microwell plates. Hombrechtikon, Switzerland, Application note:1-4.
29. Brown L 2011. Characterizing Biologics Using Dynamic Imaging Particle Analysis. *BioPharm Int*:s1-8.
30. Pan G, Tse AS, Kesavamoorthy R, Asher SA 1998. Synthesis of highly fluorinated monodisperse colloids for low refractive index crystalline colloidal arrays. *Mater Sci+* 7863:6518-6524.
31. Groh W, Zimmermann A 1991. What is the lowest refractive index of an organic polymer? *Macromolecules* 24:6660-6663.
32. <http://www.microparticles.de/eigenschaften.html>, accessed on 12/20/2012.
33. Kemper B, Kosmeier S, Langehanenberg P, von Bally G, Bredebusch I, Domschke W, Schnekenburger J 2007. Integral refractive index determination of living suspension cells by multifocus digital holographic phase contrast microscopy. *J Biomed Opt* 12:054009.
34. Curl CL, Bellair CJ, Harris T, Allman BE, Harris PJ, Stewart AG, Roberts A, Nugent KA, Delbridge LMD 2005. Refractive index measurement in viable cells using quantitative phase-amplitude microscopy and confocal microscopy. *Cytom Part A* 65:88-92.
35. Hawe A, Friess W 2007. Stabilization of a hydrophobic recombinant cytokine by human serum albumin. *J Pharm Sci* 96:2987-2999.
36. Tyagi AK, Randolph TW, Dong A, Maloney KM, Hitscherich C, Carpenter JF 2009. IgG particle formation during filling pump operation: a case study of heterogeneous nucleation on stainless steel nanoparticles. *J Pharm Sci* 98:94-104.
37. Shire SJ, Shahrokh Z, Liu J 2004. Challenges in the development of high protein concentration formulations. *J Pharm Sci* 93:1390-1402.
38. <http://www.simponi.com/sites/default/files/pdf/prescribing-information.pdf>, accessed on 12/20/2012.
39. http://www.cimzia.com/pdf/Prescribing_Information.pdf, accessed on 12/20/2012.
40. http://www.fda.gov/ohrms/dockets/ac/03/briefing/3930B1_02_B-Abbott-Humira%20Prescribing%20Info.pdf, accessed on 12/20/2012.
41. http://www.amgen.ca/Enbrel_PM.pdf, accessed on 12/20/2012.
42. Barnard JG, Rhyner MN, Carpenter JF 2012. Critical evaluation and guidance for using the coulter method for counting subvisible particles in protein solutions. *J Pharm Sci* 101:140-153.
43. Rhyner MN 2011. The Coulter principle for analysis of subvisible particles in protein formulations. *AAPS J* 13:54-58.
44. Mück C 2002. Analytik von Proteinaggregation mittels Coulter-Prinzip : Vergleich mit der Lichtblockade-Messung. Diploma thesis, Ludwig-Maximilians-Universität München / FH Albstadt-Sigmaringen.

Chapter 7

Summary of the thesis

The overall goal of this thesis was to identify and evaluate critical factors for protein particle analysis and to apply this knowledge for the development of novel standardized protein-like particles. Thorough analysis of particles in therapeutic protein formulations is crucial due to regulatory requirements, the potential immunogenicity of protein aggregates and particles, and the need for quality and stability control of the product.

Chapter 1 provides a comprehensive overview of analytical methods for the detection and characterization of particles in therapeutic protein formulations. The extensive portfolio of available methods does not only offer more flexibility and cross-validation of results, but also brings along the difficulty how to handle and to interpret differing results from several analytical techniques or instruments. In this chapter, the underlying theory, output parameters, benefits, shortcomings, and illustrative examples for each technique are described. In this context, the necessity of method evaluation before data analysis is outlined which requires the development of novel more proteinaceous particle standards.

In Chapter 2, novel techniques or instruments (Sysmex FPIA-3000 and Occhio FC200S+ (flow imaging microscopy), Coulter counter Multisizer 4 (electrical sensing zone (ESZ)), Archimedes (resonant mass measurement (RMM)), rapID (image directed Raman spectroscopy)) were evaluated regarding their performance for (protein) particle counting, sizing, or characterization. Results from flow imaging microscopy differed strongly depending on the applied settings and the used system. More established flow imaging techniques such as Micro-Flow Imaging (MFI) or FlowCAM were regarded preferable in this case. The non-optical particle techniques ESZ and RMM presented useful additions to the pool of techniques as they provided good size and count accuracy when compared to the established techniques dynamic light scattering (DLS) or nanoparticle tracking analysis (NTA). Particle identification by rapID proved to be an interesting approach, but with the need for further improvements. Chapter 2 showed that

novel techniques for particle analysis can be useful, but their strengths, weaknesses, and output parameters need to be evaluated thoroughly for the intended application.

A prominent application in the field of particle analysis is the differentiation of protein particles from silicone oil droplets. The latter may especially be introduced into products filled in prefilled syringes which are siliconized for lubrication. Chapter 3 describes this critical differentiation by MFI and RMM for samples of artificially generated silicone oil droplets and protein particles in controllable defined mixtures. MFI was identified as reliable for particles with a size above 2 μm and with moderate droplet/particle ratios (70:30 – 30:70) when using the built-in software algorithm for the identification of similar particle images. The performance could be improved, especially for more extreme ratios (95:5 – 15:85), by a customized filter which was developed specifically for this study based on particle transparency and shape. RMM was considered as highly accurate for particles from 0.5 to 2 μm if the total droplet/particle concentration was in a statistically sufficient range. As a conclusion from this chapter, MFI and RMM should be applied as orthogonal techniques in combination to achieve an accurate and reliable differentiation of protein particles and silicone oil droplets.

Flow imaging microscopy is of increasing importance due to extended particle characterization possibilities beyond sizing and counting. Therefore, regulatory agencies tend to include the technique into the pharmacopeias, in addition to the conventional technique of light obscuration (LO). However, results from flow imaging microscopy may vary substantially depending on the used instrument as observed in Chapter 2. In Chapter 4, four of the pharmaceutically most relevant flow imaging microscopy systems (MFI4100, MFI5200, FlowCAM VS1, and FlowCAM PV) were subjected to a detailed evaluation of particle quantification, characterization, image quality, differentiation of protein particles and silicone oil droplets, and handling of the systems. The FlowCAM systems provided higher image quality and were more flexible with respect to adjustment of settings, whereas the MFI systems appeared more useful for standardized applications. In detail, the FlowCAM VS1 was considered as the best choice for high resolution images, the FlowCAM PV for an accurate quantification and differentiation of protein particles and silicone oil droplets. The MFI systems showed their strength

in size and count accuracy, the MFI5200 was especially suitable for protein particle analysis under impaired optical conditions by an increased refractive index of the formulation. The results from this chapter indicate again that the choice of the appropriate instrument depends strongly on the output parameters of interest.

Based on the knowledge on critical particle properties in different analytical techniques acquired in the previous chapters, a material screening for the development of novel standardized protein-like particles for light-based techniques was performed in Chapter 5. In the screening, proteinaceous (human serum albumin (HSA)-starch particles, spray-dried HSA, gelatin particles, and zein) and non-proteinaceous materials (chitosan and polytetrafluoroethylene (PTFE)) were assessed regarding their optical similarity to particles of therapeutic proteins (represented by HSA particles generated by heat stress). Based on numerous particle properties (size, size distribution, shape, transparency, and stability) gelatin and PTFE particles were considered the most promising materials for light-based applications. The density of protein particles, as a crucial particle parameter for weight-based techniques like RMM, has not been characterized well up to now. Thus, two novel methods based on RMM for density determination of pure protein and protein particles including entrapped liquid were developed. The methods provided a density of about 1.4 g/mL for pure protein (rituximab and gelatin), in congruence with theoretically calculated values of 1.38-1.44 g/mL. For protein particles including entrapped liquid an apparent density of about 1.07 g/mL was obtained for rituximab particles generated by heat stress. This chapter indicated that both gelatin particles and PTFE might be valuable in the development of standardized protein-like particles depending on the application purpose: gelatin particles might be suitable for both light-based and weight-based techniques whereas PTFE particles could be used for light-based techniques.

As many analytical techniques for protein particles are based on the interaction of the particles with light, the particle transparency plays a crucial role for accurate particle quantification on the one hand and the development of suitable standardized protein-like particles on the other hand. Chapter 6 is focused on the relevance of the refractive index (RI), which is closely related to transparency,

for particle analysis. As the RI of protein particles has been unknown until now, a novel method for RI determination of protein particles was developed. This method provided an RI of 1.41 for particles from two different therapeutic proteins (HSA and IgG). The relevance of the RI was then investigated by increasing the RI of the surrounding formulation until particles became “invisible”, i.e. not detectable anymore by light-based systems (in this case LO and MFI) at the RI match. As an increased RI is of practical significance at high protein concentration and/or the use of excipients such as sugars, potential solution strategies were also investigated in this chapter. As a result, PTFE particles, as identified in the material screening in Chapter 5, turned out to be suitable to test a specific formulation for RI effects. Furthermore, light-independent techniques such as RMM can be beneficial in case of RI influences.

Taken together, this study provides new insight into the analysis of particles in therapeutic protein formulations. It illustrates that it is crucial to not only comprehensively understand the techniques’ principle and limitations, but to also evaluate data from different techniques carefully in order to draw reliable conclusions. In this regard, potential candidates for the development of novel standardized protein-like particles identified in this study are very valuable and can help to improve protein particle analysis in the future.

Publications and presentations associated with this thesis

Review articles

S. Zölls, R. Tantipolphan, M. Wiggernhorn, G. Winter, W. Jiskoot, W. Friess, A. Hawe: "Particles in therapeutic protein formulations, part 1: overview of analytical methods"; J Pharm Sci 101(3):914-935 (2012)

Book chapters

A. Hawe, **S. Zölls**, A. Freitag, J. F. Carpenter: "Subvisible and visible particle analysis in biopharmaceutical research and development", in Biophysical characterization of proteins in developing biopharmaceuticals, Elsevier, editors: D. Houde, S. Berkowitz (submitted)

Research articles

S. Zölls, M. Gregoritza, R. Tantipolphan, M. Wiggernhorn, G. Winter, W. Friess, A. Hawe: "How subvisible particles become invisible – relevance of the refractive index for protein particle analysis"; J Pharm Sci 102(5):1434-1446 (2013)

D. Weinbuch*, **S. Zölls***, M. Wiggernhorn, W. Friess, G. Winter, W. Jiskoot, A. Hawe: "Micro-Flow Imaging and resonant mass measurement (Archimedes) – complementary methods to quantitatively differentiate protein particles and silicone oil droplets"; J Pharm Sci 102(7):2152-2165 (2013); *joint first authors

S. Zölls*, D. Weinbuch*, M. Wiggernhorn, G. Winter, W. Friess, W. Jiskoot, A. Hawe: "Flow imaging microscopy for protein particle analysis – a comparative evaluation of four different analytical instruments"; The AAPS Journal (accepted); *joint first authors

Oral presentations

S. Zölls: "Micro-Flow Imaging for protein particles – getting more than just numbers". Protein Simple User Meeting, Basel, CH, July 3-4, 2012

Poster presentations

S. Zölls, D. Weinbuch, M. Wiggenhorn, G. Winter, W. Friess, W. Jiskoot, A. Hawe: "Comparative evaluation of four different flow imaging microscopy instruments for protein particle analysis"; National Biotech Conference, San Diego, CA, May 20-22, 2013

S. Zölls, D. Weinbuch, M. Wiggenhorn, G. Winter, W. Friess, W. Jiskoot, A. Hawe: "Micro-Flow Imaging and resonant mass measurement (Archimedes) for the differentiation of silicone oil droplets and protein particles"; PepTalk, Palm Springs, CA, January 21-25, 2013; and National Biotech Conference, San Diego, CA, May 20-22, 2013

S. Zölls, D. Weinbuch, W. Friess, A. Hawe: "Differentiation of silicone oil droplets and protein particles by MFI and RMM"; Controlled Release Society (CRS) German Local Chapter Meeting, Ludwigshafen, Germany, March 21-22, 2013

S. Zölls, R. Tantipolphan, M. Wiggenhorn, G. Winter, W. Friess, A. Hawe: "Evaluation of Archimedes and Coulter counter for the analysis of (protein) particles"; National Biotech Conference, San Diego, CA, May 21-22, 2012

S. Zölls, M. Gregoritzka, R. Tantipolphan, M. Wiggenhorn, G. Winter, W. Friess, A. Hawe: "How subvisible particles get invisible - Relevance of refractive index for protein particle analysis"; PEGS Protein engineering summit, Boston, MA, April 30 – May 3, 2012; and National Biotech Conference, San Diego, CA, May 21-22, 2012

S. Zölls, R. Tantipolphan, M. Wiggenhorn, G. Winter, W. Friess, A. Hawe: "Comparative analysis of subvisible particles induced by freeze-thawing, stirring and heating of an IgG antibody"; Colorado Protein Stability Conference, Breckenridge, CO, July 19-21, 2011; and National Biotech Conference, San Francisco, CA, May 16-18, 2011

S. Mickisch, R. Tantipolphan, M. Wiggenhorn, W. Friess, G. Winter, A. Hawe: "Subvisible particles in a monoclonal antibody formulation analyzed by nanoparticle tracking analysis and Micro-Flow Imaging"; National Biotech Conference, San Francisco, CA, May 16-19, 2010; and Workshop on protein aggregation and immunogenicity, Breckenridge, CO, July 20-22, 2010

Curriculum vitae

SARAH ZÖLLS, GEB. MICKISCH

PERSONAL DETAILS

Date of birth: 23.04.1984
Place of birth: Starnberg
Nationality: German

EDUCATION

05/2010 - 06/2013	PhD studies Coriolis Pharma, Martinsried Supervisor: Dr. Andrea Hawe in collaboration with Department of Pharmacy, Pharmaceutical Technology and Biopharmaceutics, Ludwig-Maximilians-Universität München Supervisor: Prof. Dr. Wolfgang Frieß
10/2009 - 04/2010	Research project Max Planck Institute of Biochemistry Supervisor: Prof. Dr. F.-Ulrich Hartl
10/2007 - 09/2009	Studies of Pharmaceutical Sciences (M.Sc.) Ludwig-Maximilians-Universität München
09/2007 - 04/2008	Research stay Oncology Research Institute, Greenville, SC, USA Supervisor: Prof. Dr. Xianzhong Yu
10/2004 - 08/2007	Studies of Pharmaceutical Sciences (B.Sc.) Ludwig-Maximilians-Universität München
10/2003 - 07/2004	Studies of Pharmacy Ludwig-Maximilians-Universität München
09/1994 - 07/2003	Highschool, graduation with "Abitur" Gymnasium Starnberg